NASA CR-114648

Available to the Public

NOISE REDUCTION OF A TILT-ROTOR AIRCRAFT INCLUDING EFFECTS ON WEIGHT AND PERFORMANCE

JUNE 1973

PREPARED UNDER CONTRACT NAS2-6784 (MODIFICATION I)

THE BOEING VERTOL COMPANY
P. O. Box 16858
Philadelphia, Pennsylvania 19142

for

Ames Research Center
National Aeronautics and Space Administration
and
United States Army Air Mobility Research and Development Laboratory
Ames Directorate

BOEING D222-10062-1

TABLE OF CONTENTS

		Page
SUMMARY		1
I.	INTRODUCTION	3
II.	INFLUENCE OF DESIGN PARAMETERS ON ROTOR ACOUSTICS.	6
	General Discussion	6
	Tip Speeds	13
	Number of Blades	17
	Thrust	23
	Blade Tip Shape	25
	Blade Planform	25
	Airfoil Section	34
	Blade Twist	42
	Other Noise Reduction Techniques	45
III.	TURBOSHAFT ENGINE NOISE	46
IV.	ROTOR DESIGN PARAMETER TRADEOFFS	53
	General Discussion	53
	Sensitivity Study Approach	54
	Discussion of Results of Tilt-Rotor Sensitivity to the Five Design Parameters	60
V.	PARTIAL DERIVATIVES WITH RESPECT TO OPERATIONAL AND DESIGN PARAMETERS	92
	General Remarks	92

VI. CONCEPTUAL DESIGN OF QUIET TILT-ROTOR AIRCRAFT 101

Approach 101

Criteria 101

Quiet Aircraft Selection 103

Description of New Designs 103

Performance 111

Far-Field Acoustic Signatures 118

Takeoff and Landing Trajectories 124

VII. CONCLUSIONS AND RECOMMENDATIONS 144

LIST OF APPENDICES

A. SUPPORTING ACOUSTIC DATA 150

B. SAMPLE CALCULATION OF TURBOSHAFT ENGINE INLET NOISE SUPPRESSION 161

C. HOVER OGE PERFORMANCE PREDICTION 163

D. TABULATION OF SUMMARY WEIGHT STATEMENTS AND CONFIGURATION CHARACTERISTICS 167

E. ACCURACY OF THE THEORETICAL TILT-ROTOR ACOUSTIC MODEL 171

F. AIRCRAFT SENSITIVITY PREDICTION TOLERANCES 175

G. WEIGHTS PREDICTION METHODOLOGY 186

List of References 210

LIST OF SYMBOLS

A	total rotor disc area, ft^2
AR	aspect ratio
B	number of blades per rotor
BRS	best range speed, *knots*
C	chord, *ft.*
C_P	rotor power coefficient, $RHP\ 550/\rho\pi R^2 V_t^3$
C_{T_H}	rotor thrust coefficient, $T/\rho\pi R^2 V_t^2$
C_T'	helicopter lift coefficient in forward flight, $L/\rho\pi R^2 V_t^2$
$EPNL$	effective perceived noise level, *EPNdB*
FM	hovering aerodynamic efficiency, figure-of-merit
H	height of acoustically lined engine inlet duct, *ft.*
HP	horsepower
HP_f	horsepower required in cruise flight
Hz	Hertz, *cycles per second*
I	moment of inertia, slug-ft^2
L	lift, pounds
L	length of acoustically lined engine inlet duct, *ft.*
M	Mach number, freestream velocity/speed of sound
M_{MO}	aircraft maximum operating Mach number
M_T	Mach number at rotor tip
N	noise, *dB*
$OASPL$	overall sound pressure level, *dB*
PNL	perceived noise level, *PNdB*
R	rotor radius, *dB*

LIST OF SYMBOLS (CONT'D)

REQ	required
RHP	rotor horsepower
RHP_{ind}	induced rotor horsepower required
RPM	revolutions per minute
SPL	sound pressure level, *dB*
S_w	wing area, ft^2
T	thrust, *lb.*
TLS	transmission limited speed, *knots*
T/W	thrust-to-gross weigt ratio
V	aircraft speed of flight, *knots, ft/sec.*
V_{block}	(mission range)/(mission total elapsed time), including dead time and hovering time, *knots*
V_{dive}	maximum dive speed, *knots equivalent airspeed*
V_{max}	maximum cruising speed, *knots*
V_{MO}	maximum operating speed, *knots equivalent airspeed*
V_{opt}	speed at which the aircraft maximum lift-to-drag ratio occurs, *knots, ft/sec.*
V_t	rotor tip speed, *ft/sec.*
W	gross weight, *lbs.*
W/A	nominal rotor disc loading, lb/ft^2
WE, W_E	weight empty, *lbs.*
W_h	hover gross weight, *lbs*
W_u	useful load, *lbs.*
XMSN	transmission
$XP_{\ell\ell}$	steady-state rotor performance parameter determining the rotor unsteady airload harmonic decay

LIST OF SYMBOLS (CONT'D)

a	airfoil lift curve slope, rad^{-1}
b	wing span, $ft.$
c	speed of sound in air, $knots$ or ft/sec
dB	decibel
f	frequency, Hz or cps
fe	parasite drag equivalent flat plate area, ft^2
g	acceleration of earth gravity, $32.17\ ft/sec^2$
k_{ind_h}	hover nonideal induced power correction
n	exponential slope of rotor airload as a function of rotor rotational harmonic
v	ideal rotor induced velocity, $ft/sec.$
w_b	span loading, W/b^2, lbs/ft^2
w_f	equivalent flat plate parasite drag loading, W/fe, lb/ft^2
α_p	angle between thrust line and freestream velocity, $degrees$
Δ	incremental quantity
ΔI_λ	harmonic induced force on one rotor blade
η_{ACC}	accessory losses
η_{CR}	propeller cruise design point efficiency
η_I	installation losses
η_P	propeller efficiency
η_{TR}	transmission efficiency
θ_t	rotor blade twist measured from root to tip, tip-up positive, $degrees$
$\theta_{.75}$	rotor collective angle at $.75R$ radial station, $degrees$
λ	wavelength, $meters$

LIST OF SYMBOLS (CONT'D)

λ_H	rotor inflow ratio, $(V \cos \alpha_p + v)/V_t$
μ	rotor advance ratio, V/V_t
π	3.14159
ρ	air density, $slug/ft^3$
σ	rotor solidity ratio, blade area/disc area

SUBSCRIPT

h, H	in hover
o	original or baseline value

NOISE REDUCTION OF A TILT-ROTOR AIRCRAFT INCLUDING EFFECTS ON WEIGHT AND PERFORMANCE

by

J. Gibs, W. Stepniewski,
R. Spencer and G. Kohler
Boeing Vertol Company

SUMMARY

Various methods for far-field noise reduction of a tilt-rotor acoustic signature and the performance and weight tradeoffs which result from modification of the noise sources are considered in this report. In order to provide a realistic approach for the investigation, the Boeing Tilt-Rotor Flight Research Aircraft (Model 222 as defined in Ref. 1) was selected as the baseline. This aircraft has undergone considerable engineering development. Its rotor has been manufactured and tested in the Ames full-scale wind tunnel. Therefore, the study reflects the current state-of-the art of aircraft design for far-field acoustic signature reduction and is not based solely on an engineering feasibility (paper) aircraft. This report supplements a previous study investigating reduction of noise signature through the management of the terminal flight trajectory (Ref. 2).

The following tasks comprise this study:

A. Review of rotor acoustic phenomena dependence on design parameters.

B. Definition of the tilt-rotor aircraft performance, weight and acoustic signature with respect to aircraft design parameters.

C. Definition of two new "quiet" aircraft using design ground rules applicable to the Model 222.

On the basis of Task A, the following four design and/or operational parameters were selected as potentially representing the most important inputs to noise reduction at the source using current technology.

1. Tip Speed
2. Number of blades
3. Disc loading
4. Rotor blade area.

A quantitative study of the effectiveness of those parameters was performed in Task B. Although the main effort was directed toward various aspects of noise reduction generated by the rotors, acoustic problems of the powerplants were also briefly discussed. The results of the studies performed in Task B are generalized by presenting them under the form of various derivatives about the Model 222 tilt-rotor design parameters. Rotor tip speed was identified as the most effective design parameter for noise reduction.

Finally in Task C, the most effective methods of noise attenuation at the source, resulting in the most favorable performance and/or weight tradeoffs, were applied to the design of two tilt-rotor aircraft. These aircraft were designed to have the same

basic performance (1298-pound payload over a 100 n.mi. radius mission), structural envelope and flying qualities.

In addition to the above constraints, the acoustic signatures of both aircraft (in comparison with the Model 222) must be reduced at a distance of 500 feet while hovering out-of-ground effect. For one aircraft, this reduction should amount to 10 PNdB in the perceived noise level, while for the other, 10 dB in the overall sound pressure level. This results in an increase of design gross weight of 25.3 and 5.8 percent, respectively.

I. INTRODUCTION

Reduction of the far-field noise intensity through acoustic improvements at the source and management of terminal flight trajectories of aircraft represent two of the most important inputs into improving acoustic signature on the ground. This latter aspect is significant from the military (detection, exposure of ground personnel, etc.) as well as the civilian (annoyance of the population) point of view.

Noise abatement possibilities offered by management of the terminal flight trajectories have been studied for a transport-type tilt-rotor aircraft of the 46,000-pound gross weight class (Ref. 2). In that study, penalties in increased fuel consumption and/or time required to reach prescribed cruise conditions (altitude and speed) were also indicated.

In order to complete the picture of the effectiveness of various approaches to noise abatement on the ground, it was necessary to investigate aspects of noise reduction at the source. For this task, the [illegible]ng tilt rotor flight research aircraft (Fig. 1-1, 12,00[illegible] pounds gross weight) was selected as the reference from which acoustic improvements and associated weight and performance penalties were evaluated. The selection of this aircraft as a baseline results in a more realistic study because of the five-year design effort, wind-tunnel configuration studies, and construction of a full-scale rotor and control system.

The Model 222 is not necessarily representative of the whole spectrum of tilt-rotor aircraft that may be developed in the future (from utility to transports) because of its design gross weight and weight breakdown. However, the relative (non-dimensional) trends developed in this study would be indicative of the noise reduction - performance and/or weight tradeoffs - of other tilt-rotor aircraft as well, after accounting for the differences in wing span loading, equivalent parasite drag loading, and weight-empty to gross-weight ratio. In order to best accomplish the envisioned tasks, the whole study is divided into the following sections:

- Review of the Influence of Design Parameters on Rotor Acoustics
- Turboshaft Engine Noise

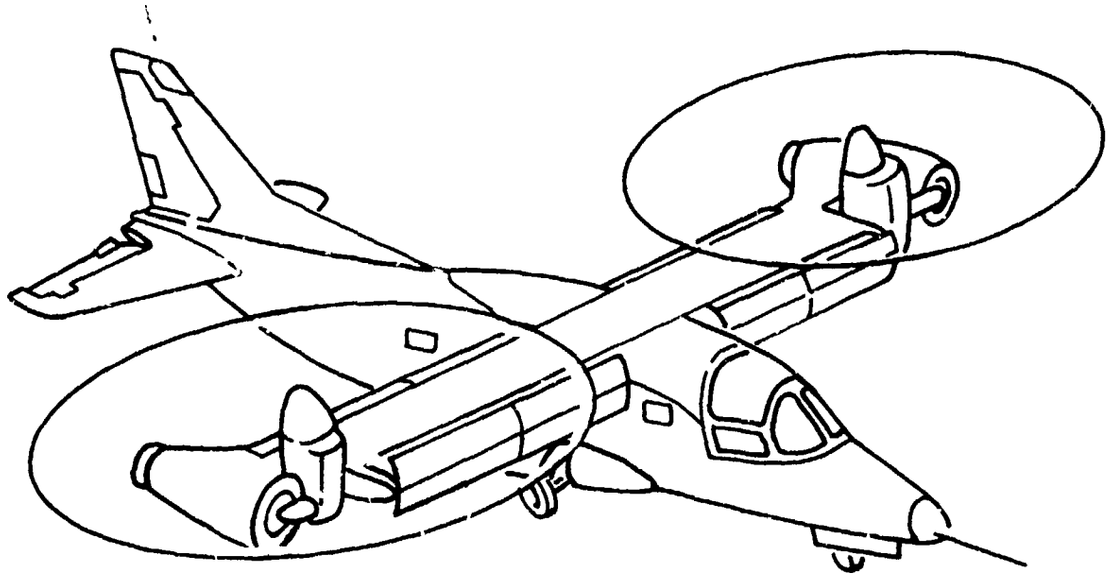

FIGURE 1–1. MODEL 222–1 TILT ROTOR NASA RESEARCH AIRCRAFT

- Rotor Design Parameters Tradeoff Studies (weight, performance, and noise)
- Partial Derivatives with Respect to Operational and Design Parameters
- Conceptual Design of Quiet Tilt Rotors
- Conclusions
- Recommendations

Each of the above sections represents, to some extent, a closed entity, but together, they show efficient methods to reduce the aircraft far-field acoustic signature as well as to indicate performance and/or weight penalties to be encountered.

In general, this report may be looked upon as a review of current design practices for the reduction of aircraft noise. However, it should be emphasized that all of the above studies reflect the present state of the art; thus, the penalties shown may be reduced with advancements in aircraft technology. Consequently, directions for R&D efforts which may contribute to smaller performance and weight penalties associated with noise reduction are pointed out.

II. INFLUENCE OF DESIGN PARAMETERS ON ROTOR ACOUSTICS

General Discussion

A major part of the acoustic/performance tradeoff study of tilt-rotor aircraft was devoted to an evaluation of state-of-the-

art regarding minimization of rotor noise. A digest of the findings is presented herein and additional data forming the background are reviewed in Appendix A.

There has been substantial data accrued in the last five years by government and industry to document the effect of various design and operational parameters on the noise of rotors, but not all of this has been applicable to tilt-rotor acoustics.

An area of particular interest was the applicability of current noise prediction methods to the tilt-rotor. The method presented in Ref. 3 has proven to be reliable for low-twist rotors; however, it had never been evaluated or substantiated for highly-twisted tilt-rotors due to a lack of suitable full-scale tests. As of this writing, it appears that a representation of airloading in terms of azimuth position and blade passage harmonics is sufficient to predict rotary-wing noise, whether helicopter or tilt-rotor. Unfortunately, the state-of-the-art for high harmonic airload prediction is not sufficient to define any but the lowest harmonics of noise. However, recent data from a 26-foot diameter rotor (Model 222) in the NASA Ames 40 × 80 facility should substantially aid the advancement of tilt-rotor acoustics.

To optimize the design of a quiet tilt-rotor aircraft, the sensitivity of trades of noise with all the operating and design variables which affect vehicle performance must be known. For

example, tip speed plays an important role in establishing rotor acoustic signature. However, while this aspect for all types of airscrews has been generally well known, precise knowledge of this particular parameter on tilt-rotor acoustic characteristics was lacking. Furthermore, most of the available data had been investigated on an individual basis, but not viewed totally.

In this study, all the meaningful data which could be amassed were evaluated for their influence on tilt-rotor noise characteristics. There are many design and operational parameters which can be applied to the design and operation to influence rotor acoustics. Some of them offer substantial control of the acoustic signature while others have only a second-order effect on the noise. An investigation into the effectiveness of the following major parameters is discussed in this report:

1. Tip Speed
2. Blade Geometry (planform and twist)
3. Airfoil Sections
4. Design Alternatives within Rotor Itself (number of blades, radii of blades, angle between blades, blade area, disc loading, power loading, etc.)
5. Special Devices (such as blade tips, leading edge modifications, boundary layer control devices, tip blowing, etc.).

Some of the information used in the study was assembled from a recent comprehensive search of contemporary literature.

Other inputs were obtained from Boeing-Vertol research as well as many years of continuous review of literature (primarily from the University of Pittsburgh's Knowledge Availability Systems Center, Abstract Search Facility). This, supplemented by personal contact with researchers working on special devices, provided the basis for the material presented in this section.

In describing the acoustic signature of a rotor, it is desirable to define the frequency spectra using a narrow filter in order to investigate harmonic as well as broadband components of noise. In so doing, a detailed definition of all frequencies reveals three spectral regions which display definable characteristics (see Figure 2-1).

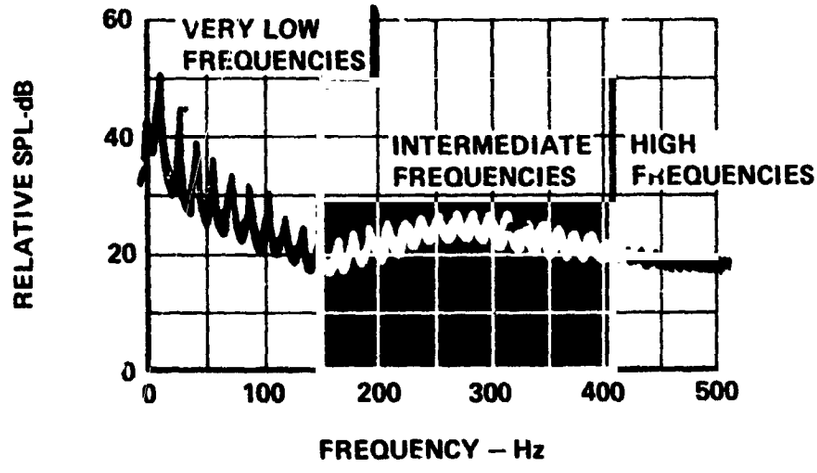

FIGURE 2-1 CHARACTERISTIC FREQUENCY RANGES FOR ROTORS

1. The very low frequency range (harmonic numbers less than 10) where the lowest harmonics may be below the audible frequency threshold. This region of the frequency spectra is characterized by a decrease in harmonic amplitude with increasing harmonic number. In this case, good correlation with theory is typical (5dB).

2. The intermediate frequency range (harmonic numbers above 10) where harmonics of blade passage are definable. Harmonic levels increase in amplitude with increasing frequency, later decreasing and finally blending in with the broadband noise. This characteristic of rotor noise may result from incident and reflected wave phasing.

3. The high frequency range (no harmonics of blade passage present) where the noise is of a broadband characteristic. The broadband noise spectra generally displays an amplitude maximum somewhere in this range.

A discussion of the effectiveness of idealized variations in a large number of design variables on far-field noise is included in Section IV.

While the impact of each of the design variables previously noted will be discussed separately, a combined summary of all the findings is presented in Figure 2-2. A review of this figure shows that for a constant thrust, the controlling parameter is tip speed, and this appears to be the factor which exerts the major

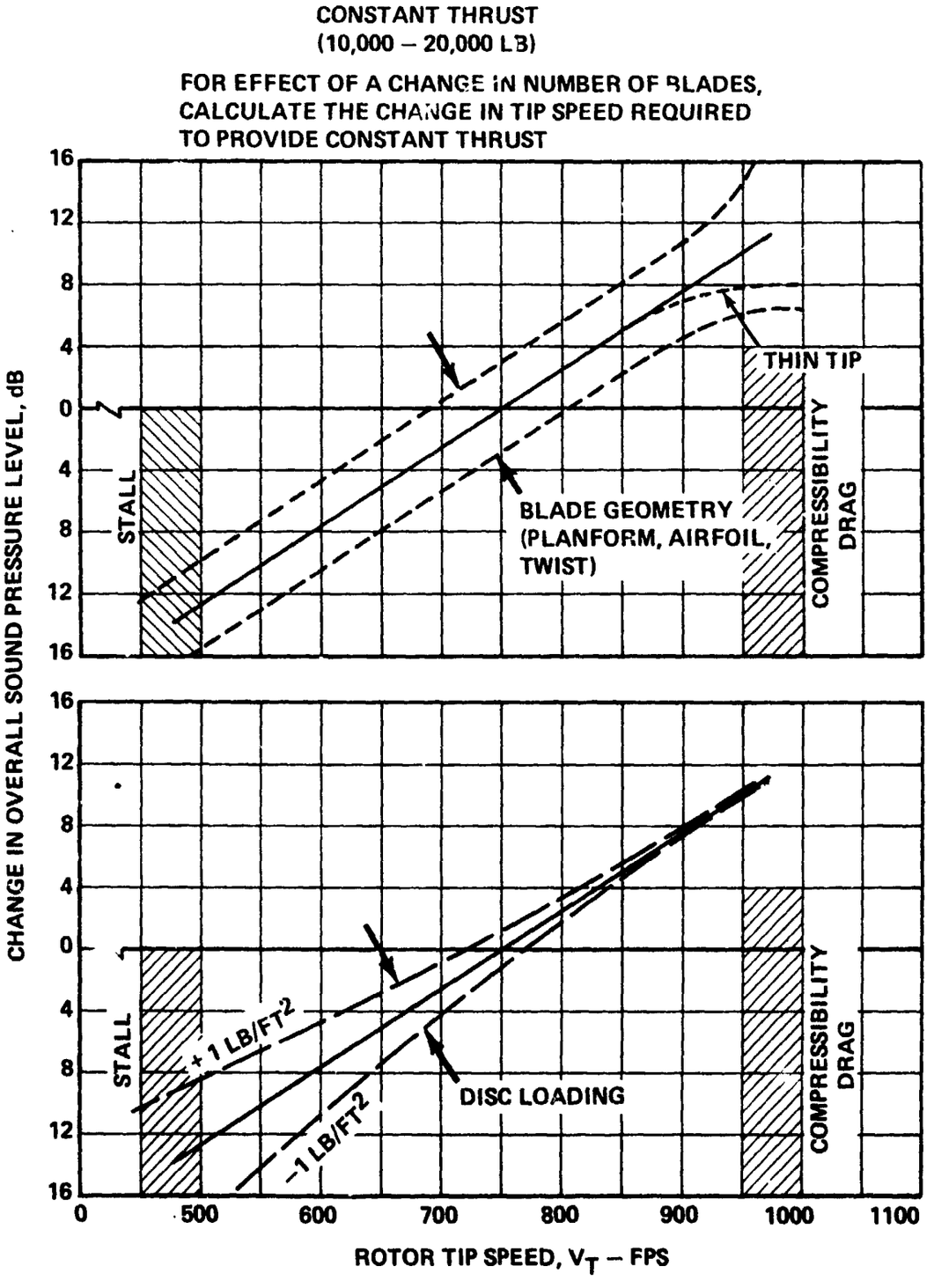

FIGURE 2-2 EFFECT OF ROTOR DESIGN ON NOISE

order of magnitude influence on the generated noise. Variations in number of blades, airfoils, planforms, and twist may combine to provide the illustrated scatter about the tip speed trend line. These tend to be of second-order influence at lower speeds, but become substantial as drag divergence is approached and thin airfoils at the blade tip become important.

In actual design practice where a given payload must be carried a specified distance, the effect of decreasing tip speed will be to increase the gross weight which would have the effect of rotating the Figure 2-2 trend line clockwise about the 750 fps point thus reducing the net acoustic benefit.

The above discussion deals with overall sound pressure level which, for propellers and rotors, is set by the lowest few harmonics. The details of airfoil and blade design, however, affect the higher harmonic noise generation in a manner which appears to defy systematic categorization. Although this has no effect on overall sound pressure level, and a very minor effect on calculated perceived noise level, it has been observed that blades of different designs have noticeably different sounds which influence subjective acceptability.

Unfortunately, the tip speed reduction comes at a performance price as illustrated in Figure 2-3. This figure, from the Ref. 4 paper by Stepniewski and Schmitz, illustrates the adverse weight trend of transmissions, blades, and control systems which accompany

reduced tip speeds. Although this figure was based on helicopter designs, it is indicative of the expected trends.

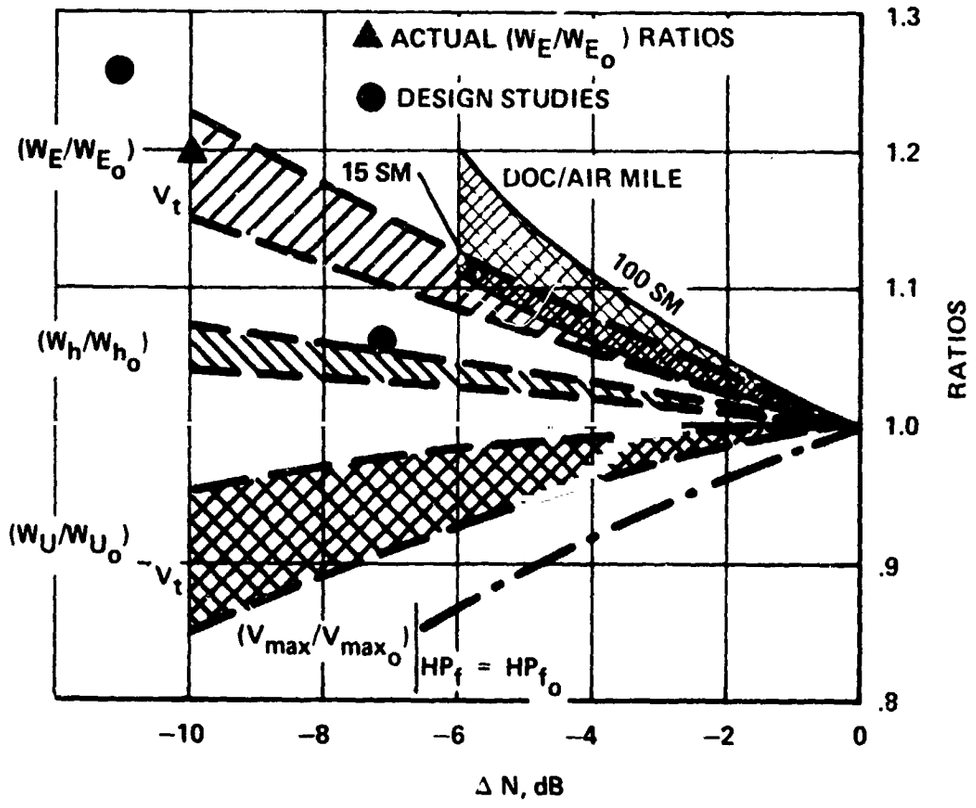

FIGURE 2-3 WEIGHTS, V_{max} AND DOC TRENDS WITH NOISE REDUCTION BY LOWERING V_t

Tip Speeds

Reduction in helicopter rotor noise as obtained by lowering tip speed is generally predictable with good accuracy and has been documented by many investigators. The data reviewed by this study

included the following:

(1) Substantial quantities of noise levels recorded on the Boeing-Vertol experimental whirl tower facility (Figure 2.4) on CH-2., CH-46, and CH-47 rotor blades (Ref. 5). In addition it included two-, three-, and four-bladed rotors with blades which were otherwise identical in design and construction, and numerous wind-tunnel noise surveys, as well as data obtained on a 13-foot diameter propeller with 41° twist.

(2) Full-scale rotor data published by Hubbard and Maglieri (Ref. 6).

(3) Whirl tower data published by Stuckey and Goddard on a Westland rotor (Ref. 7).

The above data has been summarized in the characteristic tip speed trend shown in Figure 2-5. The data shown are for overall, or low harmonics of noise. Trends of specific sets of data display variations of 3-6 dB per 100 ft/sec change in tip speed. Grouped together, the combined data shows a 4.2 dB/100 fps slope. Higher harmonics are not as consistent with variations in tip speed and, in fact, tend to be somewhat erratic. As shown in the Appendix, the higher harmonics display a slope of 3 dB/100 fps, or less.

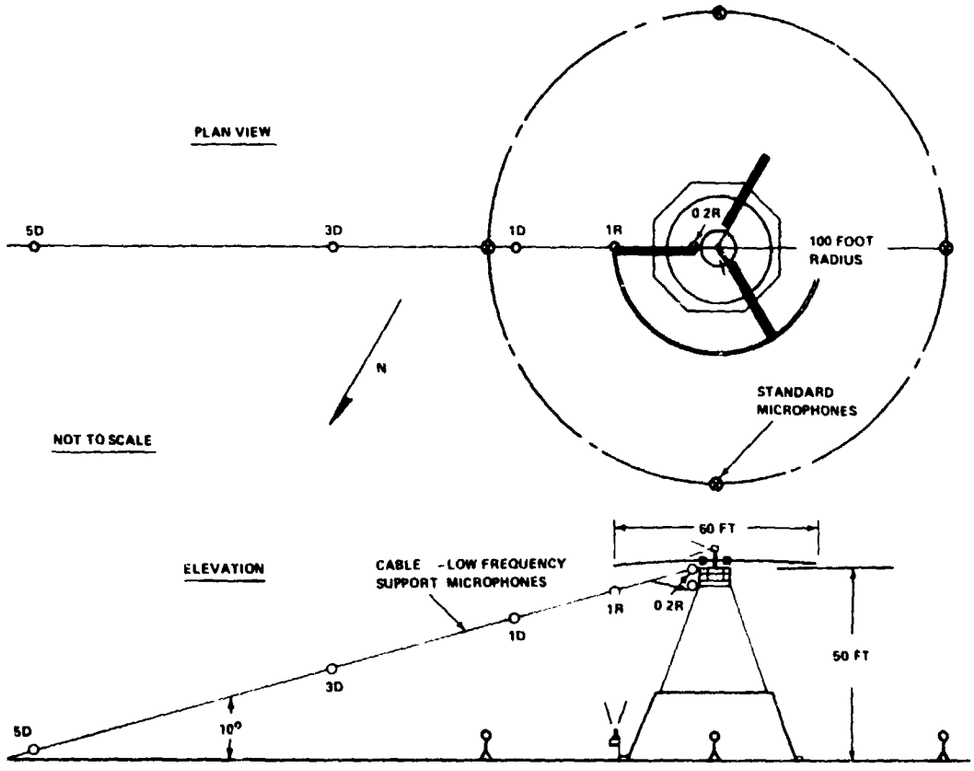

FIGURE 2-4 BOEING VERTOL EXPERIMENTAL WHIRL TOWER AND MICROPHONE ARRAY

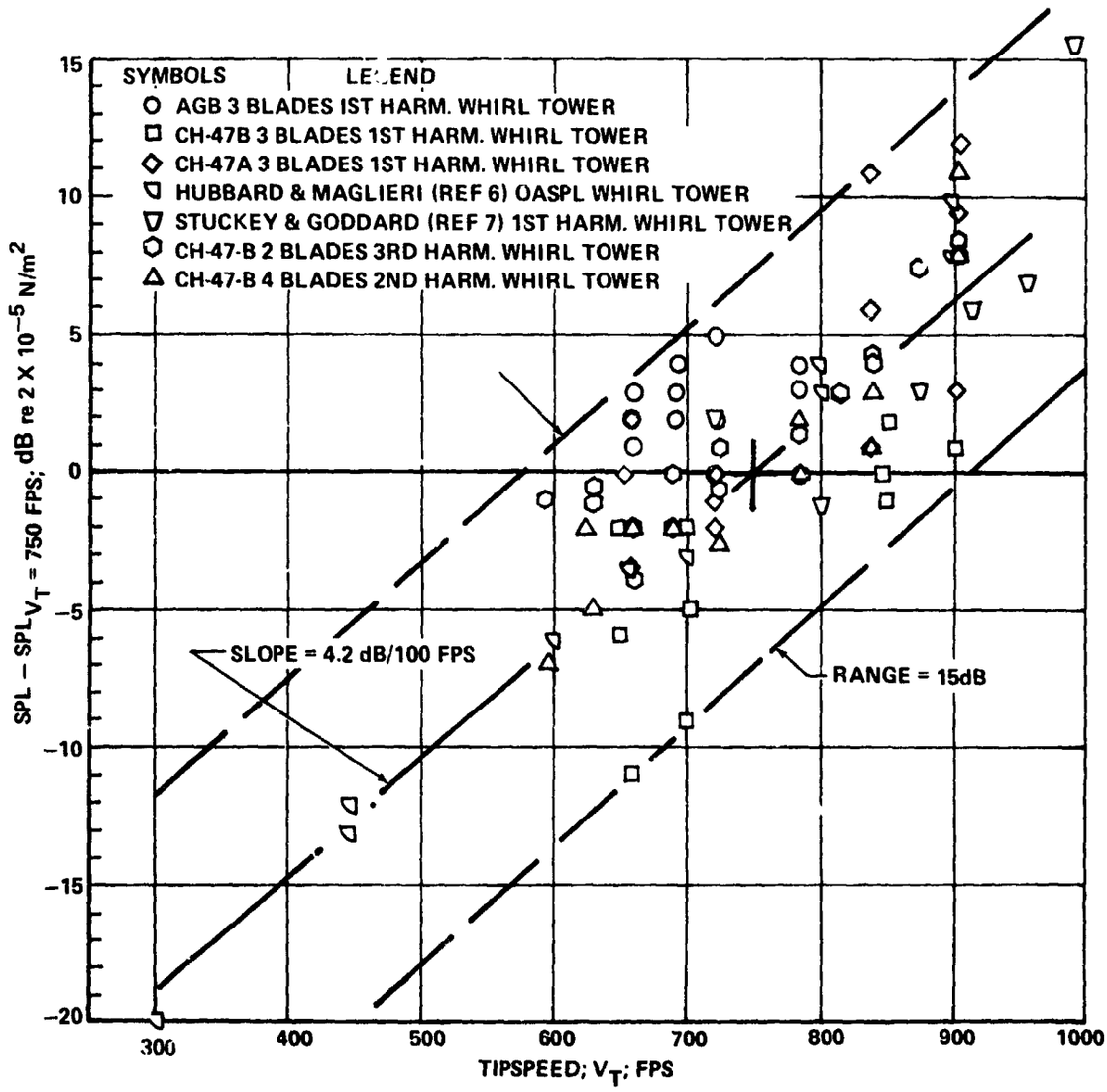

FIGURE 2-5 EFFECT OF TIP SPEED
ON ROTOR NOISE LEVELS

Number of Blades

There are several design variables that lead to noise reduction of a rotor system, but which are not clearly identifiable. This is due to the fact that they are generally incorporated into the rotor, together with changes to other rotor parameters which, in themselves, may also contribute to noise reduction. Number of blades is one of these. For example, there is no available data regarding changes of blade number where the solidity of the rotor remained constant, since all published data had been obtained from programs which added blades of the same geometrical configurations to the rotor, and thus increased rotor solidity. Adding additional blades also creates a change in blade loading. Depending on how the data on blade number is compared, several conclusions may be drawn. First, blade number at constant tip speed will be examined.

Figure 2-6 illustrates the effect of blade number of measured sound levels as a function of thrust as obtained on a whirl tower. When viewed in this manner, adding blades to the rotor clearly improves the acoustic signature.

Leverton (Ref. 8), from research at the Institute of Sound and Vibration Research, Univ. of Southampton, concludes that rotational noise will decrease by 4-5 dB per blade added, while broadband noise should decrease by the factor 10 log (B + blades added)/B).

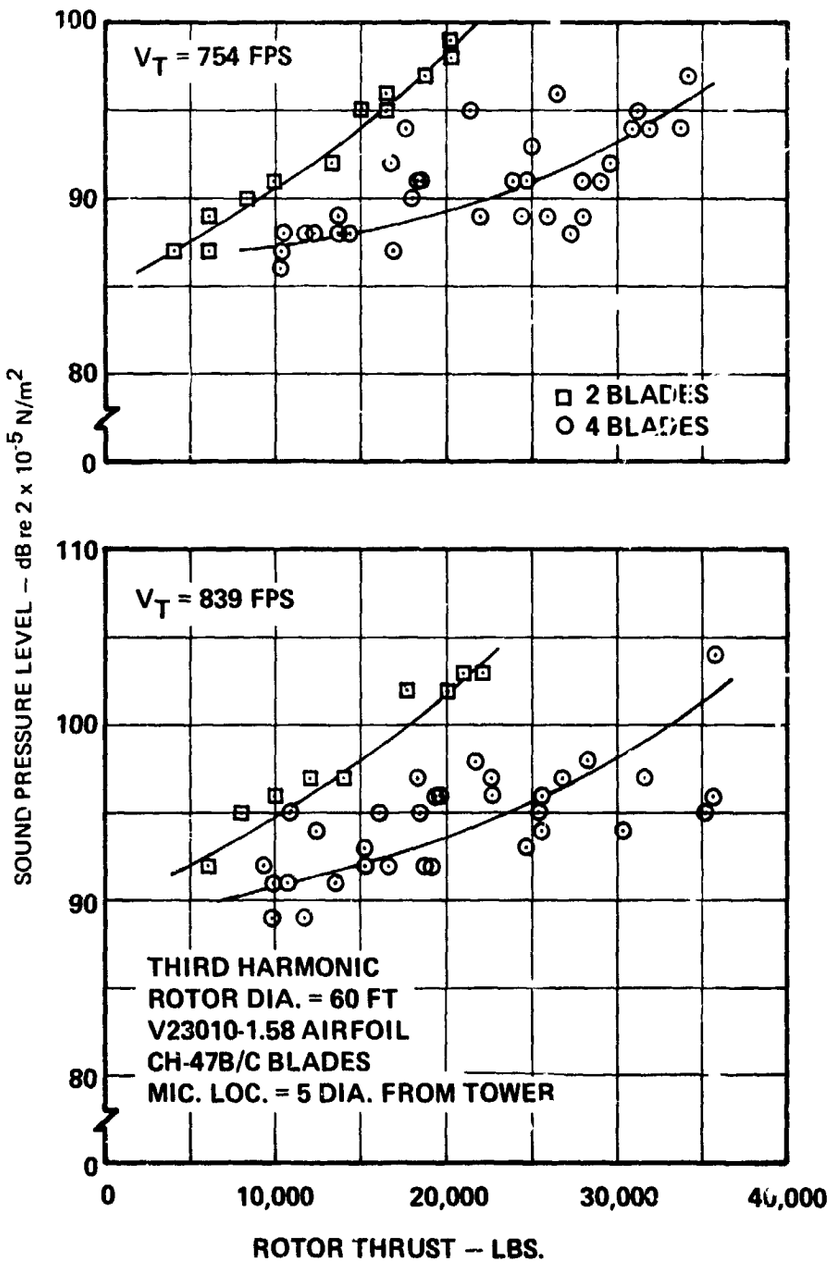

FIGURE 2-6 WHIRL TOWER NOISE OF 2 AND 4-BLADED ROTORS

Figure 2-7 compares noise produced by the 2- and 4-bladed rotors at constant thrust. For this size rotor, the noise increases rapidly with tip speeds above approximately 725 fps. Thus, for minimum noise, the number of blades should be high enough to produce the desired thrust while operating at a tip speed of 725 fps or less.

However, when 2- and 4-bladed data is compared on the basis of C_T/σ, as is typical for performance evaluation, the data collapses to a large scatterband and the value of increasing the number of blades disappears (Figure 2-8). It appears, hence, that the real advantage of adding similar blades of constant area to a rotor results from an ability to reduce tip speed because of the increased lift from the added blade.

Broadband noise produced by the 2- and 4-bladed rotors is compared in Figure 2-9. At the low thrust (9,000 pounds), the 2-bladed rotor is approximately 5 dB less noisy than the 4-bladed one throughout the range of tip speeds tested. At 18,000-pound thrust, the broadband noise again displays a 5 dB difference at V_T = 900 fps. This difference decreases with tip speed, both rotors producing the same noise below 700 fps.

In addition to permitting a reduction in tip speed, an increase in the number of blades will also result in a noise reduction if the rotor rpm and radius are maintained unchanged. The Army-NASA OH-6A Quiet Helicopter (Ref. 9) was modified by increasing the number of main rotor blades from 4 to 5 and the

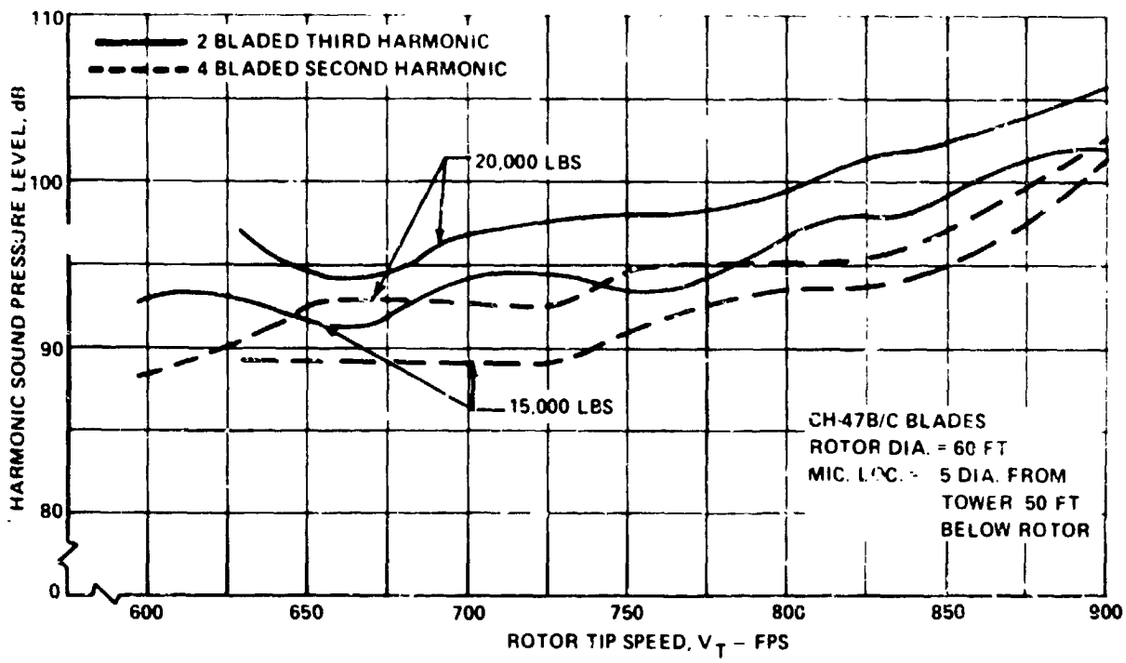

FIGURE 2-7 WHIRL TOWER ROTOR NOISE
COMPARISON OF 2 AND 4-BLADED ROTORS

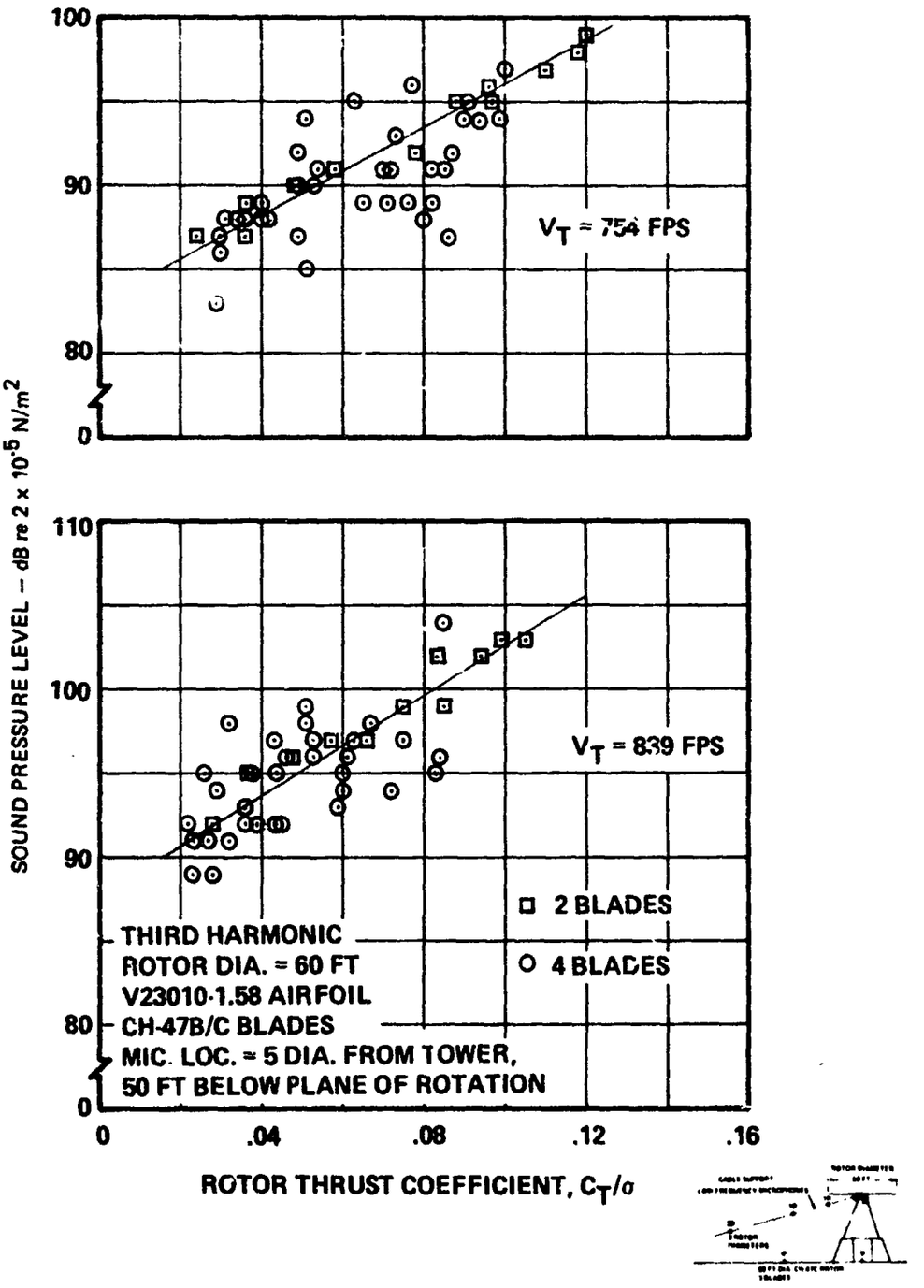

FIGURE 2-8 WHIRL TOWER NOISE OF 2 AND 4-BLADED ROTORS

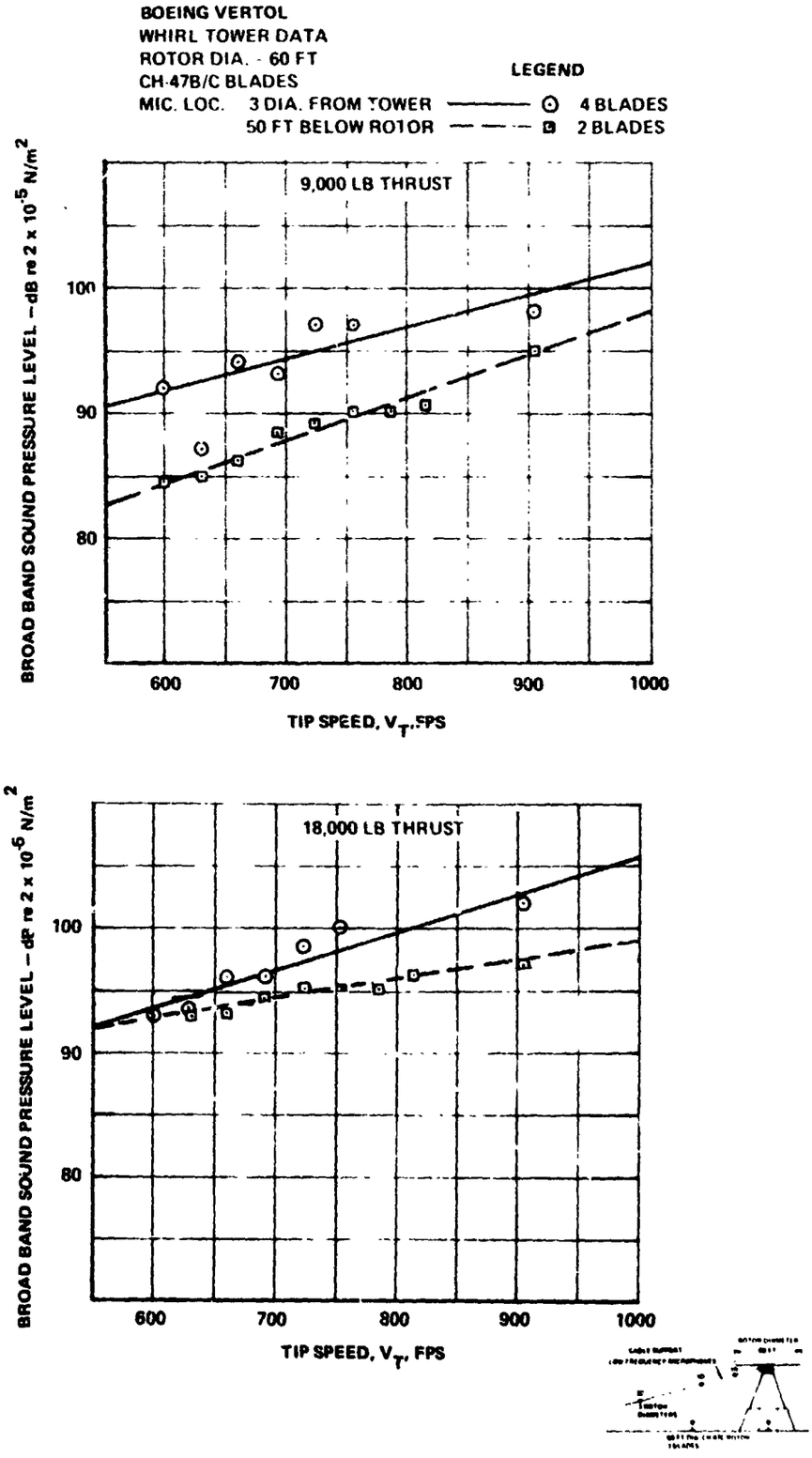

FIGURE 2-9 BROADBAND NOISE COMPARISON OF 2 AND 4-BLADED ROTORS

number of tail rotor blades from 2 to 4 without changing their original dimensions. Other minor modifications were also made, but when both the standard and modified aircraft were operated at the same rpm, the increased number of blades was primarily responsible for an average 9 dB noise reduction measured during a 100-foot altitude fly-by.

Thrust

An increase in rotor thrust results in an increase in noise level of the rotor, but it is both tip-speed and frequency dependent. Figure 2-10 was selected to illustrate the point because the data it represents was recorded on a system which measured all frequencies from 2 Hz to 10,000 Hz with the same frequency response. The increase in noise level with thrust for the 1st harmonic of blade passage frequency increases with very predictable regularity at the rate of 0.85 dB/1000 pounds of thrust at the high tip speeds (650 fps) and drops to 0.3 dB/1000 pounds of thrust at the high tip speeds (900 fps). The higher harmonics display significantly more scatter as well as increase at a lower rate: the slopes at the equivalent tip speeds being 0.5 dB/1000 pounds at V_t = 650, and 0.2 dB/1000 pounds at V_t = 900. The scatter in the higher harmonics appears to be typical of rotor data and apparently, results from the ambient condition effects such as wind gusts which affect the higher harmonic airloading. Additional data on the effect of thrust on noise may be found in the Appendix.

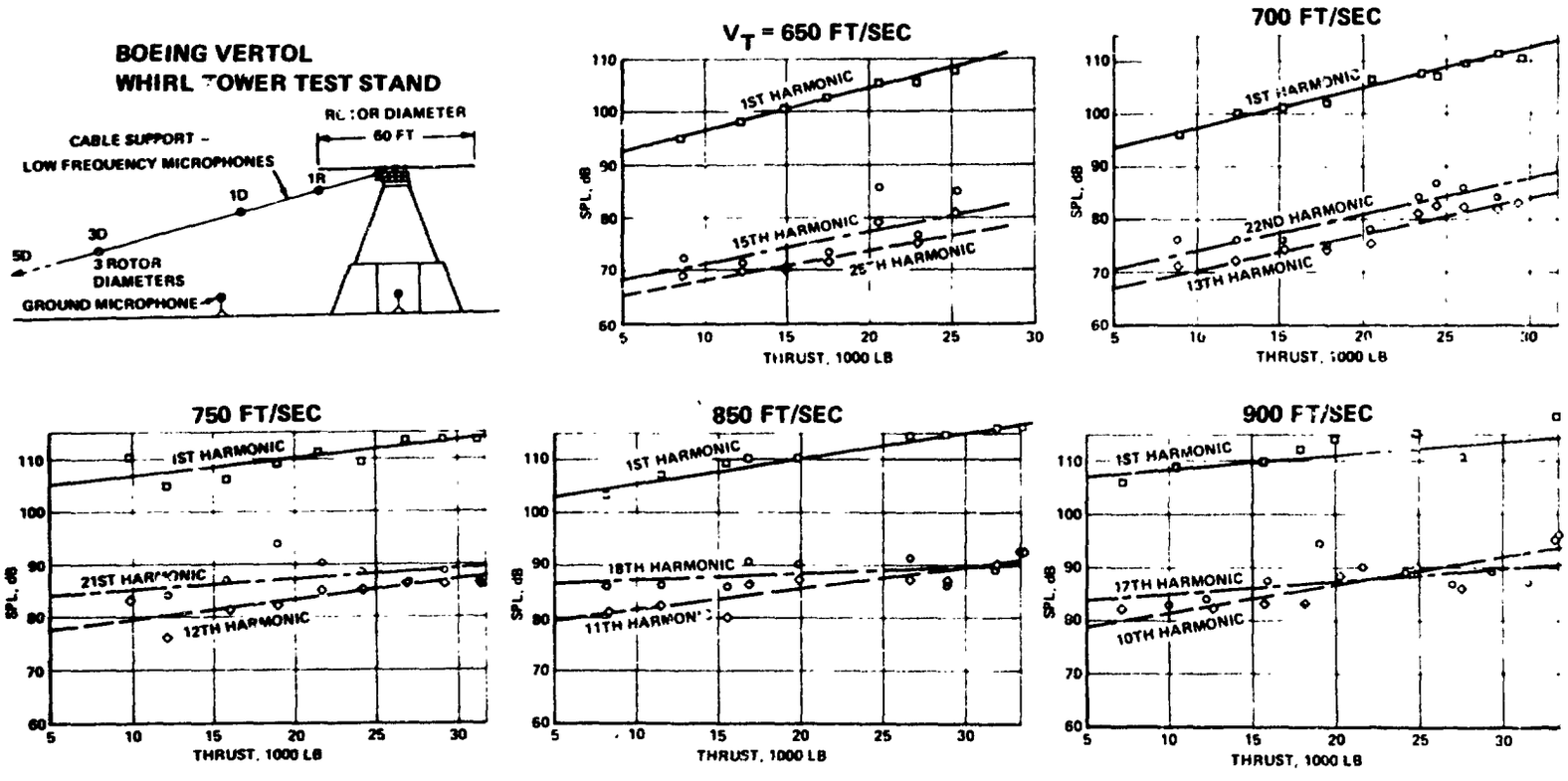

FIGURE 2-10 EFFECT OF THRUST ON ROTATIONAL NOISE HARMONICS

Blade Tip Shape

A wide variety of tip shapes have been applied to rotor blades to reduce noise. However, these attempts have met with minimal success in reducing noise below that produced by a standard square tip. Trapezoidal and square tips appear to be the two most common nonstandard shapes. A test of full-scale trapezoidal tips (Ref. 10) resulted in a reduction of broadband or 'vortex' noise by approximately 7 dB compared with a square tip at low thrust levels, but at normal thrusts, the improvement was less impressive.

Other investigations have shown the square tip to exhibit a small advantage over the trapezoidal one (see Pollard and Leverton, Ref. 11), but either of these tips appears to generate lower broadband noise than almost any other configuration evaluated. However, the latter test was conducted on a 10-foot diameter rotor at 8° collective pitch and for a V_t no greater than 367 fps. It appears, hence, that tip shape does exhibit some control over broadband noise, but has little influence on the rotational noise established by the basic airloading on the blade.

Blade Planform

With the exception of tip speed, number of blades and thrust level, all other noise control techniques which can be incorporated in the rotor system appear to have only secondary effects on rotational noise. The influence of blade planform on rotor noise for

example, was investigated by Boeing-Vertol on a whirl tower during two test programs. For one program, a set of blades was constructed with constant chord from the cutout to the 59 percent radius, and a 3:1 linear taper from 59 percent radius to the tip was incorporated. A NACA 0012 airfoil was maintained for the entire blade. The noise produced by these blades was compared to standard 0012 CH-47A blades. Plan views of these blades are shown in Figure 2-11.

Noise spectra from this test are illustrated in Figures 2-12 and 2-13. From these figures, it can be seen that little or no change in amplitude in the very low harmonics results from blade planform and corresponding solidity modifications. On the other hand, at 722 fps, the broadband noise of the tapered blade was constantly higher than for the reference blade and this probably resulted from the higher collectives required to achieve the same thrust.

In a second program, another experimental blade (designated the Advanced Geometry Blade (AGB)) was designed to demonstrate the practicality of advanced composite materials. It included both spanwise airfoil variation as well as planform taper. The airfoil section varied linearly from a V23012 at the cutout to a V23010 at the 70 percent radius, and then to a 13006 at the tip. The planform geometry also is illustrated in Figure 2-11. Although the effects of variation of airfoil sections and planform geometry cannot be separated, a noise comparison of this blade with the CH-47B blade is nevertheless interesting. The AGB spectra are compared to those

	CH-47A	CH-47C	AGB	TAPERED
AIRFOIL	0012	23010–1.58	VARIES (SEE SKETCH)	0012
RADIUS	29.5 FT	30 FT	31 FT	30 FT
CHORD,	23"	25.25"	VARIES	VARIES
TWIST	–9.0°	–9.147°	–6°	–9.0°
CUTOUT	5.7 FT	5.8 FT		5.7 FT
SOLIDITY	.062	.067	.069	.0427

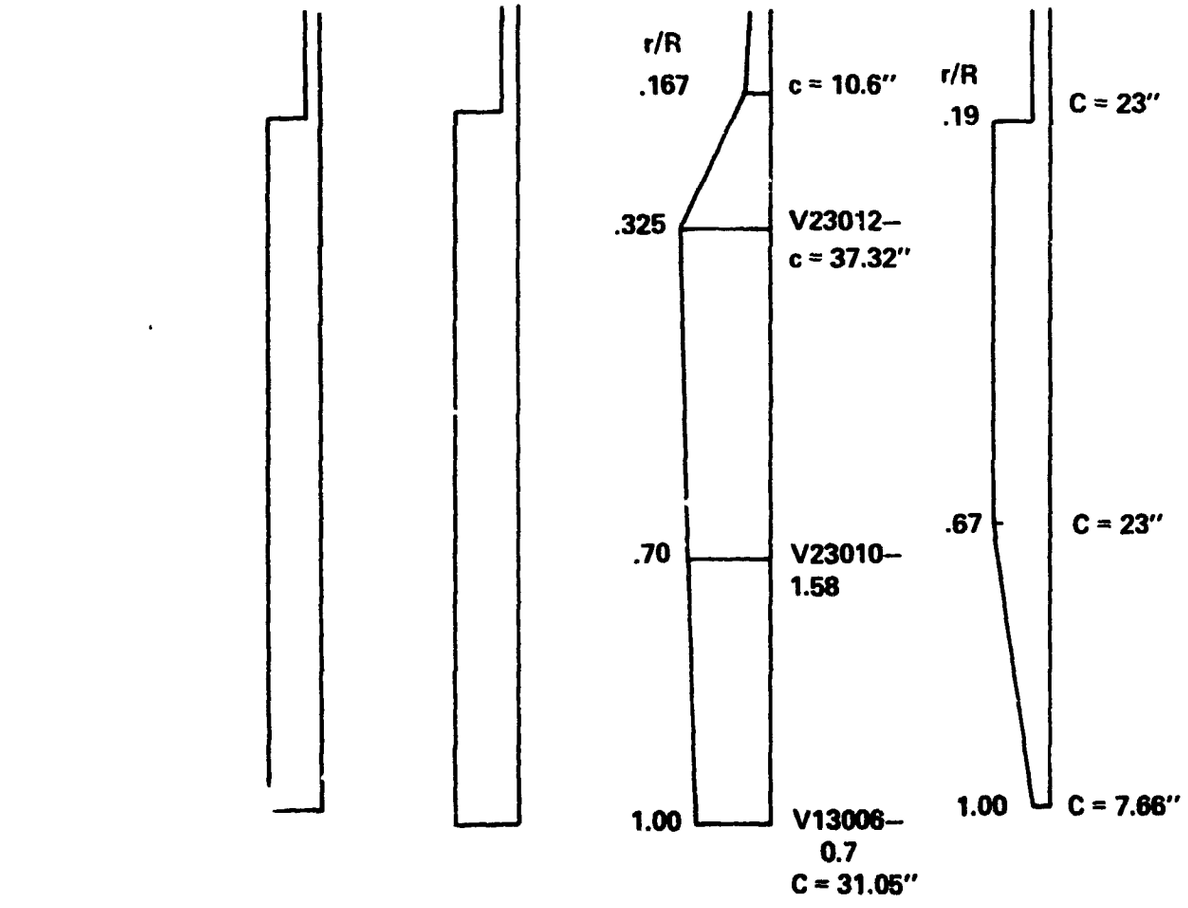

FIGURE 2-11 BLADE DESIGNS

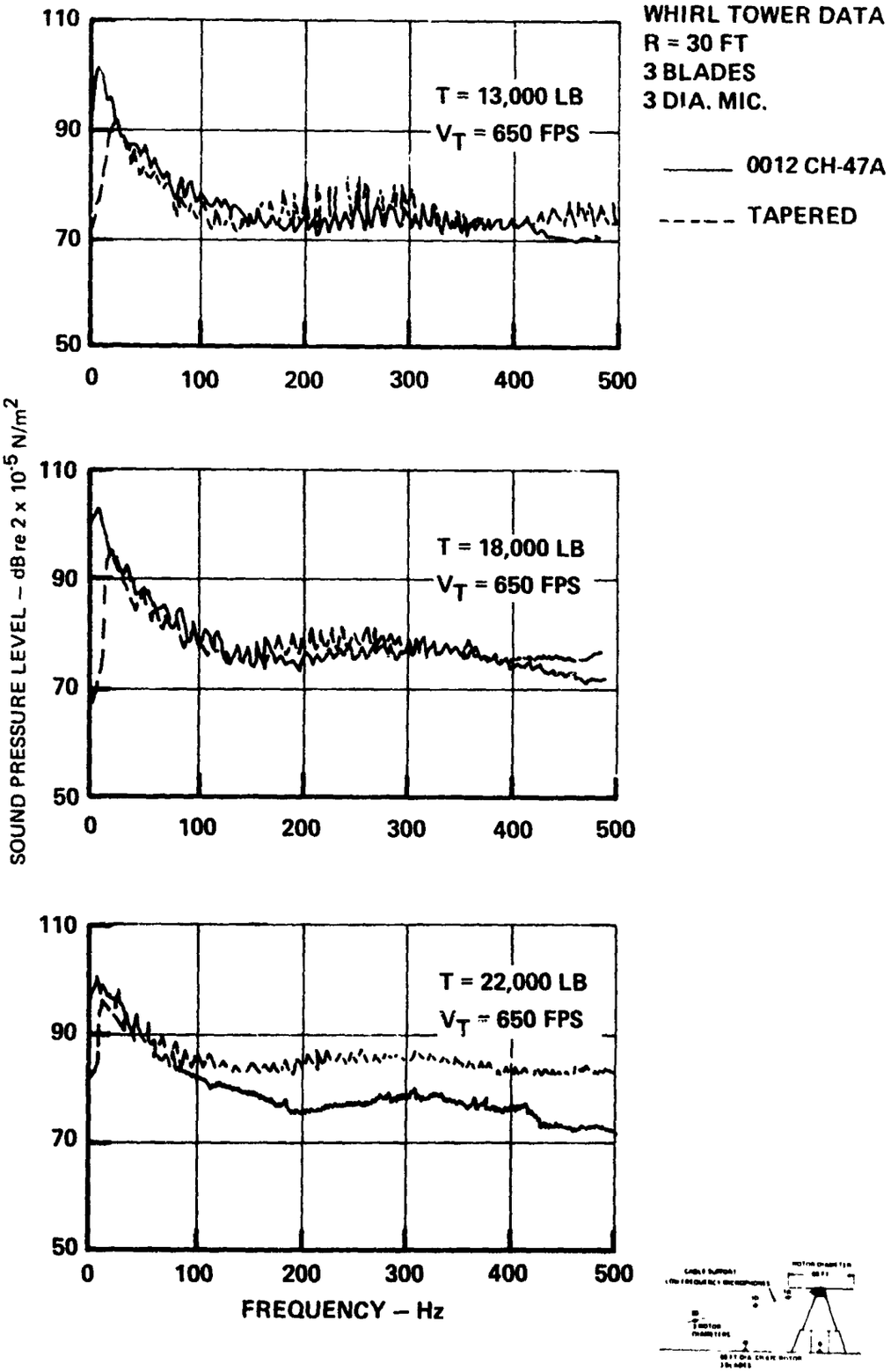

FIGURE 2-12 EFFECT OF PLANFORM

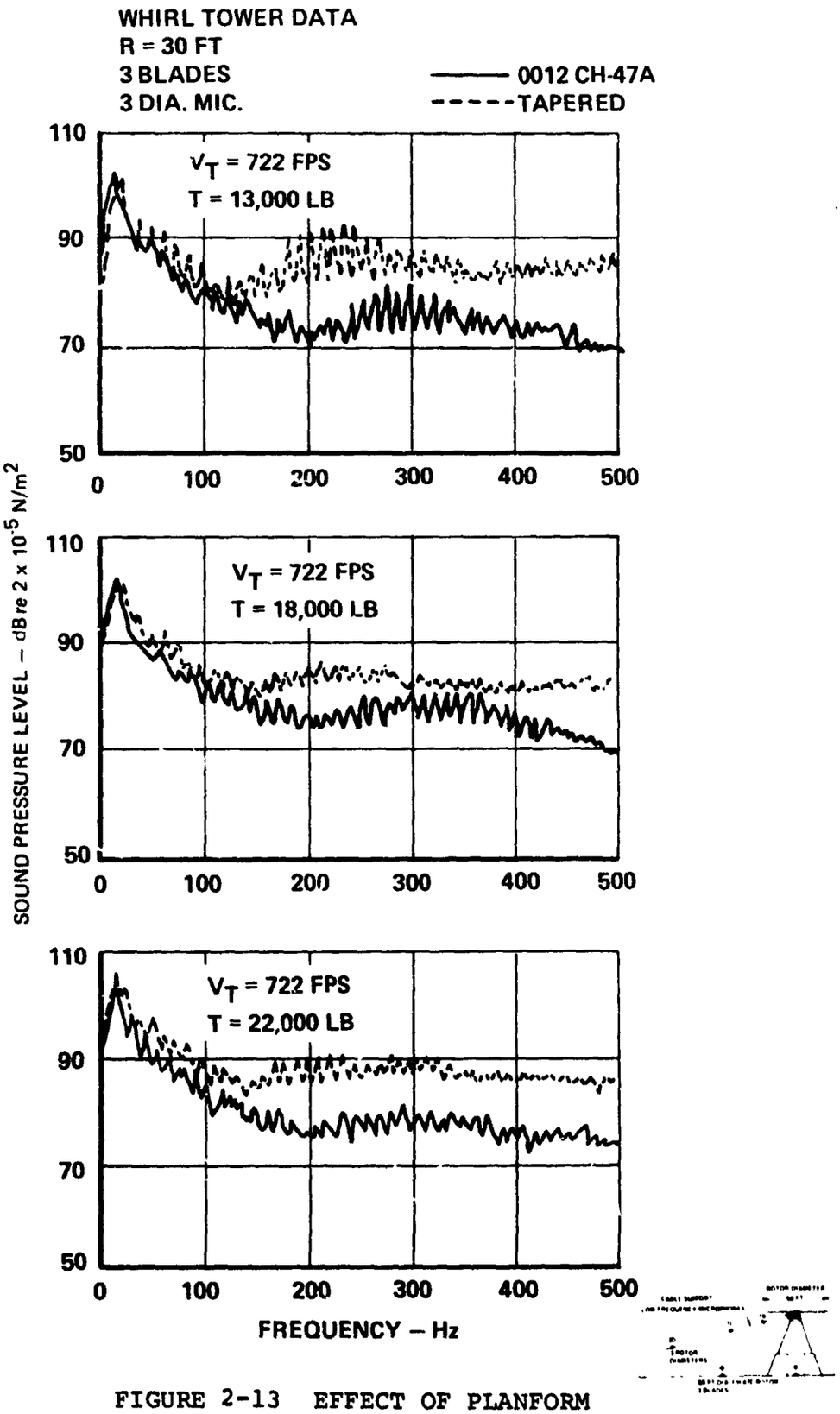

FIGURE 2-13 EFFECT OF PLANFORM

of the standard 23010 CH-47B rotor in Figures 2-14 through 2-16. There is no conclusive advantage for either blade. At a thrust of 9000 pounds and tip speed of 750 fps, the standard blade spectrum is approximately 10 dB higher at frequencies of about 30 cps. However, the standard blade has a lower spectrum than the AGB at a tip speed of 650 fps, and shows little difference at higher thrusts at 750 fps.

Note again that blade comparisons at the same tip speed and thrust show very similar sound pressure levels for the low harmonics. Differences in the spectra appear only in the high harmonics and in broadband noise. For the AGB/CH-47B rotor comparison, the change in higher harmonics which results from the blade variations is probably less significant than that due to changing ambient conditions between test runs.

Ambient wind has a substantial effect on the noise produced by a rotor (Ref. 12) and this is one reason why whirl tower measurements frequently result in data scatter of as much as 6 dB for repeated points. Consequently, the effects of such blade design parameters as planform and airfoil section (which represent second-order influences) are frequently within the scatter of repeated test points and thus, are difficult to accurately measure.

With the limited amount of data available on the noise of rotors with various planform, radii or airfoil sections, there is no strong evidence to recommend one configuration over another. Furthermore, it is also clear that a particular blade is not

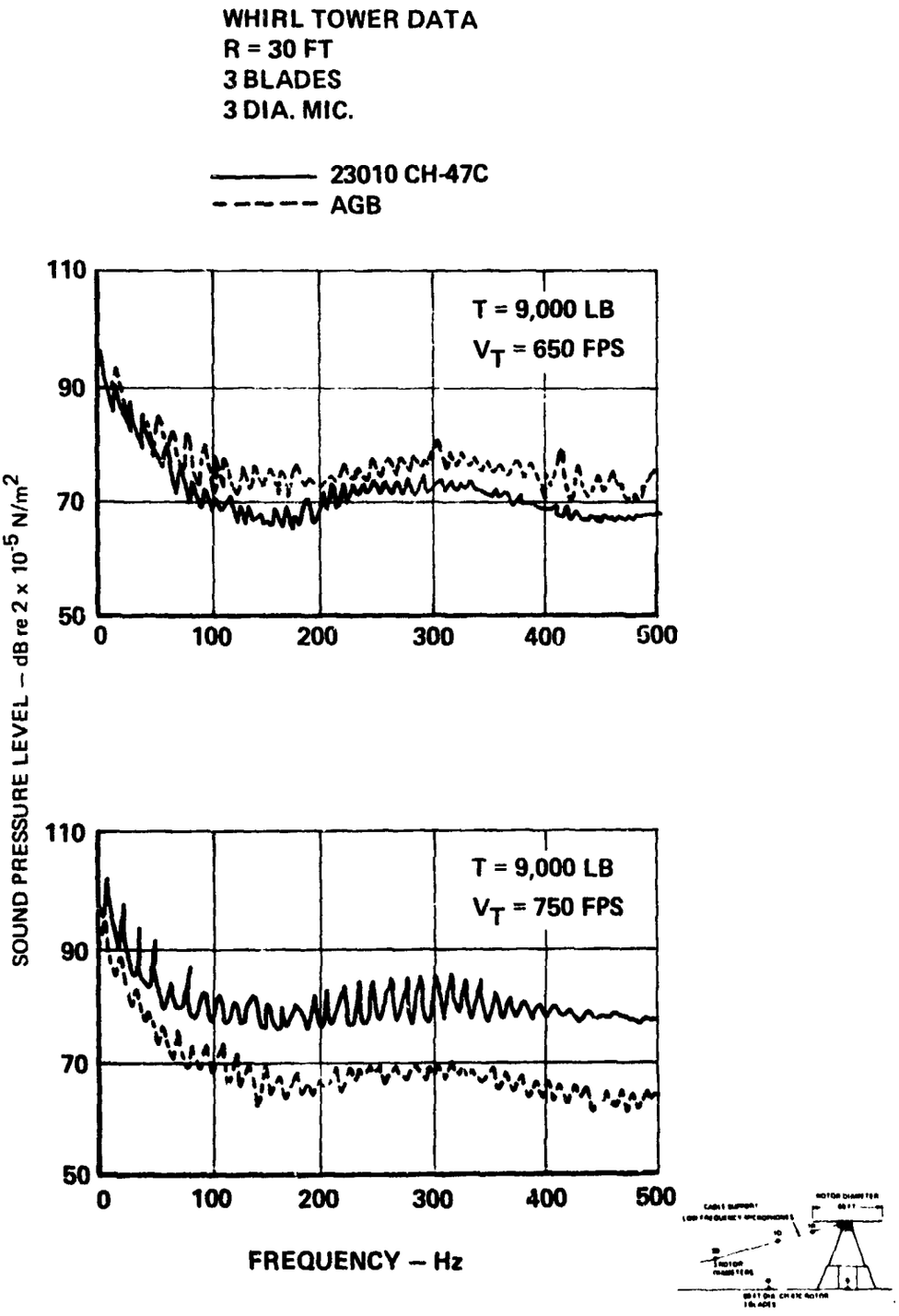

FIGURE 2-14 EFFECT OF COMBINED PLANFORM AND AIRFOIL

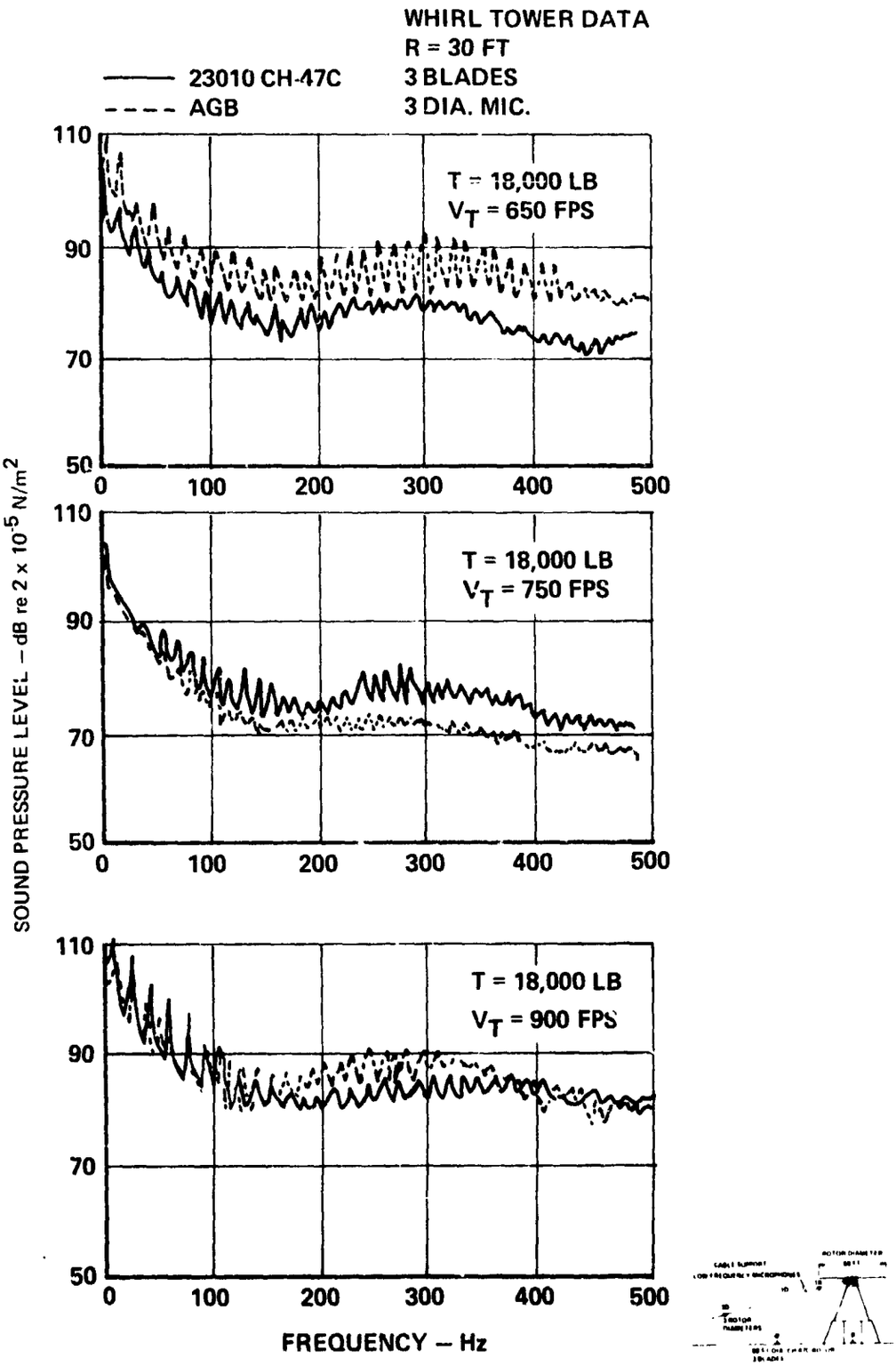

FIGURE 2-15 EFFECT OF COMBINED PLANFORM AND AIRFOIL

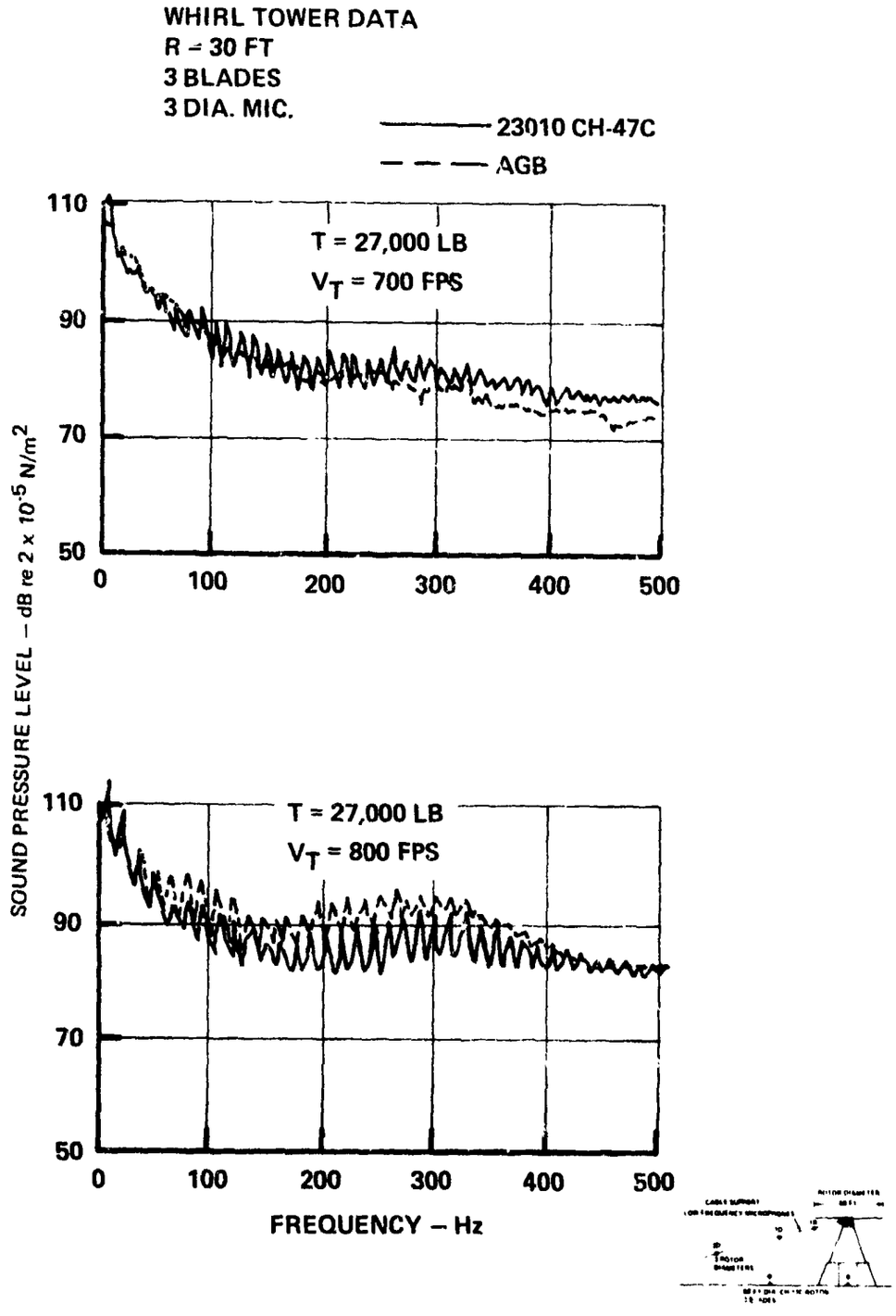

FIGURE 2-16 EFFECT OF COMBINED PLANFORM AND AIRFOIL

consistently better or worse than any other in terms of its acoustic spectrum. Based on this evidence, it appears that a rotor should be designed for its optimum performance at the lowest possible tip speed.

Airfoil Section

The airfoil sections typically used for rotor blades have little effect on the noise generated by the blades at local Mach numbers below 0.85. Above this, airfoil thickness becomes important and the inception of compressibility effects produce an undesirable impulsive noise. Below M = 0.[illegible], spanwise airloading determines the pressure amplitude fluctuation of a passing blade. Waveforms of different airfoils sometimes display different time-history characteristics, but there is little or no change in the audible characteristic.

Figure 2-17 compares the spectrum of a model with V23010-1.58 airfoil sections with another made up of VR-7 sections inboard and VR-8 sections outboard of 85 percent R. (The VR-7 and VR-8 are "high-lift" airfoils developed at Vertol for application to the HLH-ATC rotor). There is no significant difference over the entire frequency range at the thrust levels tested, which are all below stall.

Figures 2-18 through 2-20 provide a comparison between the symmetrical 0012 airfoil incorporated in CH-47A rotors and the cambered V23010-1.58 used in the CH-47B and C. These data were

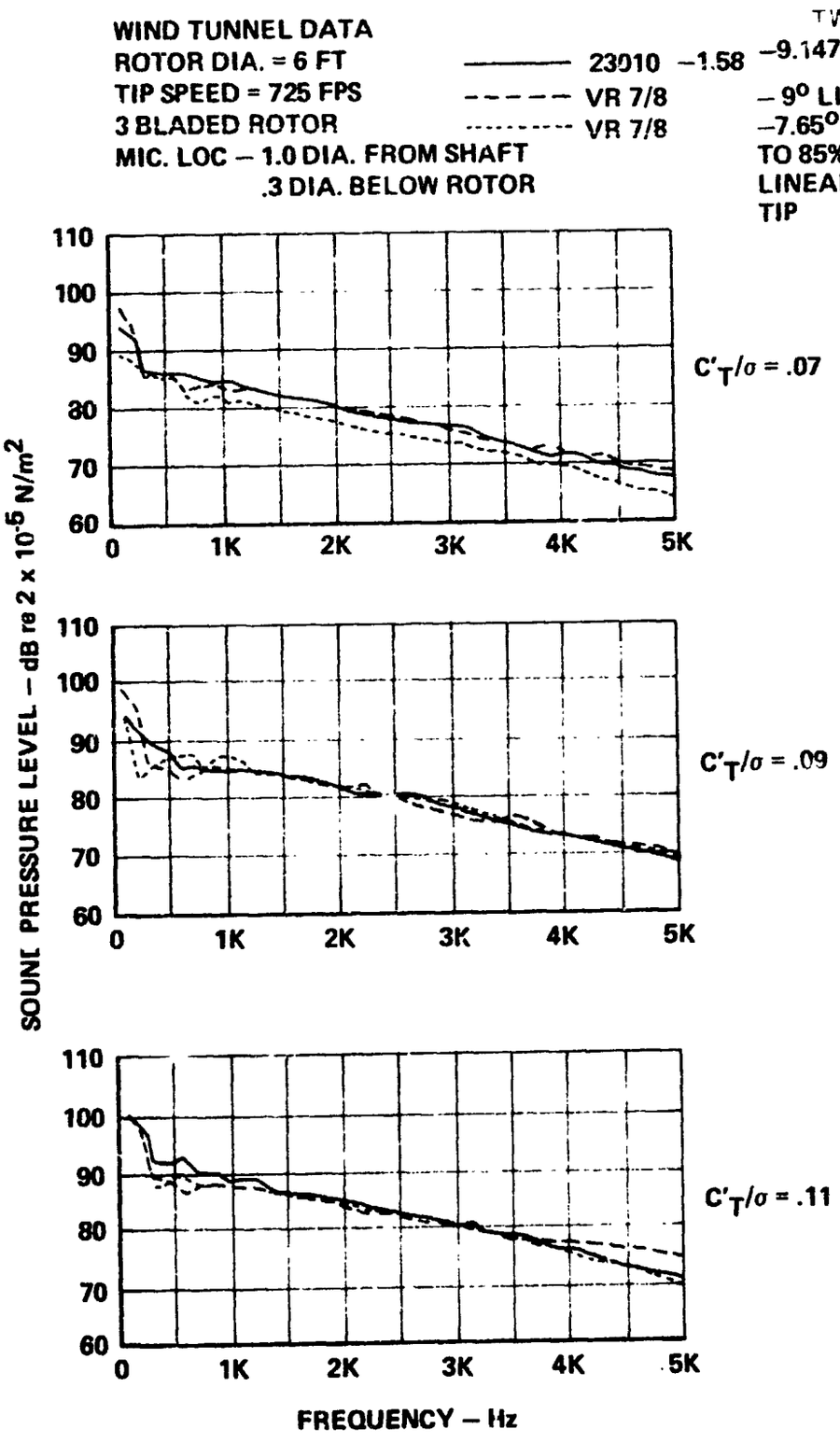

FIGURE 2-17 AIRFOIL SPECTRA IN HOVER

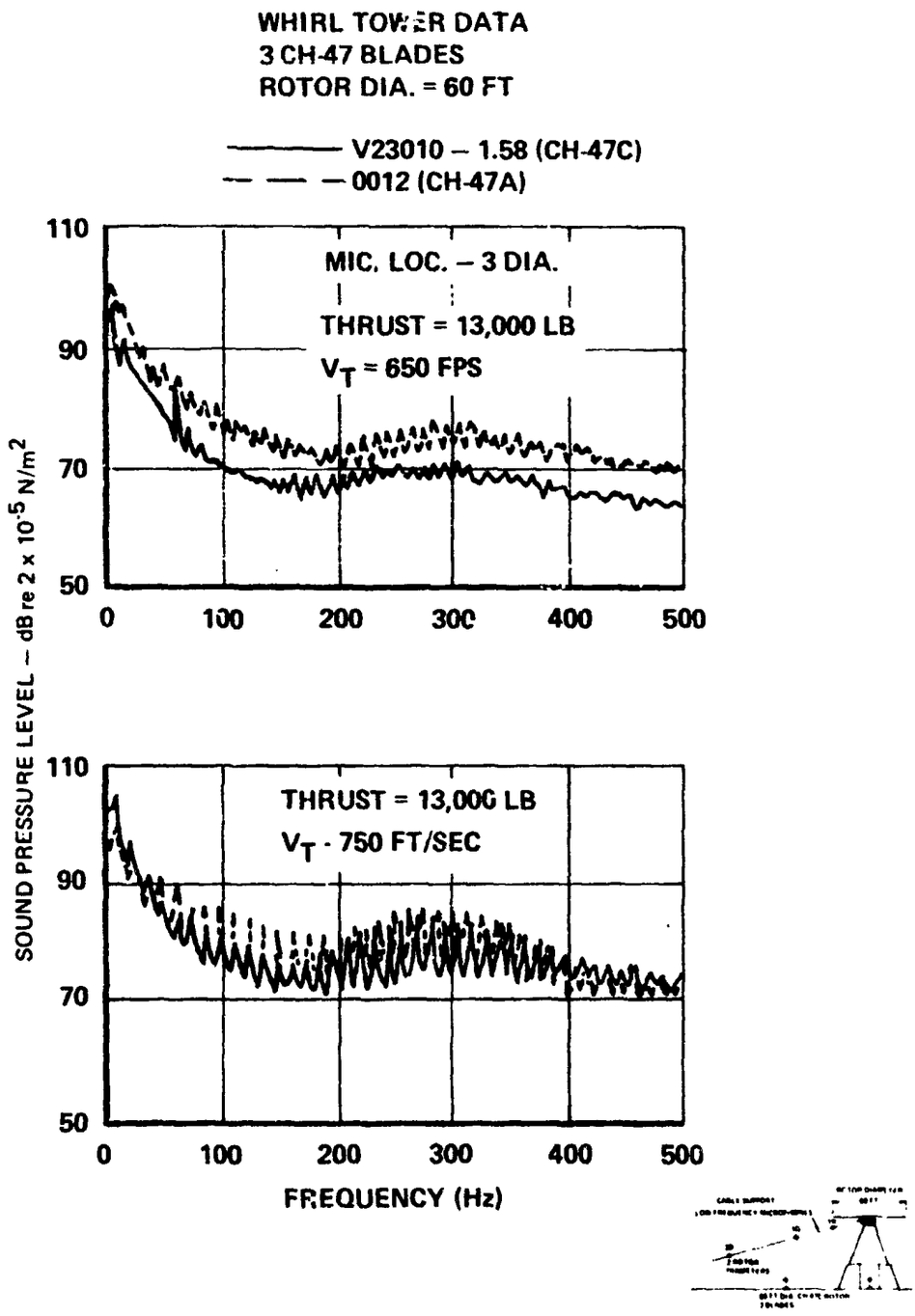

FIGURE 2-18 EFFECT OF AIRFOIL SECTION

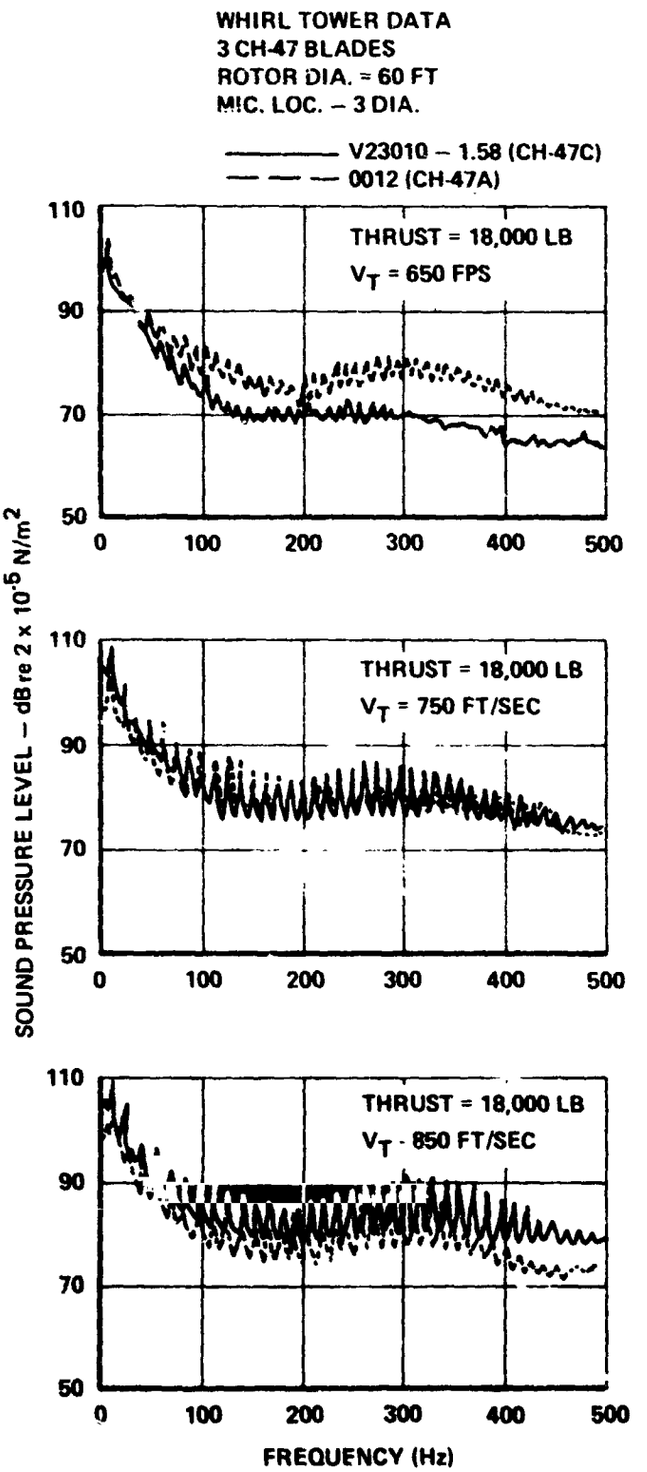

FIGURE 2-19 EFFECT OF AIRFOIL SECTION

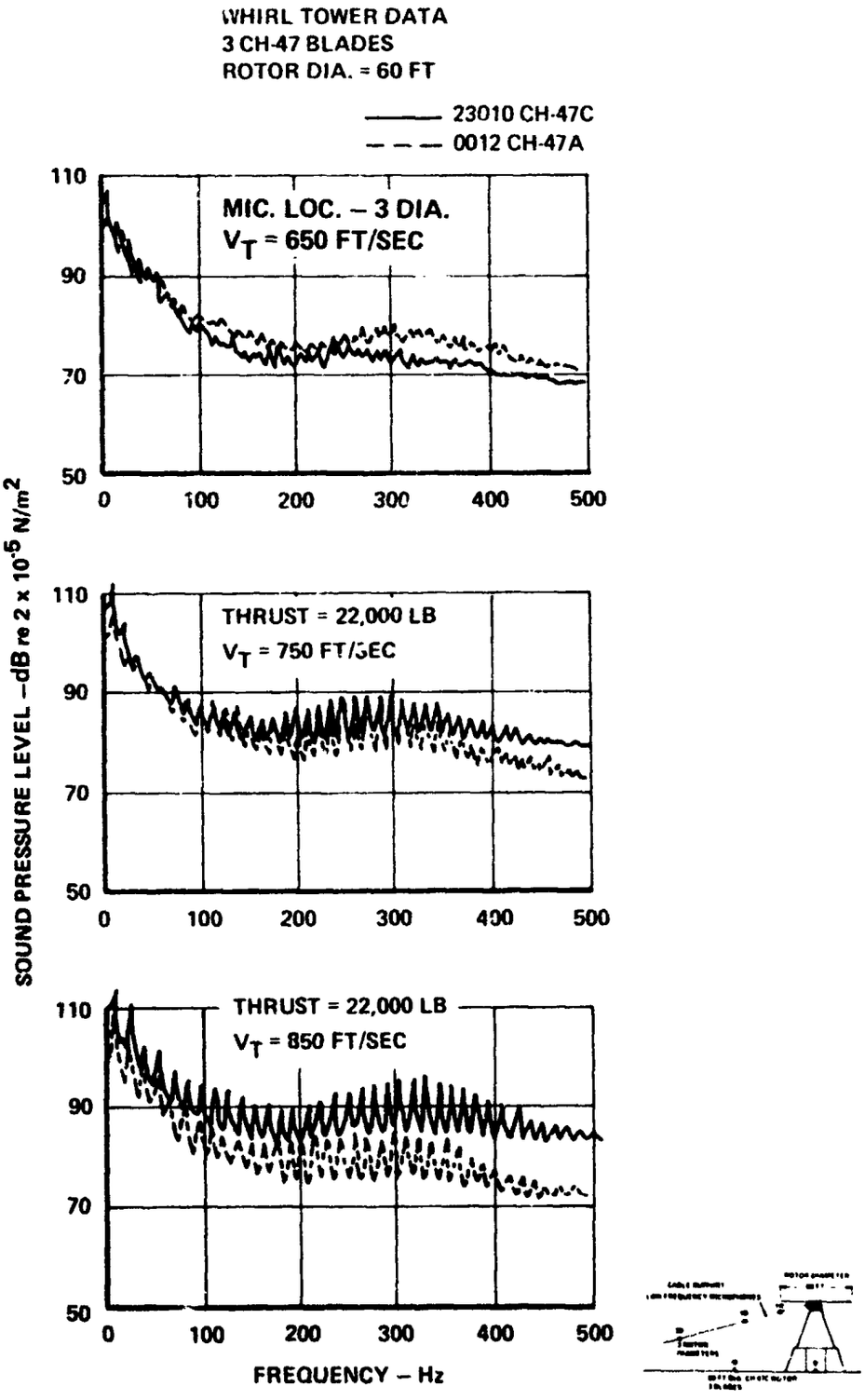

FIGURE 2-20 EFFECT OF AIRFOIL SECTION

obtained from whirl tower tests under the same conditions for each set of blades. At the lower tip speed tested (650 fps), the V23010 tends to have a lower SPL, but the reverse is true at 850 fps.

At higher thrusts and/or blade tip speeds, the airfoil section has two significant effects not apparent in the test data described above. One is related to the airfoil stall inception point. A section with the greater stall inception angle would delay the noise increase which accompanies blade stall. The importance of this can be seen from Figure 2-21, taken from Ref. 13, which compares a stalled with an unstalled propeller. The stalled propeller spectrum is approximately 5 dB greater at the mid and high frequencies, although V_t of the stalled propeller is lower.

Another effect is the reduction of "Mach bang" in the transitional Mach number range by the use of thin airfoils. Figure 2-22, from Ref. 4 depicts the advantage of the 8-percent thick VR-7 airfoil over the V23010 at high Mach numbers. At M = .92, the difference is 3 dB.

It may be concluded, hence, that very limited control over noise may be exercised by airfoils below the transonic and stall regions since, in those regimes, the effect which the airfoil may produce is not readily discernible to the listener. It is only when the local velocity is greater than M = 0.85 or when blade stall is approached, that airfoil characteristics become effective in noise control.

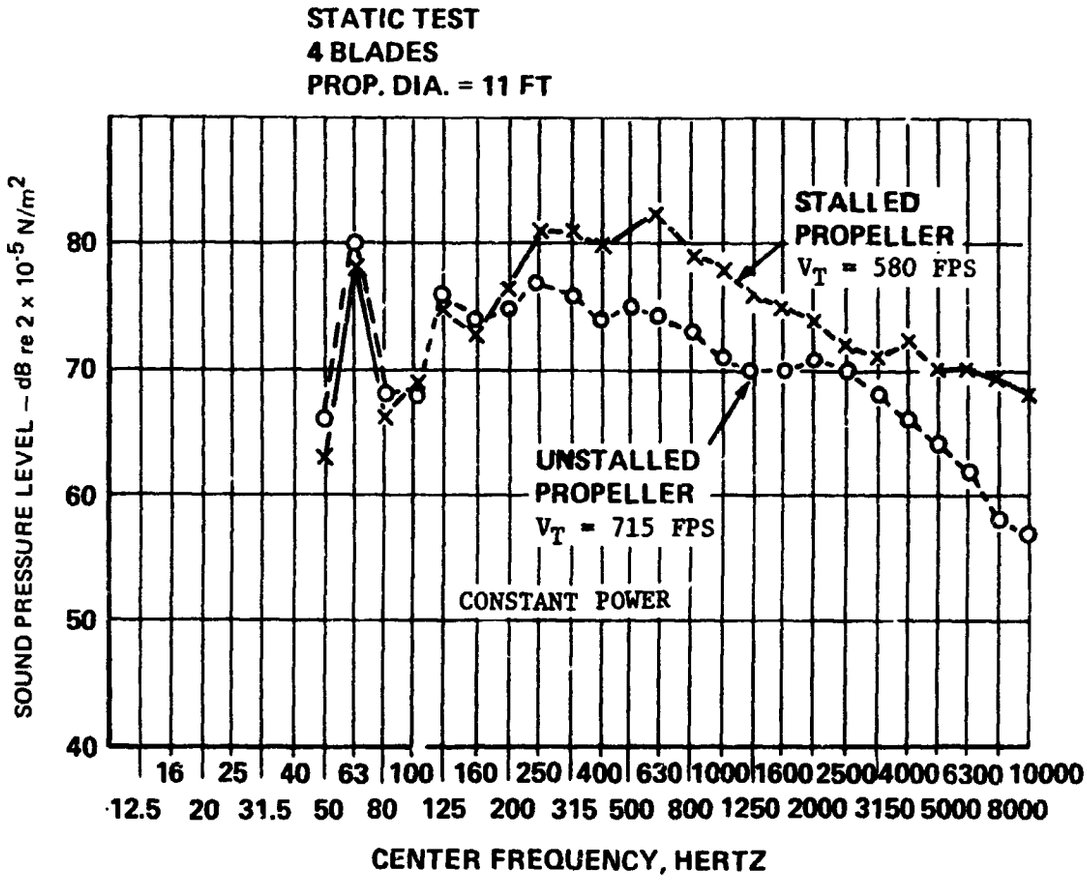

FIGURE 2-21 COMPARISON OF 1/3 OCTAVE BAND SPECTRA FROM STALLED AND UNSTALLED PROPELLERS FROM REFERENCE 13

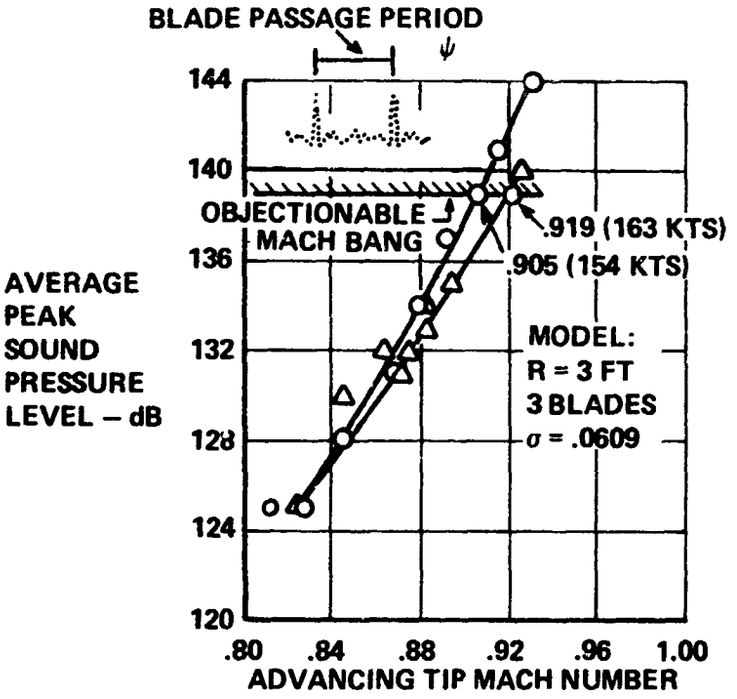

SYMBOL	ROTOR	TWIST	TRAILING EDGE DEFLECTION
○	23010 – MODIFIED	–7°	0°
△	ADVANCED AIRFOIL t/c = .08 AT THE TIP	–9°	–6°

FIGURE 2-22 EXAMPLE OF THE INFLUENCE OF AIRFOIL SECTION ON HIGH-SPEED BAND FROM REFERENCE 4

Blade Twist

Blades with large spanwise twists such as those of tilting rotors and propellers have lower spanwise blade loadings near the tip than flat blades and display, for the same thrust and tip speed, reduced noise levels when compared to helicopter rotors.

Results of a 6-foot diameter model rotor test of two helicopter rotors with different twist are depicted in Figure 2-23. The Option I rotor incorporated a -9° linear aerodynamic twist; the Option II had a -7.65° linear twist from the root cutout to the 85 percent radius station which increased linearly to -13° at the tip. The Option II configuration is approximately 2 dB quieter at the lower thrust level (C_T/σ = .07), but at higher thrusts, there is no measurable difference.

The effect of twist on near-field noise of the Boeing-Vertol 160 tilt-rotor is illustrated in Figure 2-24. (This data was measured on the ASD indoor propeller whirl rig; no free-field correction is available). An increase of twist resulted in a decrease in noise at tip speeds of 550 and 750 fps, the decrease being more apparent at the lower collective pitch values. At 900 fps, the 41° twist maintains a significant advantage at the lower collective pitch only.

Although the blade twists of Figure 2-24 are too great for helicopter rotors, they are of the magnitude being considered for tilt-rotor aircraft. Examining the plot of 10° collective

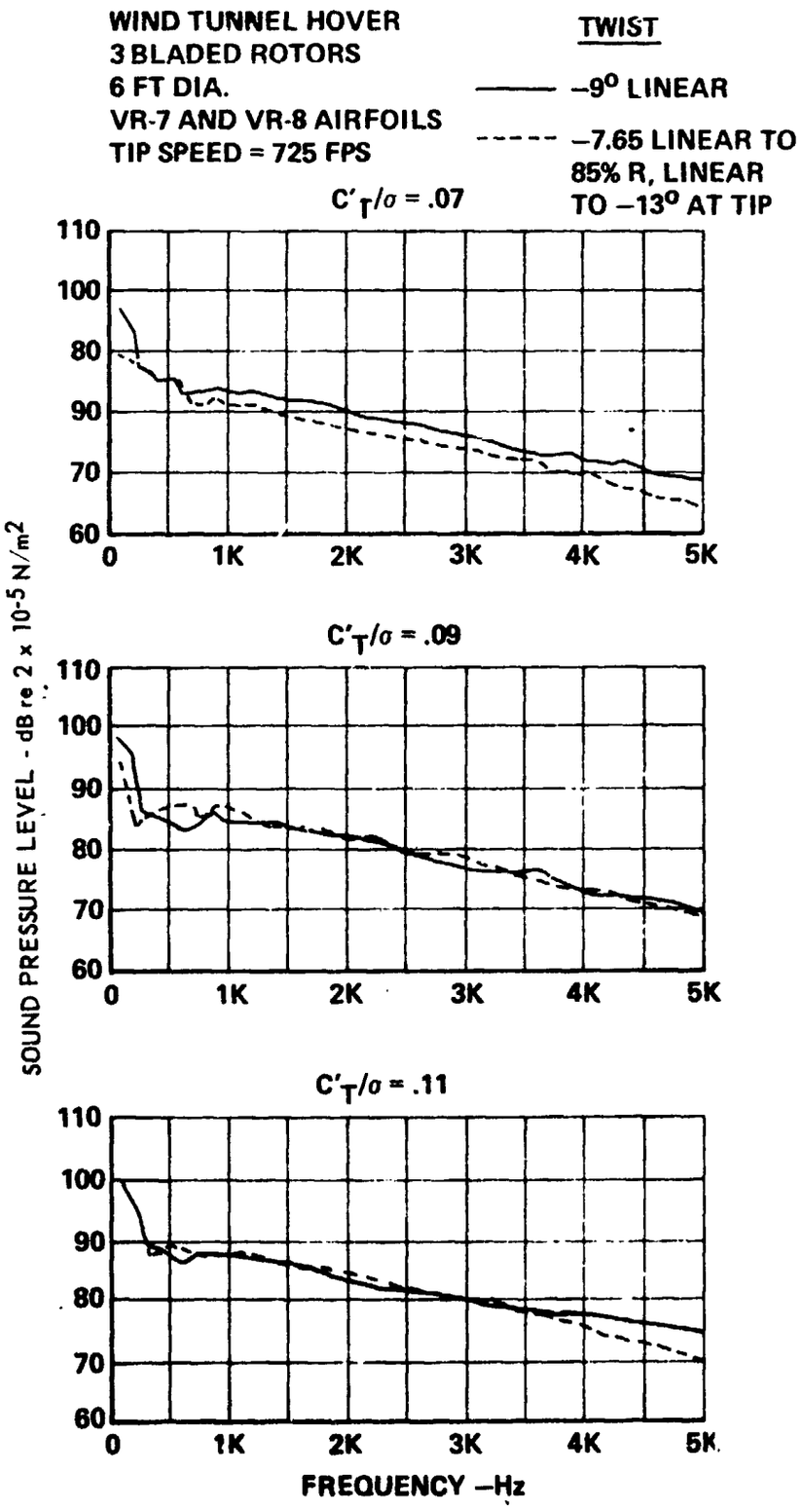

FIGURE 2-23 BLADE TWIST COMPARISONS

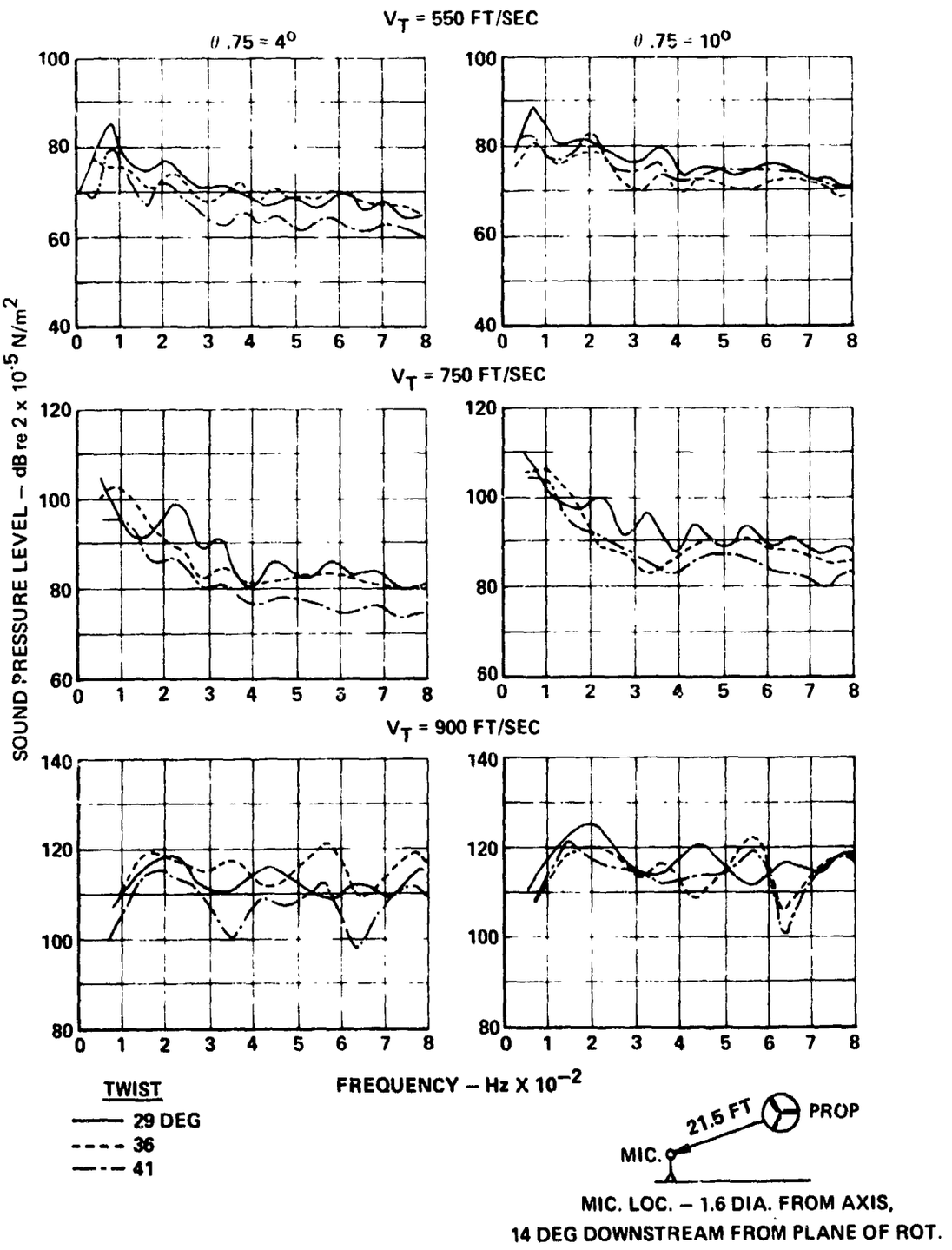

FIGURE 2-24 BLADE TWIST COMPARISON

and tip speed of 750 fps, design tip speed of the Model 222, it is seen that a difference in twist has little effect on the lower four harmonics (first harmonic frequency = 55Hz), but can have a significant effect on the higher harmonics. The 41° twist rotor, for example, shows sound pressure level 3-5dB lower than that with a 36° twist over the frequency range of 400-800 Hz. Therefore, while not affecting the overall sound pressure level, increased twist could appreciably lower the perceived noise level of a rotor with uniform flow.

Other Noise Reduction Techniques

Some research is currently underway in the areas of differential azimuth spacing between blades in the same rotor. Although the results are not definitive at this time, it appears that the overall sound levels generated by rotors with different blade spacings remain constant, with harmonic levels varying for each configuration. For example, a four-bladed rotor with equal spacing between blades displays a strong harmonic at four times the fundamental rotational speed. As the blade spacing approaches an X configuration, the harmonic frequency becomes associated with two times rotational speed. This changes the subjective quality of the sound but does not affect the amplitude of the waveform.

Other devices for reducing noise such as serrated leading edges for airfoils have demonstrated only limited success in specific frequency ranges and at low velocities. However, they have not contributed to significant reductions in the range of Reynolds number where rotors typically operate.

Expanding the tip vortex by additional fluid mass injected into the core region is currently being investigated and these tests show promise of substantial velocity reductions in rotational velocities of the core fluid. Full-scale evaluation of this concept will be conducted on the NASA Langley Whirl Tower in 1973.

III. TURBOSHAFT ENGINE NOISE

There are four sources of turboshaft engine noise: (1) compressor, (2) combustion, (3) turbine, and (4) exhaust jet. The noise emitted from the engine inlet is primarily due to the compressor, while that coming from the exhaust pipe is a combination of combustion, turbine and jet noise. Engine noise has a directivity pattern at the inlet and exhaust originating from the above four sources. Typically, the maximum acoustic output of a front-drive turboshaft engine occurs at 30° from the front of the engine for inlet and at 160° for exhaust. This directivity pattern changes, to a small extent, with power setting because the relative magnitude of the acoustic emissions from the sources are changing.

Using the trends for uninstalled engine noise shown in Figure 3-1, it is obvious that the design objective of minimization of installed power also produces a quieter aircraft.

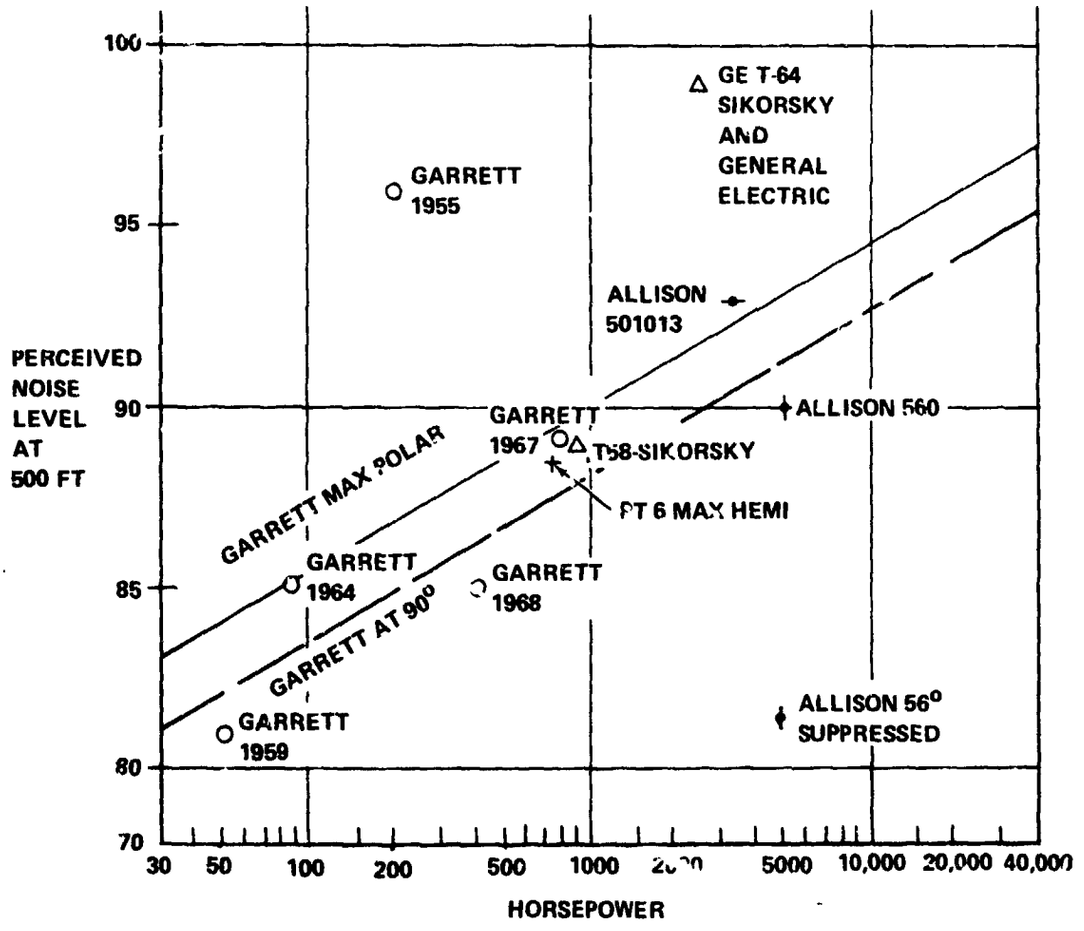

FIGURE SUMMARY CURVE -
BARE [illegible]SHAFT ENGINE NOISE

Figure 3-2 shows the sound pressure level spectra in cove: of the Model 222 rotor and Lycoming T53-L13 engine inlet and exhaust. The maximum inlet noise intensity occurs at 30° azimuth, 500 feet radially and 12° below the aircraft. The engine inlet noise, as shown on this figure is lower than the rotor spectrum level over most of the frequency range. The high frequency spike occuring in the 12,500 Hz one-third octave band is caused by fundamental blade passage frequency of the first stage of the engine compressor.

Since the engine inlet only exceeds the rotor spectrum at low frequencies (less than 160 Hz one-third octave band), and at high frequencies (12,500 Hz one-third octave band), the aircraft perceived noise level (95.0 PNdB) does not differ significantly from that of the rotors alone (93.6 PNdB).

The exhaust spectrum shown on Figure 3-2 is lower than the inlet spectrum. Thus, the exhaust is less of a factor in the aircraft perceived noise and overall sound pressure levels than the engine inlets. This is due to the relatively low exit and the resulting jet mixing velocities.

If the rotor acoustic signature (either OASPL or PNL) is significantly reduced, then further reduction of the aircraft acoustic signature may require some treatment of the engine installation. The two engine inlets can be treated by application of a sound absorptive lining to the inner surfaces. The typical attenuation characteristics of these linings are shown in Figure 3-3 (Ref. 14).

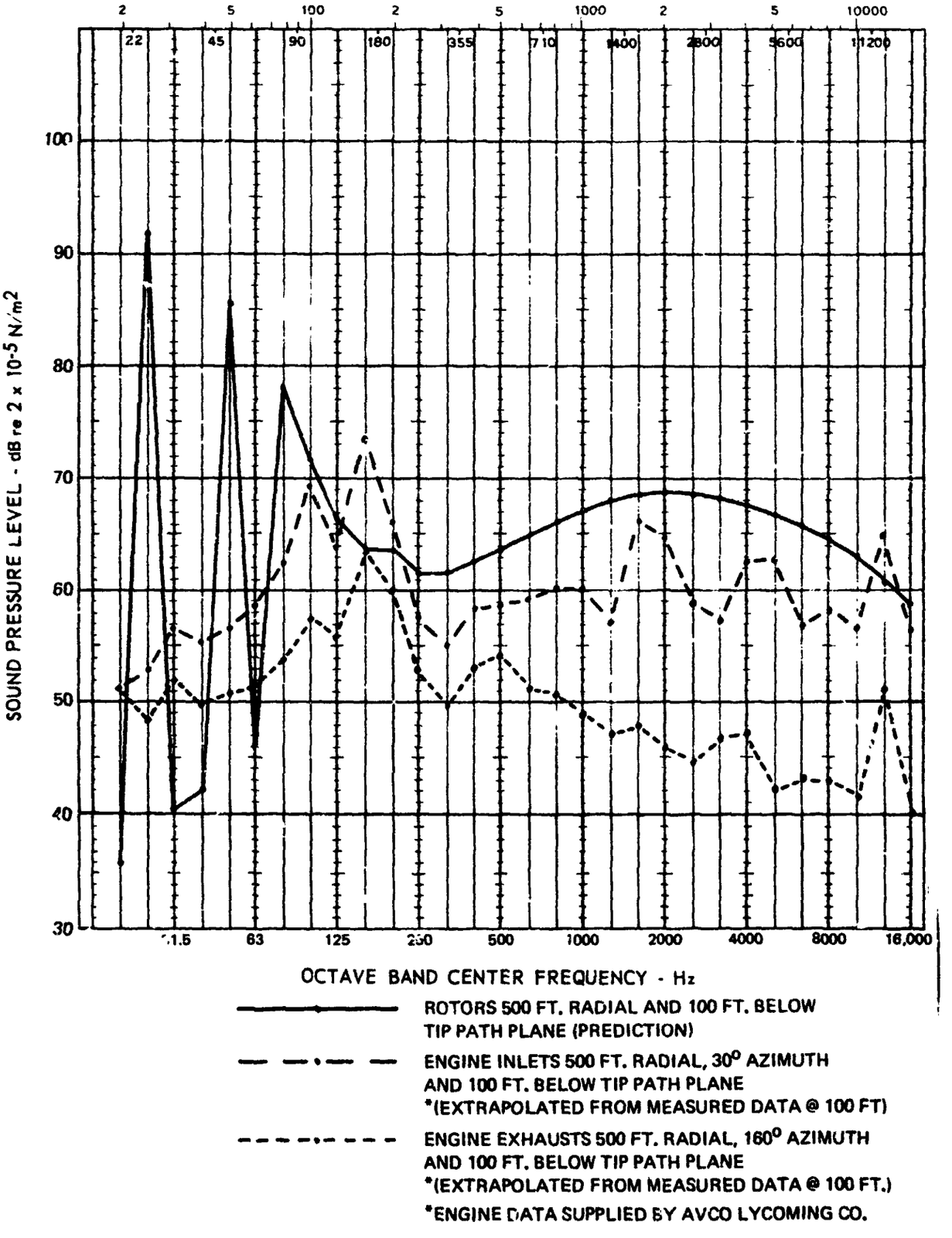

FIGURE 3-2 COMPARISON OF MODEL 222 ROTOR AND T53-L13 INLET AND EXHAUST SPECTRA IN HOVER

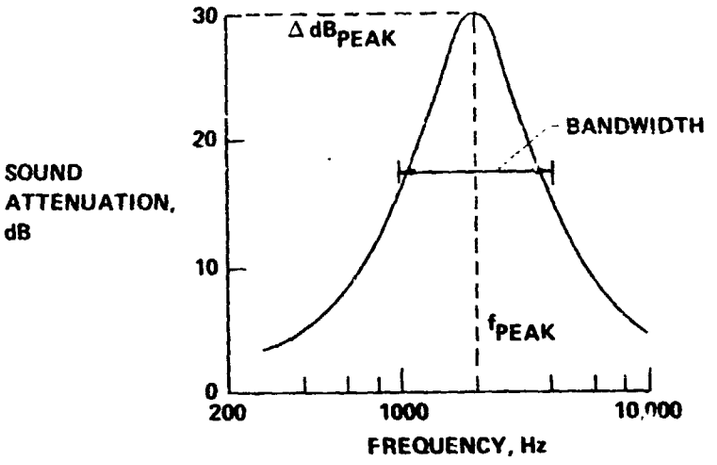

FIGURE 3-3 PARAMETERS FOR TYPICAL ATTENUATION SPECTRUM

As can be seen from this figure, the sound attenuation of these linings are frequency sensitive. Therefore, to obtain an effective inlet lining, the frequency bandwidth in the engine inlet spectra requiring the most attenuation in dB and a lining configuration giving an optimum bandwidth match are selected. Designing a lining having this optimum bandwidth match can be accomplished by two different methods: one is multiple lining layers having different attenuation spectra and peak attenuation frequencies (Figure 3-4) and the other is a longitudinal series of linings with differing properties either in parallel or in series as shown in Figure 3-5.

These attenuation characteristics are a strong function of the parameters shown in Figure 3-6. The lining geometry parameter length/height (L/H) is changed to obtain the proper attenuation over a specified frequency range once the liner material and configuration have been selected.

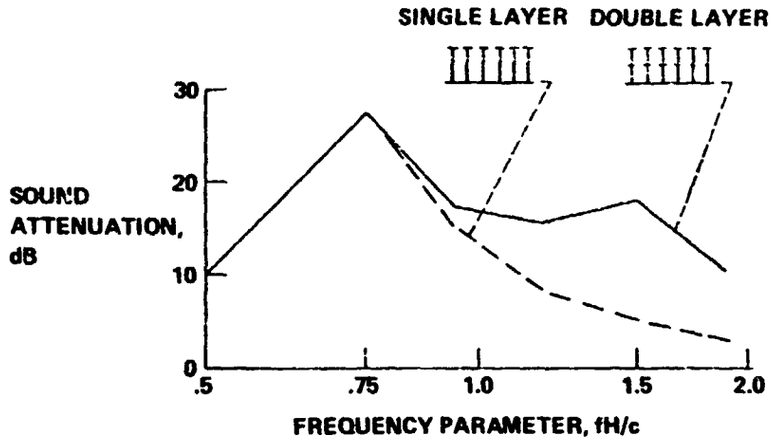

FIGURE 3-4 ATTENUATION BANDWIDTH COMPARISON

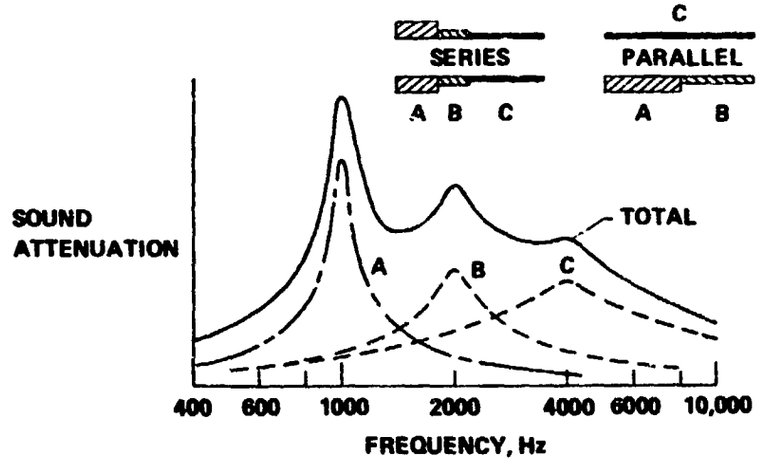

FIGURE 3-5 METHODS OF INCREASING SUPPRESSION BANDWIDTH

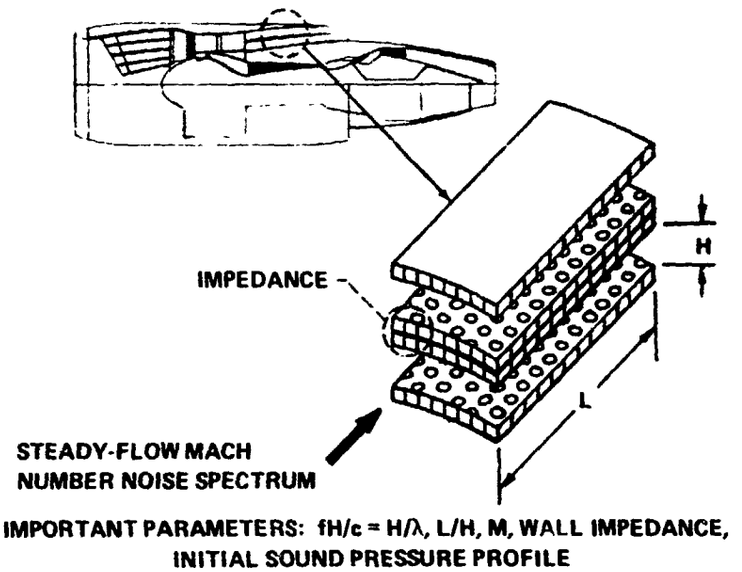

FIGURE 3-6 SUPPRESSION PARAMETERS

To determine the proper geometry, a curve such as shown in Figure 3-7 (Ref. 14) is used for a particular lining material. Refer to Appendix B for a sample calculation of the geometry of an absorptive lining installed in the engine inlets of the Model 222.

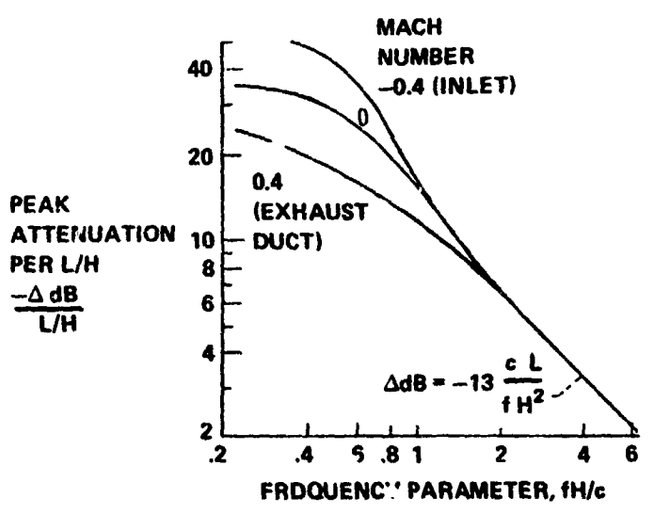

FIGURE 3-7 MACH NUMBER EFFECT ON PEAK ATTENUATION

The exhaust noise presents no problems for perceived noise level or overall sound pressure level, because the exhaust noise is more than 10 dB below that of the rotor throughout the major portion of the spectrum. If treatment of the exhaust noise is desired, a broadband absorptive muffler may be used.

There may also be a different approach to changing the engine acoustic signature other than the previously discussed treatment of the engine installation. The engine manufacturer could undertake a development program for redesign of the internal components of the engine to reduce the inlet and exhaust noise. This would result in changing the rotor/stator spacing of the compressor and/or redesign combustors to reduce the combustion rumble. Redesign of the engine components is an expensive process compared to sound suppression treatment of the aircraft engine installation. However, this initial expense would be somewhat offset by a reduction in aircraft operating costs since weight penalties for engine component redesign should not be as severe as those for the modification of the engine installation.

IV. ROTOR DESIGN PARAMETER TRADEOFFS

General Discussion

This section of the report deals with one aspect of the design problem; defining tradeoffs in performance and weight associated with the noise reduction. This is done by investigating the sensitivity of the far-field noise levels as well as performance and

weight to variations of the following selected design parameters. The acoustic importance of these parameters have been identified in Section II.

(1) tip speed

(2) rotor solidity ratio

(3) number of blades per rotor of constant area per blade

(4) number of blades per rotor of constant total blade area

(5) hover disc loading.

It should be realized that although this study is directed toward basically low disc-loading rotary-wnng aircraft, the results may not be directly applicable to such other low disc-loading configurations as helicopters. This is due to unique rotor design criteria for a compromise of performance optimization between hover and forward flight.

Sensitivity Study Approach

The establishment of a mission profile, aircraft common performance ground rules, drag trends, and prop-rotor hovering cruise performance are necessary for a comprehensive and systematic study. Aircraft performance, weight and acoustic signature resulting from changing rotor design parameters can now be compared on a common basis.

Acoustic Performance Design Study Mission. - The Boeing-Vertol Model 222 will be presented as a transport aircraft in this report. The mission shown in Figure 4-1 is derived from the above approach

ACOUSTIC–PERFORMANCE

DESIGN STUDY MISSION

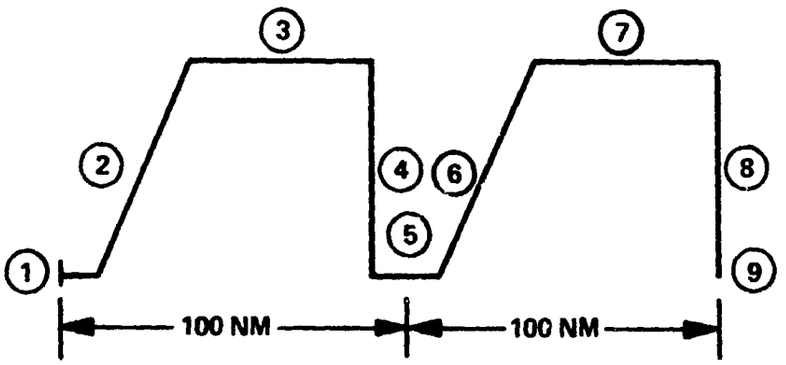

1. 5 MINUTES HOVER AT 2500 FEET, 93°F, T/W = 1.1
2. CLIMB AT MIL RATED POWER FROM 2500 FEET TO 10,000 FEET, STANDARD DAY
3. CRUISE .99 BEST RANGE SPEED AT 10,000 FEET, STANDARD DAY
4. TRANSFER ALTITUDE
5. 5 MINUTES HOVER AT 2500 FEET, 93°F, T/W = 1.1
6. CLIMB AT MIL RATED POWER FROM 2500 FEET TO 10,000 FEET, STANDARD DAY
7. CRUISE .99 BEST RANGE SPEED AT 10,000 FEET, STANDARD DAY
8. TRANSFER ALTITUDE TO 2500 FEET, 93°F
9. END MISSION WITH 10% OF INITIAL FUEL.

FIGURE 4-1 ACOUSTIC PERFORMANCE DESIGN STUDY MISSION

and thus, is not meant to show its military capability. In this section, the gross weight of the aircraft will not change from its current 12,000 pounds. Therefore, the payload will vary as the Model 222 is affected by the parameter changes.

Common Performance Ground Rules. - According to the intent of this study, the Boeing Vertol Model 222, as defined in Ref. 1, is selected as the baseline aircraft. All of the aircraft resulting from the modification of the baseline model should fulfill the following requirements:

1. All aircraft shall have a gross weight of 12,000 pounds.

2. Engine maximum rating will be equal to hover power required at a thrust-to-weight ratio = 1, IGE Sea Level Standard Day, with one engine inoperative.

3. Transmission torque limit is to be sized for rotor hover rpm and one engine maximum power at 2,500 feet, 93°F, static condition.

The above requirements do not necessarily result in a specific maximum level flight speed of the Model 222 such as 300 knots at 10,000 feet, Standard Day, at hover rpm. Instead, the maximum level flight speed will vary from changes in drag, transmission torque limit and propulsive efficiency.

The manufacturer's engine fuel flow shall be increased by 5 percent in accordance with MIL C-5011A.

The equivalent flat plate trend shown in Figure 4-2 was derived from the "Minimum Parasite Drag Breakdown" of the Model 222 (Ref. 1, Table 7, p. 126). The parasite drag is presented as a function of wing area only, as moment arms and tail volume coefficients are assumed constant.

This study investigates the influence of the 5 rotor design parameters.

1. Hover tip speed, V_{t_h}, at constant C_T/σ, B, W/A
2. Rotor solidity ratio, σ, at constant V_{t_h}, B, W/A
3. Number of blades per rotor, B, at constant σ/B, V_{t_h}, W/A
4. Number of blades per rotor, B, at constant σ, V_{t_h}, W/A
5. Hover disc loading, W/A, at constant C_T/σ, V_{t_h}, B.

To isolate the effects of each parameter, sensitivity was studied by changing one parameter while the others remained constant. Two off-baseline values for the five parameters were selected, with the baseline providing the third point. In this way, the sensitivity curve was defined in each case. The off-baseline values were expected to reduce the acoustic signature of the aircraft hovering out-of-ground effect.

The wing chord and thickness do not change and thus, wing area becomes a function of rotor diameter, since fuselage width and rotor-fuselage clearance remain constant. This approach is acceptable, since there is no need to maintain particular wing chord-to-diameter or rotor area-to-wing area ratios. For tilting-rotor aircraft, the wing does not have to support a significant portion

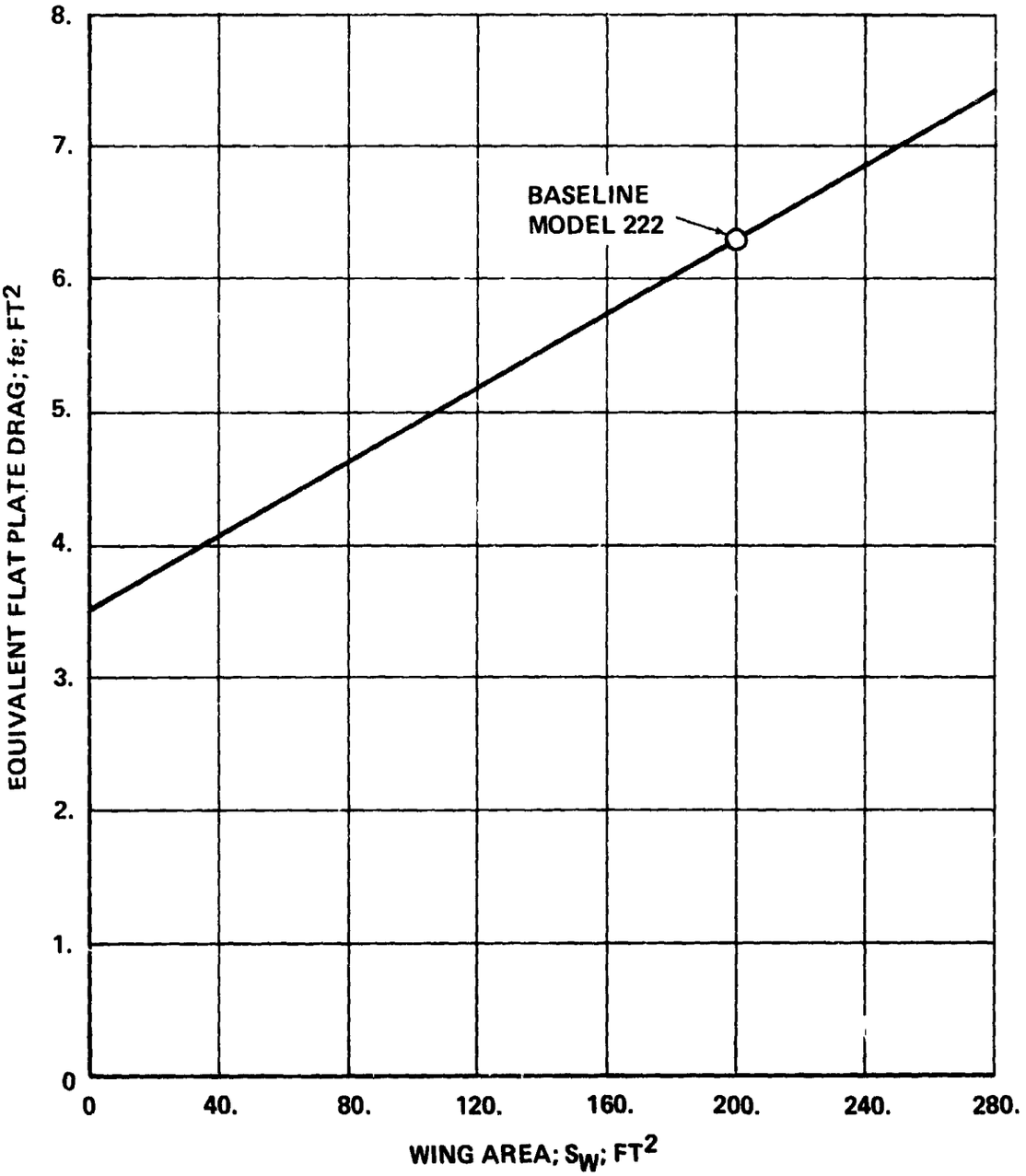

FIGURE 4-2 PARASITE DRAG TREND FOR ACOUSTIC-PERFORMANCE DESIGN STUDY

of the aircraft weight in low speed (near-hovering) flight. This permits the designer to optimize the wing geometry for airplane configuration cruise flight, while complying with the following constraints: the need for placing the rotors at the wing tips and to provide sufficient wing thickness to support the aircraft in the helicopter mode.

The rotor hover and cruise performance trends were established by the following calculation procedure. At each condition, a performance evaluation for a change in twist was calculated using the Boeing Rotor Performance Computer Program. This computer program uses a vortex wake analysis plus an empirical slipstream correction factor (see Ref. 15). The procedure outlined below assured that all rotor designs would have the same design tradeoff between hover and cruise performance. The original Model 222 blade twist increment varying linearly along the blade span was added. The manner in which the optimum twist was obtained is illustrated in the sketch below.

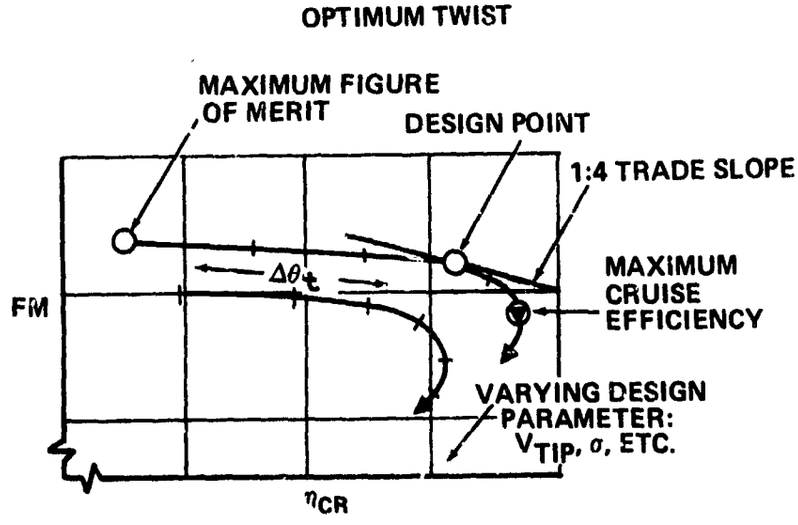

The other blade characteristics such as blade chord, thickness ratio and airfoil section distribution were kept the same as the baseline rotor (Ref. 1). Also, the rotor design operating conditions were selected to be the same as those for the Model 222 aircraft; i.e., hover at 2500 feet, 93°F, 12,000 pounds gross weight and thrust-to-weight equal to 1.05; and cruise at 300 knots, 10,000 feet standard day. Cruise thrust was based on the Model 222 drag in the cruise condition, while cruise tip speed was assumed to be 70 percent of the tip speed of the modified aircraft in hover.

The above procedure avoided excessive rotor design iterations which would have been necessary to define the optimum hover-cruise compromise twist. Thus, the rotor parameters in the sensitivity matrix were defined. Cruise performance was calculated using the same Boeing rotor performance computer program.

Discussion of Results of Tilt-Rotor Sensitivity to the Five Design Parameters

Structural Flight Envelope Limits. - The weight empty of the aircraft in this section will be dependent on the following structural limits which are the same as for the baseline aircraft.

1. V_{MO} = 350 knots, EAS
2. V_{dive} = 350 knots, EAS
3. M_{MO} = .569
4. Wing Design Maneuver Load Factor = 3g.

In general, when the parameters were changed in a manner indicating an improvement in acoustic characteristics, the result reduced aircraft performance and increased its weight empty. The exceptions to this generalization were the following parameter variations: (1) rotor hover disc loading, and (2) number of blades with constant rotor solidity. The aircraft design points establishing the sensitivity lines have their summary weight statements and configurations tabulated in Appendix D.

Rotor Performance. - The sensitivity of the rotor performance to the variation of the design parameters is shown in Figure 4-3 for hover and Figure 4-4 for cruise performance. The changes in rotor performance shown in these figures result from the following: increased profile power for changes in rotor solidity whether or not the number of blades were changed from the baseline; and twist, changing the L/D of the rotor blade by altering the spanwise lift distribution for tip speed and hover disc loading.

Aircraft Performance. - Figures 4-5 and 4-6 show the rate of change of shaft horsepower required to hover out-of-ground effect at a T/W = 1.05 and 2500 feet altitude, 93°F, with respect to the five design parameters.

Tip speed variation at a constant C_T/σ causes the hover power required to increase as V_t is reduced. This is due to the compromise in spanwise lift distribution necessary to maintain the desired

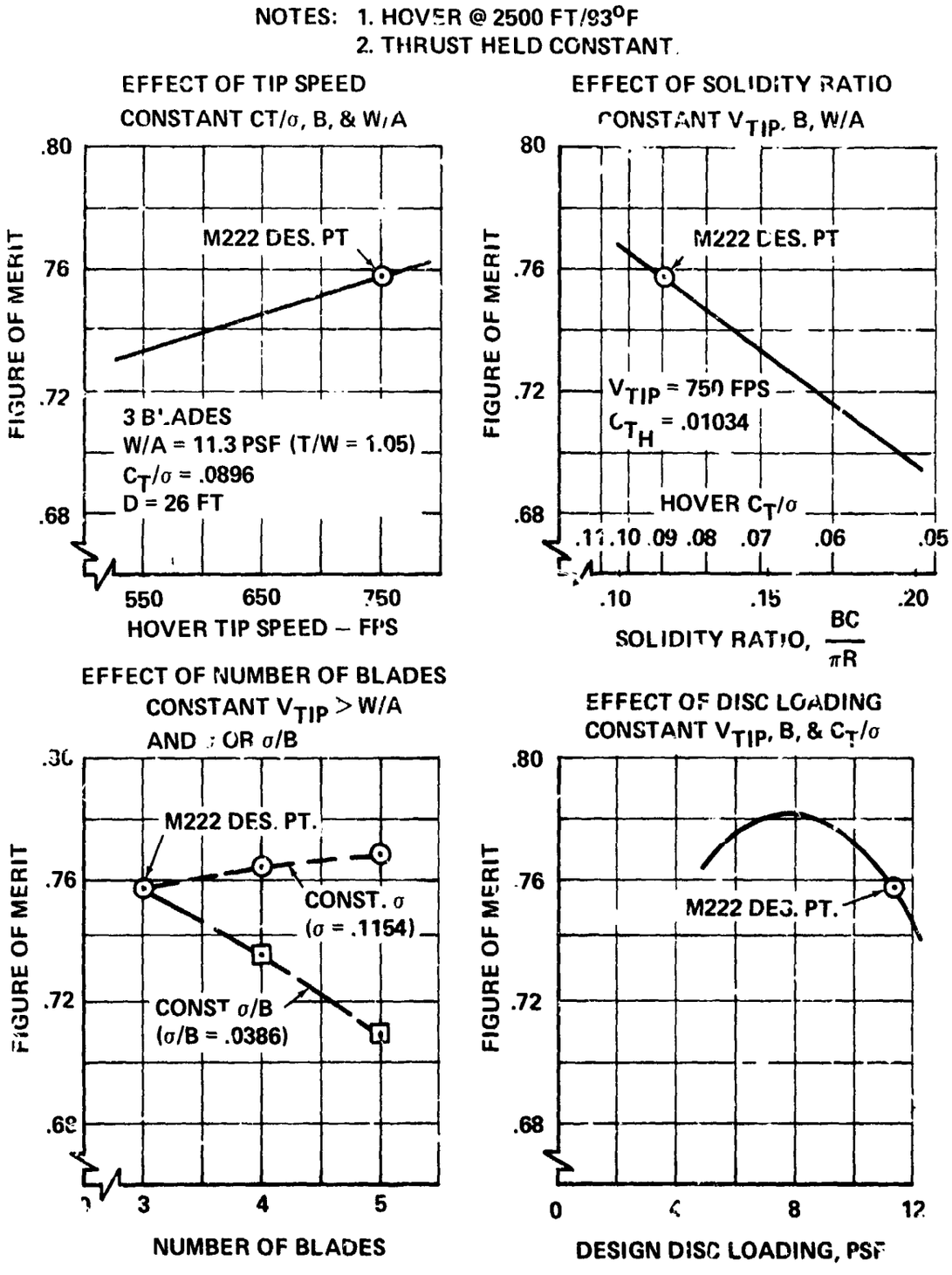

FIGURE 4-3 CHANGE IN HOVER FIGURE OF MERIT WITH VARIOUS ROTOR DESIGN PARAMETERS

NOTES: 1. CRUISE @ 10,000 FT/STD & 300 KT
2. THRUST HELD CONSTANT.

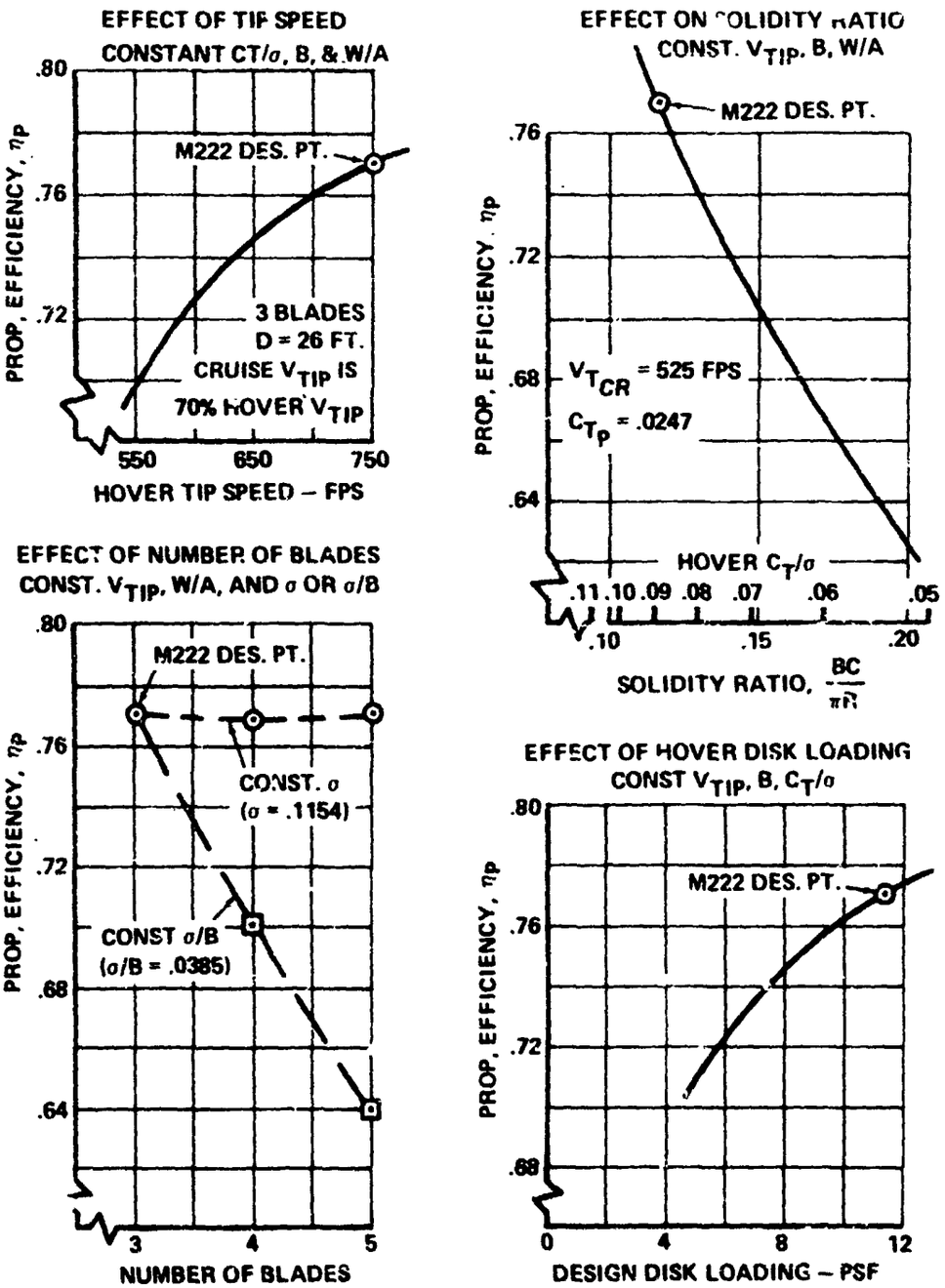

FIGURE 4-4 CHANGE IN CRUISE PROPULSIVE EFFICIENCY WITH VARIOUS ROTOR DESIGN PARAMETERS

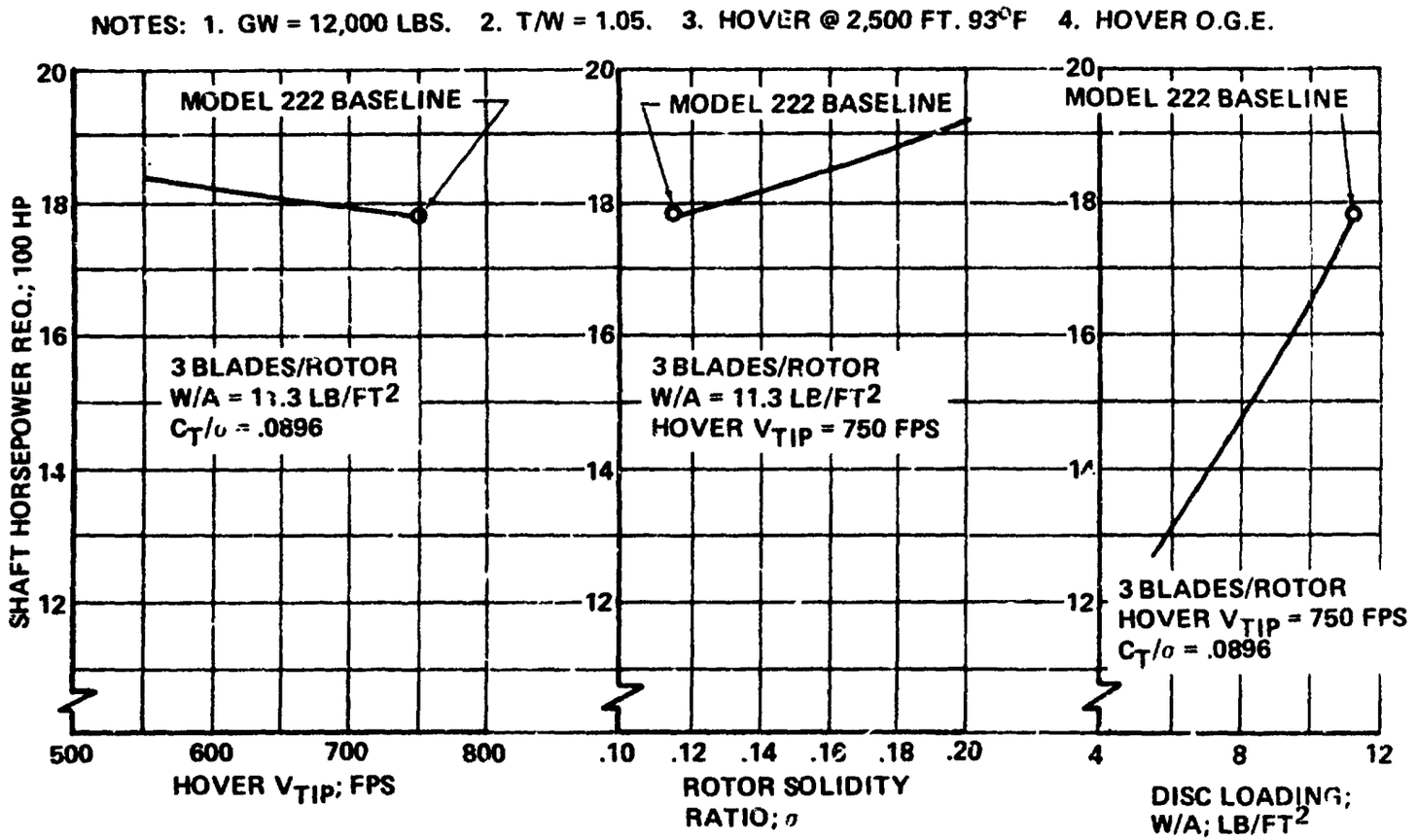

FIGURE 4-5 EFFECT OF HOVER TIPSPEED, ROTOR SOLIDITY AND DISC LOADING ON HOVER SHP REQUIRED

NOTES: 1. GW = 12,000 LBS.
2. T/W = 1.05
3. HOVER @ 2,500 FT. 93°F
4. ROTOR DIAMETER = 26 FT
5. HOVER O.G.E.

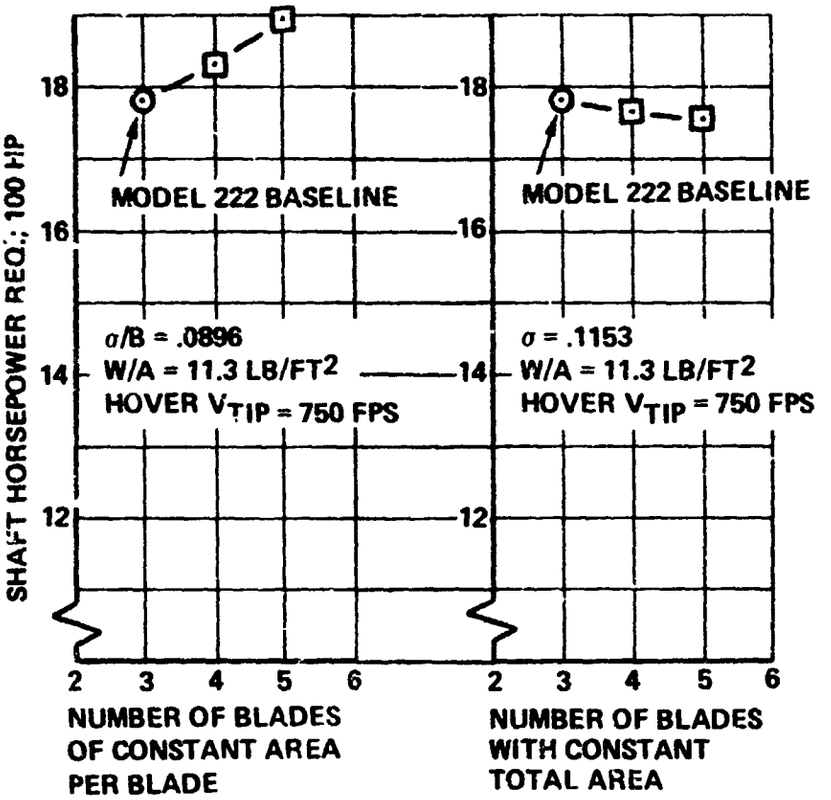

FIGURE 4-6 EFFECT OF NUMBER OF BLADES AT CONSTANT σ AND σ/B ON HOVER SHP REQUIRED

Figure-of-Merit/Cruise Propulsive Efficiency trade line of 1:4. The need to change total twist is explained by the use of the following sketch of generalized prop-rotor performance.

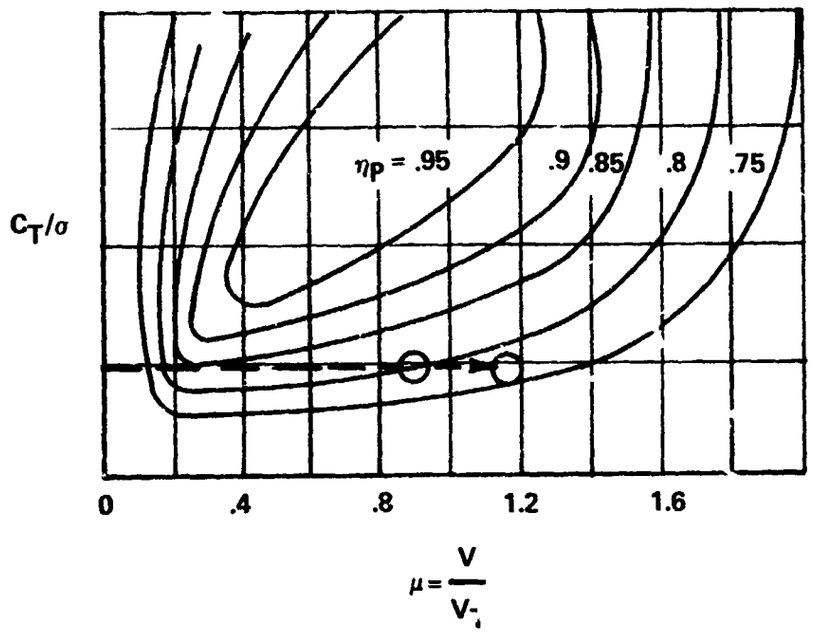

This sketch represents generalized performance for small change in rotor solidity, while the following characteristics are constant: (a) airfoil section, (b) twist distribution, and (c) planform. A hover tip speed reduction at constant C_T/σ resulting in a reduced cruise $V_t(.7V_{t_h})$ causes the cruise design point to move horizontally (arrow in chart) as design cruise speed is fixed. The degraded cruise performance is caused by an increased inflow ratio altering the angles of attack along the blade; therefore, changing the lift distribution. This indicates

a deviation from the hover-cruise performance trade slope corresponding to a hover payload/mission fuel tradeoff. Thus, the twist must be altered to maintain the study's prop-rotor performance ground rules. If the rotor were to be designed for hover only, the twist could have been selected to maximize the Figure of Merit. However, cruise efficiency at the design cruise speed would be so poor that unacceptable aircraft performance would result.

Increasing rotor blade solidity ratio at a constant tip speed, either with a constant or increasing number of blades per rotor, requires a larger hover power caused by increasing rotor profile power in direct proportion to solidity (Figures 4-5 and 4-6).

The two parameters reducing the hover power required are: increasing the number of blades per rotor at constant solidity, and reduction of disc loading at constant C_T/σ. When the number of blades is increased, a small change occurs (-8 HP/blade) which is less than 1 percent of the total power required to hover. This can be attributed to a change in the blade chord-to-radius ratio and its associated induced power because of the improved tip loss factor.

With respect to disc loading, the hover power required changes at a rate of 47.5 HP per lb/ft^2 as the induced power becomes smaller. The induced power has the following relationship to disc loading:

$$RHP_{ind_h} = \sqrt{\frac{1}{2\rho}\frac{W}{A}}\frac{W}{550}\left(\frac{T}{W}\right)^{3/2} k_{ind_h}$$

where k_{ind_h} is the nonuniform inflow and tip induced power loss factor.

$$\frac{\partial RHP_{ind_h}}{\partial(W/A)} = \frac{W}{550}\left(\frac{T}{W}\right)^{3/2}\left\{\frac{k_{ind_h}}{2\sqrt{2\rho(W/A)}} + \sqrt{\frac{W}{2\rho A}}\frac{\partial k_{ind_h}}{\partial(W/A)}\right\}$$

A further discussion of the calculation of hovering performance is contained in Appendix C.

In this study, payload is calculated on the basis of mission fuel required for 100 n.mi. radius and a takeoff gross weight. The sensitivity of payload to changes in the five design parameters is shown in Figures 4-7 through 4-11. From Figure 4-7, it appears that payload is directly proportional to tip speed. The mission fuel is increased because of reduced cruise efficiency (Figure 4-4) and Figure-of-Merit (Figure 4-3). Weight empty is also growing (Table I, Appendix D). The same factors result in the inverse proportion of payload to rotor solidity whether payload changes as a result of the varying number of blades per rotor, or the blade area at the same number of blades.

Changing the number of blades at constant solidity has no significant impact on mission payload. Increasing the blade number from 3 to 4 causes the payload to grow by 26 pounds, or 2 percent of the original payload; i.e., .22 percent of the gross weight. Another increase from 4 to 5 blades decreases the payload by 4 pounds, or .31 percent of the payload. For details, see Table I, Appendix D.

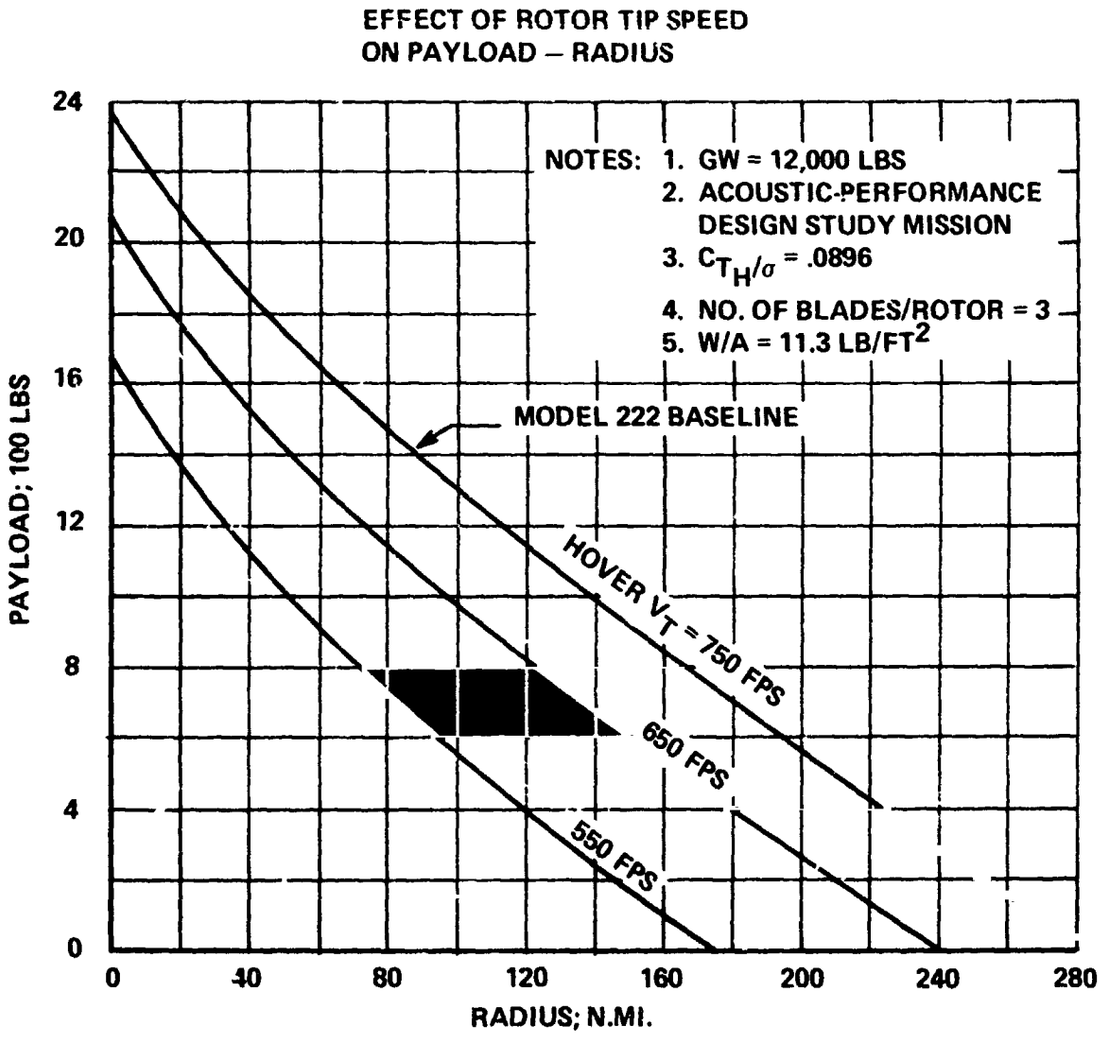

FIGURE 4-7 EFFECT OF ROTOR TIP SPEED ON PAYLOAD RADIUS

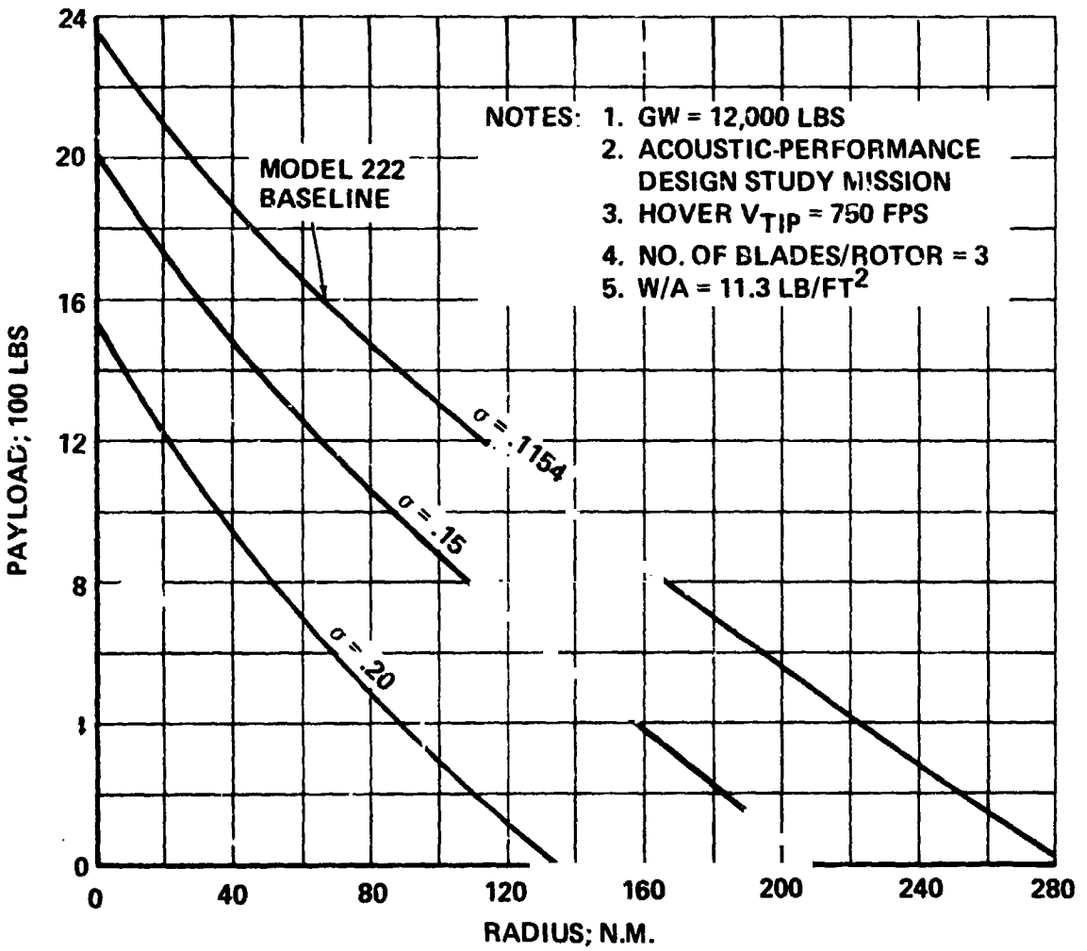

FIGURE 4-8 EFFECT OF ROTOR SOLIDITY ON PAYLOAD-RADIUS

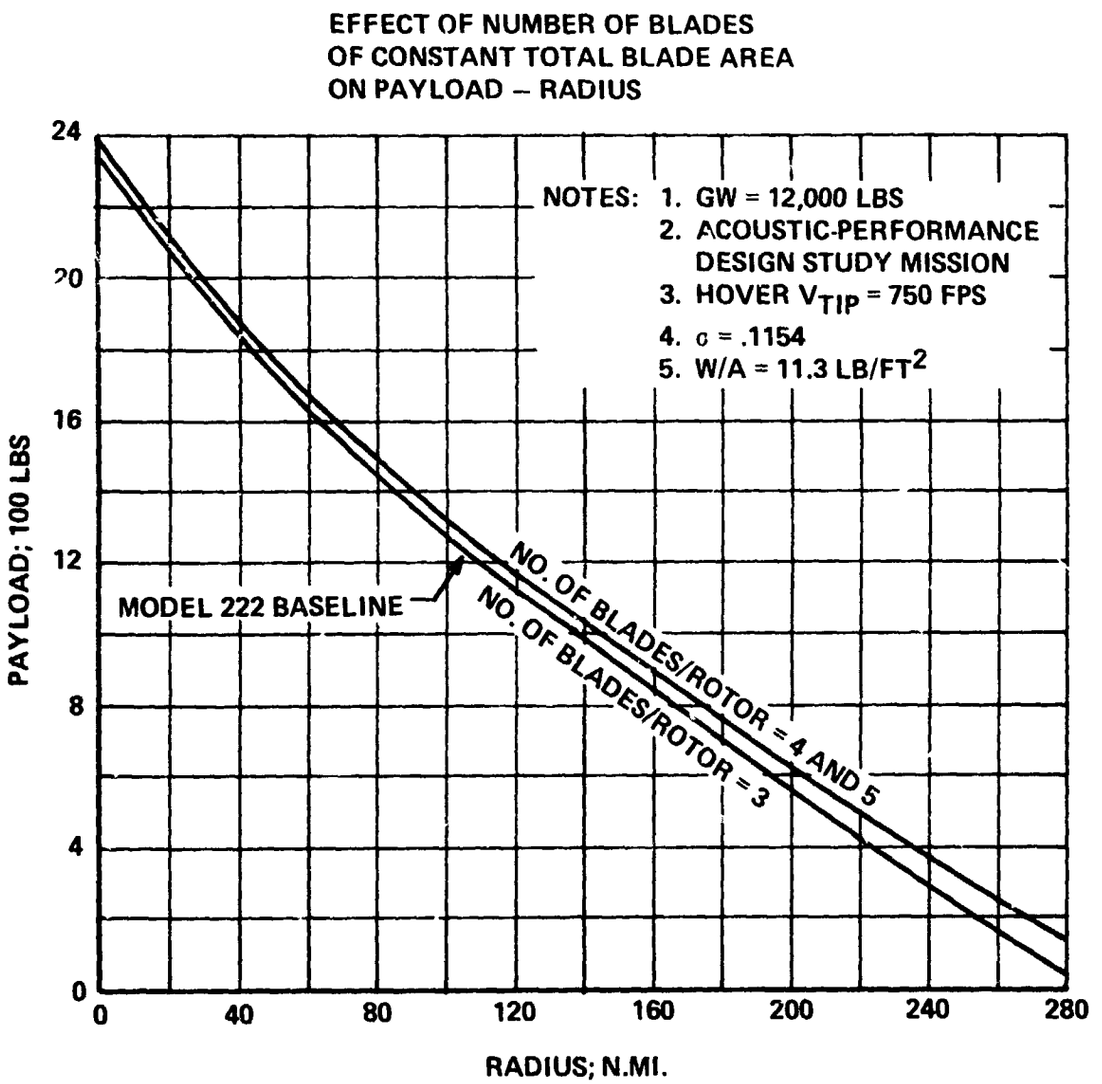

FIGURE 4-9 EFFECT OF NUMBER OF BLADES OF CONSTANT AREA PER BLADE ON PAYLOAD RADIUS

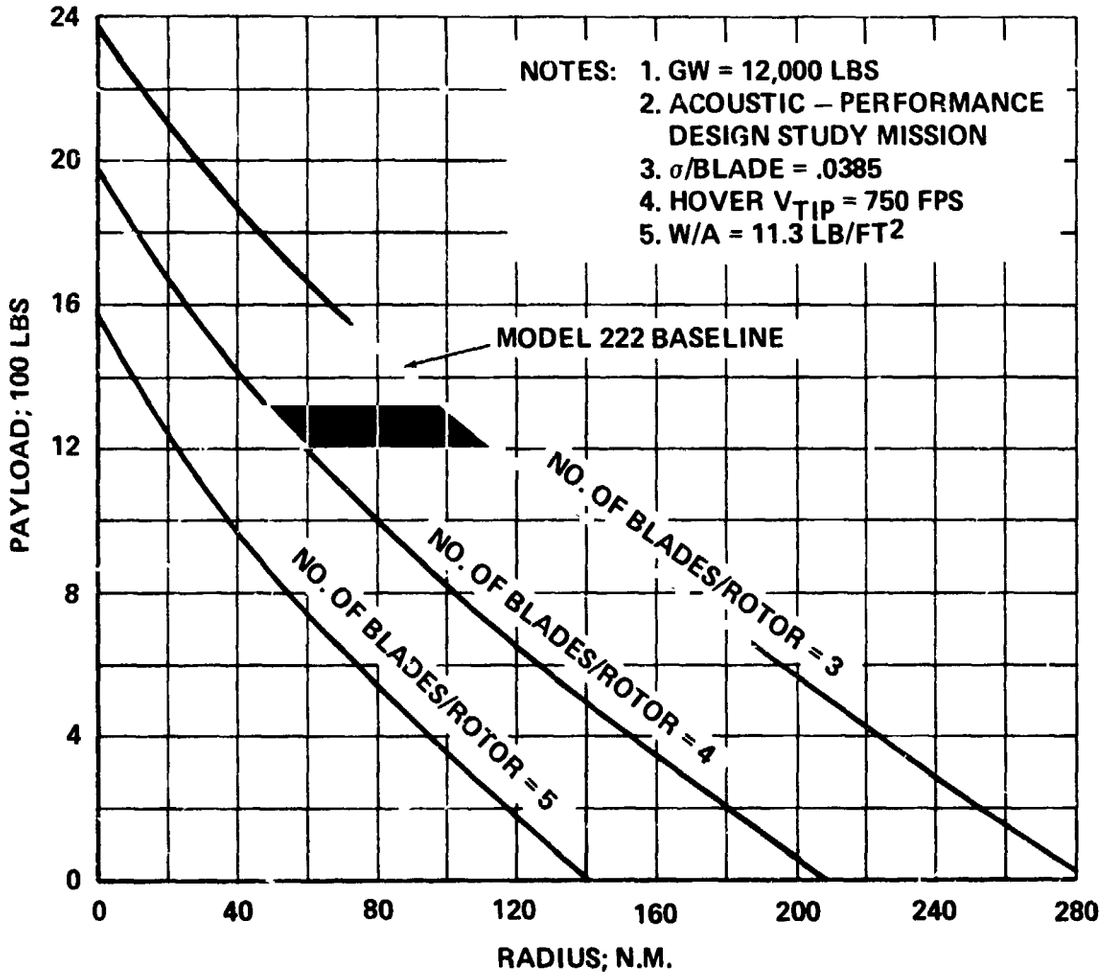

FIGURE 4-10 EFFECT OF NUMBER OF BLADES OF CONSTANT AREA PER BLADE ON PAYLOAD-RADIUS

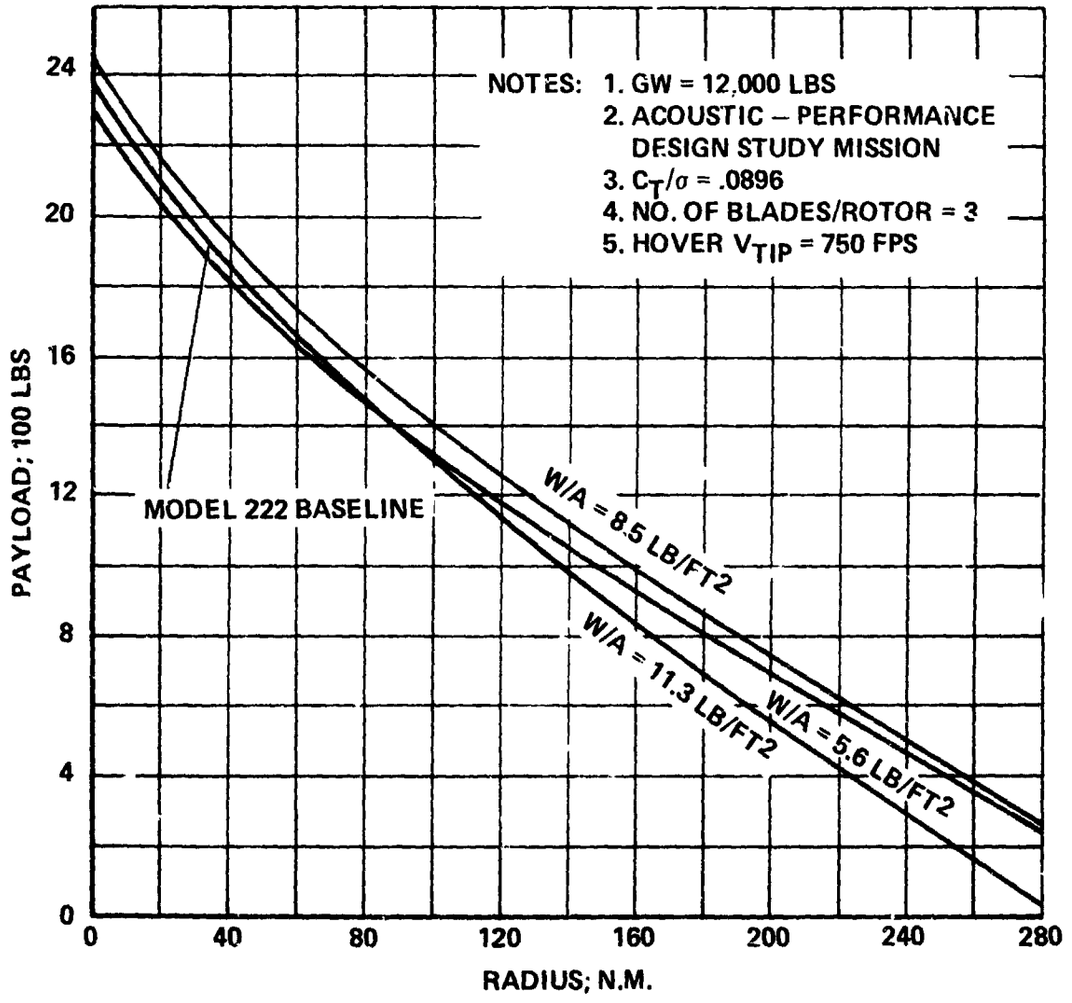

FIGURE 4-11 EFFECT OF DISC LOADING ON PAYLOAD-RADIUS

From Figures 4-11 and 4-15, it can be seen that the variation of payload with disc loading reaches a maximum at (W/A) = 9 lbs/ sq ft. This maximum is caused by a decrease and then an increase in weight empty while mission fuel is becoming smaller in a linear manner.

The hover rpm transmission limit determines the maximum level flight speed of the Boeing Vertol Model 222 at 10,000 feet standard day (Figure 63, Ref. 1). This is due to the fact that the engine power available at cruise speed, 10,000 feet Standard Day is greater than the power that can be safely input for extended periods of time to the gearbox at the hover rpm. Even though a reduced tip speed in cruise increases the propulsive efficiency of the prop-rotor because of a better rotor blade L/D, the transmission power limit at cruise rpm (70 percent of hover rpm) becomes lower. The transmission limit is set by the torque transmitted and thus, for constant torque, as rpm is reduced the power transmitted becomes smaller (30 percent). The corresponding improvement in propulsive efficiency resulting from the lower tip speed is approximately 20 percentage points. However, this does not overcome the 30 percent loss of power available. Therefore, the maximum propulsive power available occurs at the hover tip speed.

Figures 4-12 and 4-13 show the impact of the 5 design parameters on the following characteristics which influence maximum

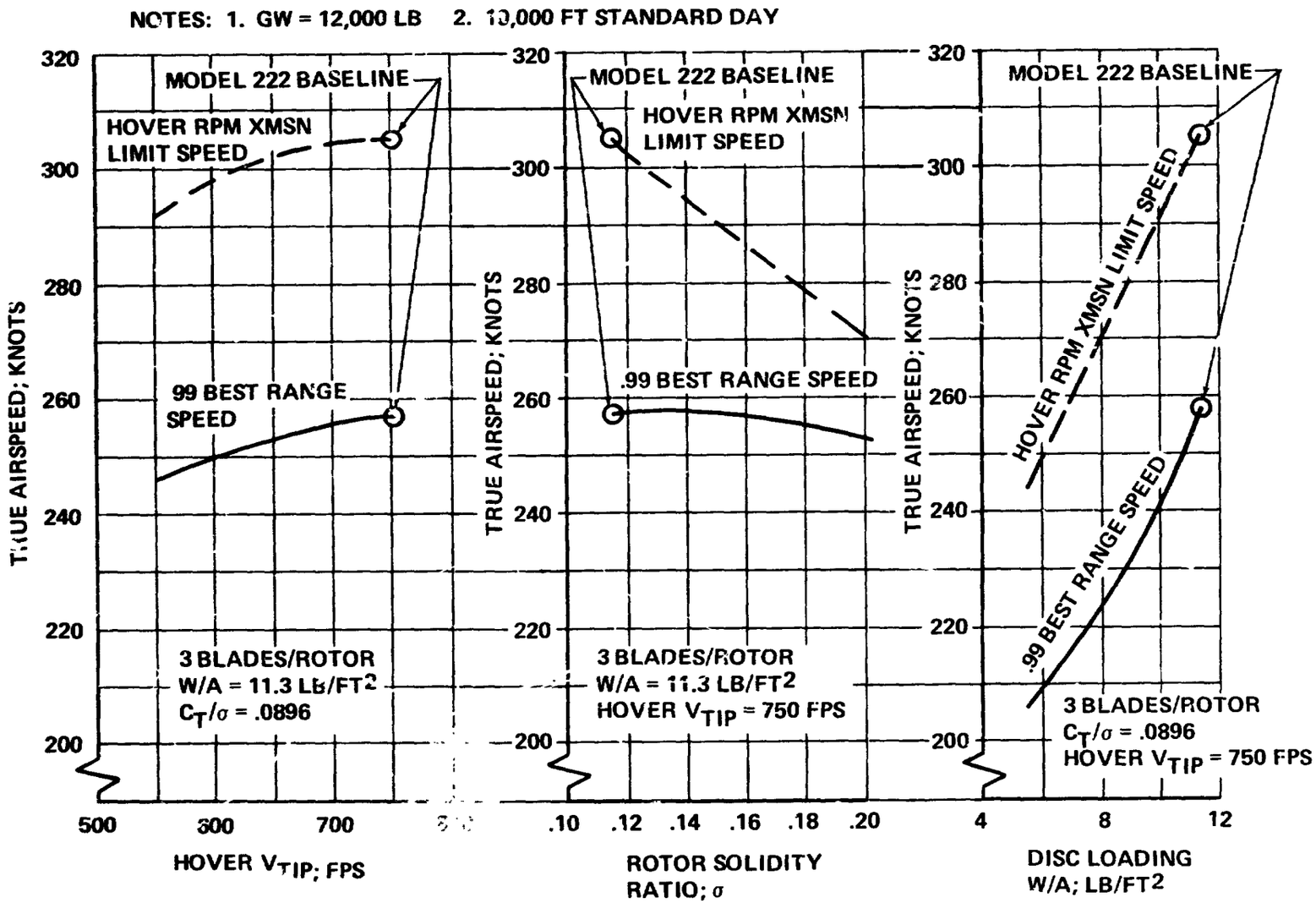

FIGURE 4-12 VARIATION OF 3 DESIGN PARAMETERS WITH .99 BEST RANGE SPEED AND XMSN LIMIT SPEED

NOTES: 1. GW = 12,000 LB 2. 10,000 FT STANDARD DAY

3. ROTOR DIAMETER = 2[illegible] FT

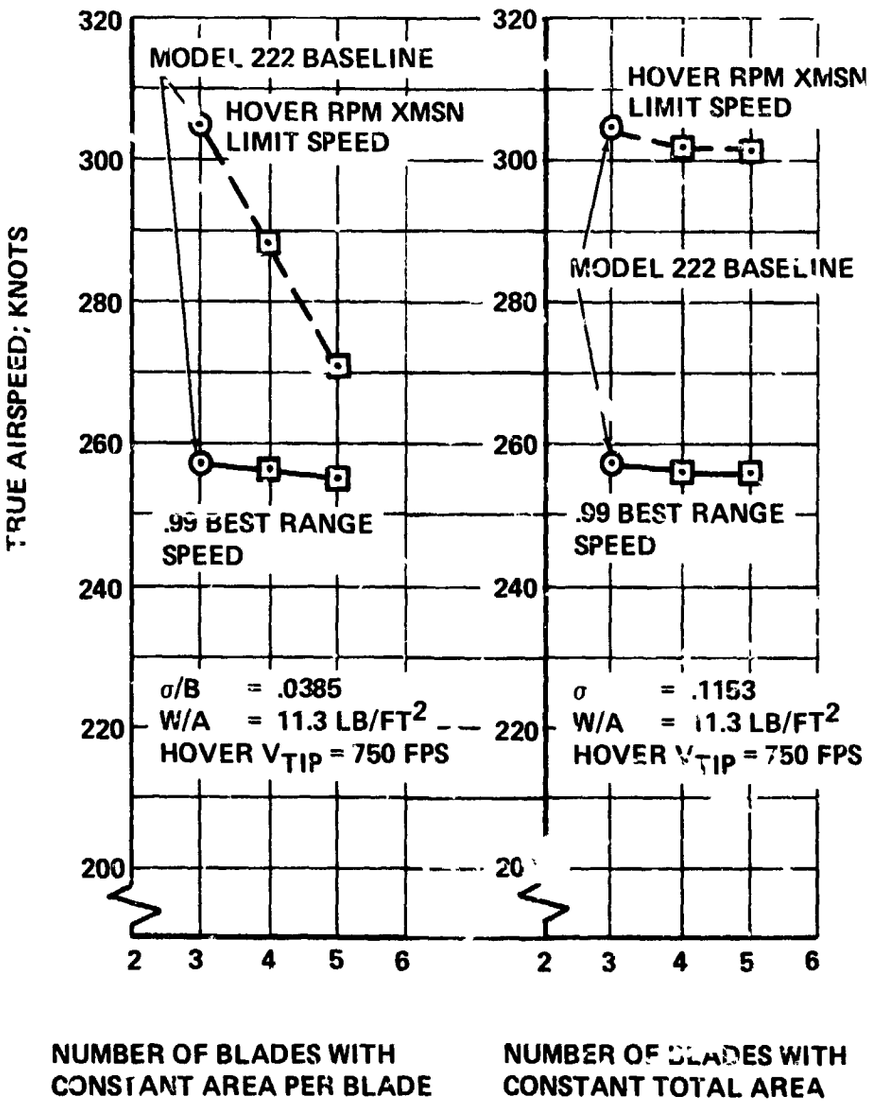

FIGURE 4-13 VARIATION OF NO. OF BLADES WITH .99 BEST RANGE SPEED AND TRANSMISSION LIMIT SPEED

level flight speed: (a) equivalent flat plate drag, (b) transmission power limit (determined from common performance ground rules), and (c) propulsive efficiency. The equivalent flat plate drag and wing span are constant, but the transmission limit undergoes small changes with the following four parameters (Table 2, Appendix D):

a. tip speed
b. rotor solidity
c. number of blades of constant area per blade
d. number of blades of constant total area.

However, their influence on the V_{max} is considerable due to the variation in propulsive efficiency.

Hover rpm transmission limit speed is directly proportional to disc loading (Figure 4-12). This results from the fact that common performance ground rules state that the transmission limit is determined by hover power required. As shown previously, hover power becomes smaller as disc loading decreases. Parasite drag increases as a function of the increasing wing area which, in turn, is inversely proportional to the square root of the disc loading. The wing geometry changes because the chord is constant while the wing span varies so that the wing tip rotors maintain a constant fuselage clearance. Both the transmission power limit and parasite drag deviations from the baseline values (Table 2, Appendix D) have a greater influence on the V_{max} level than changes of propulsive efficiency and induced drag.

The .99 best range speed is dependent on engine fuel flow which, in turn, is a function of sfc and power. The latter depends on the tilt-rotor's speed and equivalent lift-to-drag ratio (L/D_e). The specific range performance of the Model 222 aircraft is shown in Figure 70 of Ref. 1. The changes from the baseline performance of .99 best range speed are shown in Figures 4-12 and 4-13.

The performance sensitivity of the .99 best range speed to all of the design parameters except disc loading results primarily from variations of propulsive efficiency and installed power (Table 2, Appendix D). Therefore, the magnitude of the changes in the .99 best range speed from the baseline level, as caused by varying tip speed, rotor solidity at constant blade number, and increased number of blades are relatively small. The largest change (12 knots) from the baseline performance occurs when hover tip speed is reduced from 750 fps to 550 fps.

However, .99 best range speed is a very strong function of disc loading as shown in Figure 4-12. This is due to wing geometry changes as a function of disc loading. The wing loading and span loading are directly proportional and parasite drag is inversely proportional to disc loading. These factors determine the lift/drag ratio of an aircraft and in turn, the best range speed. The above factors affect the maximum L/D speed as shown below:

w_f = gross weight/fe — equivalent flat plate area loading in lb/ft^2

w_b = gross weight/b^2 — span loading in lb/ft^2

$$V_{opt} = (4w_f w_L)^{1/4} / \sqrt{\rho}$$

Aircraft Weight Sensitivity. - Sensitivity of weight empty to the five design parameters are shown in Figures 4-14 through 4-16. In addition, the summary weight statements for all the aircraft used to define the sensitivity trends are in Table I, Appendix D. The weights of the baseline aircraft subsystems were either determined from vendor information, statistical trends, or analysis of engineering drawings. The variation of weight empty from that of the baseline is determined from the weight trends created for the VASCOMP computer program (Ref. 16). These trends are substantiated in a separate document.

Except for disc loading and number of blades with constant rotor solidity, large changes in weight empty occurred as a function of the design parameter variation.

In the case of disc loading variation, the trend indicated that a weak minimum for weight empty occurs at W/A ≈ 9 lbs/sq.ft. (Figure 4-15). The unusual sensitivity relationship of weight empty to disc loading is caused by the variation of the drive system weight, which is a function of the torque limit calculated in the following way:

$$Torque = (HP \times 550 \times R)/V_t \ .$$

So, for the decreasing disc loading at a constant tip speed used in this study, the rotor radius is increasing but the horsepower limit decreases rapidly, then levels off. This causes the

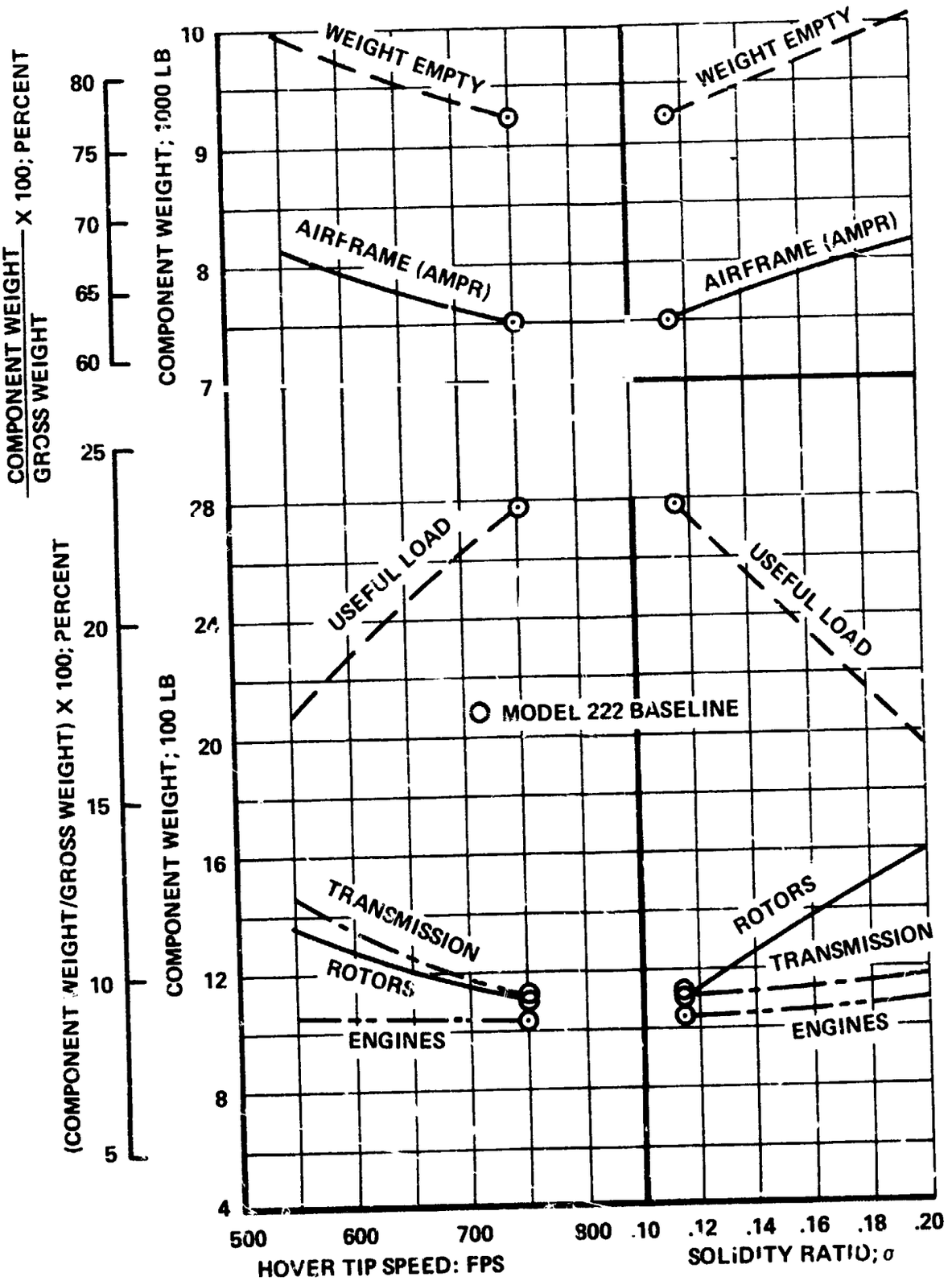

FIGURE 4-14 EFFECT OF HOVER TIP SPEED AND ROTOR SOLIDITY RATIO ON WEIGHT OF TILT-ROTOR SUBSYSTEMS

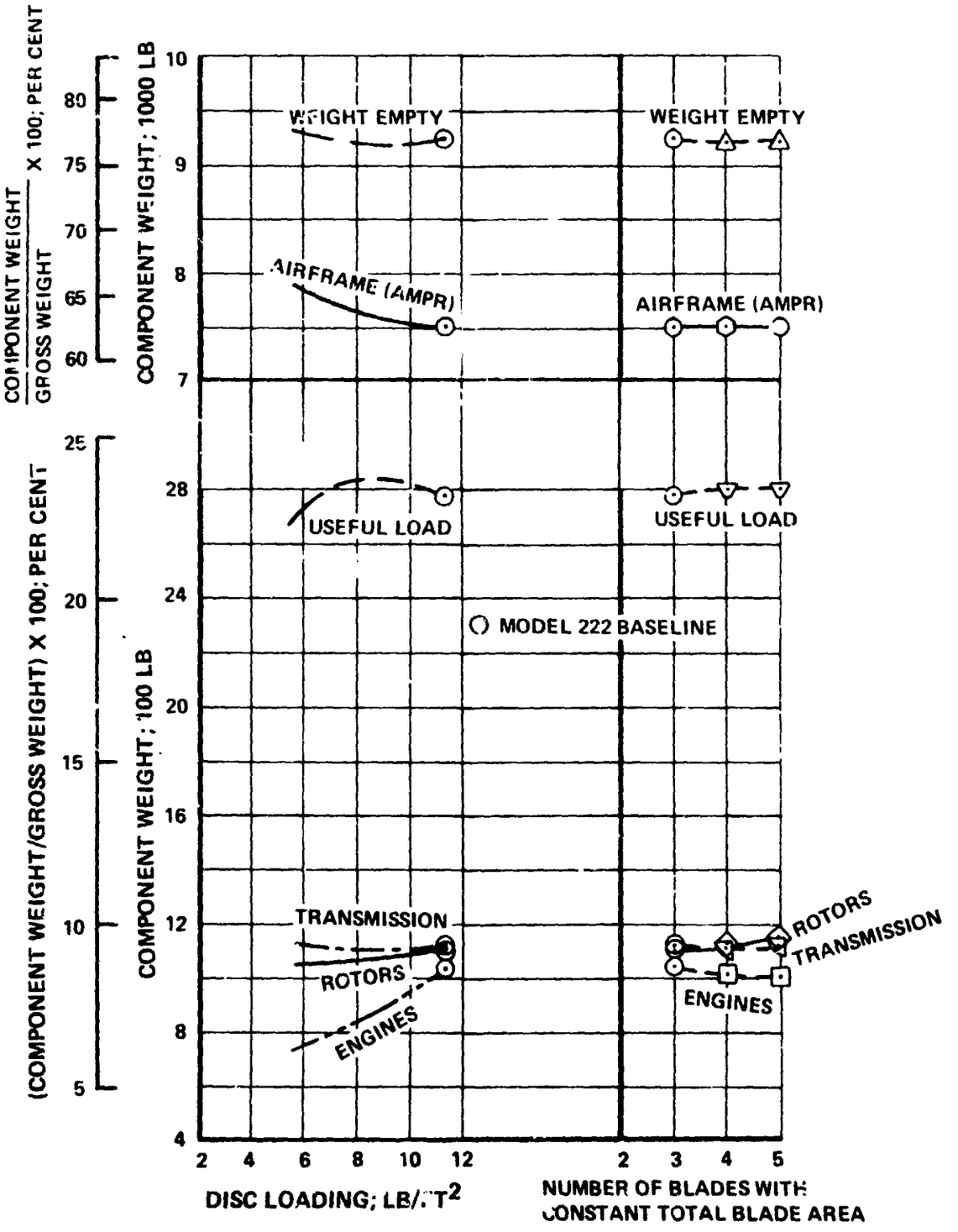

FIGURE 4-15 EFFECT OF DISC LOADING AND NO. OF BLADES WITH CONSTANT TOTAL AREA ON WEIGHT OF TILT-ROTOR SUBSYSTEMS

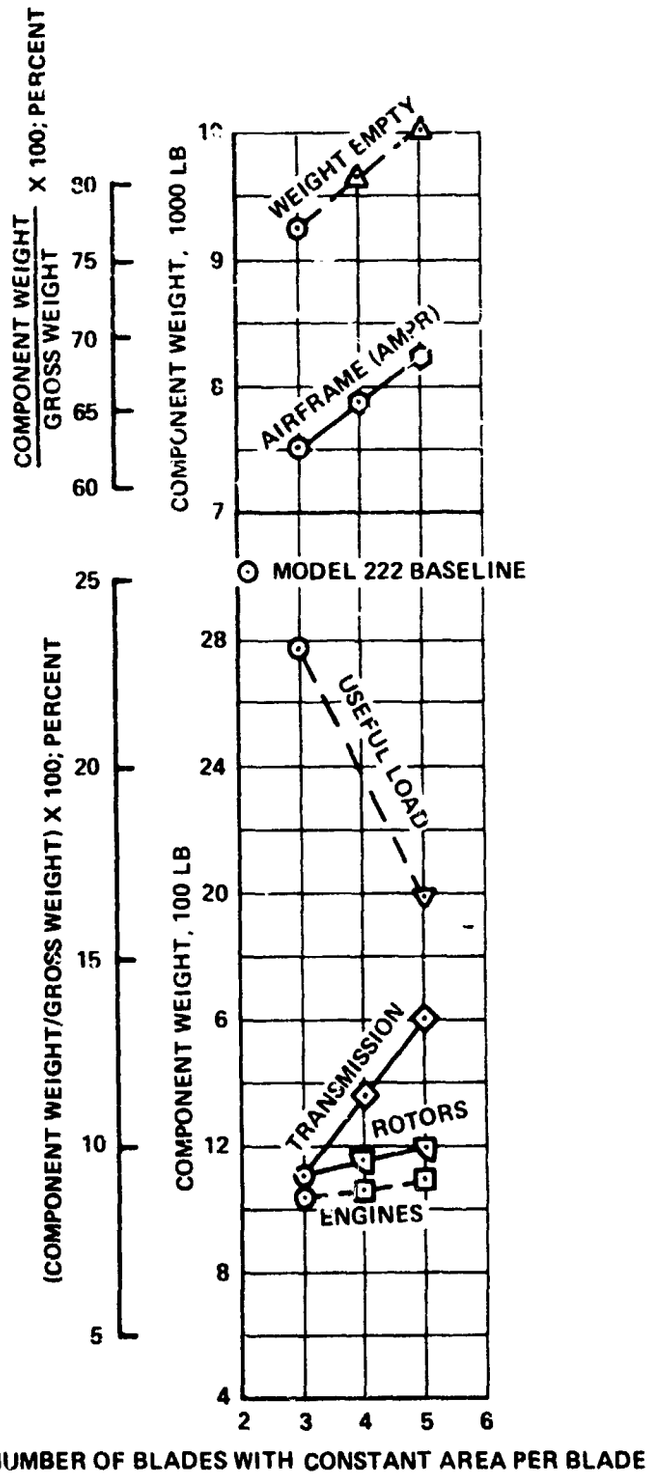

FIGURE 4-16 EFFECT OF NO. OF BLADES WITH CONSTANT AREA/BLADE ON WEIGHT OF TILT-ROTOR SUBSYSTEMS

transmission weight trend shown in Figure 4-15. The importance of this trend is that the increasing weight of the wing and tail group is balanced by the declining weight of the rotor system flight controls and engines (Table 1, Appendix D).

With respect to the variation in the number of blades at constant solidity, the weight empty remains almost constant (Figure 4-15). This is due to the fact that when the number of blades increases while keeping rotor solidity constant, the weights of the rotor and flight control systems are increasing at a faster rate than the rate at which the wing group, engines and drive system weights are declining. However, the magnitude of the variation, ranging from -.208 to .0584 percent of gross weight per blade, is so small that one could neglect it and say that there was no change in weight empty as a function of number of blades at constant rotor solidity.

Weight empty is inversely related to hover tip speed. This is caused by the increasing weight of the engines, rotor system, drive system and flight controls which is only partially offset by a decrease in wing weight due to increased weight relief of wing bending moments.

Increasing rotor solidity for either constant or varying number of blades per rotor causes weight empty to grow. The rate of increase in this case is a result of a large growth in rotor system and flight control system weight and to a smaller extent due to an increase in engine and drive system weight. As in the

previous case, the component weight increases have been somewhat offset by a decrease in wing group weight. Increasing blade number with constant area per blade increases the weight empty by 395 pounds for each additional blade over three.

The airframe weight shown in Figures 4-14 through 4-16 is that defined in the AMPR (Aircraft Manufacturers Planning Report) which is one section of the Cost Information Report.

Far-Field Acoustic Signature. - The acoustic signature discussed in this section occurs under the following conditions:

a. hover OGE

b. noise source (rotors) 100 feet above and 500 feet away from the observer

c. sea level, standard day.

The prediction method used in this section for rotor acoustic signature is based on that used in a previous Boeing-Vertol study (Ref. 2). However, the rotational noise loading law used in the above study has been modified by wind-tunnel test results (Ref. 17). The new loading law is shown in Figure 4-17. A discussion of the accuracy of the theoretical tilt-rotor acoustic model is contained in Appendix E.

The tradeoff slope or senaitivity of overall sound pressure level to the variation of the 5 design parameters is shown in Figures 4-18 and 4-19. The first harmonic of blade passage frequency is a component of the acoustic signature determining, to a large extent, the overall sound pressure level. The magnitude of this major component is a function of:

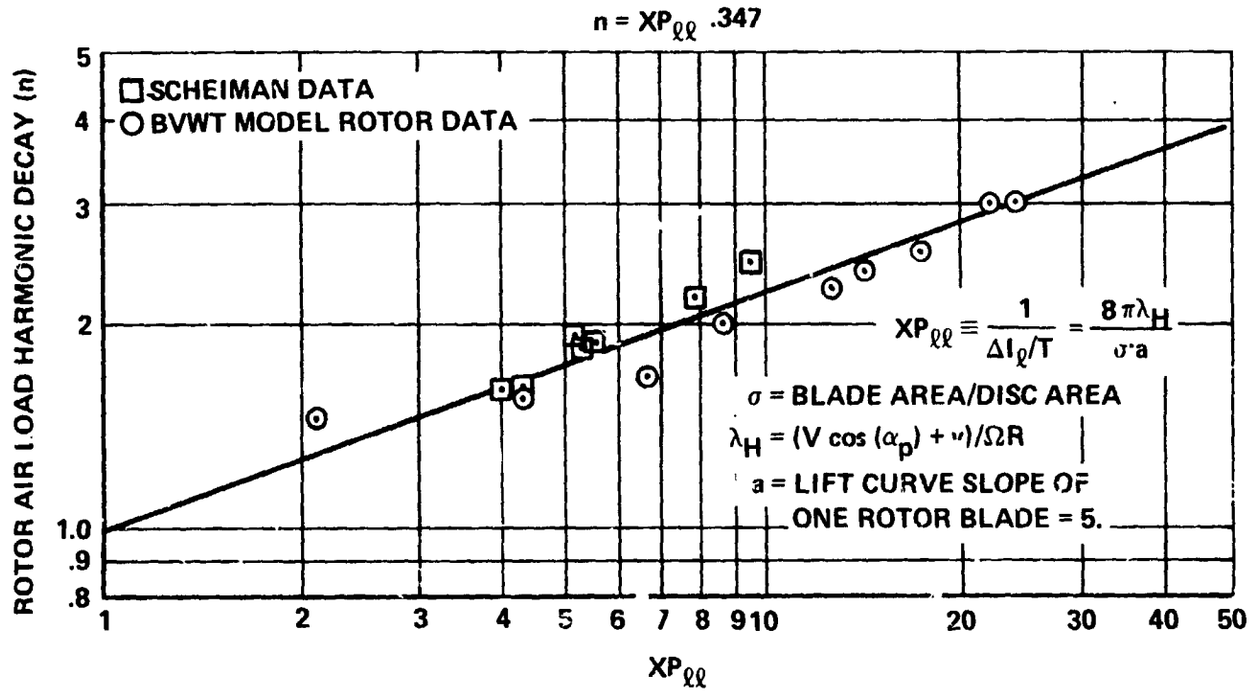

FIGURE 4-17 ROTOR FORCE HARMONIC DECAY (n) AS A FUNCTION OF OPERATING CONDITION

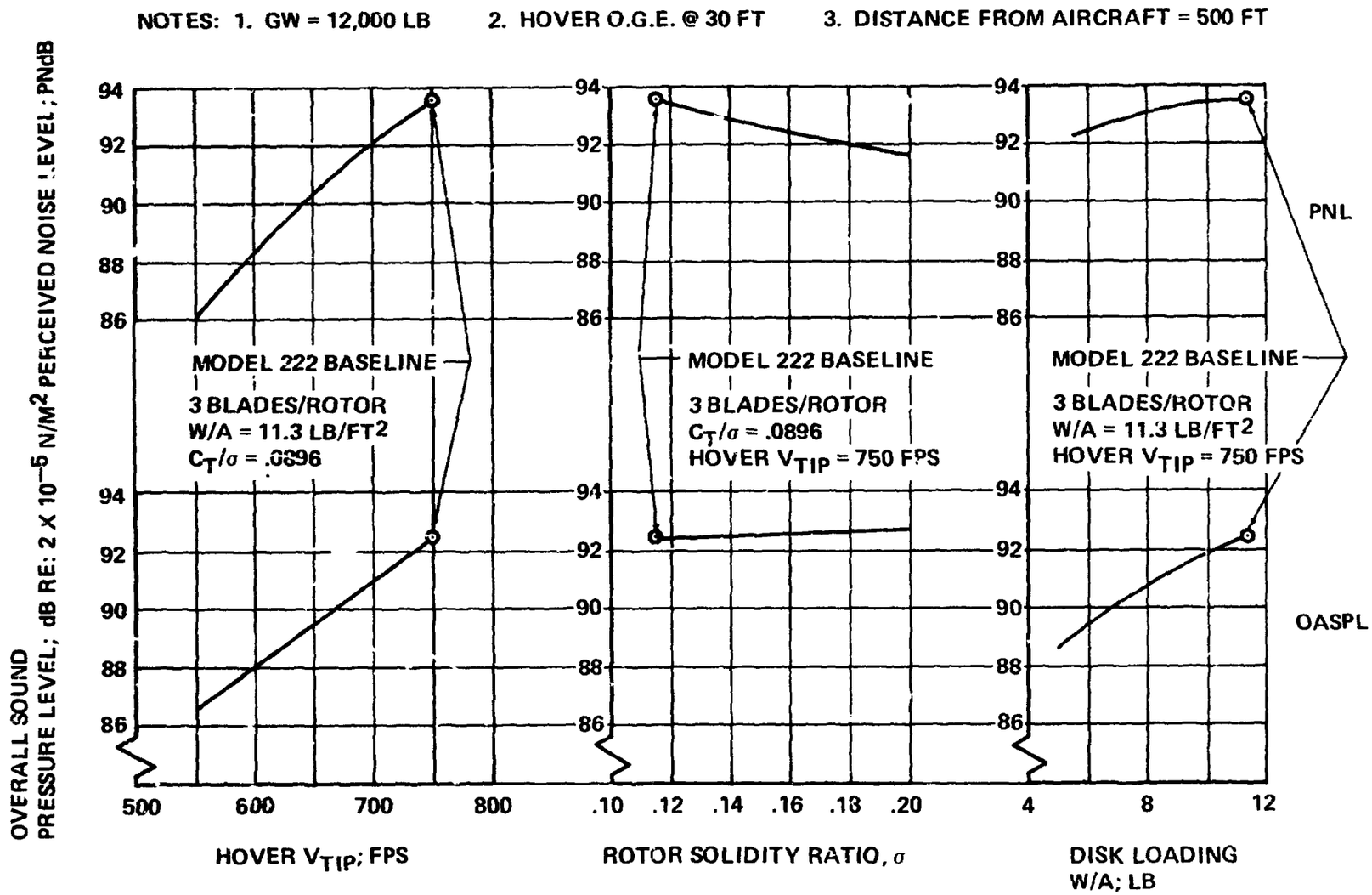

FIGURE 4-18 EFFECT OF 3 DESIGN PARAMETERS ON PERCEIVED NOISE LEVEL AND OVERALL SOUND PRESSURE LEVEL

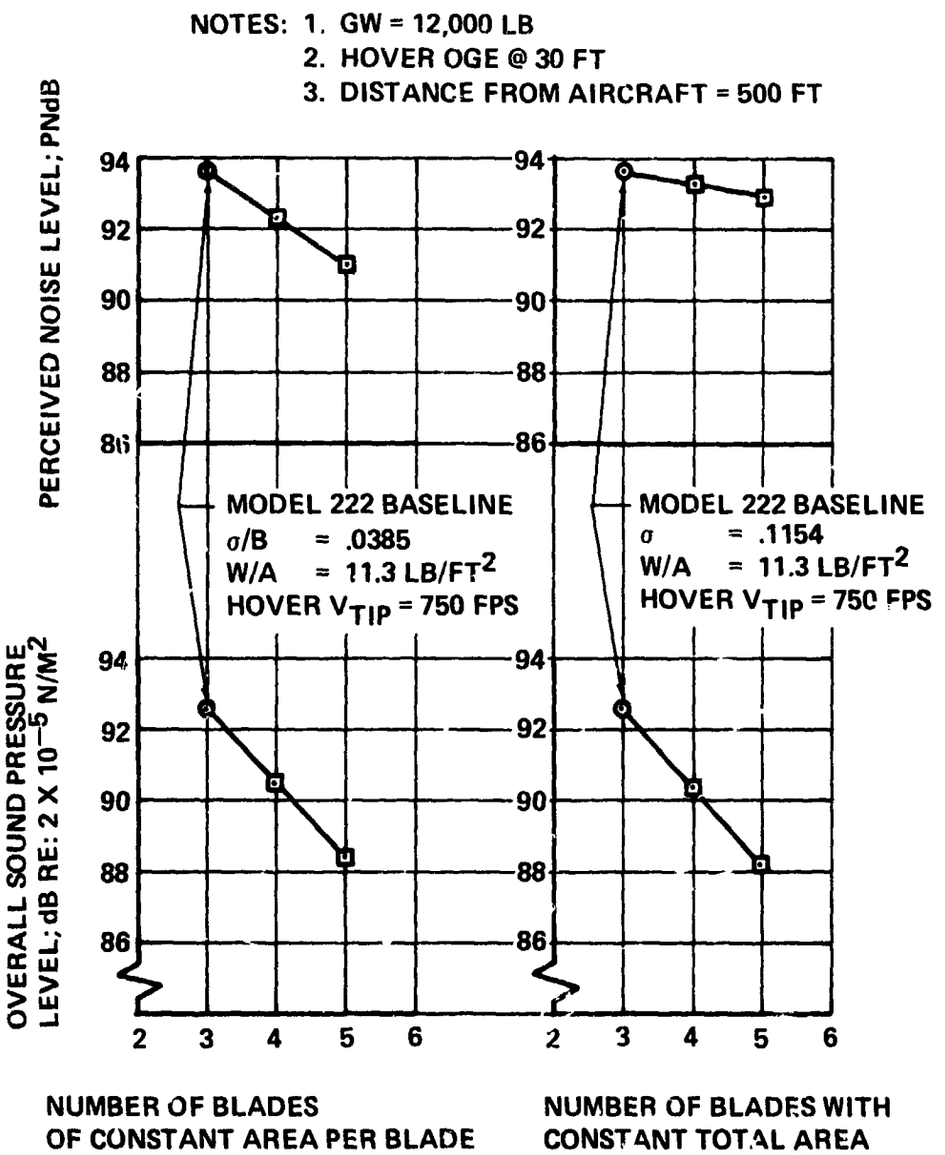

FIGURE 4-19 EFFECT OF NO. OF BLADES ON PERCEIVED NOISE LEVEL AND OVERALL SOUND PRESSURE LEVEL

(a) tip speed
(b) thrust
(c) number of blades per rotor
(d) rotor power
(e) rotor radius
(f) height and distance of source from the observer.

In this study, all acoustic aspects were investigated for constant height (100 feet) and distance (500 feet). However, it should be realized that the relative influence of power and thrust change with the height of the source over the observer for a constant horizontal distance. The rotor power becomes a more important factor as the observer approaches the tip path plane. By contrast, the sensitivity of overall sound pressure level would not be affected by variations in hover power required if the observer was 500 feet directly beneath the rotor.

Broadband noise of the rotor accustic signature is approximately 15-20 dB below the sound pressure level of the first harmonic of blade passage frequency. Thus, the overall sound pressure level is less sensitive to variation of the broadband noise sound pressure level than that of the first harmonic. Overall sound pressure level shows the smallest sensitivity to the variation of rotor solidity at a constant number of blades. Solidity varying from .1154 to .15 causes a .1 dB decrease; then, a further increase in solidity from .15 to .20 results in an increase of .4 dB.

The trend for tip speed reduction shown on Figure 4-18 indicates that the overall sound pressure level decreases with a reduced tip speed, but at smaller increments as the tip speed becomes lower.

Increasing the number of blades per rotor either at a constant or changing rotor solidity, reduced the overall sound pressure level (Figure 4-19).

Figures 4-18 and 4-19 show the effects of the variation of 5 design parameters on perceived noise level. It can be seen that the tip speed at constant C_T/σ is the most effective parameter for reducing the perceived noise level from that of the baseline aircraft. A 37.5 percent reduction in tip speed decreases the perceived noise level by 6.6 PNdB. Increasing the number of blades of constant area per blade is the second most effective parameter for reducing noise.

The effectiveness of the tip speed reduction is due to the spectrum shift to a lower frequency combined with lowering of the spectrum sound pressure level. The frequency weighting of perceived noise level requires that the broadband noise component be weighted more than that of the rotational noise. This depends on the magnitude of the fundamental blade passage frequency. Therefore, as the rotor becomes larger in diameter at a constant tip speed, the rpm drops, and thus, the dependence of PNL on the broadband component grows.

The relative tolerances of the tradeoffs discussed in this section are included in Appendix F.

Additional Design Change. - A promising design parameter other than those analyzed in the previous sections is to be selected for study. The selection process required the study and comparison of unusual or new rotor noise reduction design concepts, and determination of the most promising.

The special devices studied for possible inclusion in this report were:

1. Vertical rotor blade spacing in various planes of rotation and unequal blade azimuth spacing.

2. Tip blowing (linear mass injection causing the rapid tip vortex decay).

3. Owl Wing (leading edge serrations to favorably affect the boundary layer).

4. Special blade tips (discussed in Section II).

The investigation led to the following information about the above-listed concepts. There are some indications that a more favorable tip vortex separation can be achieved by vertical and unequal azimuth blade spacing (Ref. 18). However, no acoustic test data has been published on these concepts as of this writing. John Ward, Principle Investigator, NASA Langley Research Center, indicated that recent acoustic measurements on a small-scale model did not indicate significant changes from the acoustic signature of a conventional arrangement.

Test data on tip blowing has been published (Ref. 19), but the test results refer to a fixed-wing at relatively low tunnel speeds. The tests were performed primarily to determine the tip vortex behavior and very little acoustic information was presented. This concept of tip blowing is scheduled to be tested on a full-scale rotor (UH-1) at Langley Research Center later in 1973.

The owl wing showed very little noise reduction potential at conventional rotor Reynolds Numbers although some benefits were derived at very low Reynolds Numbers (Ref. 20). The maximum reduction obtained was 4 dB OASPL at a very large collective pitch setting of 18° on a zero twist rotor and a Reynolds Number at the tip of 1.59×10^6.

Tip shapes have been extensively discussed in published literature and a large amount of test data has been taken. However, when test data from various sources (Refs 10, 11, and 13) are compared objectively, there does not seem to be any clear-cut improvement over the conventional square tip with a thin airfoil section.

Hence, from the investigation of unconventional rotor designs, it may be concluded that the technical data available were not sufficient to permit ranking of the devices discussed above, nor could an evaluation and comparison of their relative acoustic effectiveness be performed.

V. PARTIAL DERIVATIVES WITH RESPECT TO OPERATIONAL AND DESIGN PARAMETERS

General Remarks

A linearized approach in establishing trends in performance and/or weight tradeoffs vs noise is quite attractive, since it would permit one to superimpose the influences of various operational and/or design parameters. In order to apply this approach, one must know, at the point of interest, values of partial derivatives of various significant quantities with respect to either operational or design parameters. Seven tables of such derivatives in nondimensional form, are presented in this section.

At this point, one must be cautioned that due to strong nonlinearities which may be associated with large excursions in the parameter values, validity of trends established by the linearized approach may be limited to the immediate neighborhood of the point of interest. However, large design parameter excursions from the baseline were necessary to achieve acoustically significant reductions (3dB, 3PNdB) as shown in Figures 4-18 and 4-19. One should also realize that although the derivatives are presented in nondimensional form, the values canrot be consider as general. They were established on the basis of one particular aircraft only, and consequently, they must be applied with caution to other rotary-wing configurations and even to other tilt-wing aircraft.

A comparison of OASPL nondimensional derivatives between test and prediction (Table 5-6) can be made for thrust and tip speed. The test data slopes are taken from Figures 2-5 and 2-10, and the resulting nondimensional derivatives are .28 for tip speed and .084 for thrust. The predicted derivatives (Table 5-6) agree fairly well with measured ones, considering that the measured SPL of the fundamental blade passage frequency was assumed to be directly proportional to the OASPL in the calculation of the measured data derivatives.

NONDIMENSIONAL PARTIAL DERIVATIVES	VALUE
$\frac{\Delta HOVER\ SHP_{REQ}}{HOVER\ SHP_{REQ}} \Big/ \frac{\Delta V_{t_h}}{V_{t_h}}$	-.122
$\frac{\Delta HOVER\ SHP_{REQ}}{HOVER\ SHP_{REQ}} \Big/ \frac{\Delta \sigma}{\sigma}$	.1049
$\frac{\Delta HOVER\ SHP_{REQ}}{HOVER\ SHP_{REQ}} \Big/ \frac{\Delta B}{B}\Big\vert_{\sigma=.1154}$	-.027
$\frac{\Delta HOVER\ SHP_{REQ}}{HOVER\ SHP_{REQ}} \Big/ \frac{\Delta B}{B}\Big\vert_{\sigma/B=.0385}$	.0809
$\frac{\Delta HOVER\ SHP_{REQ}}{HOVER\ SHP_{REQ}} \Big/ \frac{\Delta T}{T}$	1.31
$\frac{\Delta HOVER\ SHP_{REQ}}{HOVER\ SHP_{REQ}} \Big/ \frac{\Delta V_{t_h}}{V_{t_h}}\Big\vert_{C_T/\sigma=.0896}$	-.118
$\frac{\Delta HOVER\ SHP_{REQ}}{HOVER\ SHP_{REQ}} \Big/ \frac{(\Delta W/A)}{(W/A)}\Big\vert_{C_T/\sigma=.0896}$	.149

TABLE 5-1

SENSITIVITY OF $HOVER\ SHP_{REQ}$ @ 2500'93°F
TO DESIGN PARAMETER CHANGES

NONDIMENSIONAL PARTIAL DERIVATIVES	VALUE
$\frac{\Delta .99\ BRS}{.99\ BRS} \Big/ \frac{\Delta V_{th}}{V_{th}}$	.0292
$\frac{\Delta .99\ BRS}{.99\ BRS} \Big/ \frac{\Delta \sigma}{\sigma}$	.00649
$\frac{\Delta .99\ BRS}{.99\ BRS} \Big/ \frac{\Delta B}{B}\Big\vert_{\sigma=.1154}$	-.00584
$\frac{\Delta .99\ BRS}{.99\ BRS} \Big/ \frac{\Delta B}{B}\Big\vert_{\sigma/B=.0385}$	-.0117
$\frac{\Delta .99\ BRS}{.99\ BRS} \Big/ \frac{\Delta T}{T}$	.1776
$\frac{\Delta .99\ BRS}{.99\ BRS} \Big/ \frac{\Delta V_{th}}{V_{th}}\Big\vert_{C_T/\sigma=.0896}$	.1025
$\frac{\Delta .99\ BRS}{.99\ BRS} \Big/ \frac{(\Delta W/A)}{(W/A)}\Big\vert_{C_T/\sigma=.0896}$	.463

TABLE 5-2

SENSITIVITY OF .99 BEST RANGE SPEED
TO DESIGN PARAMETER CHANGES

NONDIMENSIONAL PARTIAL DERIVATIVES	VALUE
$\frac{\Delta TLS}{TLS} \Big/ \frac{\Delta V_{t_h}}{V_{t_h}}$	-.0369
$\frac{\Delta TLS}{TLS} \Big/ \frac{\Delta \sigma}{\sigma}$	-.153
$\frac{\Delta TLS}{TLS} \Big/ \frac{\Delta B}{B}\Big\|_{\sigma=.1154}$	-.02
$\frac{\Delta TLS}{TLS} \Big/ \frac{\Delta B}{B}\Big\|_{\sigma/B=.0385}$	-.163
$\frac{\Delta TLS}{TLS} \Big/ \frac{\Delta T}{T}$	0.0
$\frac{\Delta TLS}{TLS} \Big/ \frac{\Delta V_{t_h}}{V_{t_h}}\Big\|_{C_T/\sigma=.0896}$	.0616
$\frac{\Delta TLS}{TLS} \Big/ \frac{(\Delta W/A)}{(W/A)}\Big\|_{C_T/\sigma=.0896}$	.390

TABLE 5-3

SENSITIVITY OF HOVER RPM TRANSMISSION LIMIT SPEED TO DESIGN PARAMETER CHANGES

NONDIMENSIONAL PARTIAL DERIVATIVES	VALUE
$\frac{\Delta WE}{WE} \Big/ \frac{\Delta V_{th}}{V_{th}}$	0.0
$\frac{\Delta WE}{WE} \Big/ \frac{\Delta \sigma}{\sigma}$	.124
$\frac{\Delta WE}{WE} \Big/ \frac{\Delta B}{B}\Big\|_{\sigma=.1154}$	-.00813
$\frac{\Delta WE}{WE} \Big/ \frac{\Delta B}{B}\Big\|_{\sigma/B=.0385}$	.128
$\frac{\Delta WE}{WE} \Big/ \frac{\Delta T}{T}$	0.0
$\frac{\Delta WE}{WE} \Big/ \frac{\Delta V_{th}}{V_{th}}\Big\|_{C_T/\sigma= .0896}$	-.248
$\frac{\Delta WE}{WE} \Big/ \frac{(\Delta W/A)}{(W/A)}\Big\|_{C_T/\sigma= .0896}$	.00607

TABLE 5-4

SENSITIVITY OF WEIGHT EMPTY
TO DESIGN PARAMETER CHANGES

NONDIMENSIONAL PARTIAL DERIVATIVES	VALUE
$\frac{\Delta PAYLOAD}{PAYLOAD} / \frac{\Delta V_{th}}{V_{th}}$	-.184
$\frac{\Delta PAYLOAD}{PAYLOAD} / \frac{\Delta \sigma}{\sigma}$	-1.078
$\frac{\Delta PAYLOAD}{PAYLOAD} / \frac{\Delta B}{B}\Big\|_{\sigma=.1154}$	.0601
$\frac{\Delta PAYLOAD}{PAYLOAD} / \frac{\Delta B}{B}\Big\|_{\sigma/B=.0385}$	-1.086
$\frac{\Delta PAYLOAD}{PAYLOAD} / \frac{\Delta T}{T}$	.804
$\frac{\Delta PAYLOAD}{PAYLOAD} / \frac{\Delta V_{th}}{V_{th}}\Big\|_{C_T/\sigma=.0896}$	1.88
$\frac{\Delta PAYLOAD}{PAYLOAD} / \frac{(\Delta W/A)}{(W/A)}\Big\|_{C_T/\sigma=.0896}$	-.357

TABLE 5-5

SENSITIVITY OF MISSION PAYLOAD
TO DESIGN PARAMETER CHANGES

NONDIMENSIONAL PARTIAL DERIVATIVES	VALUE
$\frac{\Delta OASPL}{OASPL} \Big/ \frac{\Delta V_{th}}{V_{th}}$	.243
$\frac{\Delta OASPL}{OASPL} \Big/ \frac{\Delta \sigma}{\sigma}$	-.000721
$\frac{\Delta OASPL}{OASPL} \Big/ \frac{\Delta B}{B}\Big\vert_{\sigma=.1154}$	-.0681
$\frac{\Delta OASPL}{OASPL} \Big/ \frac{\Delta B}{B}\Big\vert_{\sigma/B=.0385}$	-.0649
$\frac{\Delta OASPL}{OASPL} \Big/ \frac{\Delta T}{T}$	.1038
$\frac{\Delta OASPL}{OASPL} \Big/ \frac{\Delta V_{th}}{V_{th}}\Big\vert_{C_T/\sigma=.0896}$	.235
$\frac{OASPL}{OASPL} \Big/ \frac{(\Delta W/A)}{(W/A)}\Big\vert_{C_T/\sigma=.0896}$	.0151

TABLE 5-6

SENSITIVITY OF OVERALL SOUND PRESSURE LEVEL
TO DESIGN PARAMETER CHANGES

NONDIMENSIONAL PARTIAL DERIVATIVES	VALUE
$\frac{\Delta PNL}{PNL} \Big/ \frac{\Delta V_{th}}{V_{th}}$	.176
$\frac{\Delta PNL}{PNL} \Big/ \frac{\Delta \sigma}{\sigma}$	-.0213
$\frac{\Delta PNL}{PNL} \Big/ \frac{\Delta B}{B}\Big\vert_{\sigma=.1154}$	-.00362
$\frac{\Delta PNL}{PNL} \Big/ \frac{\Delta B}{B}\Big\vert_{\sigma/B=.0385}$	-.0353
$\frac{\Delta PNL}{PNL} \Big/ \frac{\Delta T}{T}$	.1026
$\frac{\Delta PNL}{PNL} \Big/ \frac{\Delta V_{th}}{V_{th}}\Big\vert_{C_T/\sigma = .0896}$	.224
$\frac{\Delta PNL}{PNL} \Big/ \frac{(\Delta W/A)}{(W/A)}\Big\vert_{C_T/\sigma=.0896}$	.00428

TABLE 5-7

SENSITIVITY OF PERCEIVED NOISE LEVEL
TO DESIGN PARAMETER CHANGES

VI. CONCEPTUAL DESIGN OF QUIET TILT-ROTOR AIRCRAFT

Approach

This section covers the problems of reducing the signature of the baseline rotor design by: (1) -10 dB OASPL and (2) -10 PNdB, while maintaining a specified payload over a radius of 100 n.mi. and performing the mission defined in Section IV. The three parameters shown in Section IV to be most effective in changing the rotor acoustic signature are: (1) number of blades at constant solidity, (2) tip speed (V_t) at constant C_T/σ, and (3) hover disc loading (W/A) at constant C_T/σ. When these parameters are varied, the gross weight will change from that of the Model 222.

In this section, an effort is presented of designing for a specified noise level while pursuing the traditional design goals of performance, flying qualities, and structural flight envelope.

Criteria

All aircraft shall carry the reference aircraft payload (1298 pounds) for the design study mission as shown in Figure 4-1. One design shall have a PNL 10 PNdB lower than that of the Model 222 and the other one, an OASPL 10 dB less than that of the baseline aircraft. For convenience, the design shall be designated throughout the rest of the report as M222-10 PNdB and M222-10 dB OASPL. The two aircraft shall have

tail volume coefficients and overall fuselage dimensions identical to that of the Model 222. The engine and transmission sizing requirements as stated in Section IV shall be met by all aircraft. The landing gear shall be able to withstand a vertical sink speed of 14 fps. The study structural limits which remain the same as for the baseline aircraft are: (1) V_{MO} = 350 knots EAS, (2) V_{dive} = 350 knots EAS, (3) M_{MO} = .569, and (4) wing design maneuver load factor of 3 g's.

The wing chord shall be a function of gross weight only. The rotor diameter plus fuselage and rotor fuselage clearance will determine the wing span. The wing sizing criteria stated above is identical to that used in Section IV. The tilt-rotor has no need to maintain a specific wing chord to rotor diameter ratio as other convertible aircraft, because the wing does not contribute a significant portion of lift in low-speed flight. Thus, the wing loading may be designed for cruise only, except as limited by the placement of the rotors at the wing tips and the requirement of sufficient thickness to support the fuselage in near-hovering flight.

The engine specific fuel consumption shall be increased by 5 percent as required in MIL-C-5011A. The engine performance shall be scalable from that of the Lycoming T53-L13.

The end result of the above criteria is that the two new aircraft(M222-10 PNdB and M222-10 dB OASPL) will be similar in external appearance; however, rotors and wings as well as performance characteristics differ from the M222 model as defined in Ref. 1.

Quiet Aircraft Selection

The three rotor parameters were varied one at a time in the direction shown in Section IV to be most effective. The disc loading of the baseline was reduced to one-half its original value in two equal steps. The hover tip speed was reduced by 100 fps increments from the baseline. Then, the above matrix of rotor design was repeated for 4 and 5 blades per rotor. Thus, 27 designs were evaluated. The final selection of an aircraft meeting each acoustic criteria was made on the basis of minimum design gross weight.

The process of selecting the minimum design gross weight was facilitated by the three figures (Figures 6-1, -2 and -3) showing the variation of design gross weight as a function of hover tip speed and disc loading (W/A) for 3, 4 and 5 blades per rotor. Also, shown on these figures are the lines of constant PNL and OASPL which are 10 dB lower than that of the baseline aircraft. In Figure 6-1, however, the OASPL - 10 dB line is missing because it does not occur in the range of parameters investigated. This graphical optimization method not only shows the minimum, but also the parameter values about the minimum, thus determining the penalty involved in a nonoptimum design.

Description of New Designs

The selected aircraft have a lower disc loading, a larger number of blades per rotor, and higher design gross weight than the reference model. The aircraft with a reduced overall sound

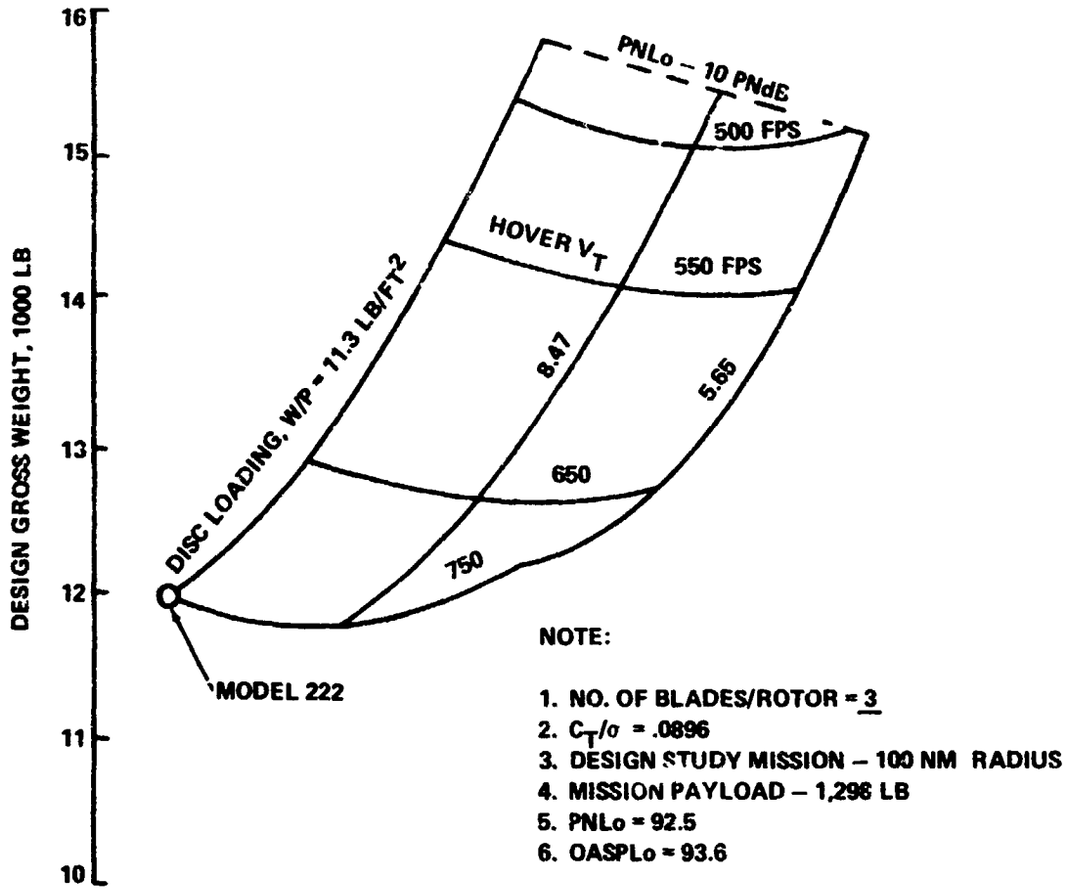

FIGURE 6-1 TILT-ROTOR DESIGN SELECTION CHART
(3 BLADES PER ROTOR)

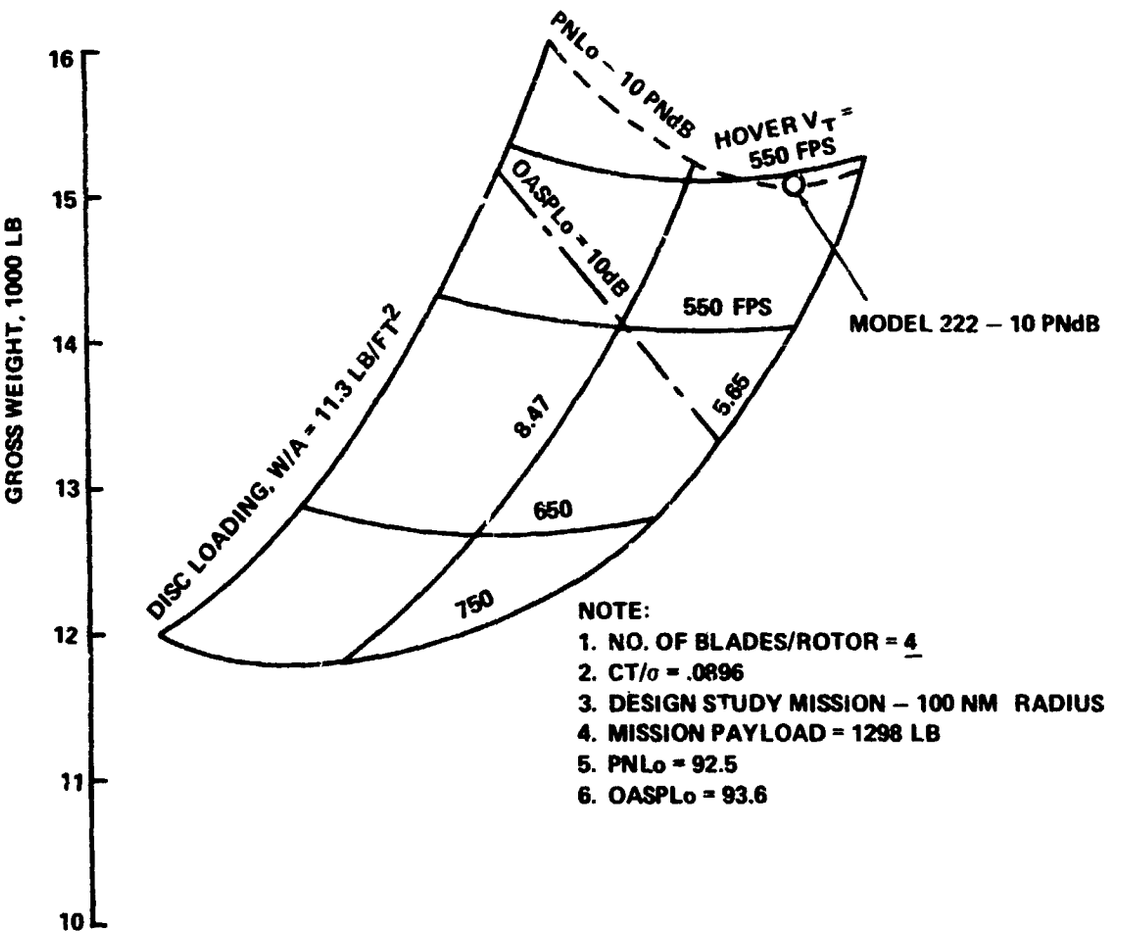

FIGURE 6-2 TILT-ROTOR DESIGN SELECTION CHART
(4 BLADES PER ROTOR)

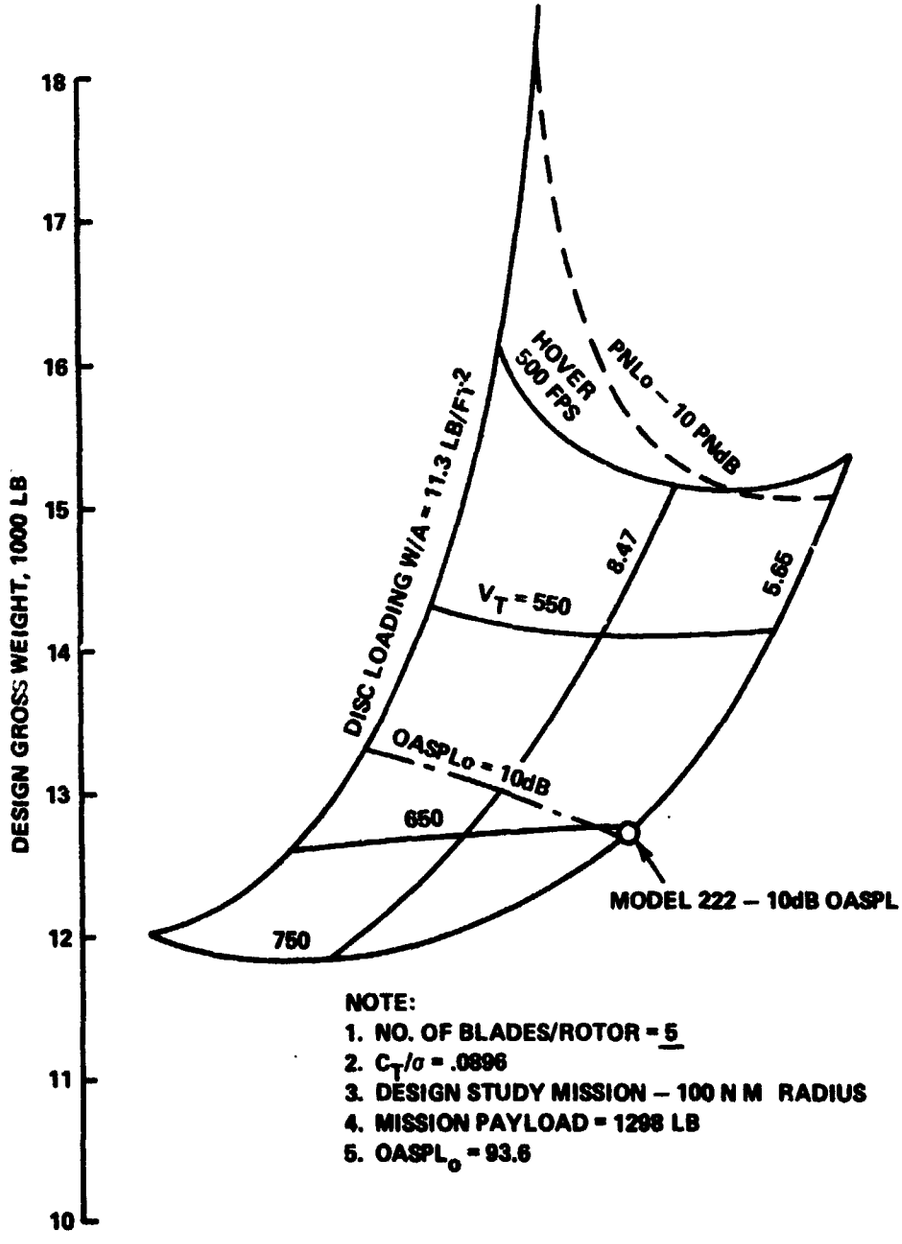

FIGURE 6-3 TILT-ROTOR DESIGN SELECTION CHART
(5-BLADES PER ROTOR)

[illegible] pressure level [illegible] dB OASPL. [illegible] 3 blades per rotor and a design gross weight of [illegible] 11,711 pounds. The aircraft meeting a noise goal [illegible] level M222-10 PNdB has a rotor diameter of [illegible] blades per rotor and a design gross weight of [illegible] pounds. The two aircraft are depicted in three-view sketches [illegible] and SK 25111, respectively.

A comparison of the summary weight statements for the baseline aircraft and the two new aircraft is presented in Table [illegible]. The greatest relative increase (in percentage) of component weight of M222-10 dB OASPL and M222-10 PNdB occur in the rotor (11 and 58 percent, respectively), wing ([illegible] percent), empennage (43, 70 percent), flight controls and the drive system (15, 82.5 percent). This is offset by a decrease in engine weight (43, 4 percent), and mission fuel for the M222-10 dB OASPL (13 percent).

Tables 6-2 and 6-3 show the mass properties of M222-10 dB OASPL and M222-10 PNdB, respectively. In both aircraft, because of larger and heavier rotors, wing and nacelles, the roll and yaw inertias increased from the M222 mass properties shown in Table G-2, Appendix G. In the case of M222-10 dB OASPL, the nacelle horizontal roll and yaw inertias are 182 and 172 percent of the baseline aircraft. The nacelle vertical (helicopter configuration) roll and yaw inertias undergo similar increases. The much greater inertias about the two axes of the 2 quiet aircraft will result in lower acceleration

	MODEL 222	MODEL 222 - 10 dB OASPL	MODEL 222 - 10 PNdB			
ROTOR GROUP	1100	1211	1743			
WING GROUP	800	1402	1416			
TAIL GROUP	213	305	361			
BODY GROUP	1211	1274	1282			
BASIC						
SECONDARY						
SECOND.-DOORS, ETC.						
ALIGHTING GEAR	590	623	737			
FLIGHT CONTROLS	1183	1262	1623			
ENGINE SECTION	400	400	400			
PROPULSION GROUP	(2533)	(2387)	(3405)			
ENGINES(S)	1026	718	988			
AIR INDUCTION						
EXHAUST SYSTEM	200	200	200			
COOLING SYSTEM						
LUBRICATING SYSTEM						
FUEL SYSTEM	200	200	200			
ENGINE CONTROLS						
STARTING SYSTEM						
PROPELLER INST.						
*DRIVE SYSTEM	1107	1269	2017			
AUX. POWER PLANT						
INSTR. AND NAV.	108	108	108			
HYDR. AND PNEU.						
ELECTRICAL GROUP	305	305	305			
ELECTRONICS GROUP	230	230	230			
ARMAMENT GROUP						
FURN. & EQUIP. GROUP	(439)	(439)	(439)			
PERSON., ACCOM.	299	299	299			
MISC. EQUIPMENT	63	63	63			
FURNISHINGS	35	35	35			
EMERG. EQUIPMENT	42	42	42			
AIR COND. & DE-ICING	108	108	108			
PHOTOGRAPHIC						
AUXILIARY GEAR	10	10	10			
MFG. VARIATION						
WEIGHT EMPTY	9230	10064	12167			
FIXED USEFUL LOAD	(400)	(400)	(400)			
CREW (2)	360	360	360			
TRAPPED LIQUIDS	40	40	40			
ENGINE OIL						
FUEL	1072	945	1180			
CARGO and/or	1298	1298	1298			
PASSENGERS/TROOPS						
GROSS WEIGHT	12000	12707	15045			

TABLE 6-1 SUMMARY WEIGHT STATEMENT COMPARISON

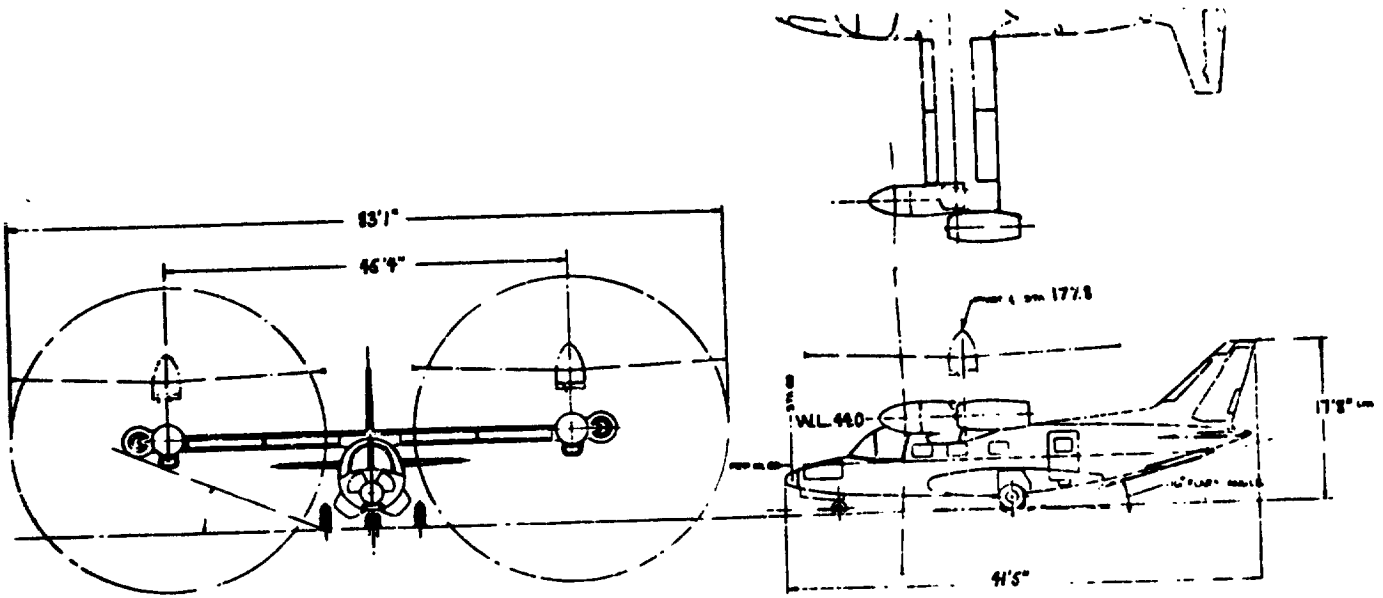

SUB-GROUPS	NACELLE HORIZ. BALANCE WEIGHT	X (F.S.)	Y (B.L.)	Z (W.L.)	INERTIA - SLUG PT.² I_{XX} (ROLL)	I_{YY} (PITCH)	I_{ZZ} (YAW)	NACELLE VERTICAL BALANCE X (P.S.)	Y (B.L.)	Z (W.L.)	INERTIA - SLUG FT² I_{XX} (ROLL)	I_{YY} (PITCH)	I_{ZZ} (YAW)
[1]FUSE & CONTENTS													
FWD	164	14.2		- 19.6	6	12	12						
CENTER	2723	140.4		- 7.9	384	2371	2371						
AFT	376	304.0		.6	36	264	264						
[2]HORIZONTAL TAIL	223	413.3	30.7	18.5	20	13	31	SAME					
[3]VERTICAL TAIL	190	395.3		63.5	24	66	42						
[4]WING/CONTENTS	2091	171.2	137.5	41.0	1956	260	2120						
[5]NACELLE & CONTENTS	4697	141.6	278.6	45.3	241	997	1031	174.1	278.6	175.7	1031	997	241
OPER. WT. EMPTY	10464	181.4		27.7	91288	13779	101582	176.0		41.4	93645	14622	100069
FUEL - INBOARD	946	171.3	93.0	40.5	442	64	606						
- OUTBOARD													
CARGO	1298	171.3		.5	600	450	315						
DESIGN GROSS WEIGHT	12707	163.2		25.9	94312	14500	104262	175.2		37.1	96915	15579	102736

NOTE: ROTOR BLADE INERTIAS (I_o)
BLADE WT. EA. (WITH CUFF) I_{XX} (ROLL) I_{YY} (PITCH) I_{ZZ} (YAW) SLUG FT²

TABLE 6-2 M222-10 dB OASPL MASS PROPERTIES

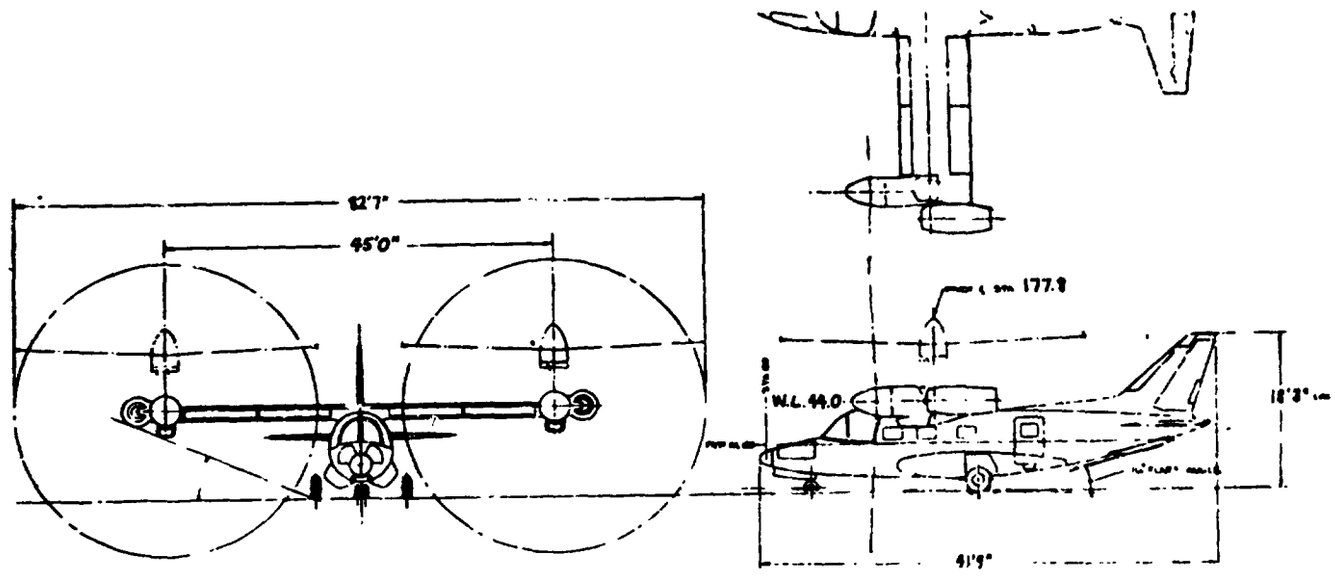

		NACELLE HORIZ.						NACELLE VERTICAL					
		BALANCE			INERTIA - SLUG PT.^{2}			BALANCE			INERTIA - SLUG FT.^{2}		
SUB-GROUPS	WEIGHT	X (F.S.)	Y (B.L.)	Z (W.L.)	I_{XX} (ROLL)	I_{YY} (PITCH)	I_{ZZ} (YAW)	X (F.S.)	Y (B.L.)	Z (W.L.)	I_{XX} (ROLL)	I_{YY} (PITCH)	I_{ZZ} (YAW)
°FUSE & CONTENTS													
FWD	166	14.2		-19.6	6	12	12						
CENTER	2949	140.4		-7.9	384	2371	2371						
AFT	380	304.0		0.6	36	264	264						
°HORIZONTAL TAIL	257	438.0	55.0	15.0	23	76	38			SAME			
°VERTICAL TAIL	215	430.8		89.0	24	66	66						
°WING/CONTENTS	2192	169.4	137.5	40.5	1956	260	2120						
°NACELLE & CONTENTS	6408	140.5	278.6	44.8	363	1507	1730	178.6	278.6	79.5	1730	1507	363
OPER. WT. EMPTY	12507	159.8		29.6	120P92	17131	134071	179.3		47.3	124529	18280	131584
FUEL - INBOARD	1181	171.3	93.0	40.5	482	70	666						
- OUTBOARD													
CARGO	1297	171.3		0.5	600	450	315						
DESIGN GROSS WEIGHT	15045	161.7		28.0	124303	17918	137310	178.0		42.8	128310	19302	134778

NOTE: ROTOR BLADE INERTIAS (I_o)
BLADE WT. EA. (WITH CUFF) I_{XX} (ROLL) I_{YY} (PITCH) I_{ZZ} (YAW) SLUG FT^2

TABLE 6-3 M222-10 PNdB MASS PROPERTIES

than for the Model 222. Flying qualities have not been investigated in this study. Thus, the pilot acceptance is unknown. However, an effort was made to keep the flying qualities similar to the original model by the sizing constraint of constant tail control volumes. Nevertheless, each aircraft has different characteristics.

Performance

The performance estimates for the reference aircraft and the two designs with acoustic constraints were made in the following areas:

1. Rotor hover performance (Figure 6-4)
2. Level flight power required (Figure 6-5)
3. Mission payload - radius (Figure 6-6)
4. Mission productivity as a function of range (Figure 6-7).

The design hover Figure-of-Merit for the three aircraft are:

1. M222 FM = .757
2. M222 - 10 dB OASPL FM = .796
3. M222 - 10 PNdB FM = .751

The above Figures of Merit correspond to the design points shown in Figure 6-4. This figure indicates that no large hover/performance penalty is encountered by a quiet design. However, the same cannot be said for cruise performance, as the aircraft propeller efficiencies decrease from the baseline values for the design condition of 300 knots, 10,000 feet Standard Day.

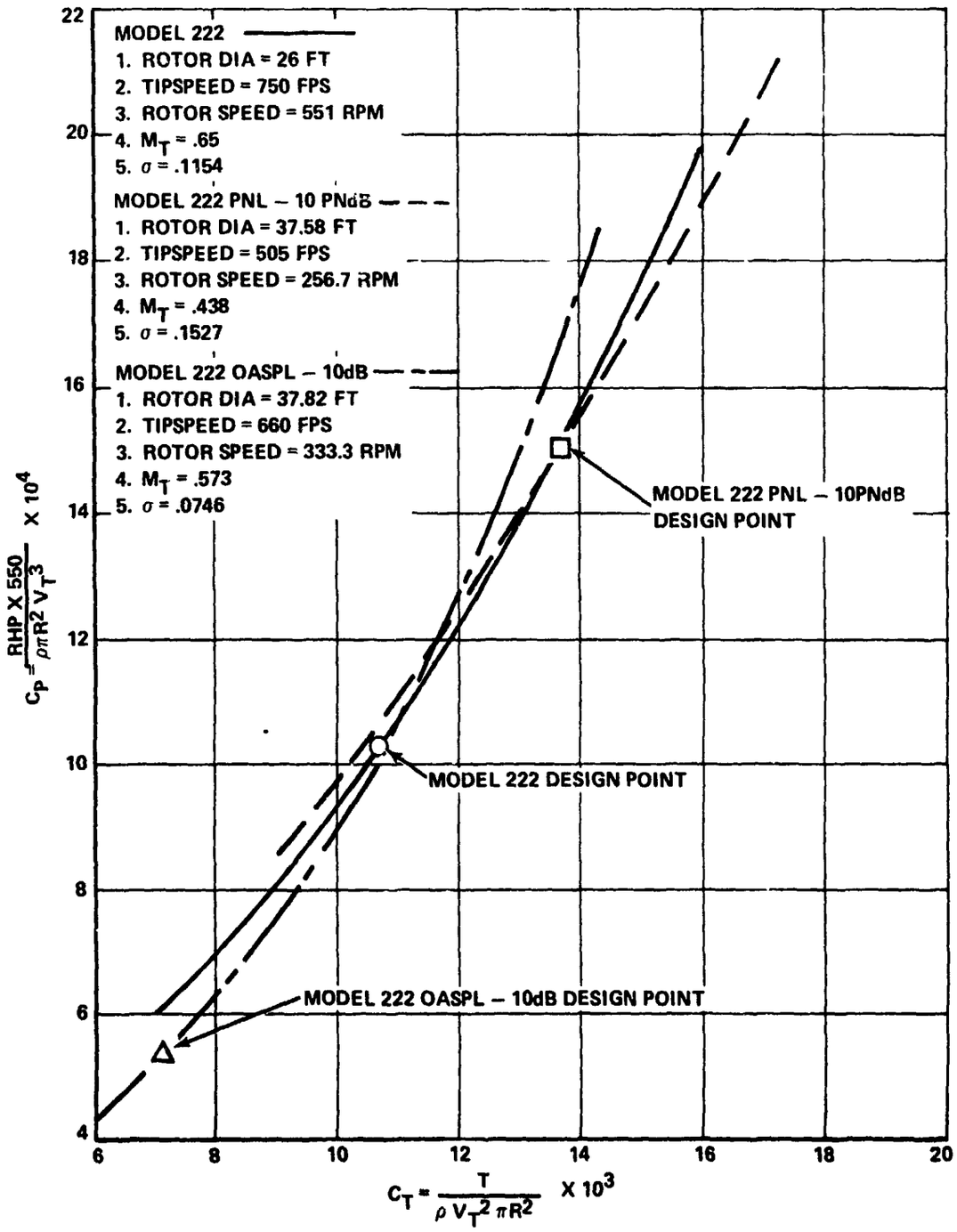

FIGURE 6-4 COMPARISON OF ROTOR HOVER PERFORMANCE

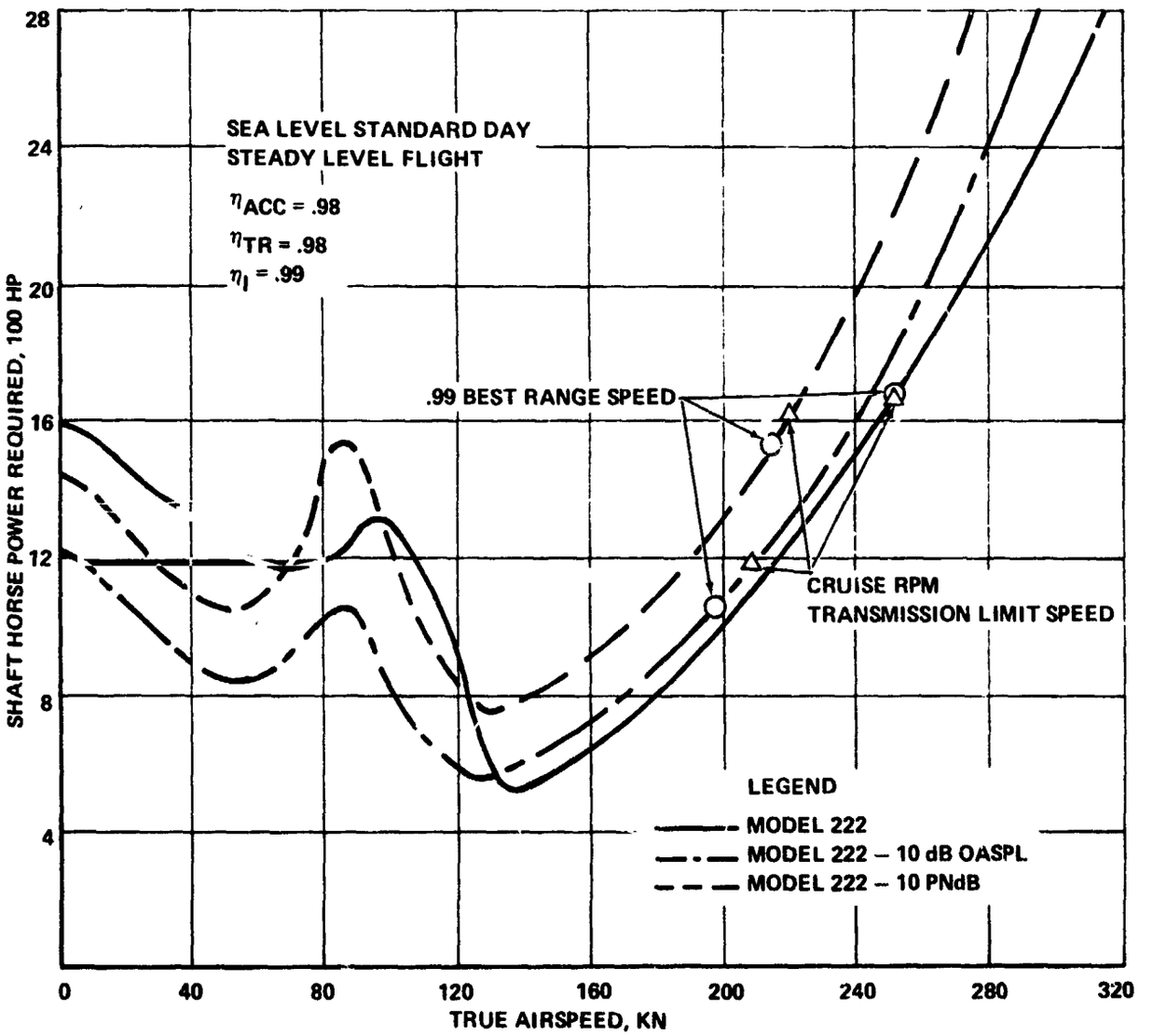

FIGURE 6-5 EFFECT OF AIRCRAFT DESIGN FOR NOISE REDUCTION ON POWER REQUIRED

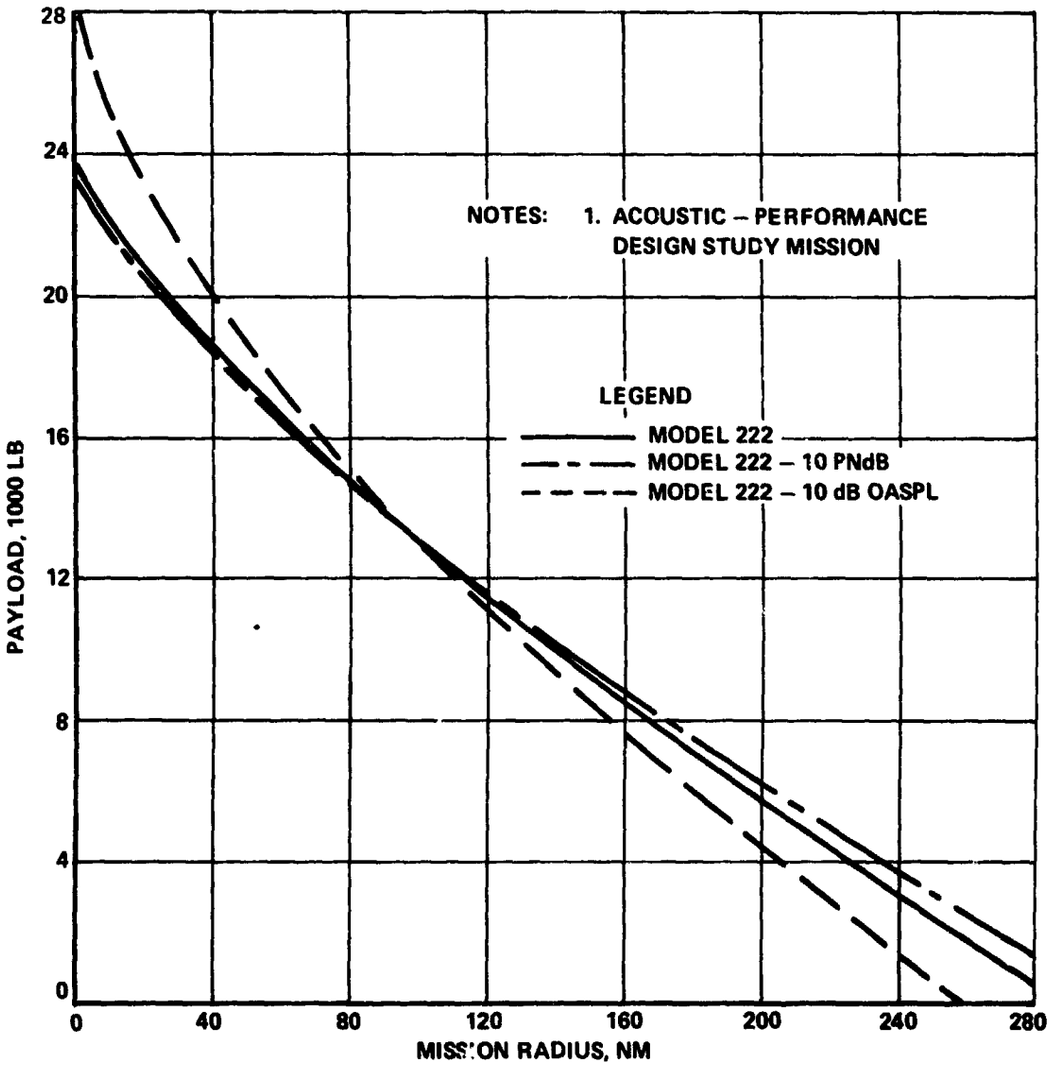

FIGURE 6-6 PAYLOAD VS RADIUS COMPARISONS OF STANDARD AND NOISE REDUCTION DESIGNS

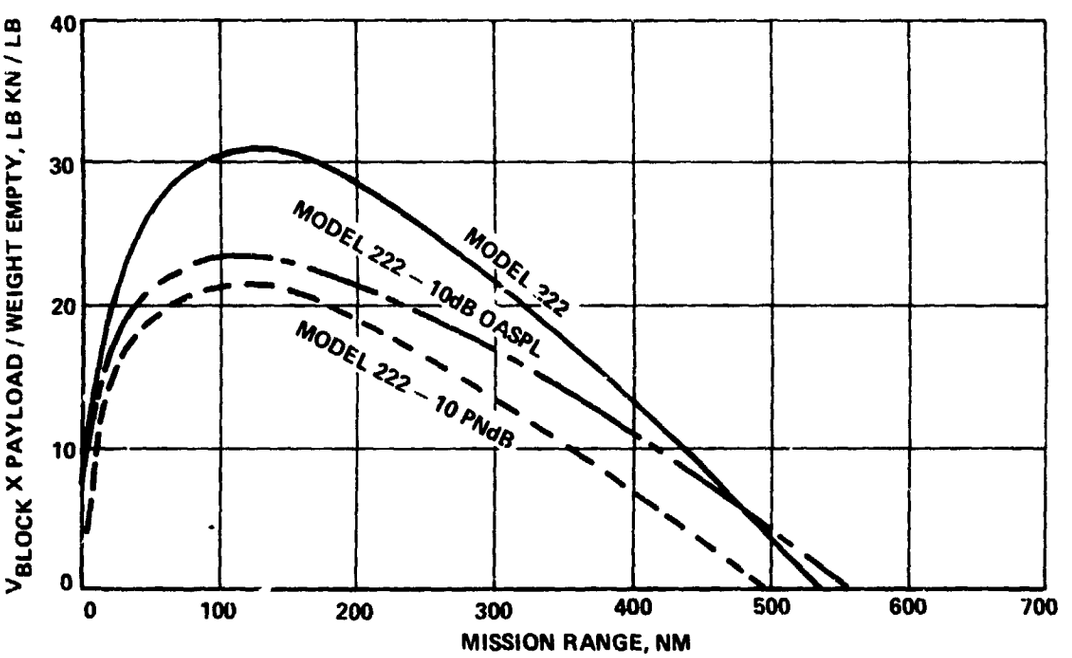

FIGURE 6-7 COMPARISON OF MISSION PRODUCTIVITY

	M222	η_p = .71
2.	M222 - 10 dB OASPL	η_p = .728
3.	M222 - 10 PNdB	η_p = .683

The comparison of level flight power required (Figure 6-5) shows that the common performance ground rules chosen for this study result in balanced design, as all three aircraft have a .99 best range speed (cruise condition) very close to the cruise rpm transmission limit. Taking into account the differences in parasite drag, wing span loading, rotor area to wing area ratio and hover disc loading, the only unusual item in the comparison is the relative increase in power required through conversion with respect to that in hover, as the design hover tip speed is decreased (M222, V_{t_h} = *750 fps;* M222 - 10dB OASPL, V_{t_h} = *660 fps;* and M22 - 10 PNdB, V_{t_h} = *505 fps*). The transition power required increase occurs at advance ratios $(V/V_t) \approx .20$ and a nacelle angle of $\approx$ *45 degrees*. The increasing power is attributable to *retreating blade stall* despite the rotor blade area increasing as the square of the reduction of design hover tip speed.

Design approaches for reducing power required through conversion are: (1) lower the C_T/σ, (2) decrease wing loading, and/or (3) incorporate sophisticated high-lift devices on the wing. The above design alternatives penalize the aircraft performance and weight. The two new aircraft have had their wing area increased over that of the baseline (Table 6-4), but not enough to permit conversion to the airplane mode at sufficiently low speeds to

CONFIGURATIONS	CERL [illegible]	[illegible]	[illegible]
ITEM	BASELINE	[illegible]	[illegible]
ROTOR			
Rotor Radius, Ft.	[illegible]	[illegible]	
No. of Blades	[illegible]	[illegible]	
Tip Speed, FPS	[illegible]	[illegible]	
σ	.1284	[illegible]	
Disc Loading, LB FT^2	11.3	[illegible]	
WING			
Wing Area, FT^2	[illegible]	[illegible]	[illegible]
Wing Span, Ft.	33.42	[illegible]	[illegible]
Aspect Ratio	[illegible]	[illegible]	
Taper Ratio, $\frac{C_T}{C_R}$	[illegible]	[illegible]	[illegible]
HORIZONTAL TAIL			
Area, $Ft.^2$	58.3	[illegible]	[illegible]
Span, Ft.	[illegible]	19.8	[illegible]
Aspect Ratio	4.22	[illegible]	[illegible]
Taper Ratio	.337	[illegible]	[illegible]
Tail Volume Coeff.	[illegible]	[illegible]	[illegible]
Moment Arm, Ft.	20.3	20.3	[illegible]
VERTICAL TAIL			
Area, $Ft.^2$	43.3	[illegible]	[illegible]
Span, Ft.	8.12	[illegible]	[illegible]
Aspect Ratio	1.52	[illegible]	[illegible]
Taper Ratio, $\frac{C_T}{C_R}$	.329	[illegible]	[illegible]
Tail Volume Coeff.	.127	[illegible]	[illegible]
Moment Arm, Ft.	19.55	19.6	[illegible]
NO. OF ENGINES	2	2	2
SHP*/ENGINE	1550.	1100.	1510.
XMSN HP LIMIT/ROTOR	1150.	820.	1125.
fe, $Ft.^2$	6.279	7.404	[illegible]
HOVER OGE, 100 FT. ALT.			
OASPL @ 500 Ft.	92.5	79.4	[illegible]
PNL @ 500 Ft.	93.6	83.6	[illegible]

TABLE 6-4

avoid an increase in power required. It is left to a more detailed study to determine the optimum design of the wing and rotor in the conversion flight regime.

The payload vs mission radius comparison (Figure 6-6) illustrates that as a result of the common performance ground rules adopted in this study, the capability of all three aircraft does not vary widely. The same cannot be said of the comparison of mission productivity (Figure 6-7) where the productivity of the noise constrained designs is lower than that of the Model 222.

Far Field Acoustic Signatures

The two noise constrained designs have sound absorptive linings in the inlets of the engines. Thus, the rotor spectrum represents the major influence in determining either OASPL or PNL. Acoustic signature resulting from engine inlet treatment and rotor design in hover is shown in Figures 6-8 through 6-10. As a result of the design changes, the aircraft acoustic directivity pattern also changes from that of the baseline aircraft (Figure 6-11). A comparison of the relative aural detectability of the baseline and the two noise constrained designs in airplane configuration level flight is shown in Figure 6-12. The baseline aircraft (Model 222) is shown to be less detectable (shorter detection distance) at some airspeeds than the design with reduced OASPL. The aural detection distance for the tilt-rotor aircraft in this study is set by the broadband component of the rotor spectrum (typically, the 315 Hz, 1/3-octave

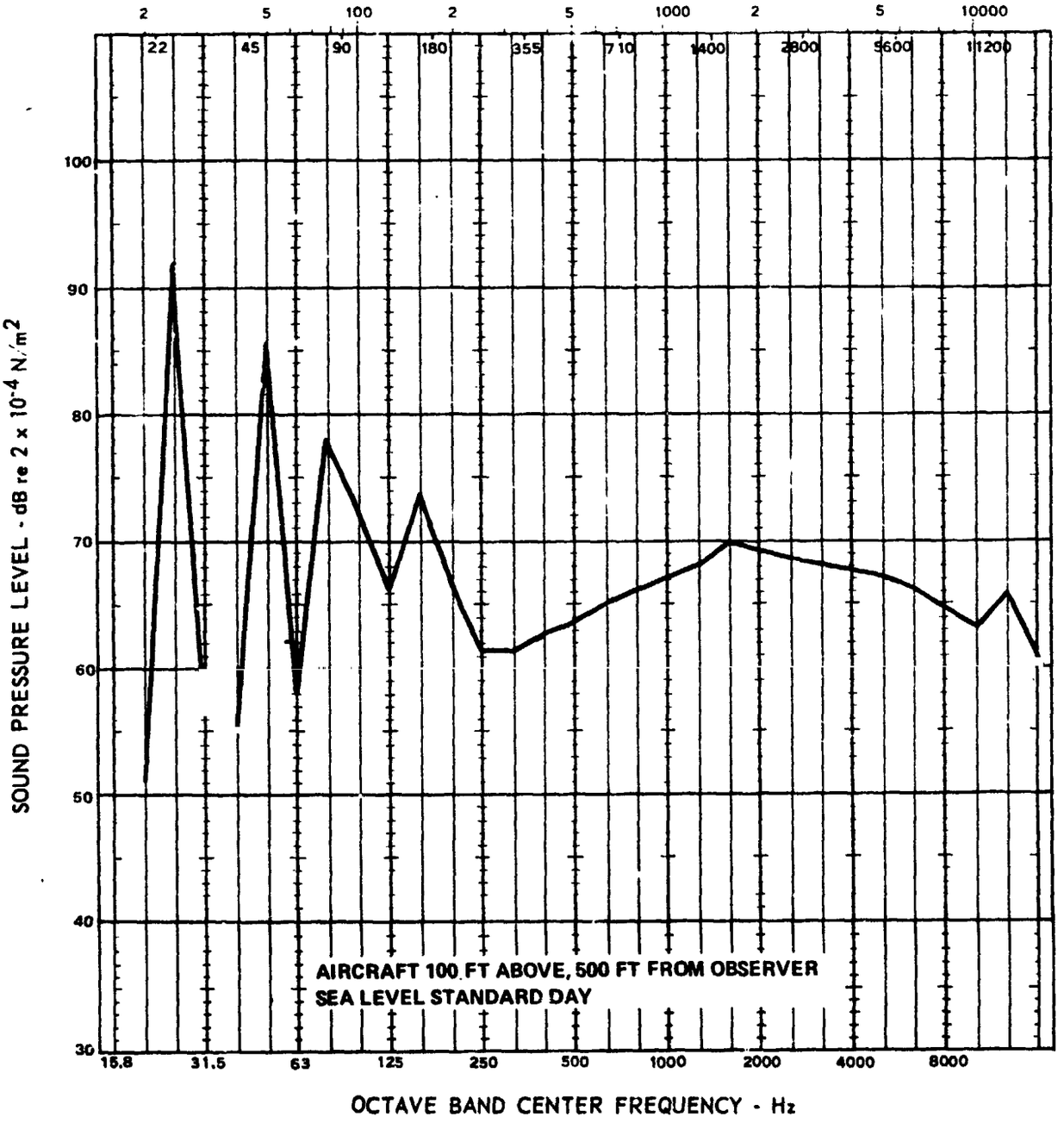

FIGURE 6-8 MODEL 222 HOVER OGE SPECTRUM

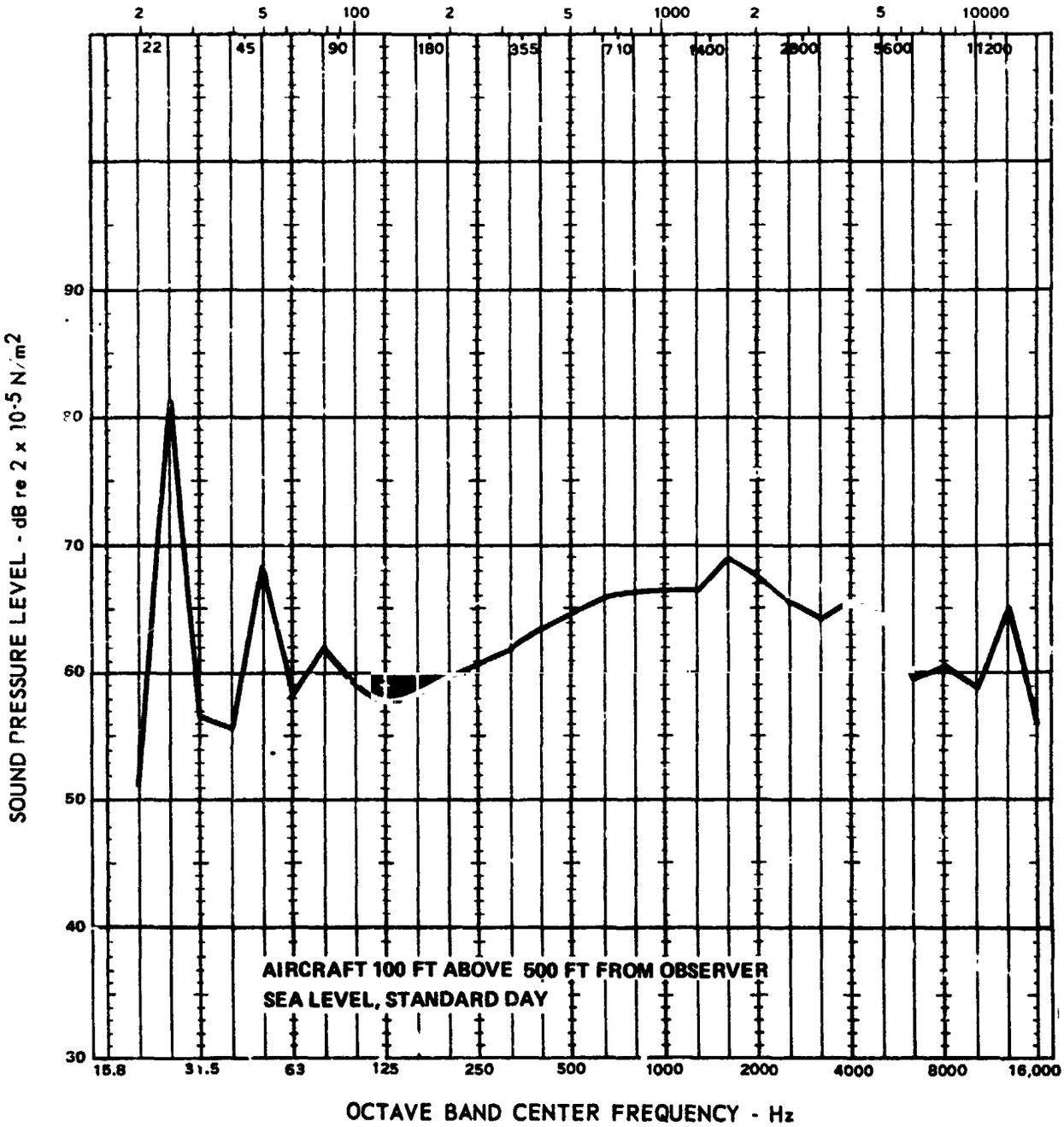

FIGURE 6-9 MODEL 222 - 10 dB OASPL HOVER OGE SPECTRUM

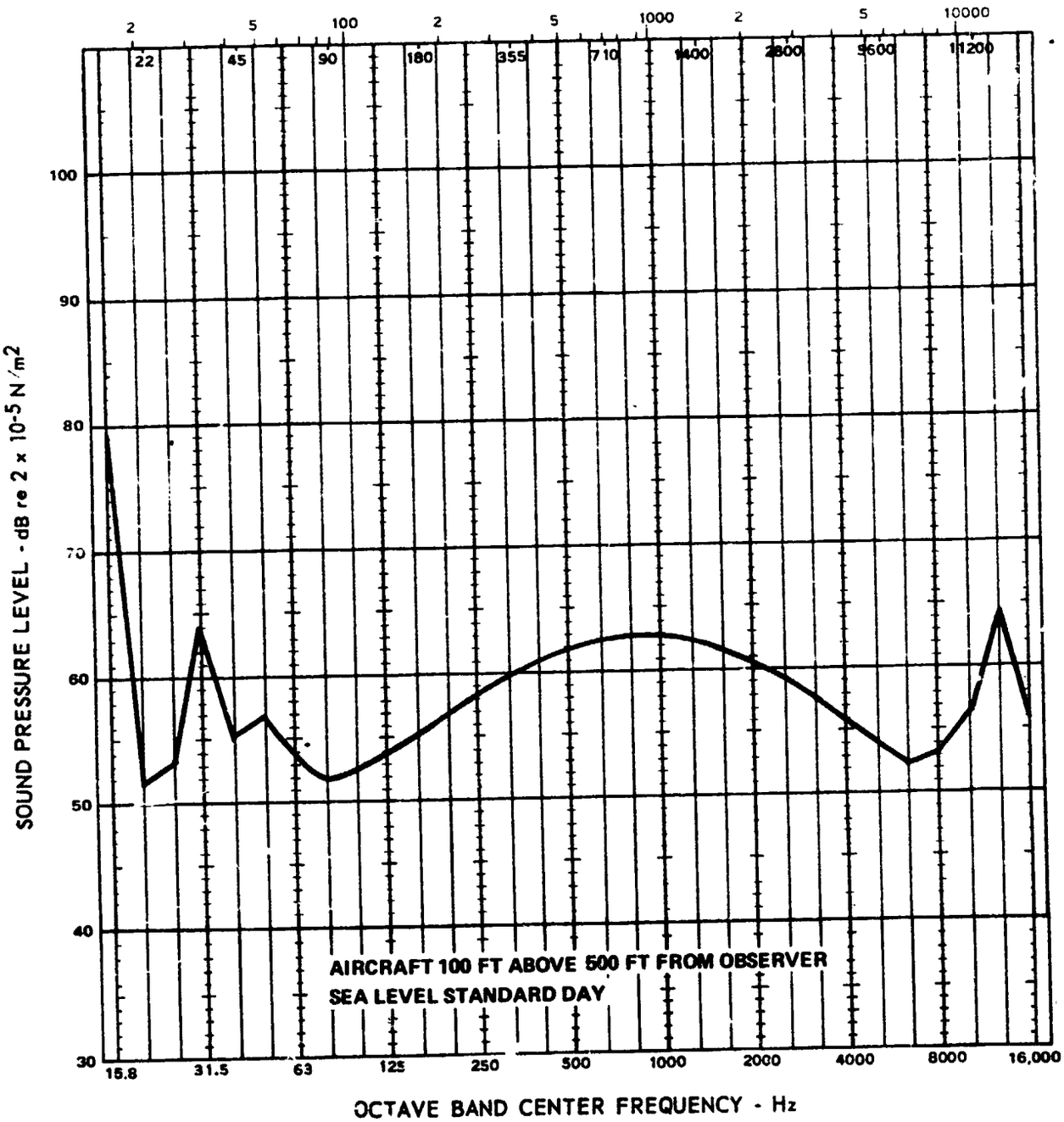

FIGURE 6-10 MODEL 222 - 10 PNdB HOVER OGE SPECTRUM

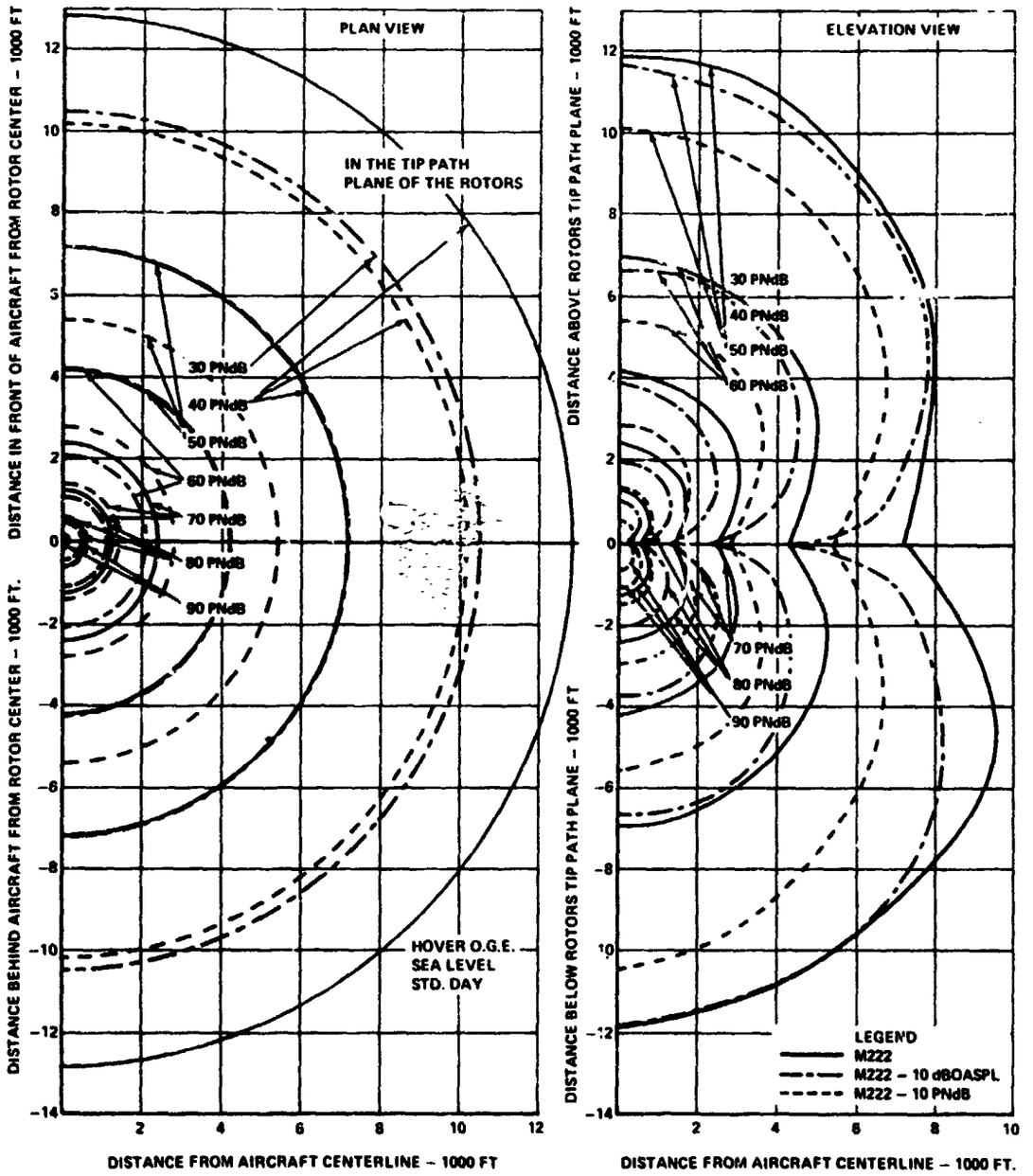

THREE DIMENSIONAL PERCEIVED NOISE LEVEL CONTOURS OF THE MODELS 222 – 10 d BOASPL, 222 – 10 PNdB, AND 222

FIGURE 6-11 HOVER PNL DIRECTIVITY COMPARISON

NOTES:

1. OBSERVER DIRECTLY UNDERNEATH FLIGHT PATH
2. LINE OF SIGHT DETECTION
3. DETECTION BASED ON THRESHOLD OF HEARING
4. ZERO AMBIENT NOISE LEVEL
5. ZERO TERRAIN ABSORPTION
6. OBSERVER AT SEA LEVEL

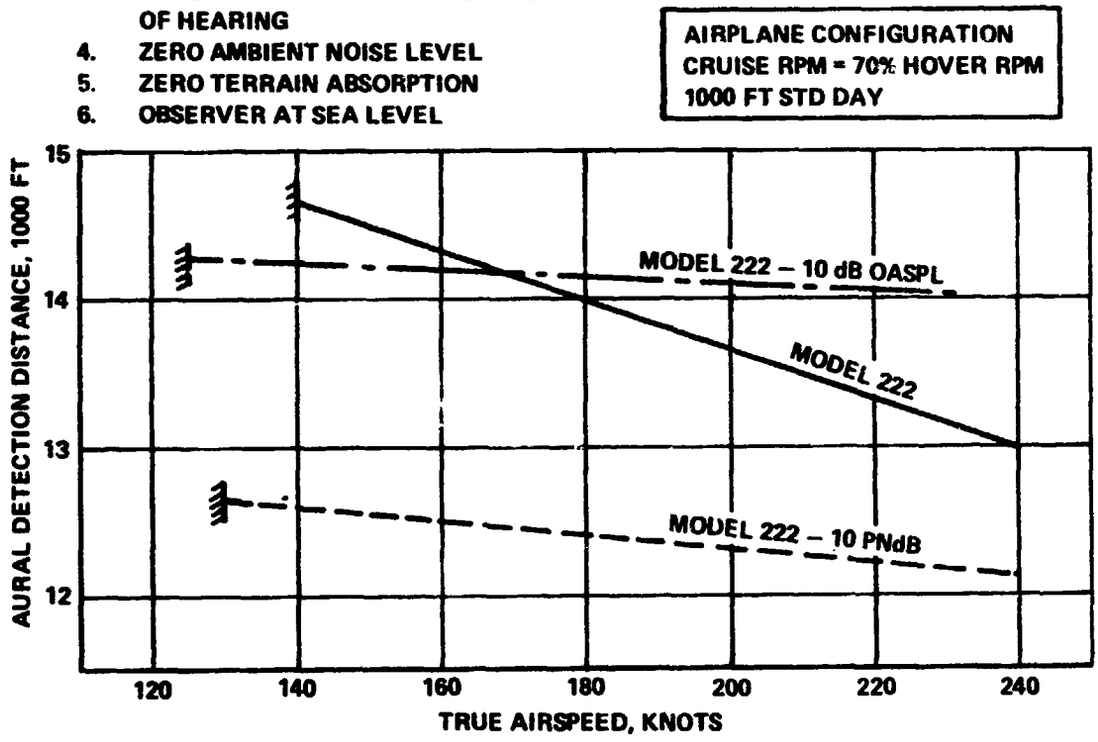

FIGURE 6-12 COMPARISON OF TILT-ROTOR AIRCRAFT AURAL DETECTABILITY FOR STANDARD AND NOISE REDUCTION DESIGNS

band). Broadband noise is a function of thrust, tip speed and blade area. However, there is not much difference in rotor blade areas between the baseline and the M222-10 dB OASPL. The difference in aural detectability of the new design with reduced OASPL is attributable to the larger thrust (drag) at the higher speeds shown in Figure 6-12. The equivalent flat plate drag is shown in Table 6-4 for all three designs.

Takeoff and Landing Trajectories

The trajectories performed by these designs show their off-design point performance and perceived noise level. An aircraft designed to improve the acoustic signature in hover, but acoustically unacceptable in takeoff or landing, would not represent much improvement over an aircraft with no claims of being designed with such a constraint. The three types of trajectories show the tradeoff between acoustically constrained designs and performance capability defining the trajectory and thus the distance between aircraft and observer. The three types of trajectories performed are:

1. Conventional Takeoff (nacelle tilts from vertical to horizontal while climbing)

2. Conventional Landing (nacelle tilts from horizontal to vertical while descending)

3. Helicopter-Type Takeoff (nacelle remains at an angle $i_n \approx 60°$ such that the wing contributes no lift while climbing).

The spectra of the maximum PNL of each aircraft in both the helicopter and airplane modes, if occurring in the trajectory, are also shown. A review of Figures 6-13 through 6-27 reveals that the peaks in the PNL time histories for the two climbing trajectories of the M222 - 10 dB OASPL and M222 - 10 PNdB aircraft are lower than the baseline Model 222. However, the duration of the peak PNL is longer for the two quiet designs. The longer durations are the result of both quiet designs having less excess power than the baseline; hence, the result is a lower rate of climb. The landing trajectory information shown in Figures 6-28 through 6-36 indicates that as in the takeoffs, the two quiet designs have lower peak PNL than the baseline. However, the durations of the peak levels do not change very much from the Model 222 to M222 - 10dB OASPL and M222 - 10 PNdB.

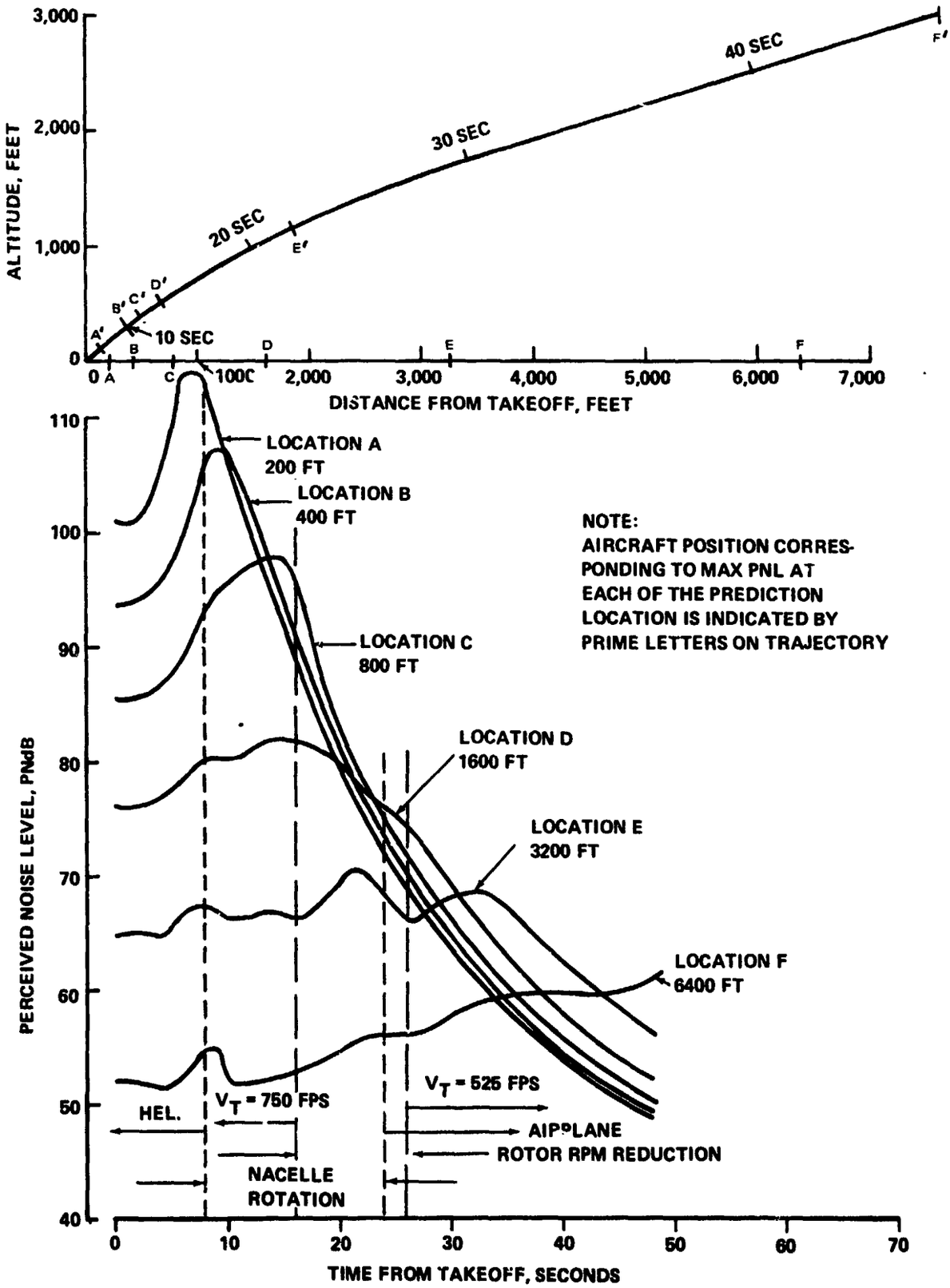

FIGURE 6-13 MODEL 222 STANDARD TAKEOFF AND CLIMBOUT TO 3,000-FOOT TRAJECTORY AND TIME HISTORY

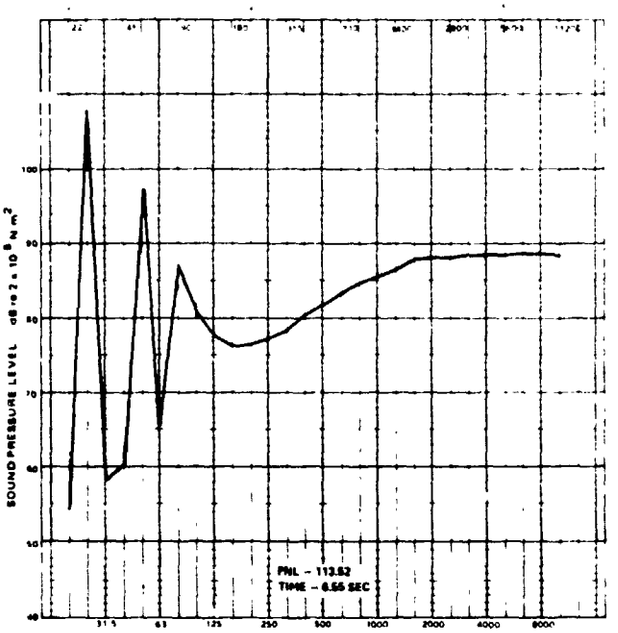

MODEL 222 STANDARD TAKEOFF AND CLIMBOUT TO 3,000 FT
MAX PNL SPECTRUM IN THE HELICOPTER MODE

FIGURE 6-14

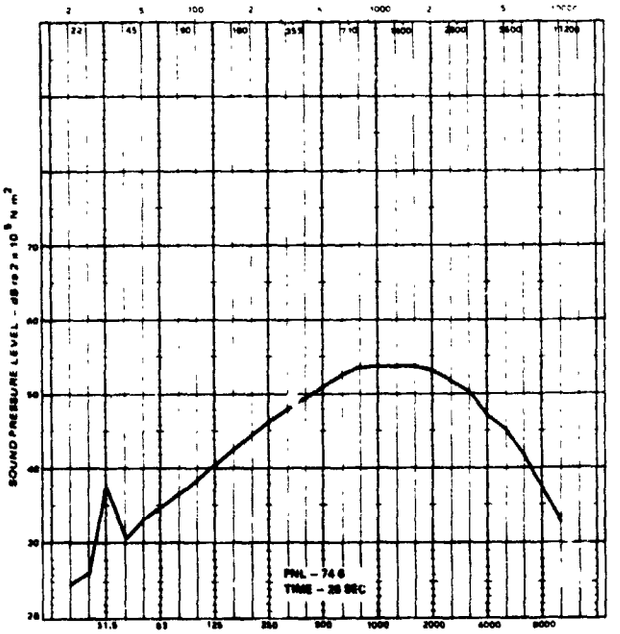

MODEL 222 STANDARD TAKEOFF AND CLIMBOUT TO 3,000 FT
MAX PNL SPECTRUM IN THE AIRCRAFT MODE

FIGURE 6-15

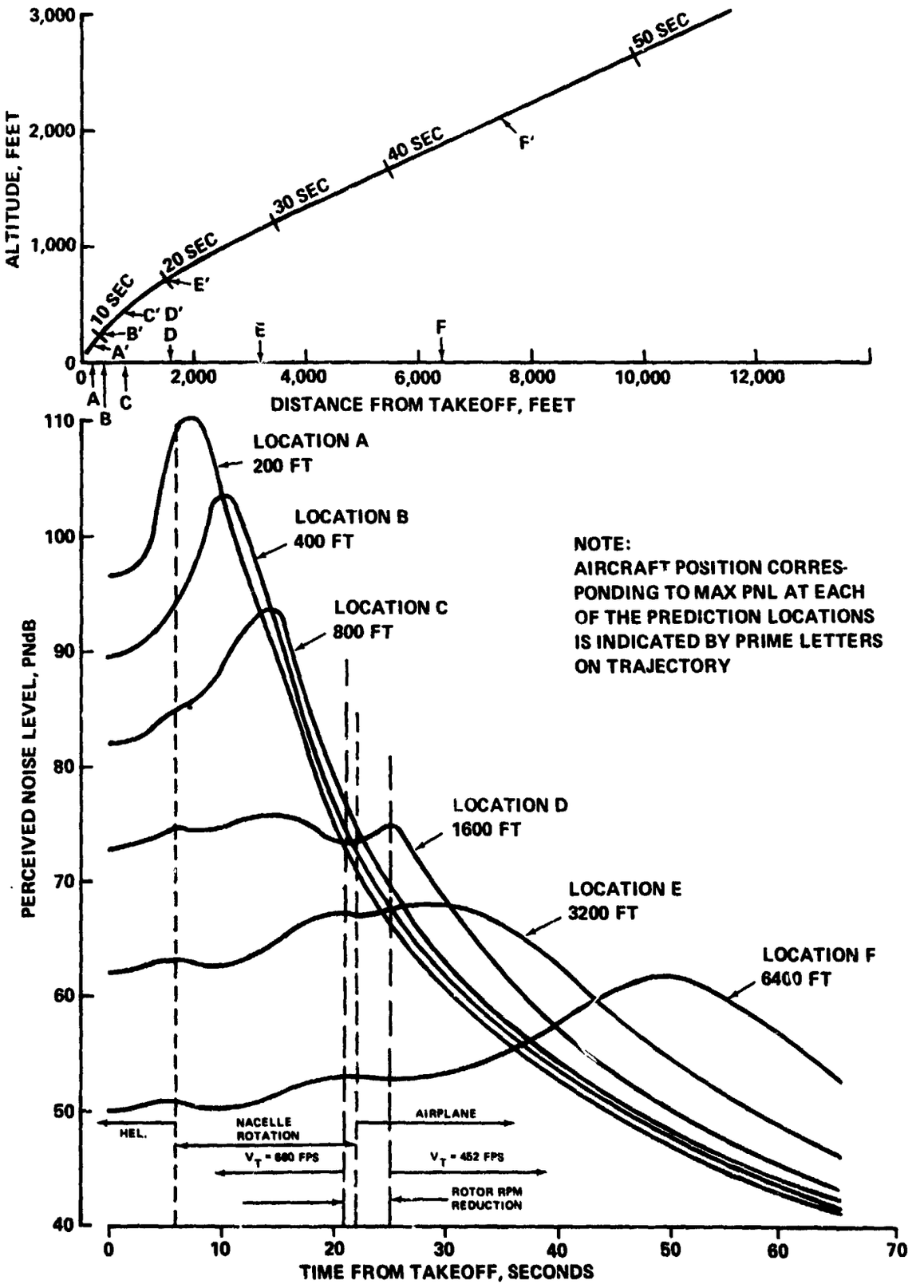

FIGURE 6-16 MODEL 222 - 10 dB OASPL STANDARD TAKEOFF AND CLIMBOUT TO 3,000-FOOT TRAJECTORY AND PNL TIME HISTORY

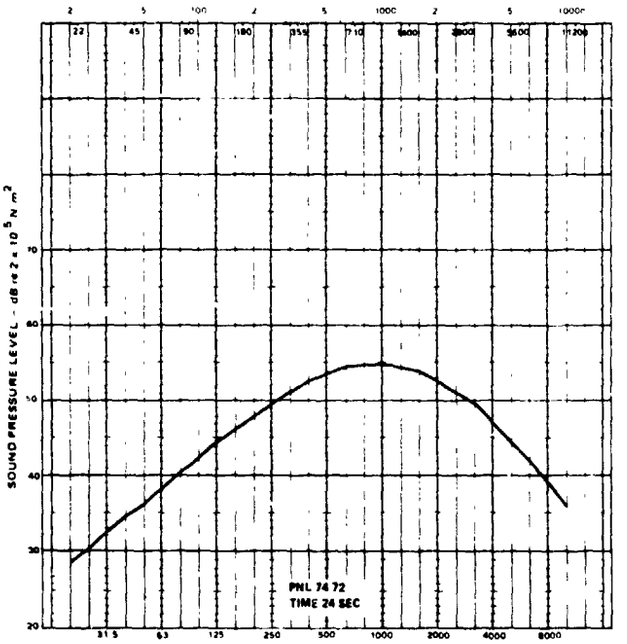

MODEL 222 – 10 dB OASPL STANDARD TAKEOFF AND CLIMBOUT TO 3,000 FT
MAX PNL SPECTRUM IN THE AIRCRAFT MODE

FIGURE 6-17

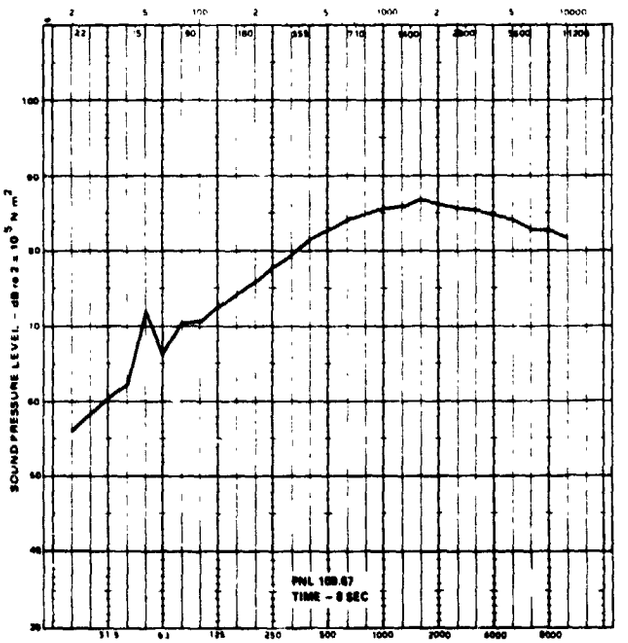

MODEL 222 – 10 dB OASPL STANDARD TAKEOFF AND CLIMBOUT TO 3,000 FT
MAX PNL SPECTRUM IN THE HELICOPTER MODE

FIGURE 6-18

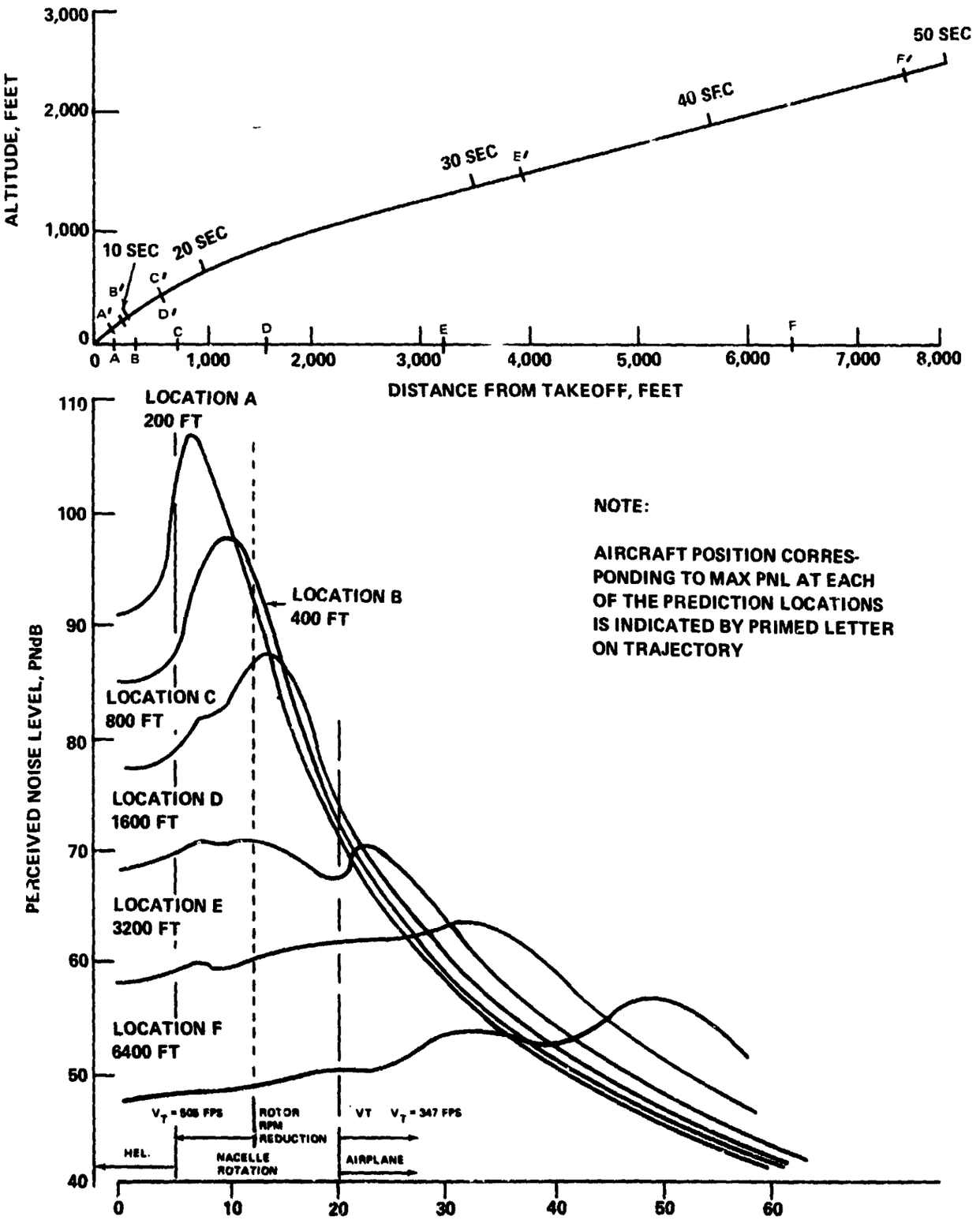

FIGURE 6-19 MODEL 222 - 10 PNdB STANDARD TAKEOFF AND CLIMBOUT TO 3,000-FOOT TRAJECTORY AND PNL TIME HISTORY

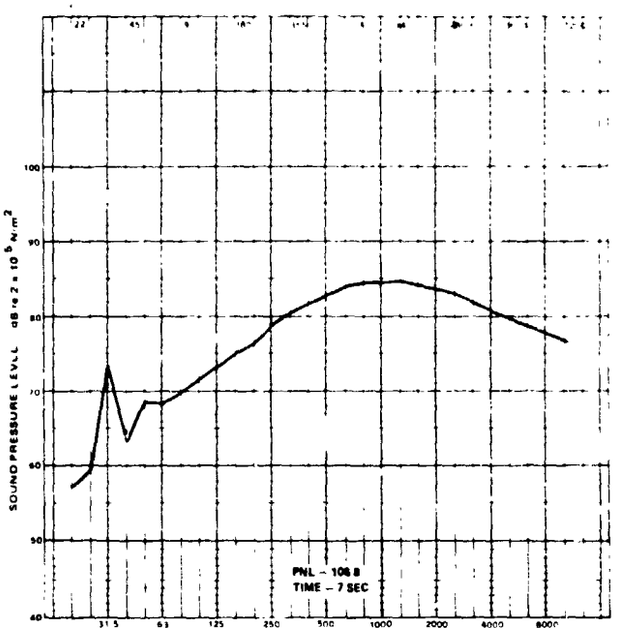

MODEL 222 – 10 PNdB STANDARD TAKEOFF AND CLIMBOUT TO 3,000 FT
MAX PNL SPECTRUM IN THE HELICOPTER MODE

FIGURE 6-20

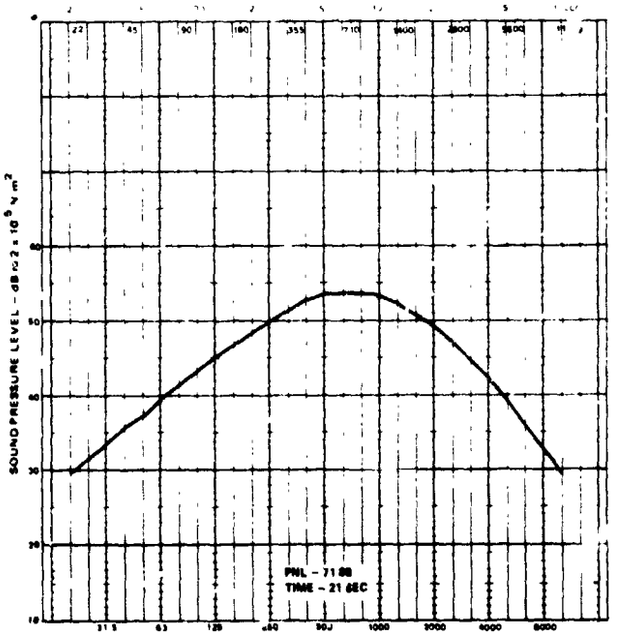

MODEL 222 – 10 PNdB STANDARD TAKEOFF AND CLIMBOUT TO 3,000 FT
MAX PNL SPECTRUM IN THE AIRCRAFT MODE

FIGURE 6-21

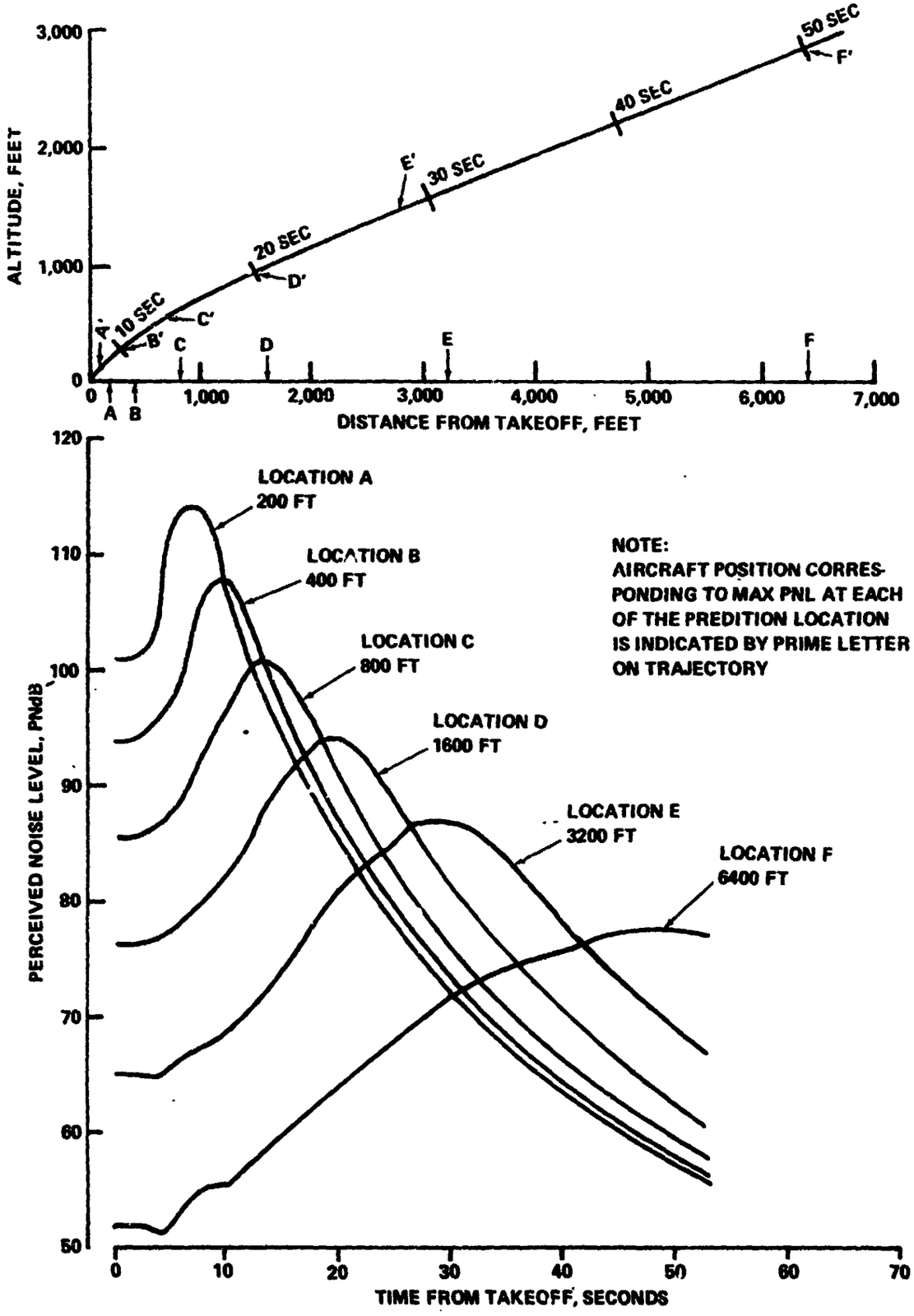

FIGURE 6-22 MODEL 222 HELICOPTER TAKEOFF AND CLIMBOUT TO 3,000-FOOT TRAJECTORY AND PNL TIME HISTORY

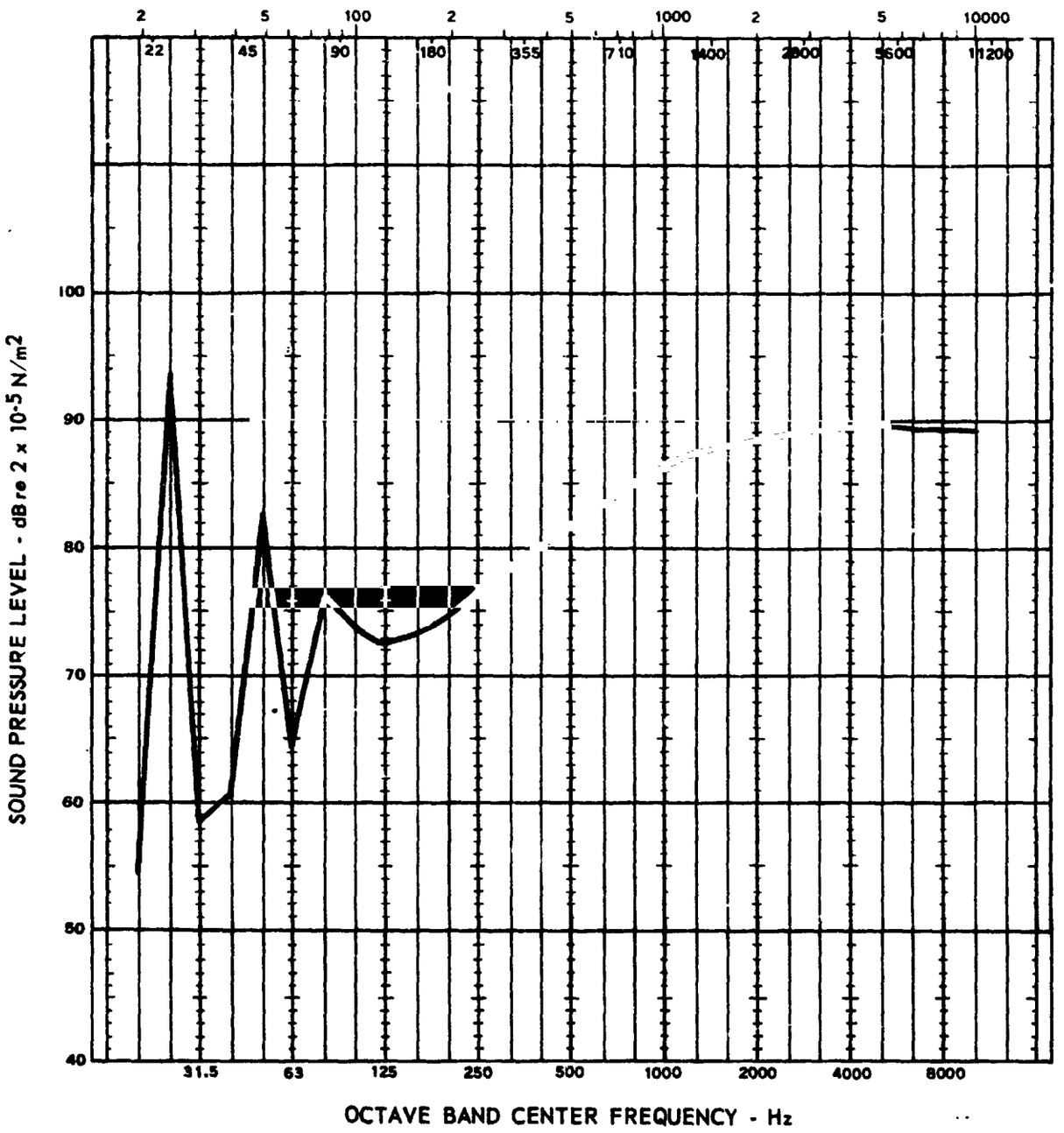

MAX PNL SPECTRUM IN THE HELICOPTER MODE
PNL = 113.2
TIME = 8 SEC

FIGURE 6-23 MODEL 222 HELICOPTER TAKEOFF AND CLIMBOUT TO 3,000 FEET

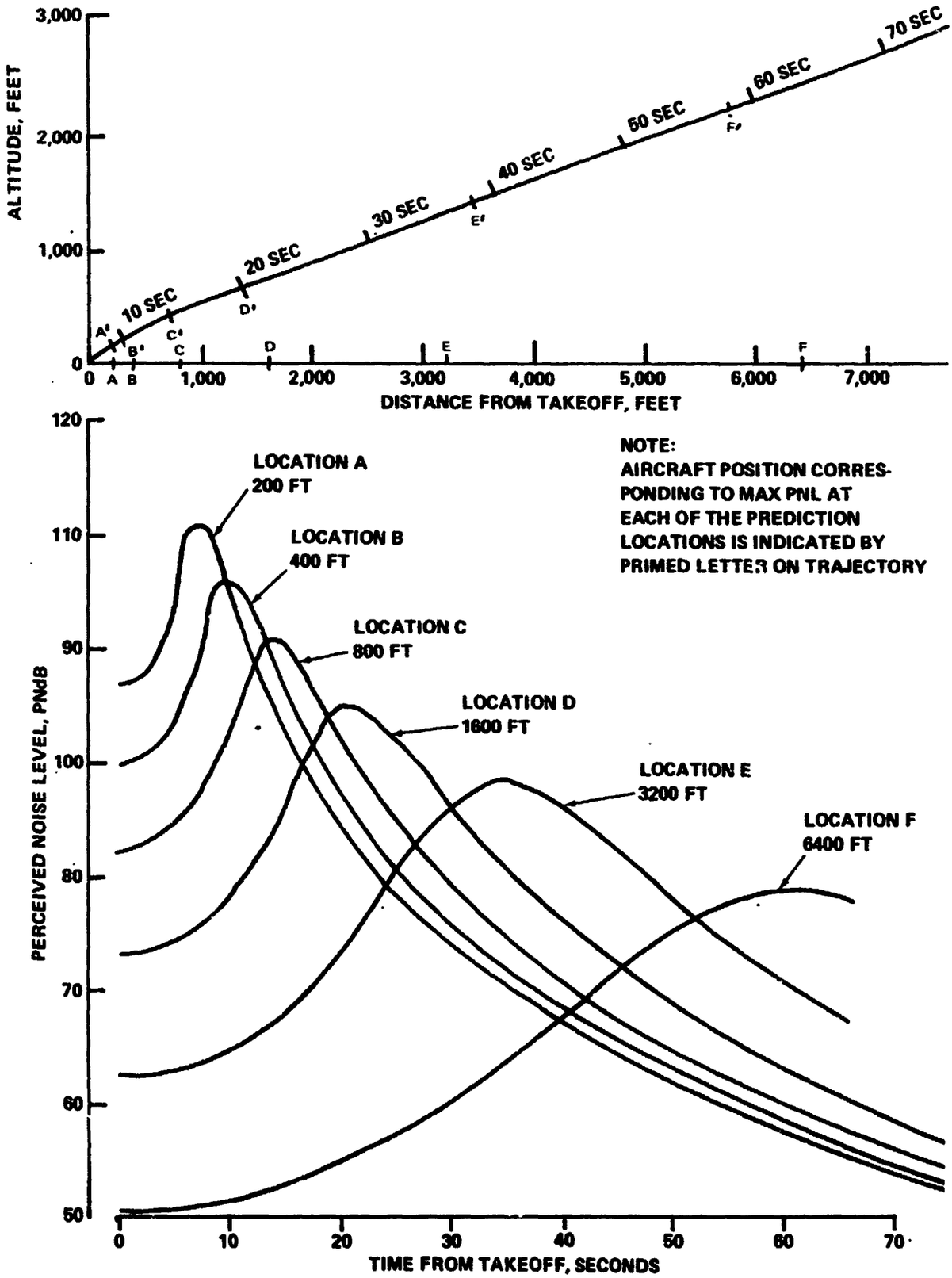

FIGURE 6-24 MODEL 222 - 10 dB OASPL HELICOPTER TAKEOFF AND CLIMBOUT TO 3,000-FOOT TRAJECTORY AND PNL TIME HISTORY

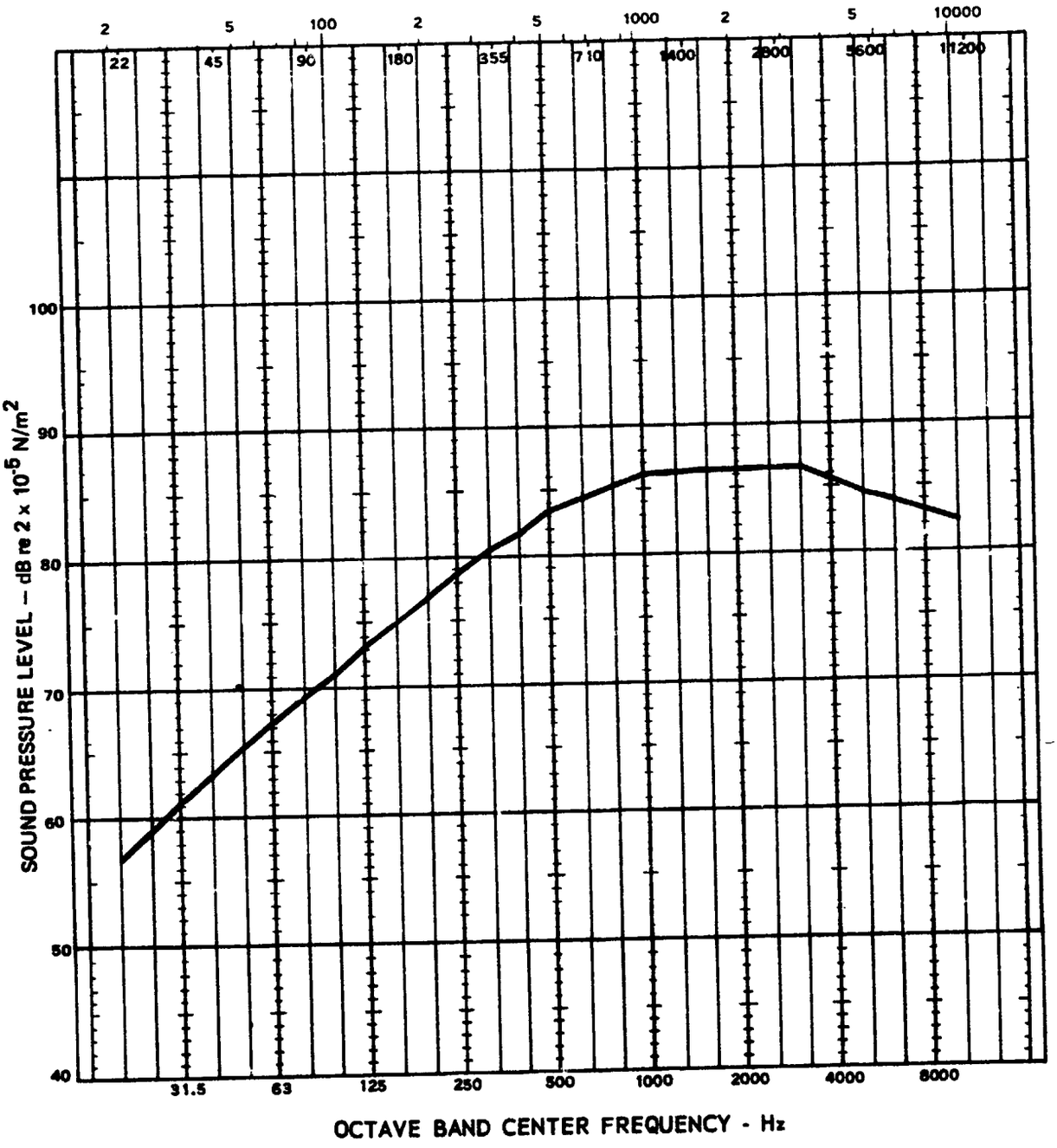

FIGURE 6-25 MODEL 222 - 10 dB OASPL HELICOPTER TAKEOFF AND CLIMBOUT TO 3,000 FEET

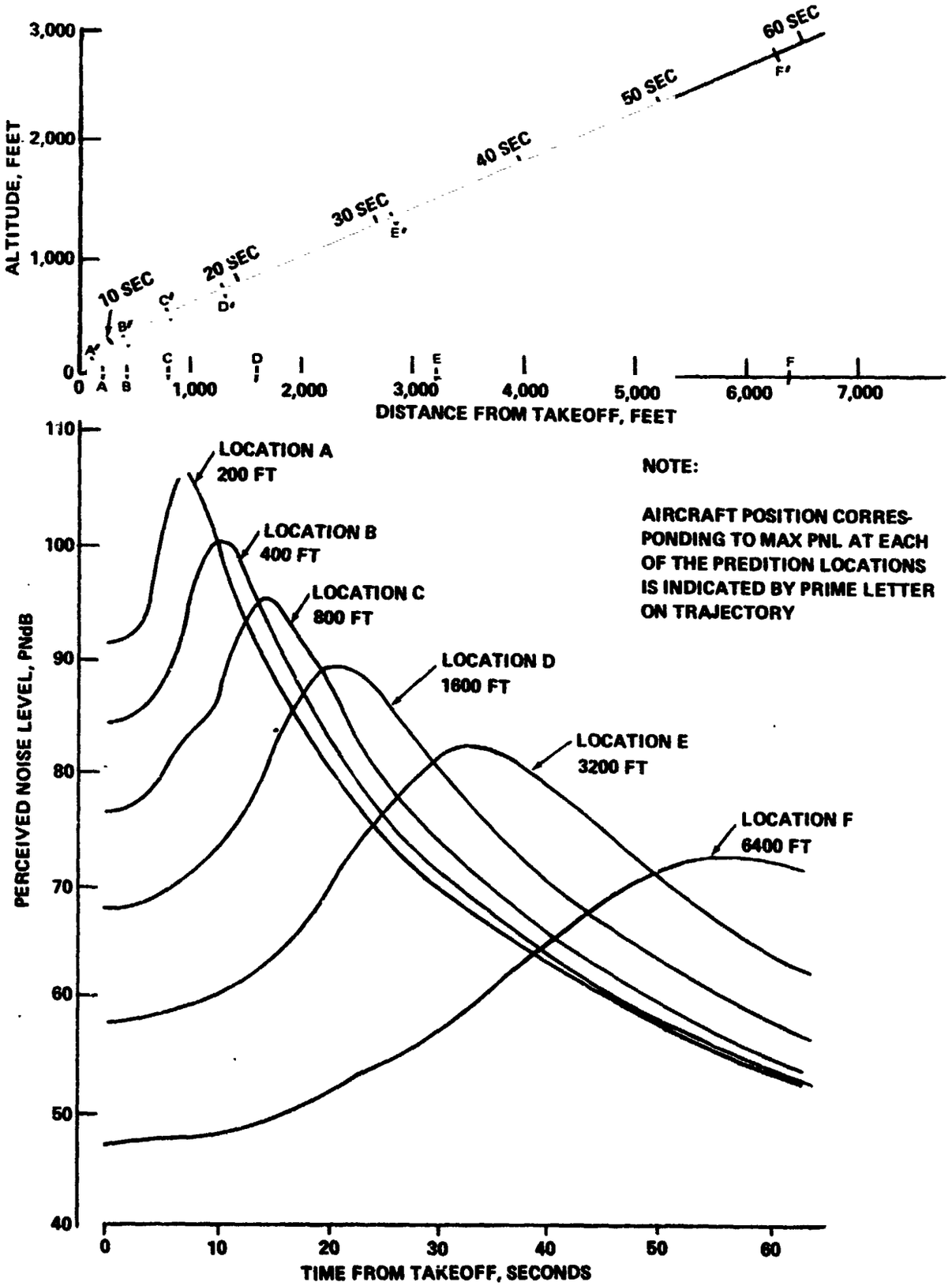

FIGURE 6-26 MODEL 222 - 10 PNdB HELICOPTER TAKEOFF AND CLIMBOUT TO 3,000-FOOT TRAJECTORY AND PNL TIME HISTORY

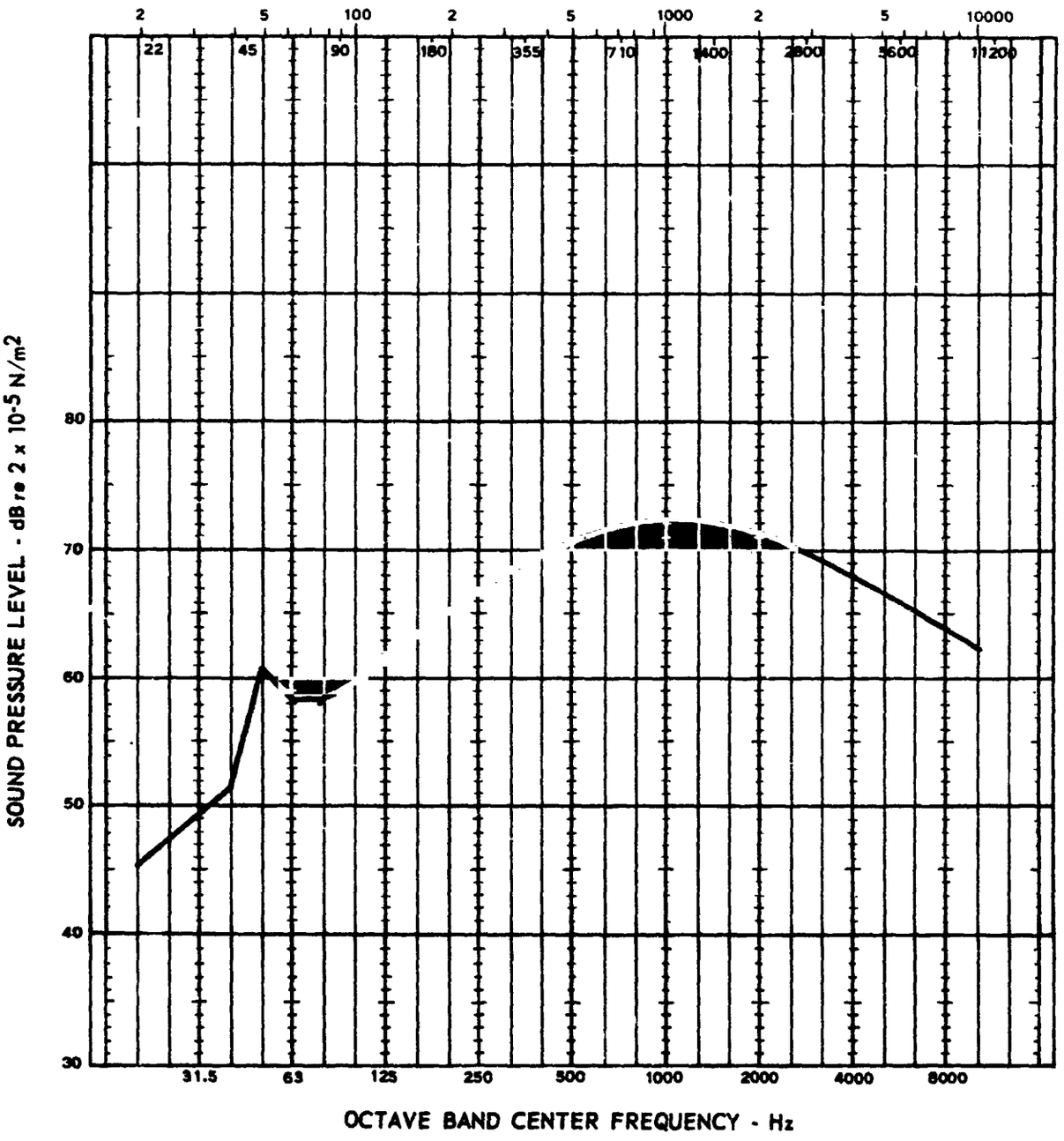

MAX PNL SPECTRUM IN THE HELICOPTER MODE
PNL = 106.8
TIME = 7 SEC

FIGURE 6-27 MODEL 222 - 10 PNdB HELICOPTER TAKEOFF AND CLIMBOUT TO 3,000 FT

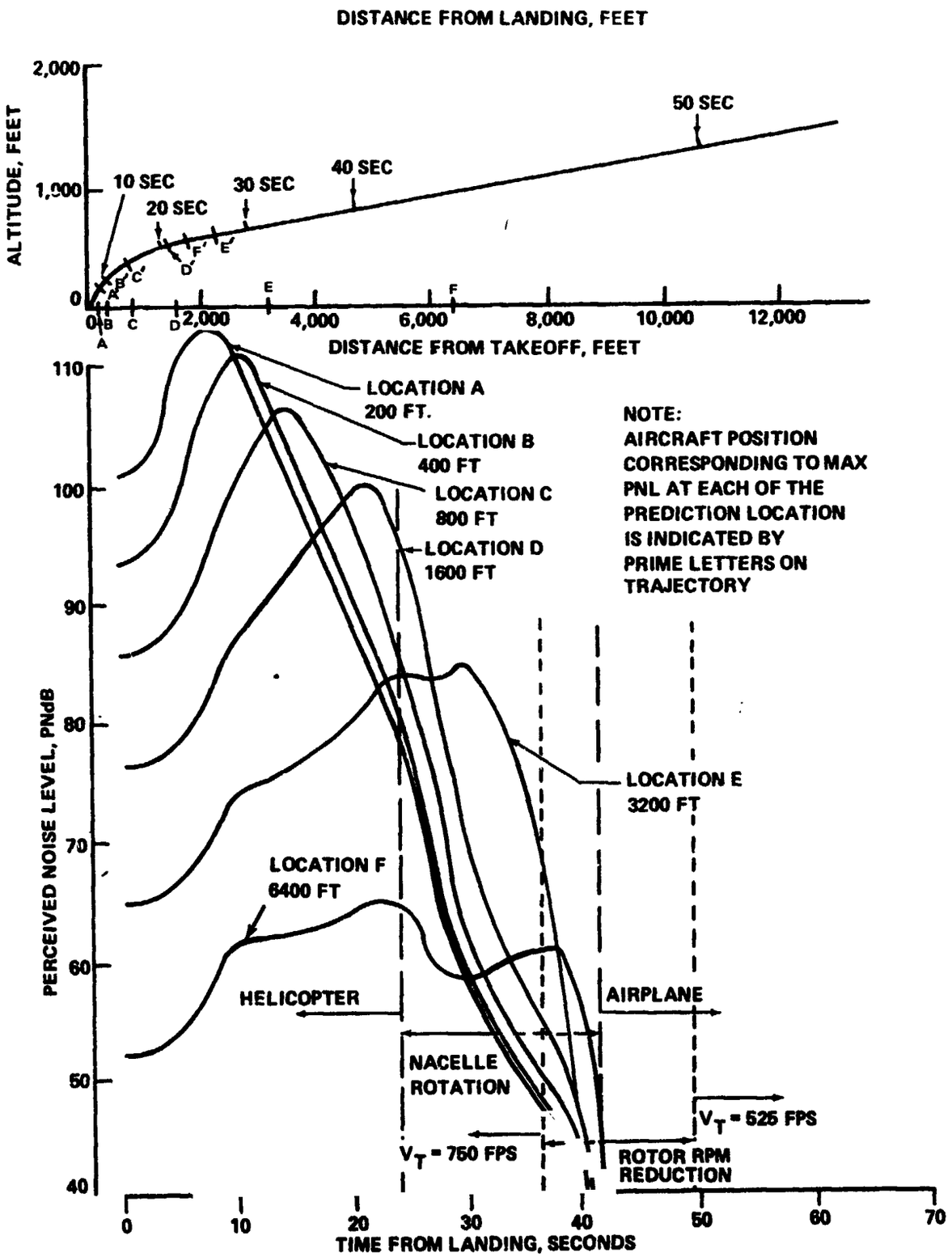

FIGURE 6-28 MODEL 222 - STANDARD LANDING FROM 3,000-FOOT TRAJECTORY AND PNL TIME HISTORY

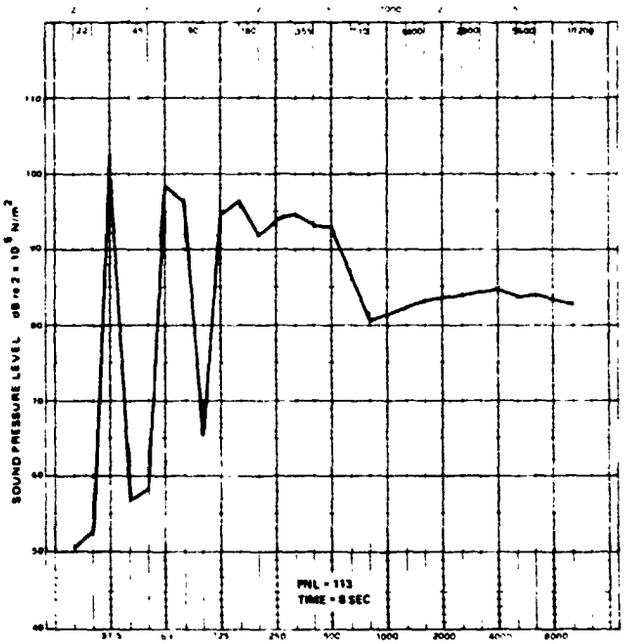

FIGURE 6-29

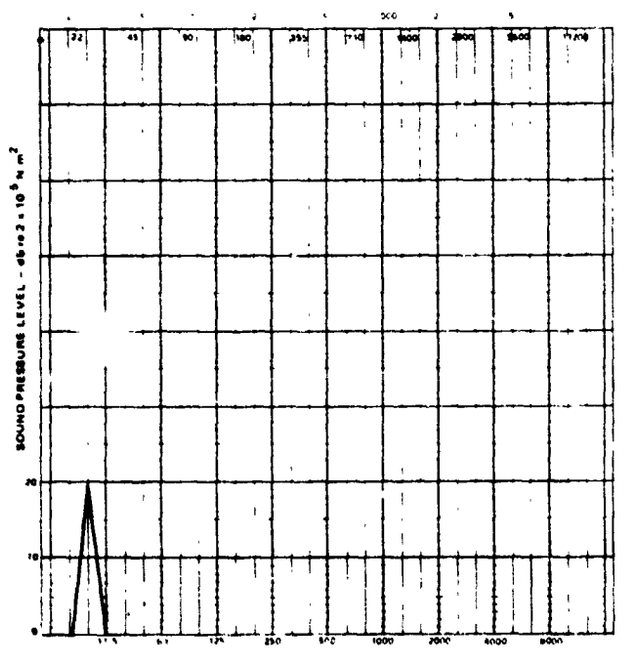

FIGURE 6-30

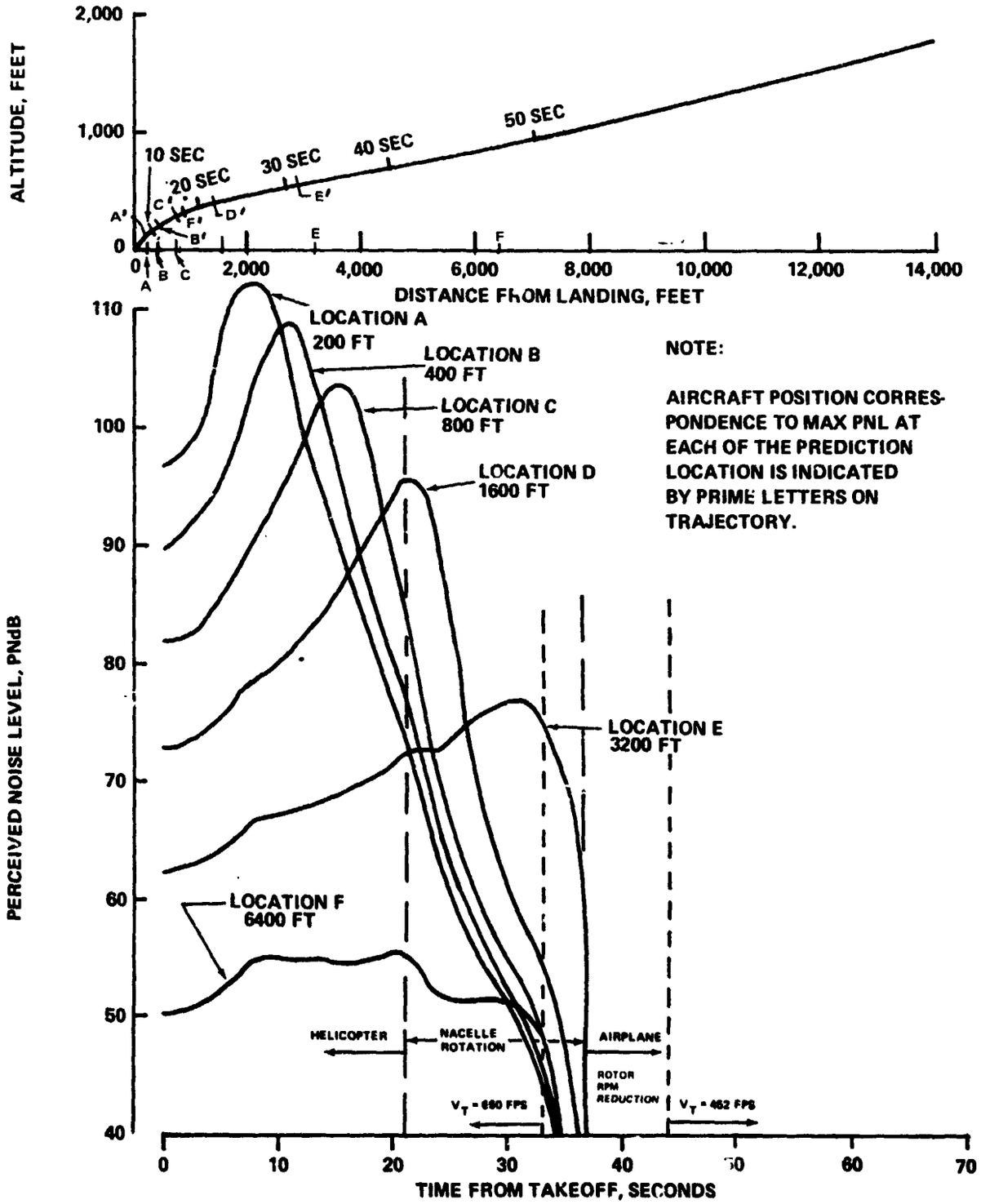

FIGURE 6-31 10 dB OASPL STANDARD LANDING FROM 3,000-FOOT TRAJECTORY AND PNL TIME HISTORY

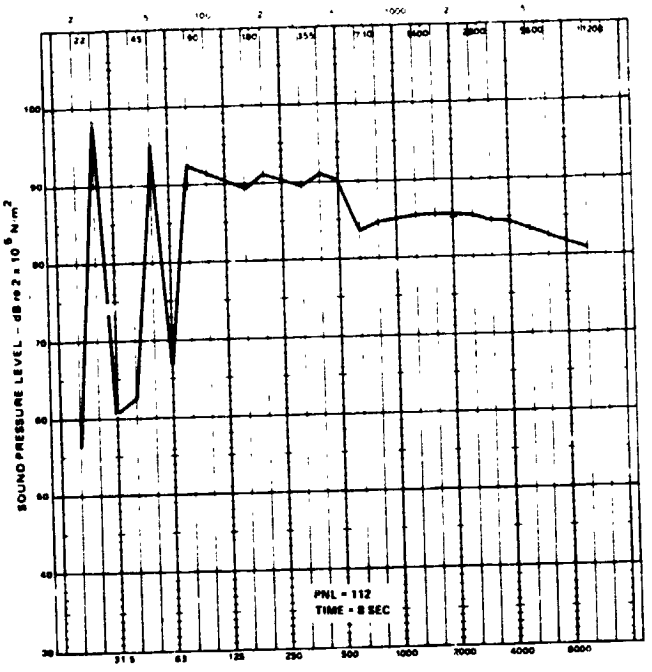

MODEL 222 – 10 dB OASPL STANDARD LANDING FROM 3,000 FT
MAX PNL SPECTRUM IN THE HELICOPTER MODE

FIGURE 6-32

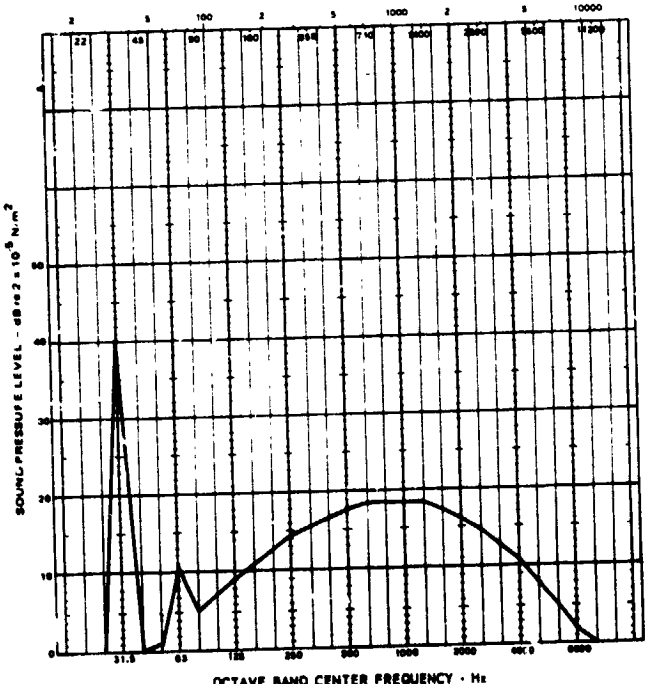

MODEL 222 – 10 dB OASPL STANDARD LANDING FROM 3000 FT
MAX PNL SPECTRUM IN THE AIRCRAFT MODE

FIGURE 6-33

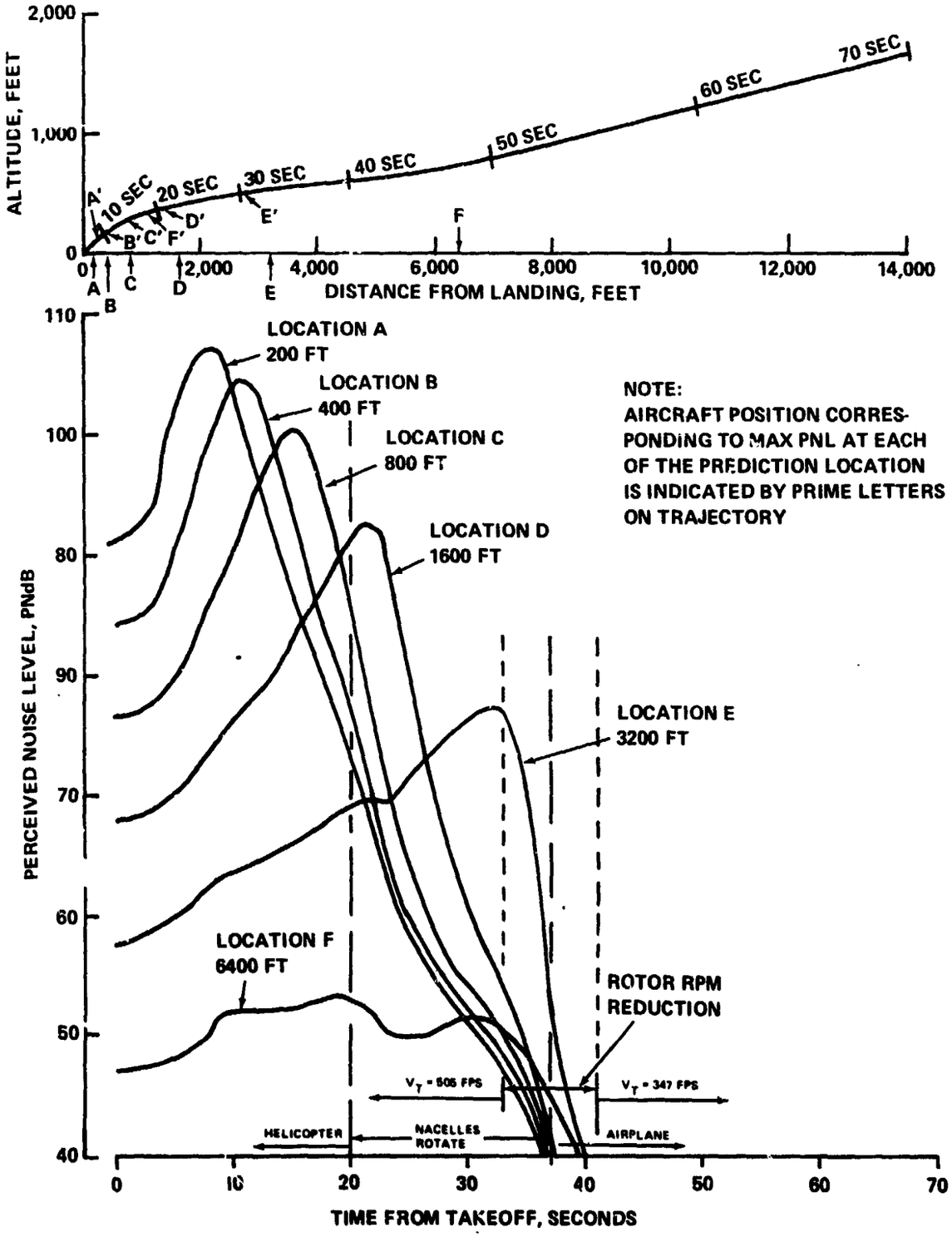

FIGURE 6-34 MODEL 222 - 10 PNdB STANDARD LANDING FROM 3,000-FOOT TRAJECTORY AND PNL TIME HISTORY

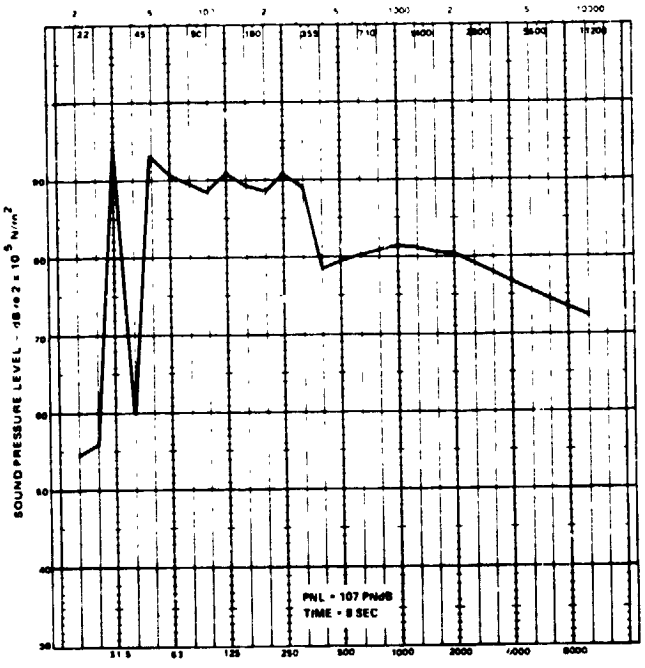

MODEL 222 – 10 PNdB STANDARD LANDING FROM 3,000 FT
MAX PNL SPECTRUM IN THE HELICOPTER MODE

FIGURE 6-35

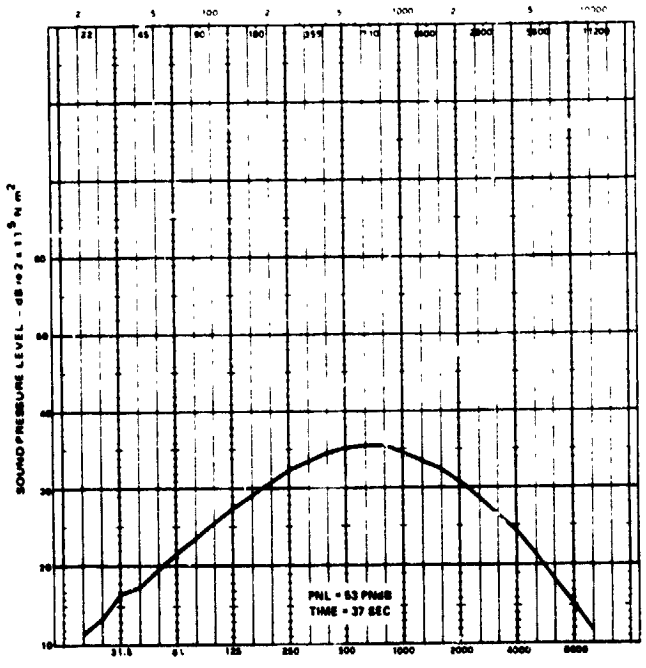

MODEL 222 – 10 PNdB STANDARD LANDING FROM 3,000 FT
MAX PNL SPECTRUM IN THE AIRCRAFT MODE

FIGURE 6-36

VII. CONCLUSIONS AND RECOMMENDATIONS

CONCLUSIONS:

A. The only design parameter change producing a significant reduction of perceived noise level at constant gross weight is lowering the hover tip speed at a constant C_T/σ. However, the following performance and weight penalties are associated with this approach.

1. A lower payload due to increases in weight empty and mission fuel.

2. Small increase in power required to hover.

3. A small decline in both hover rpm transmission limit and .99 best range speed.

Example: A reduction in hover tip speed from 750 fps to 550 fps caused a 7.6 PNdB reduction in PNL, while

a. Weight empty increased 8.7 percent,
Mission Fuel increased 4.3 percent, and
Payload declined 57.7 percent.

b. Hover Power Required increased 2.6 percent.

c. Hover rpm Transmission Limit and .99 Best Range Speed both declined 4.3 percent.

B. The design parameter variations most effective in decreasing the overall sound pressure level are as follows:

1. Reducing tip speed.

2. Lowering Disc Loading.

3. Increasing number of blades with constant rotor solidity.

Lowering the hover tip speed from 750 fps to 550 fps reduces the overall sound pressure level by 5.9 dB. The performance and weight penalties are the same as those identified for perceived noise level reduction.

Reducing the disc loading changes the performance and weight as follows:

a. A large decrease in power required to hover.

b. A large decline in both hover rpm transmission limit speed and .99 best range speed.

c. Very small variation of weight empty* and payload.

d. A lower mission fuel consumption.

Example: A reduction in disc loading from 11.3 to 5.6 lb/ft causes the overall sound pressure level to decrease from 92.5 to 89.1 dB, while:

---

*The very small variation in weight empty as a function of disc loading is the result of the common performance ground rule requiring that the engines supply sufficient power to meet the hovering condition only.

- Hover power required was reduced by 26.6 percent.
- Hover rpm transmission limit speed declined 19.4 percent and .99 best range speed decreased by 20.2 percent.
- Weight empty increased 1 percent and payload increased 1.9 percent.
- Mission fuel declined 11 percent.

Increasing the number of blades at constant rotor solidity from 3 to 4 blades results in the following:

a. 2.1 dB decrease in OASPL.

b. No noticeable change in weight empty, mission fuel and payload.

c. A small decline in power required to hover.

d. No noticeable change in .99 best range speed.

e. A small decrease in hover rpm transmission limit speed.

Example: An increase in the number of blades at constant solidity from 3 to 5 blades reduces the overall sound pressure level by 1.8 dB per blade or 3.6 dB, while:

- Hover power required declined 1.6 percent.
- Hover rpm transmission limit speed decreased 1 percent.

C. Design of tilt-rotors with significantly lower OASPL (-10dB) in hover than an unconstrained design may be accomplished with a moderate increase in design gross weight of 5.84 percent. However, the increase in design gross weight for a design constraint of a significant reduction in PNL (-10 PNdB) increases the DGW by 25.4 percent over that of the unconstrained design.

D. Mission productivity (V_{block} x Payload/WE) significantly declines from that of the reference.

E. A tradeoff exists between an acoustic design constraint in hover and maximum rate of climb capability on the resulting duration corrected annoyance (EPNL) underneath the takeoff trajectory. The same tradeoff is not applicable to landing.

F. The tradeoffs shown in Section IV and used in Section VI are dependent on the criteria used to size the engines and transmissions. If the criteria were based on a high-speed dash capability (300 knots) rather than hover, the weight penalties would be much larger than those used. It should be realized, hence, that many of the above conclusions are particular to the selected design and performance ground rules.

RECOMMENDATIONS:

A. The 57.7 percent decrease of payload at constant gross weight caused by a tip speed reduction of 200 fps is too severe a penalty to be accepted as a normal design practice. An effort to reduce this penalty through advanced drive systems and

advanced composite materials in the rotor system is necessary if tip speed is to be the route used for reduction of far-field acoustic signature.

B. Airfoils should be developed which have a higher L/D over a wider range of Reynolds Number and angles of attack than present ones. This would make possible a better compromise between hover and cruise performance when the hover tip speed is reduced in order to improve acoustic far-field characteristics.

C. The influence of (1) rotor blade span loading distribution, (2) number of blades per rotor with constant total area, and (3) airfoil characteristics, on the far-field rotor acoustic signature is not well understood. An investigation should be conducted to establish a consistent data base and empirical relationships for the above design parameters.

D. Continuing theoretical and experimental research should be carried out to improve the quantitative predictions of prop-rotor noise. If the measure of acoustic acceptability is frequency weighted, then emphasis should be placed on prediction of the rotor acoustic signature above 250 Hz.

Acknowledgements

The authors wish to express their indebtedness to Dr. F. H. Schmitz of USAAMRDL for his general guidance and numerous technical suggestions. They also wish to thank the following personnal from Boeing Vertol Company: H. Sternfeld for his guidance in acoustics, V. Soule for rotor performance calculations, J.S. Wisniewski for

estimates of weight and mass properties, and J. Schneider for the Quiet Aircraft design sketches. Special thanks are due to Mrs. Wanda Metz for her most valuable help in editing, typing, and arranging this report. The assistance of Mr. K. Collinge of AVCO Lycoming Division with respect to the turboshaft engine noise aspects is greatly appreciated.

APPENDIX A

SUPPORTING ACOUSTIC DATA

The following material on tip speed and blade tips is supplementary to that presented in Section II. It is included for information purposes.

Tip Speed

The relationships presented in Section II on Tip Speed were found to be supported in most of the literature. However, the data reported by Stuckey and Goddard (Ref. 7) and presented in Figure A-1, show a lesser effect of tip speed on noise than those reported elsewhere. The sound pressure levels shown are for constant nominal thrust of a full-scale 3-bladed rotor. The first harmonic noise levels increase (with a few exceptions) with tip speed as expected. However, the higher 10th and 15th harmonics are essentially constant below a tip speed of 1000 fps.

Other available data show an increase in noise with tip speed even in the higher harmonics. Figure A-2, for example, shows the results of a whirl-tower test of CH-47B/C rotor blades operated at three different nominal thrusts (Ref. 5). The microphone located at a three-diameter distance registered an average 6 dB increase in first harmonic SPL for each 100 fps of tip speed increase. The data gathered by the ground microphone indicates

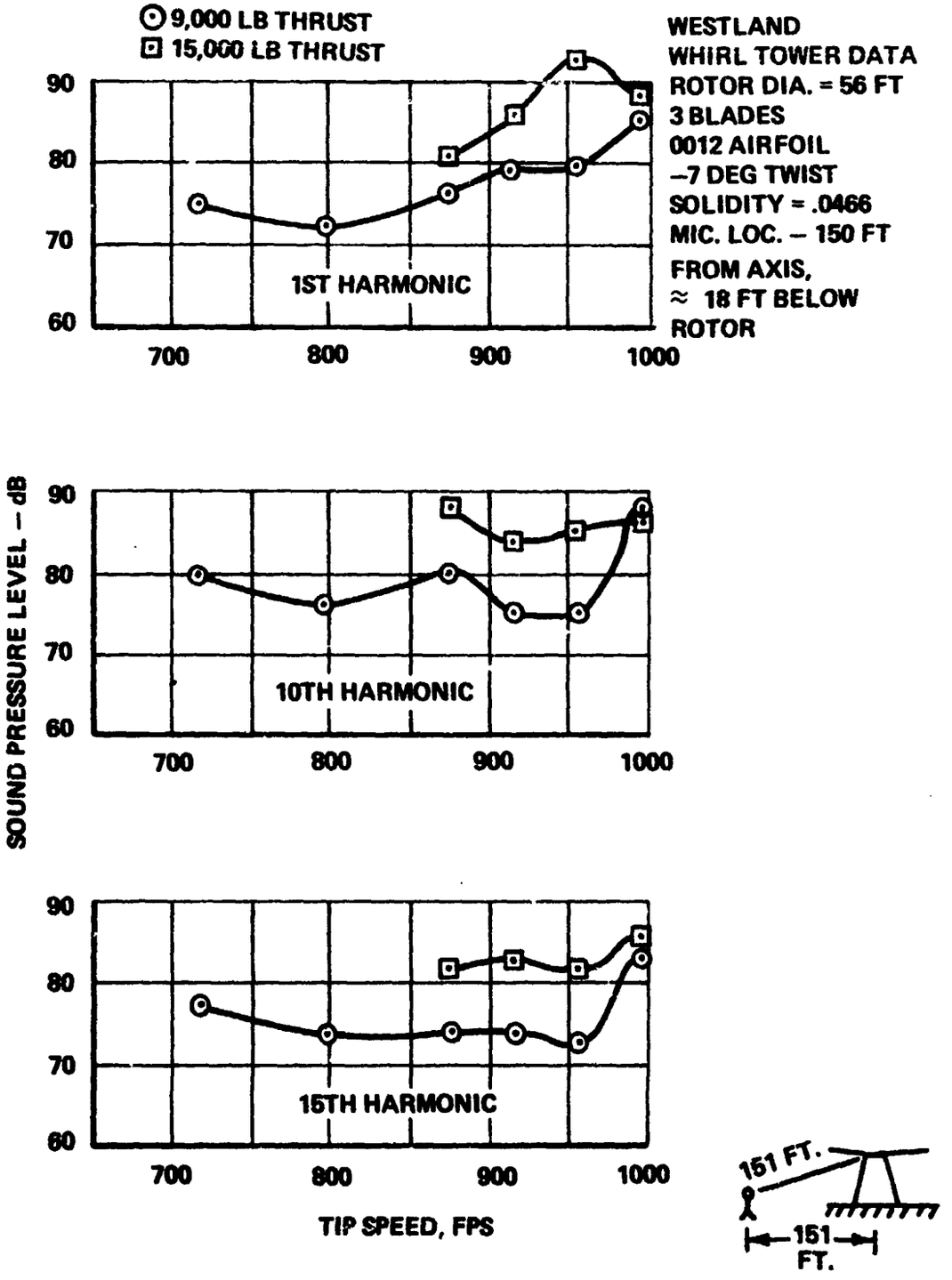

FIGURE A-1 EFFECT OF TIP SPEED ON ROTATIONAL NOISE HARMONICS FROM REFERENCE 7

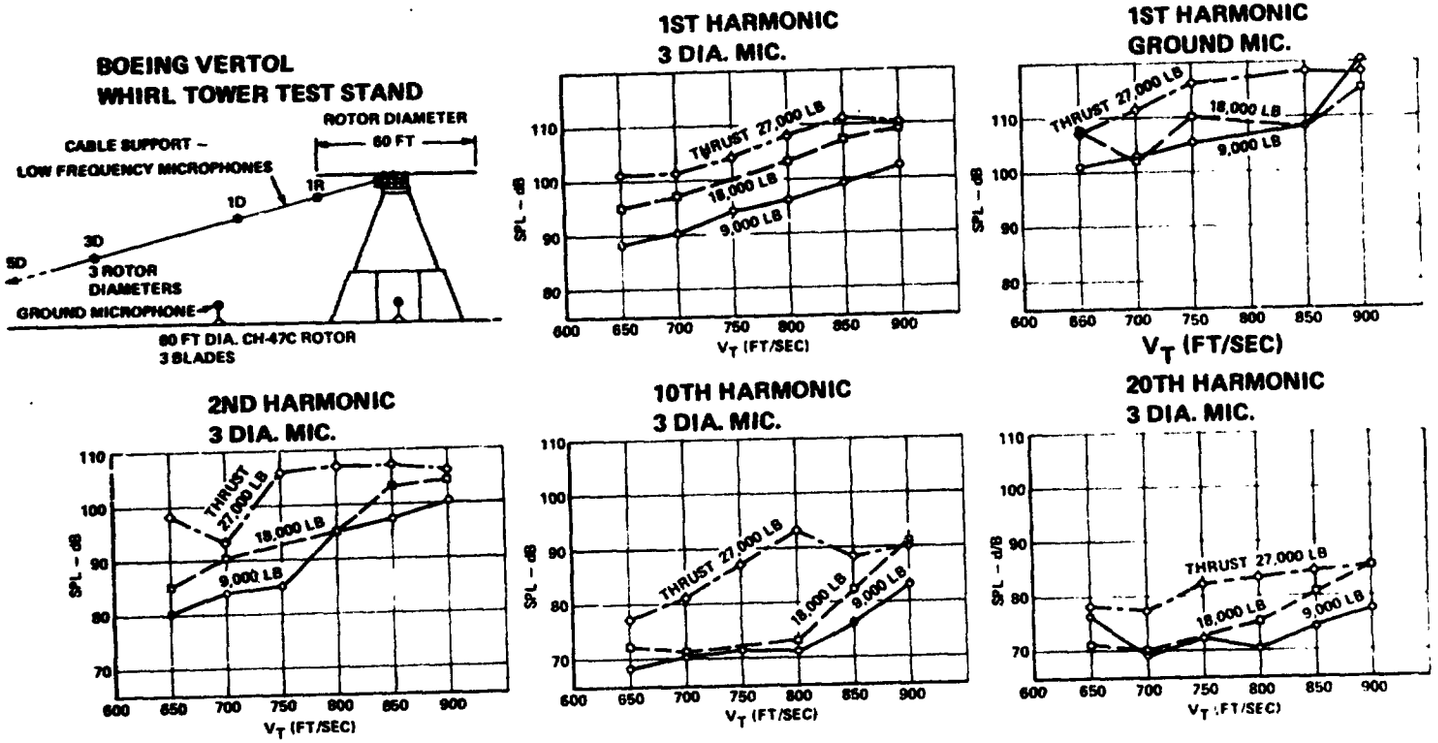

FIGURE A-2 EFFECT OF TIP SPEEL ON ROTATIONAL NOISE HARMONICS

a somewhat lower rate of increase, and does not display the same uniformity with increasing tip speed as the aerial microphone.

The higher harmonic amplitudes generally increase with tip speed, but the trends are not as well defined as for the lower harmonics of sound pressure.

A cross-plot of Hubbard and Maglieri full-scale rotor data (Ref. 6) illustrates rotor noise in terms of tip speed and is given in Figure A-3. The overall SPL is approximately linear, increasing at 5 dB per 100 fps. This agrees well with the Vertol data of Figure A-2.

Figure A-4 illustrates the sound pressure level for several harmonics of the 13-foot diameter Model 160 propeller (-41° twist). For this configuration, the increase in sound pressure is approximately linear for all harmonics shown up to 850 fps tip speed, with a 6 dB increase for each 100 fps of tip speed between 550 and 850 fps for the lower two harmonics. Above 850 fps, the higher harmonics increase at a diverging rate.

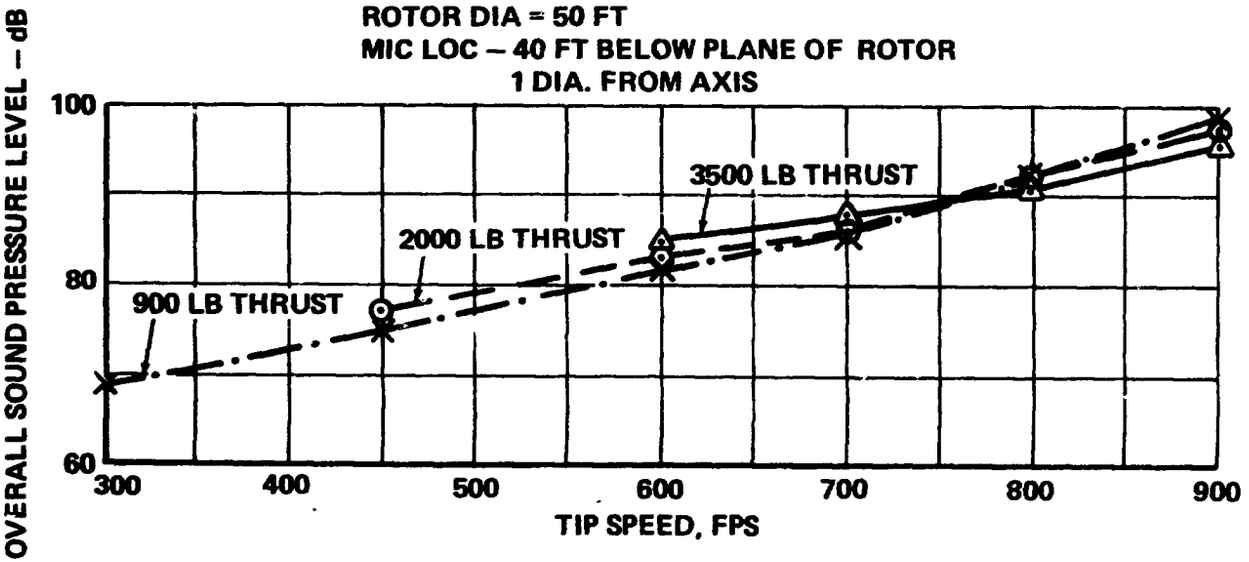

FIGURE A-3 EFFECT OF TIP SPEED FROM REFERENCE 6

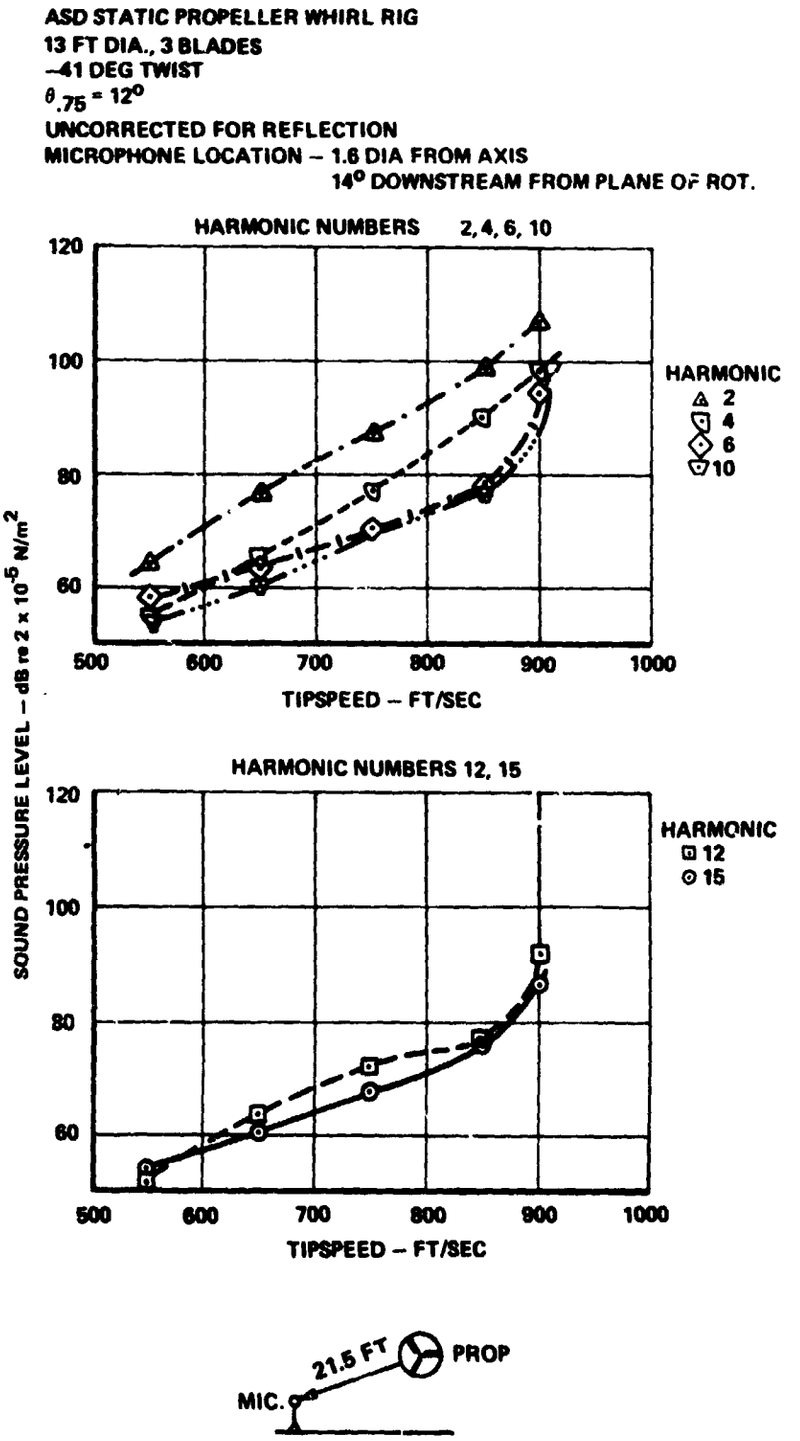

FIGURE A-4 EFFECT OF TIP SPEED ON HARMONIC SOUND LEVELS

Blade Tip Modifications

Blade tip modifications can have a moderate effect on far-field noise. A Boeing-Vertol investigation in 1961 on a tied-down CH-46 revealed that several modifications to the tip could be made to achieve amplitude reductions in certain frequency ranges relative to the unmodified, revolved airfoil tip. These tests were conducted on an overlapped tandem-rotor aircraft and the results shown in Figure A-5 would be expected to be less pronounced than for a single isolated rotor. The greatest reduction in noise at all frequencies was displayed by the square tip which averaged 5 dB over 6 octave bands.

A recent test reported by Pollard and Leverton (Ref. 11) also confirms that the square tip is as quiet as any tip yet tested, at least at the low tip speeds. Figure A-6 from their report shows the results for a 10-foot diameter rotor at 8° pitch. By contrast, Sikorsky data (Figure A-7), taken from Ref. 10 show a contradictory trend for trapezoidal tips when compared with that of Pollard and Leverton. However, the maximum tip speed in Figure A-6 is only 367 fps.

A double-swept tip was installed by Bell on a UH-1 and the results reported in Ref. 21. Figure A-8, reproduced from this reference, shows a very small benefit (in the 75-150 Hz band) except at an advancing tip Mach number of .8 where the difference is 6 dB.

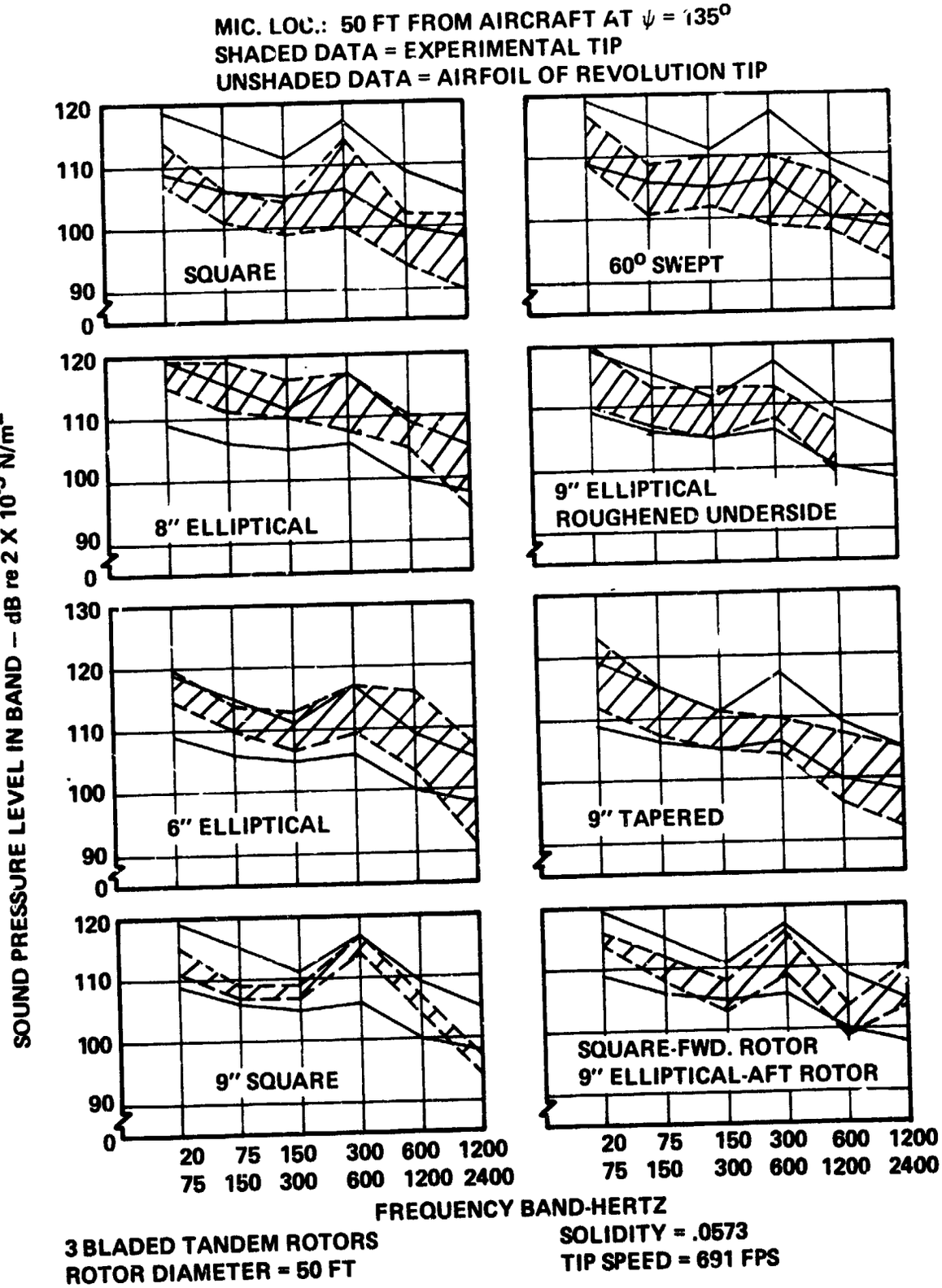

FIGURE A-5 NOISE LEVELS OF EXPERIMENTAL TIP SHAPES ON TIEDOWN CH-46 AIRCRAFT

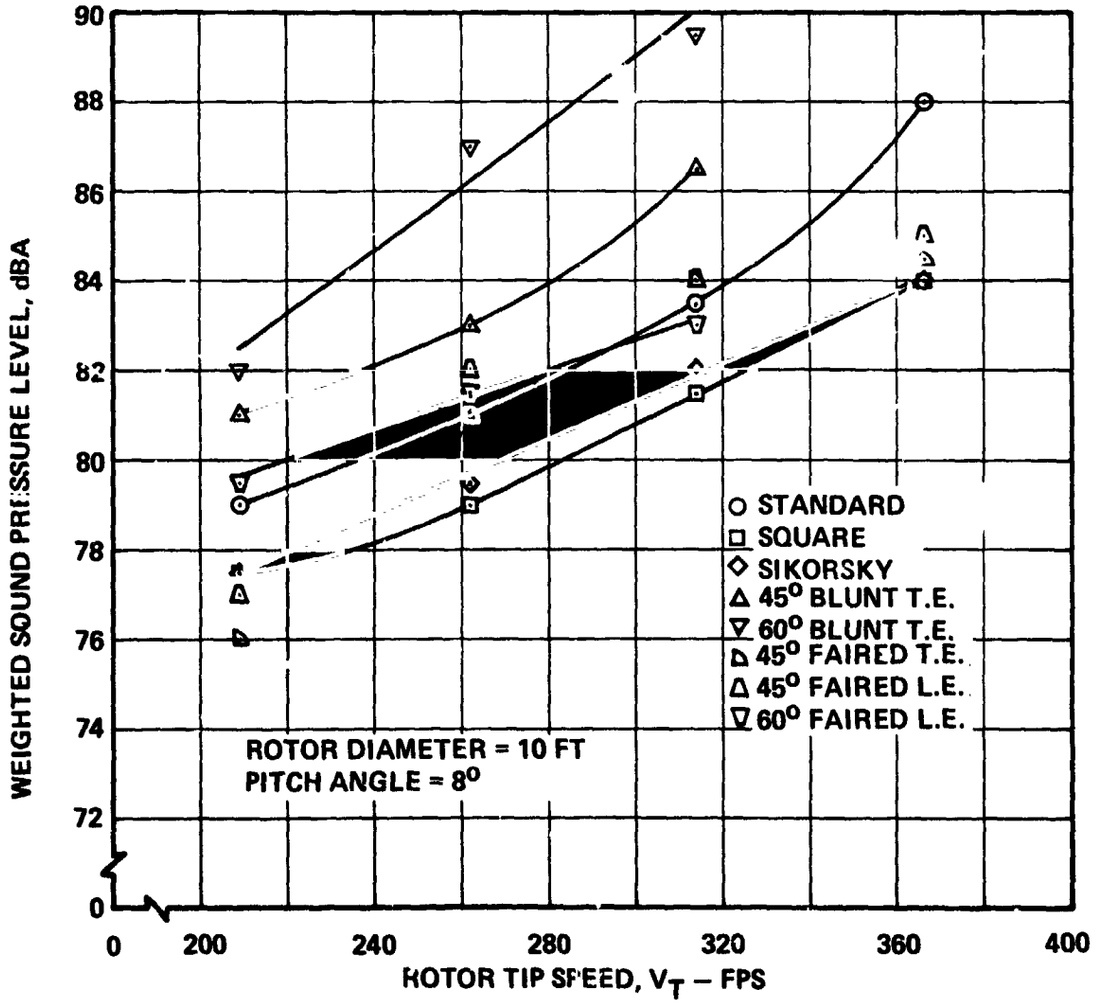

FIGURE A-6 TIP SHAPE COMPARISON FROM REFERENCE 11

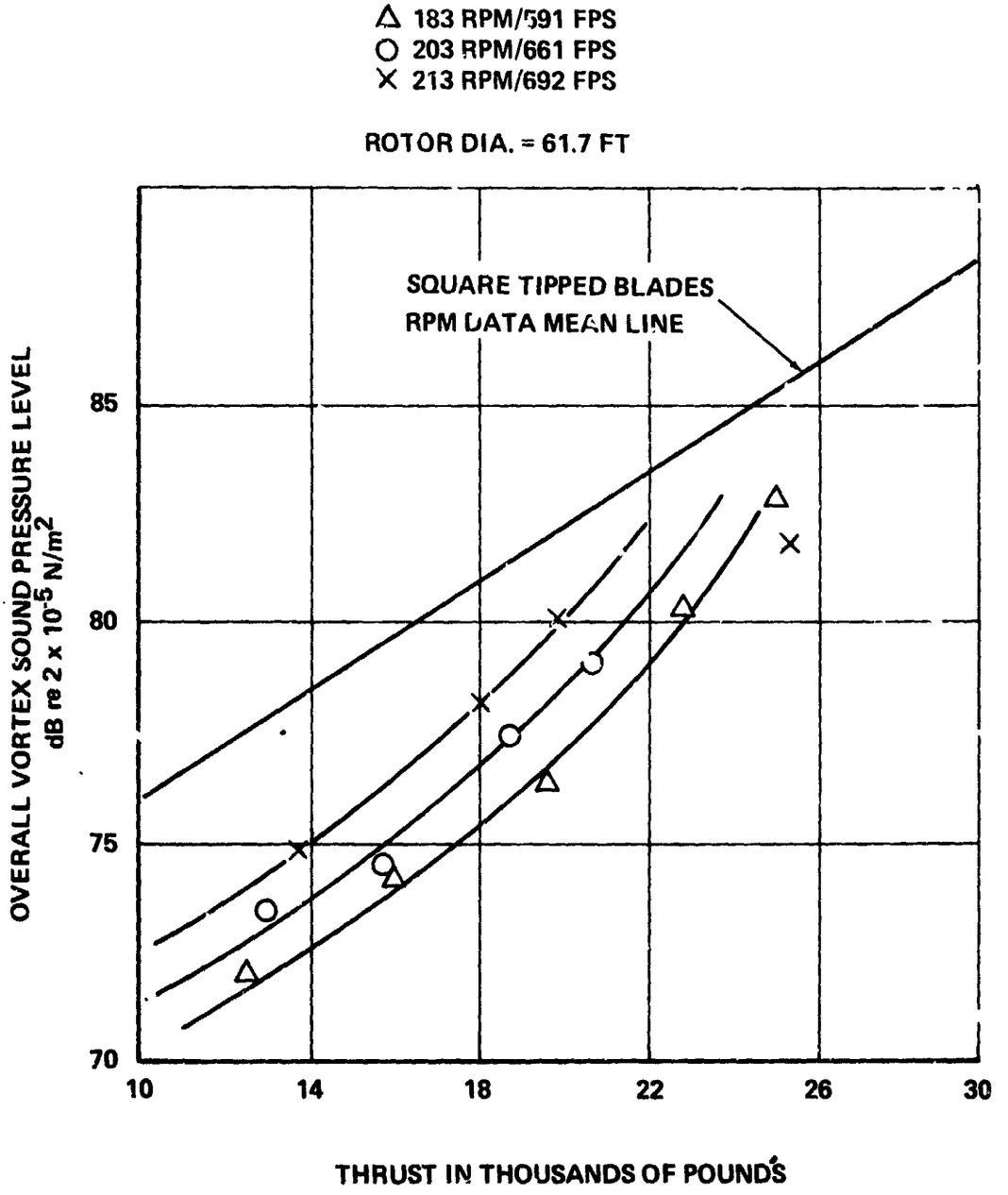

FIGURE A-7 COMPARISON OF SQUARE AND TRAPEZOIDAL TIPS FROM REFERENCE 10

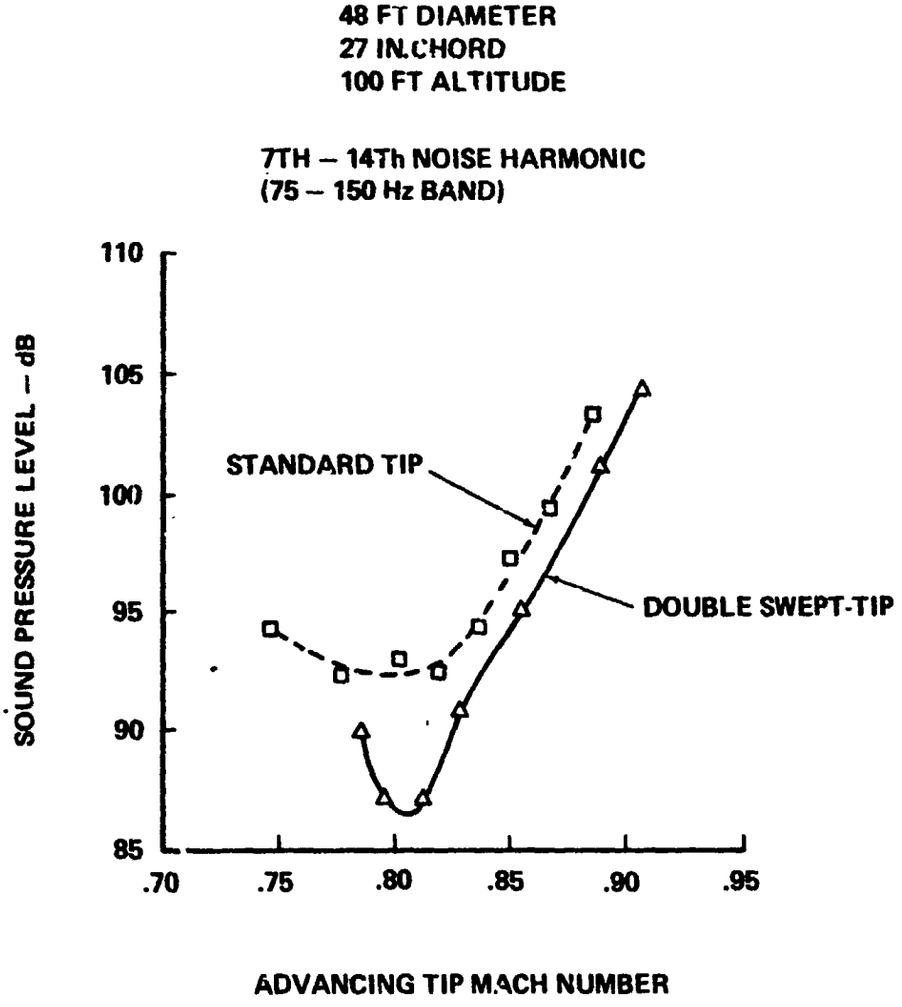

FIGURE A-8 EFFECT OF SWEPT-TIP MAIN ROTOR BLADES ON HELICOPTER FLYOVER NOISE (REF. 21)

APPENDIX B

SAMPLE CALCULATION OF TURBO-SHAFT ENGINE INLET NOISE SUPPRESSION

The following sample calculation is included to familiarize the reader with design parameters controlling the installation of sound attenuating linings. The calculation procedure will utilize figures from Section III which are representative of the current state-of-the-art sound absorption lining design. The parameters represent the Model 222 and typical noise attenuation requirements.

Peak attenuation frequency (f)	=	*4000 Hz*
Distance between inside inlet surface & transmission fairing (H)	=	*.5 ft.*
Speed of sound (c)	=	*1117 ft/sec*
Desired attenuation	=	*-10 dB*

Therefore, the *frequency parameter* $(fH/c) = \frac{4000 \times .5}{1117} = 1.79$ (non-dimensional)

Then, using Figure 3-7, the resulting peak attenuation per L/H is $-7.5dB/(L/H)$ at $M = 0$.

Since the desired peak attenuation is $10dB$, the L/H ratio needed is

$$\left(\frac{7.5dB}{L/H}\right)\left(\frac{L}{H}\right)_N = 10dB$$

$$(L/H)_N = \frac{10dB}{7.5dB/(L/H)} = 1.333$$

Thus, the length of inlet lining needed is

$$L_N = (L/H)_N H = 1.333 \times .5 = .67 \text{ ft.}$$

This procedure ignores the modifications that might be needed to de-ice the new noise suppression inlet.

APPENDIX C

HOVER OGE PERFORMANCE PREDICTION

Hover and axial flow rotor performance presented in this report is calculated by a computer program consisting of vortex theory with empirical corrections for the wake structure. The Boeing Vertol Company uses this program as a primary design tool in the optimization of aerodynamic performance of rotors in axial flow. Confidence in the prediction capability of this method was gained by comparing test results and predictions for many rotors, propellers, and convertible proprotors. Examples of such comparisons may be seen in References 22 and 23.

In hover, the interaction of the wake vortex structure and the induced velocity at the rotor plane caused by the wake determine the wake vorticity. The calculation procedure uses momentum theory to establish the reference or *normal* vortex structure. A new blade loading is calculated from the reference wake vortex structure which is then updated to account for the new blade loading. The procedure is repeated until a solution is found.

Wake structure reflects the vortex law requiring vortex filaments to travel at the same velocity as the flow in the wake. The wake flow is the sum of the axial speed of the airscrew *(V)* and the three components of flow induced by the vortex filaments. Thus, the axial variation of the slipstream velocities are a prime factor

in the vortex arrangement of the wake. Glauert's approximation (Ref. 24, pg. 367) of the downstream variation of the slipstream velocity with distance from the tip path plane was used.

This finally led to the approximate formula

$$v_x/v_\infty = (1/2)\left[2 - (1 - AF)e^{-Nx/R}\right], \qquad \text{(C-1)}$$

where the slipstream acceleration factor AF is about 0.19 and falls asymptotically to zero as v increases.

The slipstream model based on the above relationship worked quite well for low disc loadings, but gave too optimistic results for propellers as used in the tilt-wing configurations. Assuming that the general form of Equation (C-1) is correct, values of the so-called contraction rate parameter N were selected to match theoretical results against experimental data. In this way, a curve of "correct" values of N versus airscrew thrust coefficient values $(C_T = T/A\rho V_t^2)$ was obtained. The thus established relationship of $N = f(C_T)$ was used in the computer program.

Combined blade element and momentum theory may be used for rapid calculation of rotor hover performance. Fairly accurate results *(±.5% Figure of Merit)* should be attained by suitable correction factors based on the more detailed description of a hovering rotor contained in the vortex theory computer program.

Thus:

$$C_P = \frac{C_T^{3/2}}{\sqrt{2}} k_{ind_h} + \frac{\bar{\sigma} d_0 \sigma}{8} \qquad \text{(C-2)}$$

and

$$Figure\ of\ Merit = \frac{C_T^{3/2}/\sqrt{2}}{C_T^{3/2}\, k_{ind_h}/\sqrt{2} + (\bar{c}_{d_o}\sigma/8)} \qquad \text{(C-3)}$$

where:

$k_{ind_h} \equiv$ *nonideal induced power correction*

$\bar{c}_{d_o} \equiv$ *average blade profile drag.*

A reasonable average profile drag for the spanwise airfoil section distribution (Reference 1) of the Model 222 rotor is .00831 at the design operating condition. The nonideal induced power correction factor is shown to be a function of thrust coefficient (C_T) in Figure C-1. The dependence of the nonideal induced power correction on C_T is consistent with the explicit vortex interference theory because the wake structure of the vortex theory was defined empirically as a function of C_T. The trend of the nonideal induced power correction shown in Figure C-1 is only good for the assumed hover figure-of-merit to propeller cruise efficiency tradeoff and can be represented over the range $.006 \leq C_T \leq .028$ by the following equation:

$$k_{ind_h} = .8733 + 43.30C_T - 1774.9C_T^2 + 28664C_T^3 \qquad \text{(C-4)}$$

If k_{ind_h}, C_T/σ and disc loading (W/A) are assumed to be constant, it can be shown that the figure-of-merit would increase as hover tip speed decreases.

$$C_T/\sigma = .0896$$

$$C_T|_{W/A} = constant/V_t^2 \equiv K/V_t^2 \qquad \text{(C-5)}$$

$$FM|_{C_T/\sigma,\ W/A} = \frac{K^{1/2}/\sqrt{2}}{K^{1/2}k_{ind_h}/\sqrt{2} + .0116V_t}. \qquad \text{(C-6)}$$

Equation (C-6) contradicts the trend shown in Figure 4.3. However, k_{ind_h} is not a constant as assumed in Equation (C-6), but has been shown to be a function of C_T. Therefore, Equation (C-6) is consistent with the methodology used for performance calculations and supports the rotor performance trends shown in Figure 4.3 if k_{ind_h} varies.

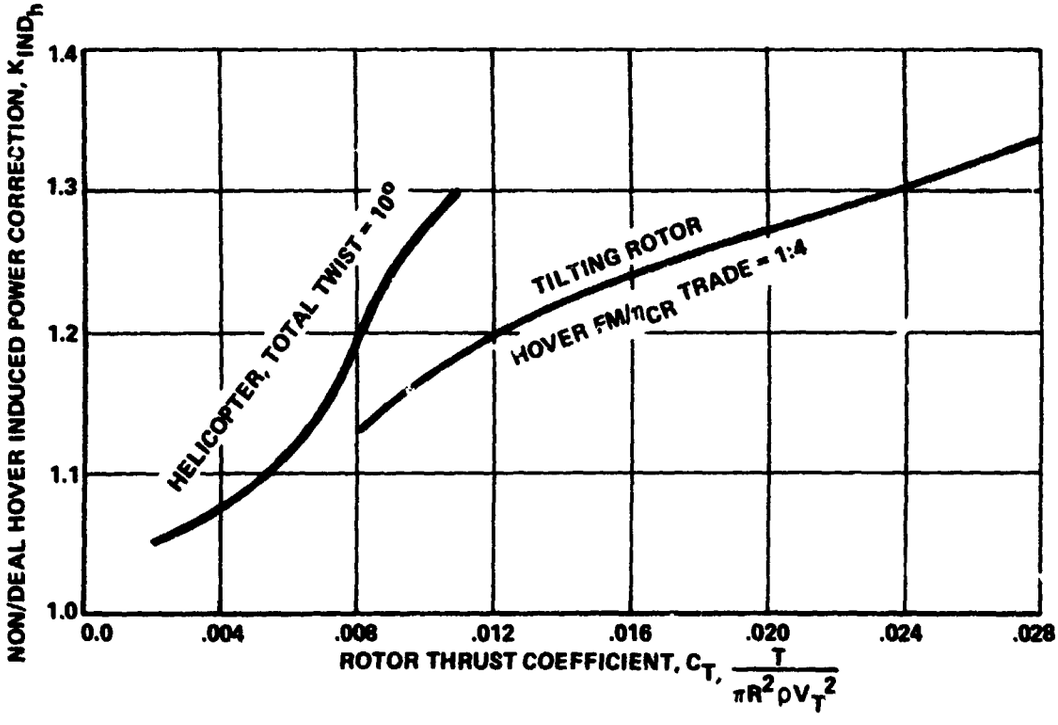

FIGURE C-1. HOVER INDUCED POWER CORRECTION FOR TILT-ROTOR AIRCRAFT AND HELICOPTERS

APPENDIX D

TABULATION OF SUMMARY WEIGHT STATEMENTS AND CONFIGURATION CHARACTERISTICS

WING	
SPAN	35ft 5in
CHORD	71.8 in
AREA	200 ft²
ASPECT RATIO	5.61
TAPER RATIO	1.0
THICKNESS-CHORD RATIO	.21
WING LOADING	60 lbs/ft²
HORIZONTAL TAIL	
SPAN	15 ft 3 in
AREA	58.3 ft²
VERTICAL TAIL	
SPAN	8 ft 9 in
AREA	43.3 ft²
ROTOR	
DIAMETER	26 ft - 0 in
SOLIDITY	.115
DISC LOADING	11.3 lbs/ft² (DL/σ)
NR BLADES	3
WEIGHTS	
DESIGN GROSS WT.	12,000 lbs
WT EMPTY	9,230 lbs

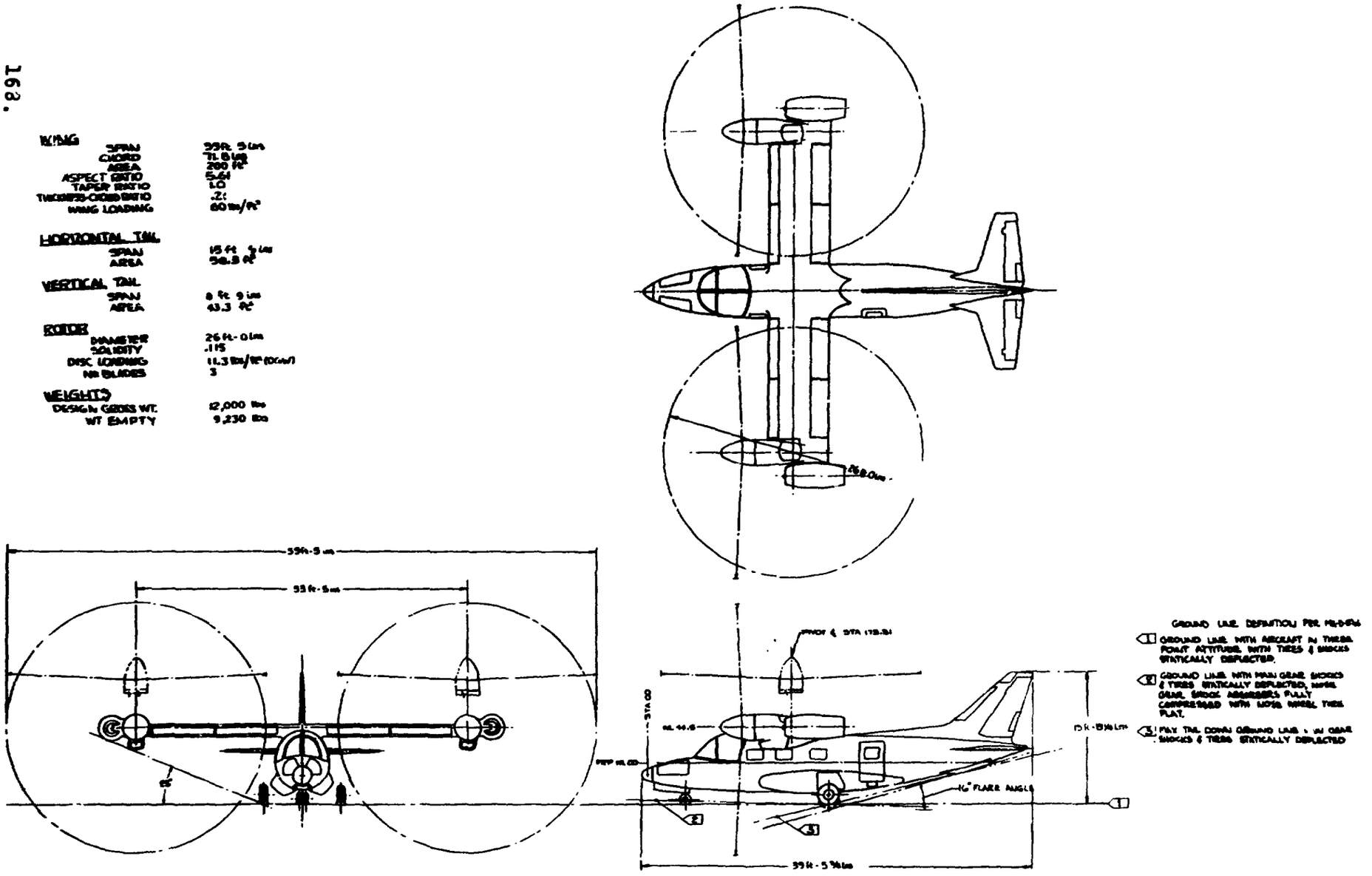

FIGURE D-1 MODEL 222-1 TILT ROTOR NASA RESEARCH AIRCRAFT

	① MODEL 222	② V_{TH}= 650 B=3 C_T/σ=.0886	③ V_{TH}= 550 B = 3 C_T/σ=.0896	② V_{TH}= 750 B = 3 σ = .15	③ V_{TH}=750 B = 3 σ = .20	② V_{TH}= 750 B = 4 σ =.0885	③ V_{TH}=750 B = 5 σ/B=.0385	② V_{TH}=750 B = 4 σ=.1154	③ V_{TH}= 750 B = 5 σ=.1154	② V_{TH}= 750 B = 3 W/A= 8.5	③ V_{TH}=750 B = 3 W/A= 5.6
ROTOR GROUP	1100	1212	1354	1312	1600	1354	1596	1114	1126	1072	1048
WING GROUP	800	780	750	774	734	771	737	780	780	942	1195
TAIL GROUP	213	213	213	213	213	213	213	213	213	231	267
BODY GROUP	1211	1211	1211	1211	1211	1211	1211	1211	1211	1211	1211
BASIC											
SECONDARY											
SECOND.-DOORS, ETC.											
ALIGHTING GEAR	590	590	590	590	590	590	590	590	590	590	590
FLIGHT CONTROLS	1183	1239	1309	1289	1428	1309	1427	1191	1196	1170	1158
ENGINE SECTION	400	400	400	400	400	400	400	400	400	400	400
PROPULSION GROUP	(2533)	(2690)	(2904)	(2565)	(2677)	(2577)	(2645)	(2506)	(2496)	(2358)	(2254)
ENGINE(S)	1026	1037	1053	1043	1103	1049	1086	1011	1006	868	732
AIR INDUCTION	35	35	35	35	35	35	35	35	35	35	35
EXHAUST SYSTEM	40	40	40	40	40	40	40	40	40	40	40
COOLING SYSTEM	60	60	60	60	60	60	60	60	60	60	60
LUBRICATING SYSTEM	20	20	20	20	20	20	20	20	20	20	20
FUEL SYSTEM	200	200	200	200	200	200	200	200	200	200	200
ENGINE CONTROLS	20	20	20	20	20	20	20	20	20	20	20
STARTING SYSTEM	25	25	25	25	25	25	25	25	25	25	25
PROPELLER INST.											
DRIVE SYSTEM	1107	1253	1451	1132	1174	1128	1159	1095	1090	1087	1122
MISC. POWER PLANT											
ASSR. AND NAV.	108	108	108	108	108	108	108	108	108	108	108
HYDR. AND PNEU.											
ELECTRICAL GROUP	305	305	305	305	305	305	305	305	305	305	305
ELECTRONICS GROUP	230	230	230	230	230	230	230	230	230	230	230
ARMAMENT GROUP											
FURN. & EQUIP. GROUP	(439)	(439)	(439)	(439)	(439)	(439)	(439)	(439)	(439)	(439)	(439)
PERSON. ACCOM.	299	299	299	299	299	299	299	299	299	299	299
MISC. EQUIPMENT	63	63	63	63	63	63	63	63	63	63	63
FURNISHINGS	35	35	35	35	35	35	35	35	35	35	35
ENVIRO. EQUIPMENT	42	42	42	42	42	42	42	42	42	42	42
AIR CONDR. & DEICING	108	108	108	108	108	108	108	108	108	108	108
PHOTOGRAPHIC											
AUXILIARY GEAR	10	10	10	10	10	10	10	10	10	10	10
MISC. VARIATION											
WEIGHT EMPTY	9230	9535	9931	9574	10053	9625	10019	9205	9212	9174	9323
FIXED USEFUL LOAD											
CREW (2)	360	360	360	360	360	360	360	360	360	360	360
TRAPPED LIQUIDS	40	40	40	40	40	40	40	40	40	40	40
ENGINE OIL											
FUEL	1072	1093	1118	1148	1247	1147	1231	1071	1068	1013	954
CARGO	1298	972	551	878	300	828	350	1324	1320	1413	1323
PASSENGERS/TROOPS											
GROSS WEIGHT	12000	12000	12000	12000	12000	12000	12000	12000	12000	12000	12000

* INCLUDES LB. SUMS. OIL REV.

TABLE D-1 LISTING OF SUMMARY WEIGHT STATEMENTS FOR ALL SENSITIVITY LINE AIRCRAFT

	①	②	③	②	③	②	③	②	③	②	③
CASE / ITEM	M 222 BASELINE	V_T = 650	V_T = 550	σ = .15	σ = .20	σ/B = .0385 B = 4	σ/B = .0385 B = 5	σ = .1154 B = 4	σ = .1154 B = 5	W/A = 3.5	W/A = 5.6
ROTOR											
ROTOR RADIUS; FT	13	13	13	13	13	13	13	13	13	15	18.5
NO. OF BLADES	3	3	3	3	3	4	5	4	5	3	3
$V_{T_{HOVER}}$; FPS	750	650	550	750	750	750	750	750	750	750	750
σ	.1154	.1540	.2150	.15	.20	.1540	.1925	.1154	.1154	.087	.057
DISC LOADING; LB/FT^2	11.3	11.3	11.3	11.3	11.3	11.3	11.3	11.3	11.3	8.5	5.6
WING											
WING AREA; FT^2	200	200	200	200	200	200	200	200	200	224	266
WING SPAN; FT	33.42	33.42	33.42	33.42	33.42	33.42	33.42	33.42	33.42	37.42	44.42
AR	5.61	5.61	5.61	5.61	5.61	5.61	5.61	5.61	5.61	6.25	7.42
TAPER RATIO	1.0	1.0	1.0	1.0	1.0	1.0	1.0	1.0	1.0	1.0	1.0
HORIZONTAL TAIL											
AREA; FT^2	58.3	58.3	58.3	58.3	58.3	58.3	58.3	58.3	58.3	66.3	78.7
SPAN; FT	15.67	15.67	15.67	15.67	15.67	15.67	15.67	15.67	15.67	16.7	18.2
AR	4.22	4.22	4.22	4.22	4.22	4.22	4.22	4.22	4.22	4.22	4.22
TAPER RATIO	.337	.337	.337	.337	.337	.337	.337	.337	.337	.337	.337
TAIL VOLUME COEFF	1.0	1.0	1.0	1.0	1.0	1.0	1.0	1.0	1.0	1.0	1.0
MOMENT ARM; FT	20.3	20.3	20.3	20.3	20.3	20.3	20.3	20.3	20.3	20.3	20.3
VERTICAL TAIL											
AREA; FT^2	43.3	43.3	43.3	43.3	43.3	43.3	43.3	43.3	43.3	54.2	76.5
SPAN; FT	8.12	8.12	8.12	8.12	8.12	8.12	8.12	8.12	8.12	9.08	10.75
AR	1.52	1.52	1.52	1.52	1.52	1.52	1.52	1.52	1.52	1.52	1.52
TAPER RATIO	.329	.329	.329	.329	.329	.329	.329	.329	.329	.329	.329
TAIL VOLUME COEFF.	.127	.127	.127	.127	.127	.127	.127	.127	.127	.127	.127
MOMENT ARM; FT	19.55	19.55	19.55	19.55	19.55	19.55	19.55	19.55	19.55	19.55	19.55
NO. OF ENGINES	2	2	2	2	2	2	2	2	2	2	2
SHP*/ENGINE	1550.	1572.	1598.	1601.	1677.	1595.	1650.	1537.	1530.	1318.	1114.
XMSN HP LIMIT/ROTOR	1150.	1167.	1186.	1188.	1243.	1183.	1224.	1140.	1135.	978.	826.
fe; FT^2	6.279	6.279	6.279	6.279	6.279	6.279	6.279	6.279	6.279	6.706	7.186
HOVER O.G.E. 100 FT ALT											
OASPL @ 500 FT	92.5	89.6	86.6	92.7	92.8	90.5	88.4	90.4	88.2	91.1	89.1
PNL @ 500 FT	93.6	90.3	86.0	92.7	91.7	92.3	91.0	93.3	92.9	93.3	92.3

*MAXIMUM STATIC HORSEPOWER @ S.L. STD DAY

TABLE D-2 CHANGES IN AIRCRAFT CONFIGURATION CAUSED BY DESIGN PARAMETER CHANGES

APPENDIX E

ACCURACY OF THE THEORETICAL TILT-ROTOR ACOUSTIC MODEL

The acoustical mathematical model used in this report to predict the aircraft signature is the same as that in Reference 2, with a minor change in the loading law as shown in Figure 4-17.

The accuracy of the acoustic model in predicting the signature of a tilt-rotor has not been defined in depth due primarily to a lack of data on full-scale rotors. However, a valid comparison of prediction and experimental rotor data has been made with a CH-47B/C for a range of rotor tip speed and thrust sweeps on the Boeing Vertol experimental whirl tower. This comparison is shown in Table E-1 and E-2. These blades have less than 9° twist, however, tilt-rotor blades have 30-40 degrees. For correlation, harmonically related data is analyzed with narrow band filtering (2 Hz bandwidth) and averaged over approximately 30 rotor cycles or 3 seconds. For comparison with broadband theory, the data is analyzed with 1/3 or 1/1 octave filters and the average of 3 seconds of data is also read.

The only comparisons of prediction and measurement to be incorporated into this report are test data published in Reference 5, pages 47, 48, and 49. To accurately interpret the comparisons shown in Tables E-1 and E-2 for OASPL and PNL respectively, the following must be taken into account.

(1) Whirl Tower Data may vary by as much as 6 dB for identical test conditions.

(2) The rotor height was approximately one diameter above the ground. To be out of aerodynamic effects of the ground plane, the rotor should be 1.5 diameters, or higher, above the ground.

(3) The acoustic model assumes 1/3-octave bands with an infinite roll-off of 1/3 octave; the rotor to be out-of-ground effect with zero forward speed.

(4) The acoustic model prediction has not been corrected for the reflections of the rotor acoustic signature from the ground. See Ref. 12, pgs. 96 - 100 for pure tone correction.

(5) The octave band filters used are 3 dB down at bandwidth limits and have a rolloff of 25 dB/octave.

(6) The prediction of the rotor fundamental blade passage frequency is not included in the OASPL or PNL presented in Tables E-1 and E-2.

The theoretical acoustic model for harmonically related noise consistently predicts the first five harmonics of the rotor signature with good accuracy (Ref. 5). The empirical theory or algorithm for broadband noise, however, does not achieve the same amount of

precision and consistently underpredicts data (Ref. 5). Although a generalized empirical correction has been made to this theory to improve the agreement with rotor data, it cannot be verified with any accuracy at this time due to a lack of available data for comparison. When compared with CH-47B rotor data from whirl tower experiment, the acoustic model consistently underpredicts both OASPL and PNL by an average of 6.9 dB and 6.6 PNdB, respectively.

The OASPL deviations vary from a minimum of 4.2 dB and a maximum of 11.5 dB. The PNL deviations have a minimum of 1.5 PNdB and a maximum of 13.5 PNdB. It cannot be determined from this small data sample whether the theoretical model is correctly predicting the change of the acoustic signature as a function of either tip speed or thrust.

The authors caution the reader that the trends of the small number of data points presented in Tables E-1 and E-2 are not sufficient to be conclusive evidence of the accuracy of the acoustic model. For statistical accuracy, a minimum of 8 data points per design parameter variation (while maintaining other design parameters as constants) would be desirable, including repeated measurements to define the data variance. It is recommended that this be pursued so as to create a data base against which any mathematic representation of rotor acoustics can be compared. This would be useful to the whole rotary-wing industry, as the rotor acoustic far-field signature becomes more important to operators of rotary-wing aircraft.

MEASURED AND PREDICTED OVERALL SOUND PRESSURE LEVELS FOR A CH-47B/C ROTOR ON A WHIRL TOWER				
TIP SPEED ∿ V_t ∿	THRUST ∿ *LB* ∿	CALCULATED ∿ *dB* ∿	MEASURED ∿ *dB* ∿	Δ ∿ *dB* ∿
650	8,600	85.3	96.8	11.5
	17,500	90.9	96.1	5.2
	23,000	93.4	97.6	4.2
750	9,700	94.0	99.6	5.6
	19,000	103.2	109.5	6.3
850	8,300	93.2	102.3	9.1
	17,000	98.7	106.9	8.2
	26,600	102.5	107.4	4.9
			Average Δ*dB*	6.87

TABLE E-1

MEASURED AND PREDICTED PERCEIVED NOISE LEVELS FOR A CH47B/C ROTOR ON A WHIRL TOWER				
TIP SPEED ∿ V_t ∿	THRUST ∿ *LB* ∿	CALCULATED ∿ *dB* ∿	MEASURED ∿ *dB* ∿	Δ ∿ *dB* ∿
650	8,600	93.5	107.0	13.5
	17,500	99.5	101.2	1.7
	23,000	101.9	103.5	1.6
750	9,700	97.2	108.3	11.1
	19,000	102.0	113.1	11.1
850	8,300	98.9	106.9	8.0
	17,000	104.9	109.2	4.3
	26,600	108.6	110.1	1.5
			Average Δ*dB*	6.6

TABLE E-2

APPENDIX F

AIRCRAFT SENSITIVITY PREDICTION TOLERANCES

This section contains sensitivity prediction tolerance charts. To provide further insight into this assessment, an Evaluation Diagram is presented which summarizes the analytical process used to calculate the most probable predicted value. In addition, optimistic (low cumulative probability) and pessimistic (high cumulative probability) values are estimated and plotted as a probability curve to indicate the range of possible deviations.

Evaluation diagrams and prediction ranges for the following characteristics are contained in this Appendix.

1.	Weight Empty	Figures F-1 and F-2
2.	Hover RPM Transmission Limit Speed	F-3 and F-4
3.	Mission Payload	F-5 and F-6
4.	99% Best Range Speed	F-7 and F-8
5.	Overall Sound Pressure Level	F-9 and F-10
6.	Perceived Noise Level	F-11 and F-12

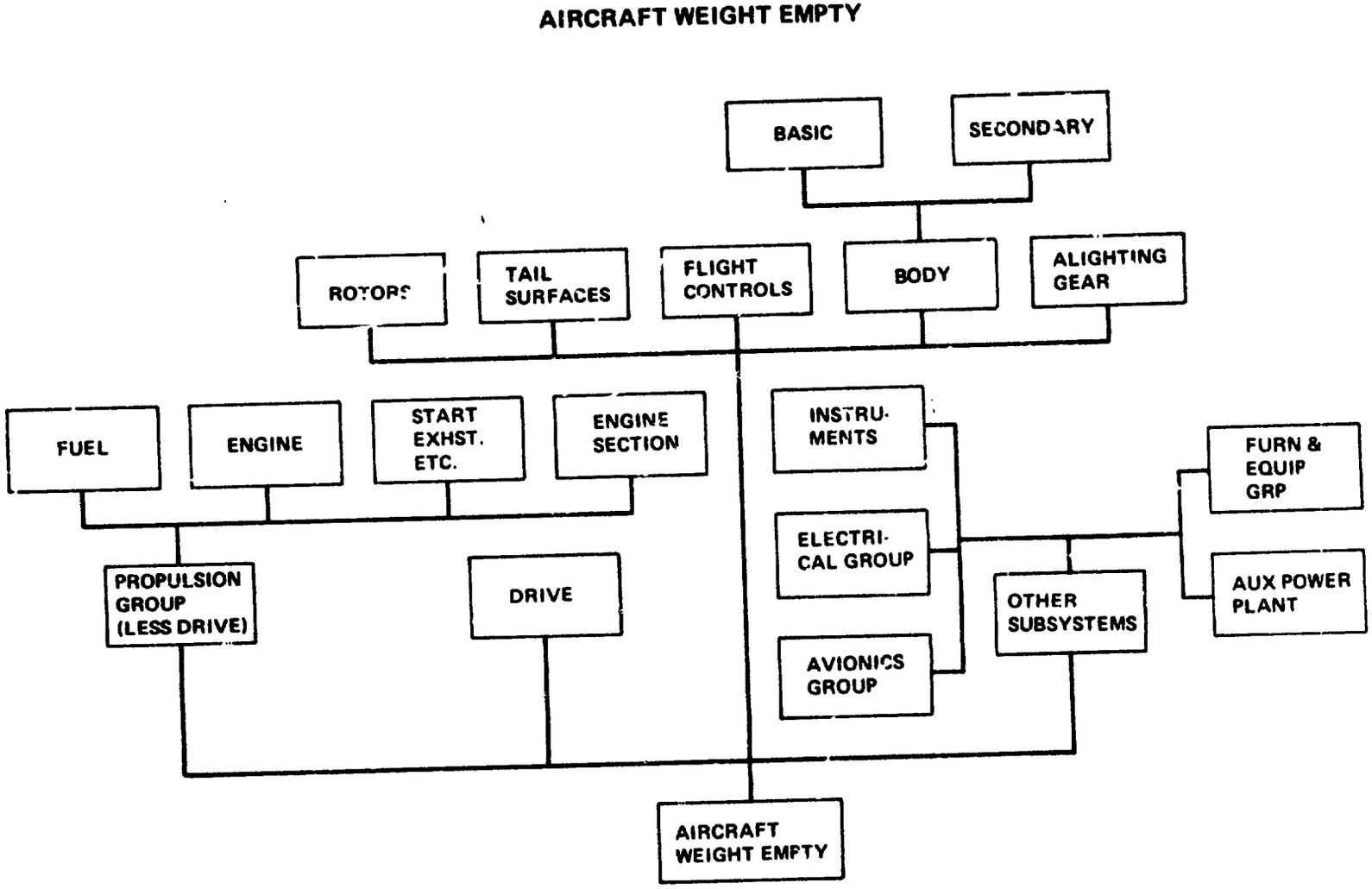

FIGURE F-1 EVALUATION DIAGRAM
(WEIGHT EMPTY)

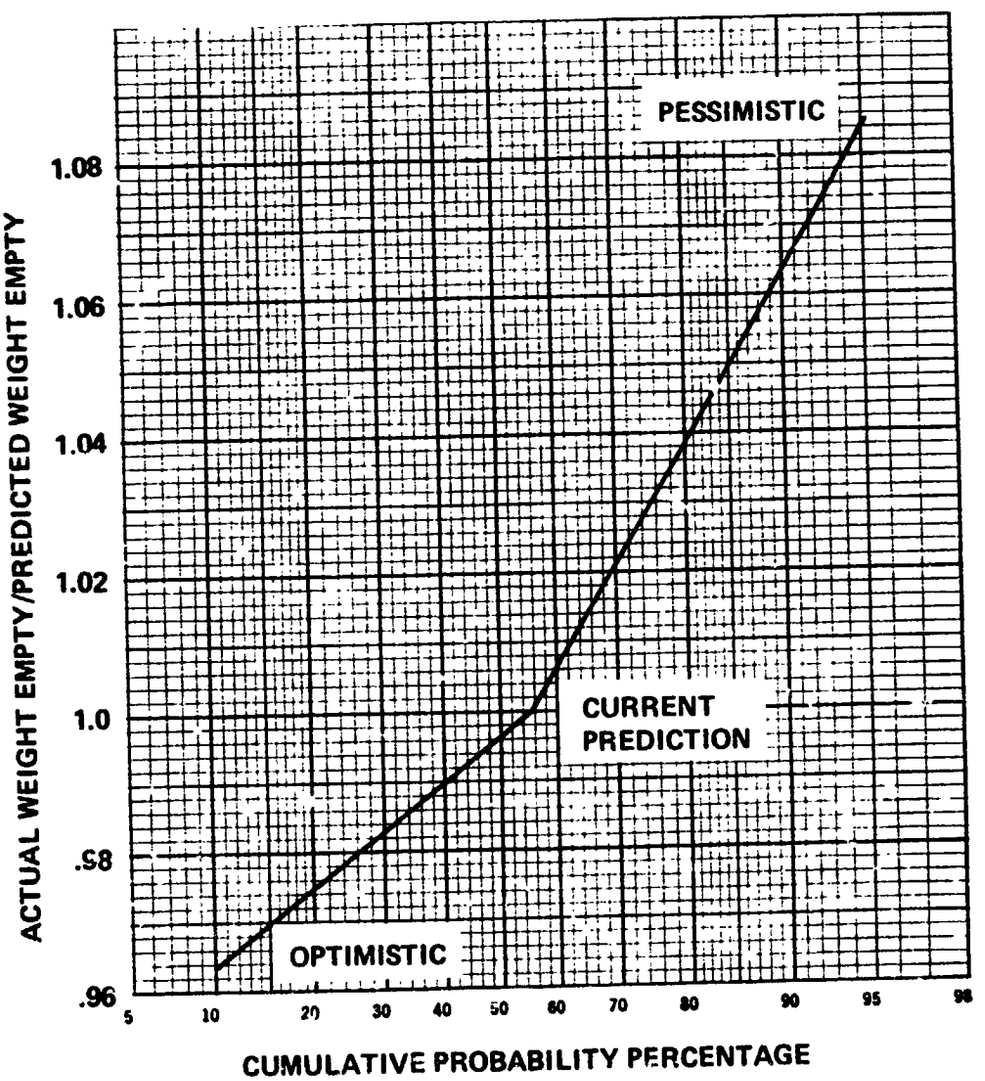

FIGURE F-2 PREDICTION RANGE FOR WEIGHT EMPTY

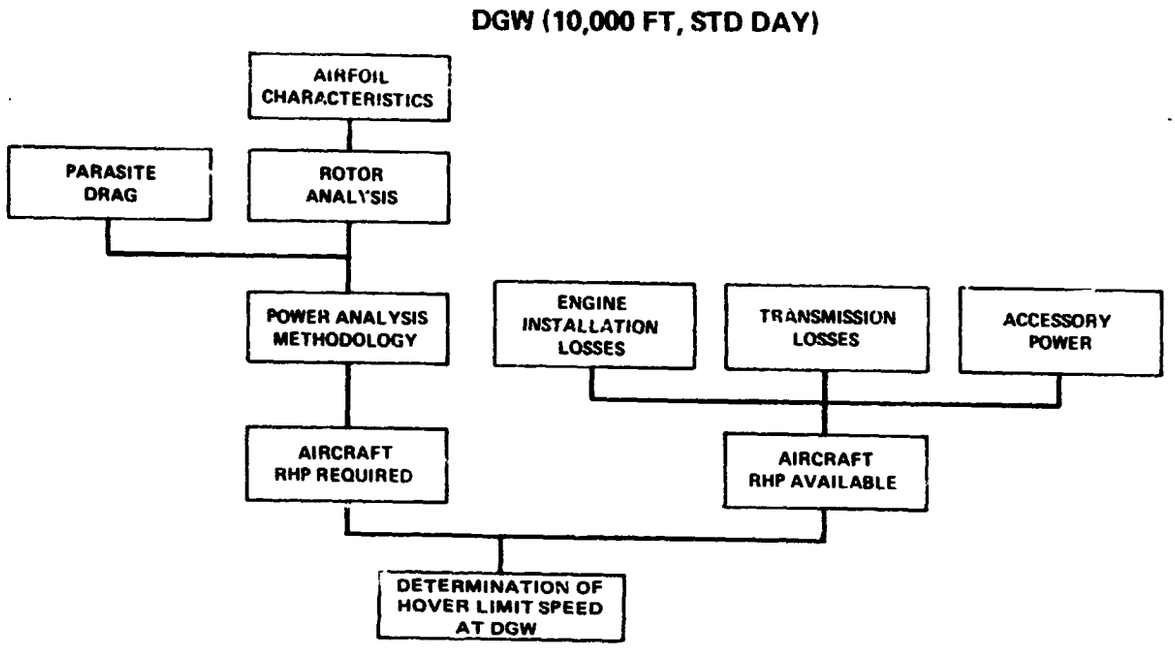

FIGURE F-3 EVALUATION DIAGRAM
(HOVER RPM TRANSMISSION SPEED)

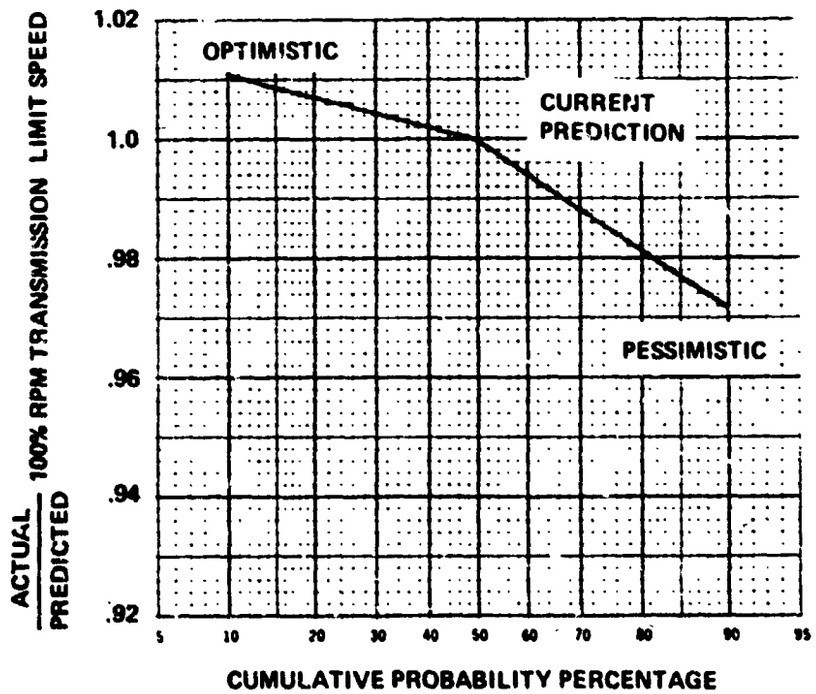

FIGURE F-4 PREDICTION RANGE FOR HOVER RPM XMSN LIMIT SPEED

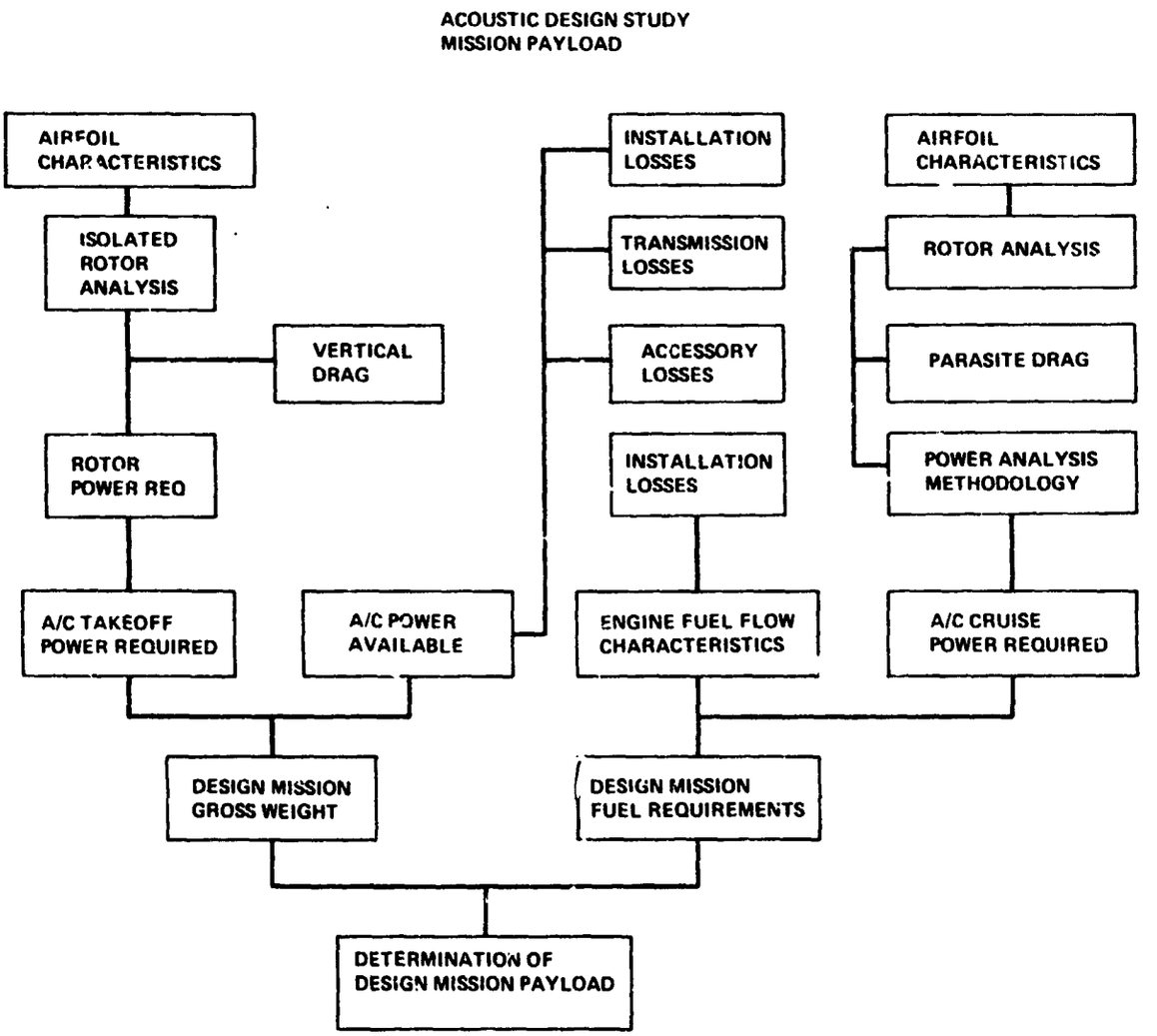

FIGURE F-5 EVALUATION DIAGRAM ACOUSTIC DESIGN STUDY MISSION PAYLOAD

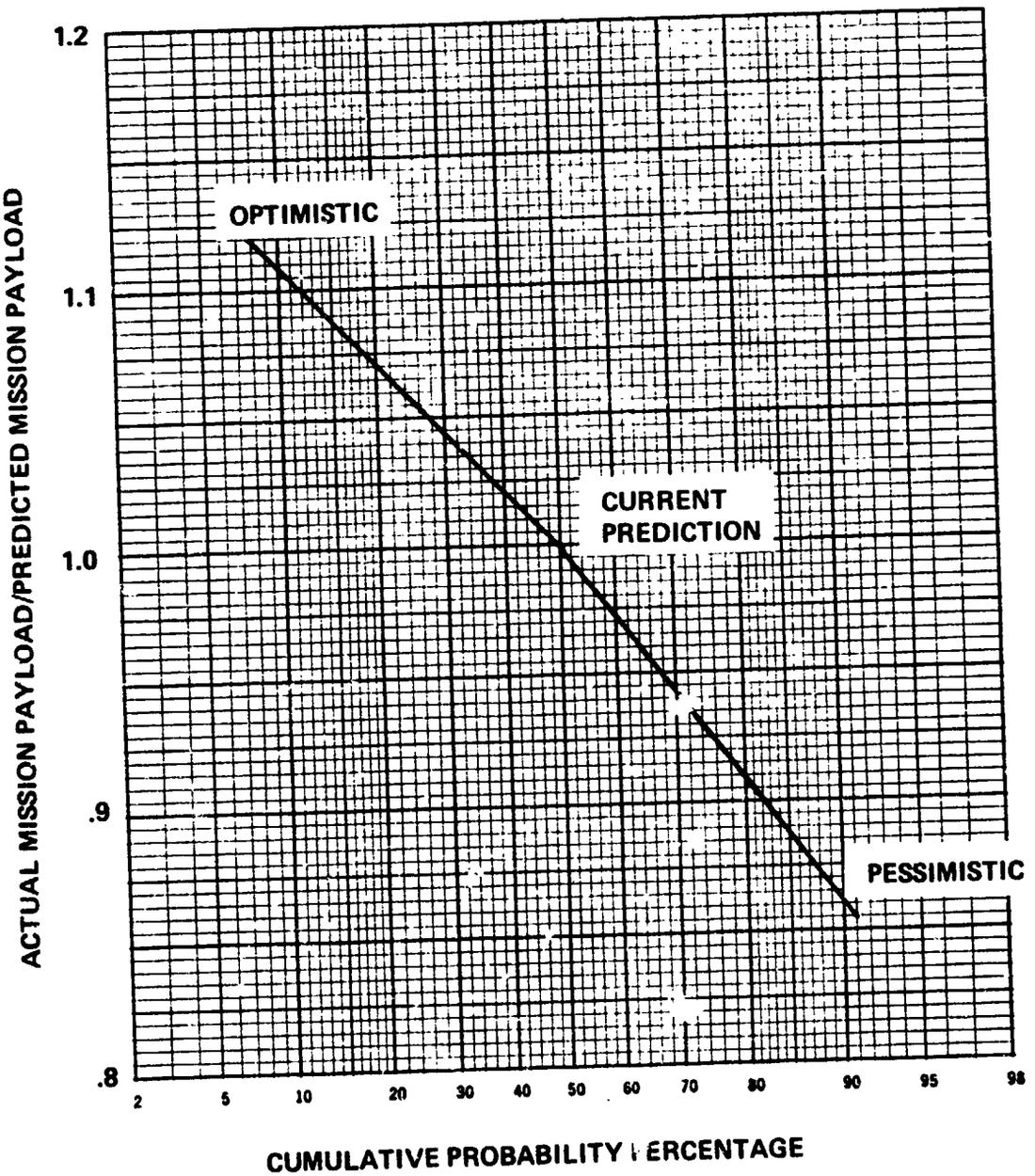

FIGURE F-6 PREDICTION RANGE FOR MISSION PAYLOAD

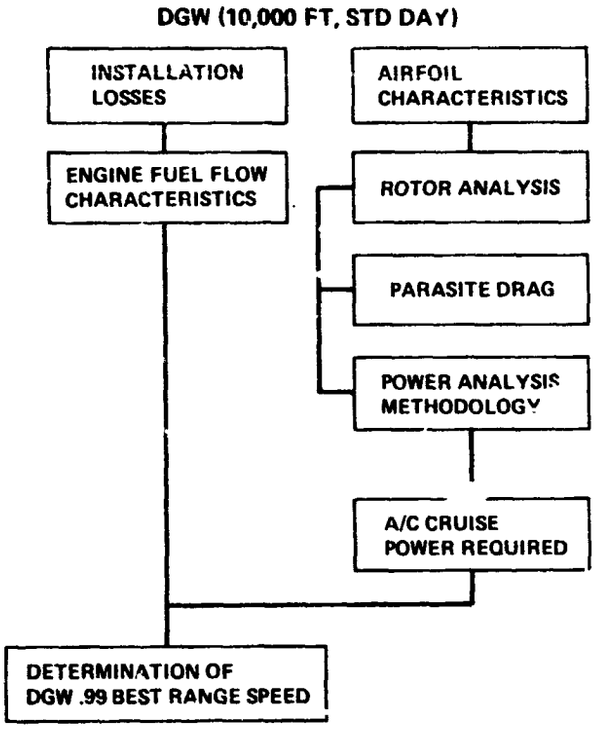

FIGURE F-7 EVALUATION DIAGRAM
(.99 BEST RANGE SPEED)

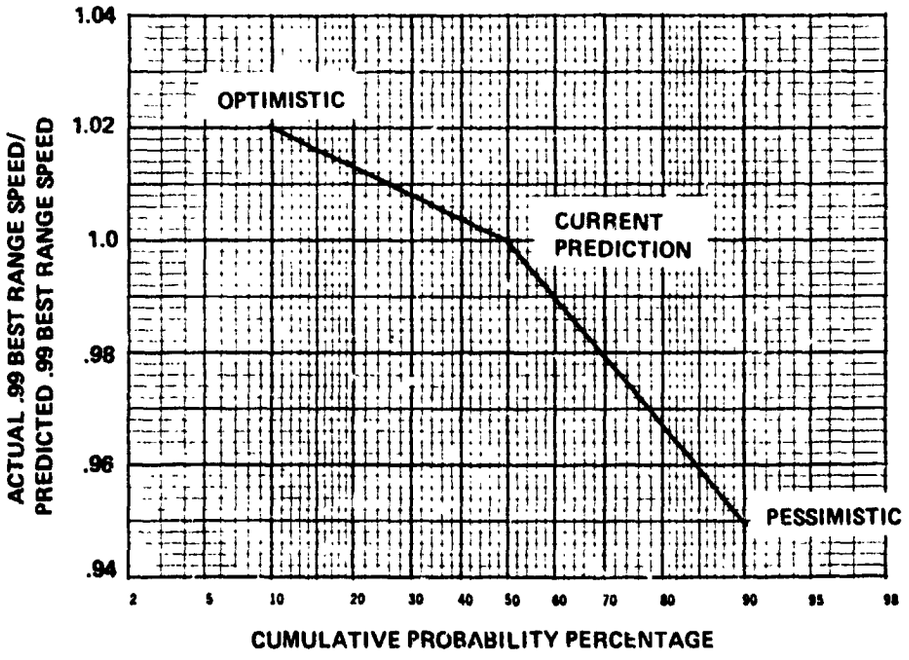

FIGURE F-8 PREDICTION RANGE FOR .99 BEST RANGE SPEED

EXTERNAL NOISE IN HOVER – DGW @ 500 FT DISTANCE

OVERALL SOUND PRESSURE LEVEL

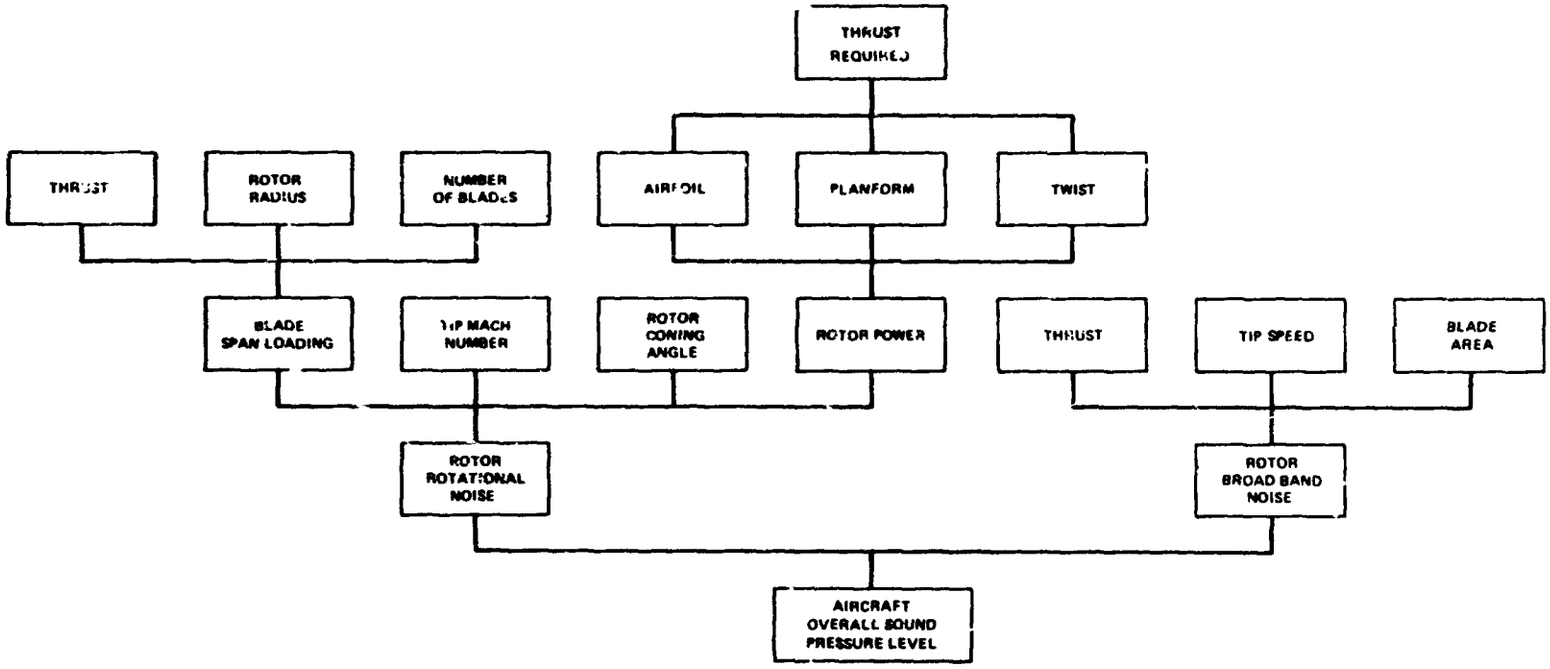

FIGURE F-9 EVALUATION DIAGRAM

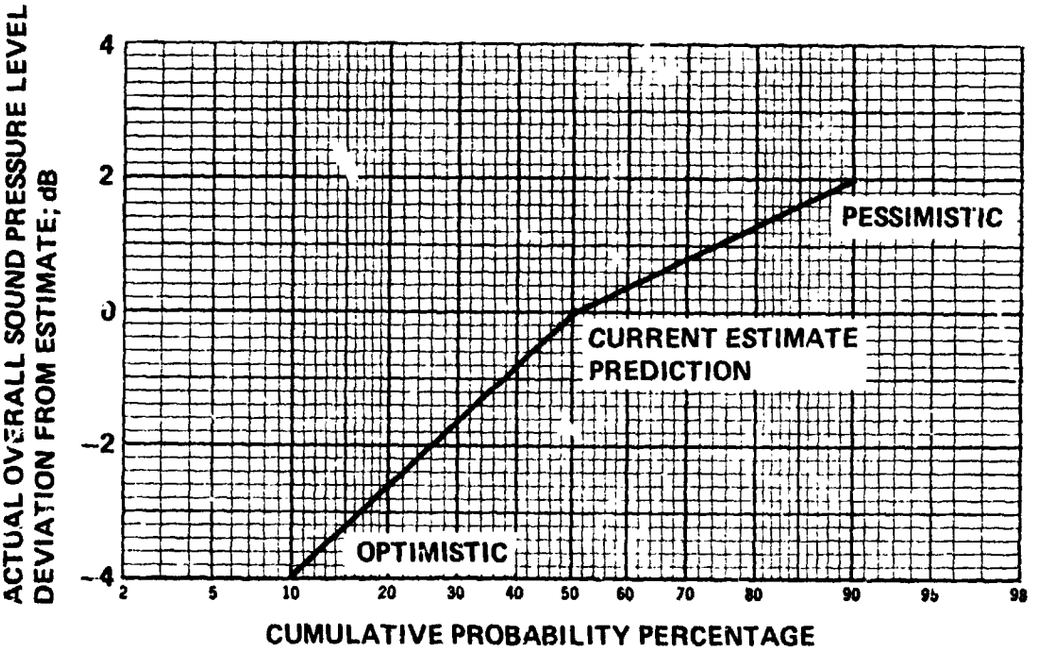

FIGURE F-10 PREDICTION RANGE FOR OVERALL SOUND PRESSURE LEVEL

EXTERNAL NOISE IN HOVER – DGW @ 500 FT DISTANCE

PERCEIVED NOISE LEVEL

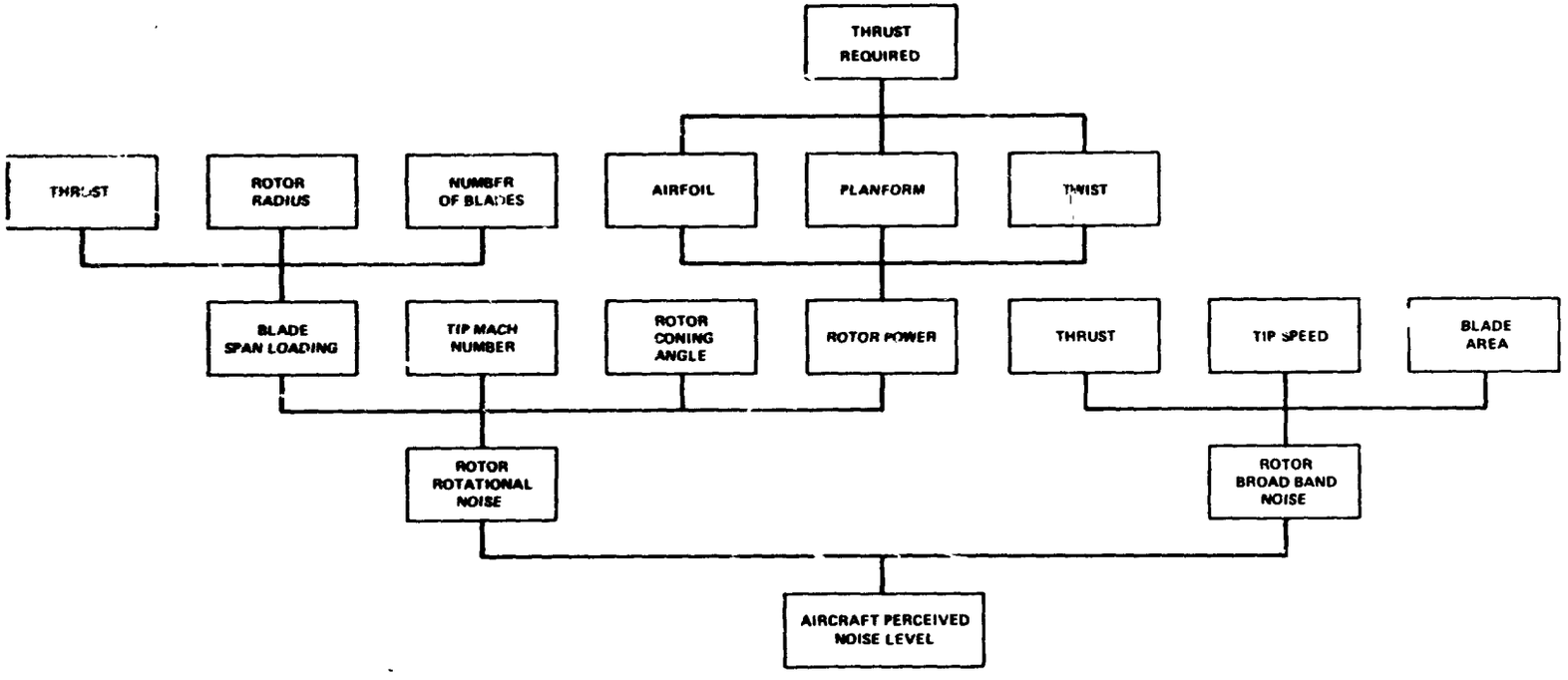

FIGURE F-11 EVALUATION DIAGRAM

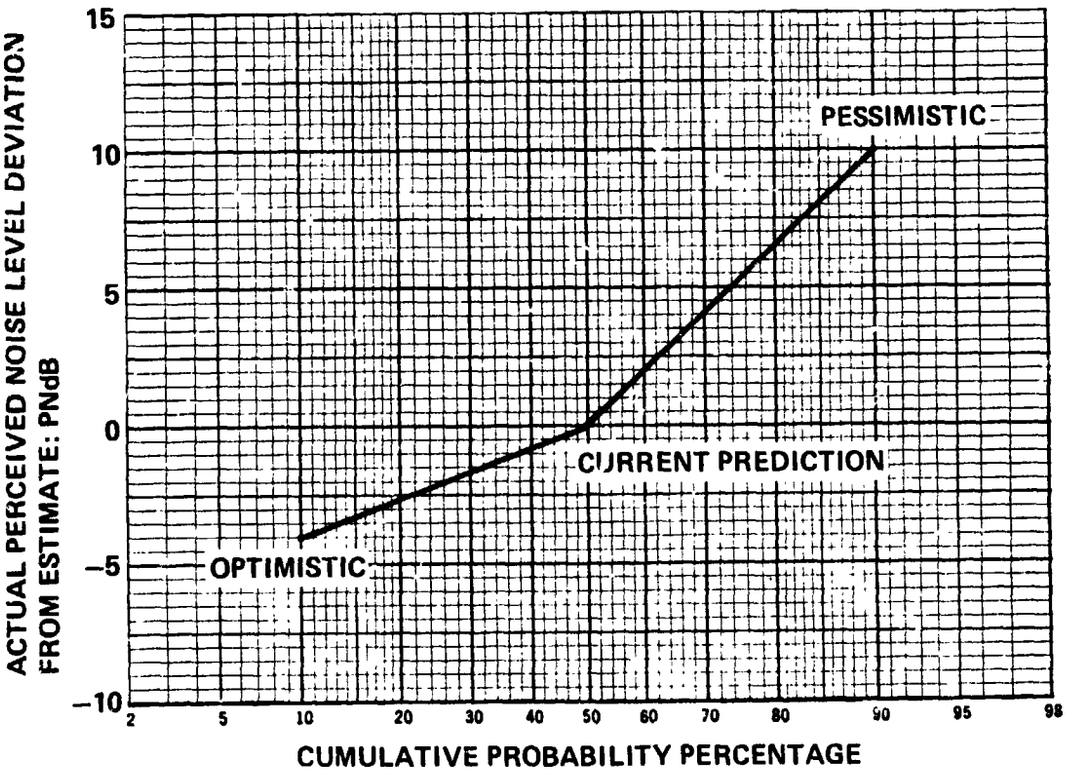

FIGURE F-12 PREDICTION RANGE FOR PERCEIVED NOISE LEVEL

APPENDIX G

WEIGHTS PREDICTION METHODOLOGY

This appendix contains the summary, development and validation of the mass properites (weight, balance and moments of inertia) for the Model 222, 26-foot diameter tilt-rotor aircraft (baseline). Preliminary estimates indicate only minor changes to the quantitative data presented in this report.

Summary and Development

The significant weights developed for the Model 222 are:

Weight Empty	9,230 lbs
Operating Weight Empty	9,630 lbs
Design Gross Weight	12,000 lbs
Alternate Gross Weight	14,400 lbs
Airframe Weight*	7,499 lbs

*DCPR (or AMPR)

The aircraft weight empty was determined using a combination of methods, including:

Statistical Weight Trend Equations	21%
Actual Weights of Existing Aircraft and/or Components	22%
Vendor Information	16%
Calculated Weights (Layout and Detail Drawings)	31%

Similar Components of Existing Aircraft 10%

(Percentages pertain to the weight empty of the aircraft.)

A summary weight statement for the aircraft is presented in Table G-1. Balance and mass moments of inertia for the configuration are included in Table G-2. The data in this table is distributed by sections of the aircraft to facilitate mass properties studies. Balance reference datums (X, Y and Z) defined in the table correspond to those used on the Mitsubishi MU-2J aircraft. Balance arms were determined by scaling the various layout drawings.

The group weights in Table G-1 consider current technology and the use of existing materials and manufacturing techniques.

Validation of Weights

The weight trends were developed around the aircraft geometry, design parameters, materials and structural criteria. A discussion of the various groups and the methods used to determine their weights follows:

MODEL 222 TILT ROTOR AIRCRAFT - NASA RESEARCH AIRCRAFT

ENGINES (2) T53-L-13 H.P. EACH - 1550 ROTOR DIA.- 26'	DESIGN GROSS WEIGHT	ALT. GROSS WEIGHT				AMPR WEIGHTS
ROTOR GROUP	1100					1100
WING GROUP	800					800
TAIL GROUP	213					213
BODY GROUP	1211					1211
BASIC						
SECONDARY						
SECOND.-DOORS, ETC.						
ALIGHTING GEAR	590	LESS: WHEELS, TIRES, BRAKES, AIR			-100	490
FLIGHT CONTROLS	1183					1183
ENGINE SECTION	400					400
PROPULSION GROUP	(2533)					(1357)
ENGINE(S)	1026	LESS: ENGINES			-1026	-
AIR INDUCTION	35					35
EXHAUST SYSTEM	40					40
COOLING SYSTEM	60					60
LUBRICATING SYSTEM	20					20
FUEL SYSTEM	200	LESS: BLADDER FUEL TANKS			- 50	150
ENGINE CONTROLS	20					20
STARTING SYSTEM	25					25
PROPELLER INST.						
*DRIVE SYSTEM	1107	LESS: XMSN OIL			-100	1007
AUX. POWER PLANT	-					
INSTR. AND NAV.	108	LESS: INDIC., XMTR, AMPL.			- 60	48
HYDR. AND PNEU.	-					
ELECTRICAL GROUP	305	LESS: BATTERY & AC, DC COMP.			-180	125
ELECTRONICS GROUP	230	LESS: CFE & GFAE EQUIP.			-175	55
ARMAMENT GROUP	-					
FURN. & EQUIP. GROUP	(439)					439
PERSON. ACCOM.	299	1200				
MISC. EQUIPMENT	63					
FURNISHINGS	35					
EMERG. EQUIPMENT	42					
AIR COND. & DE-ICING	108	LESS: ENVIRONMENTAL CONT.			- 40	68
PHOTOGRAPHIC	-					
AUXILIARY GEAR	10					10
MISC. VARIATION	-					-
WEIGHT EMPTY	9230	9230			-1731	7499
FIXED USEFUL LOAD		OPERATING WEIGHT EMPTY				
CREW (2)	360	360				
TRAPPED LIQUIDS	40	40				
ENGINE OIL						
FUEL	1170	4770				
Instrumentation	1200					
PASSENGERS/TROOPS						
GROSS WEIGHT	12000	14400				

TABLE G-1 SUMMARY WEIGHT STATEMENT

(Weight, Balance & Moments of Inertia)
NASA RESEARCH AIRCRAFT

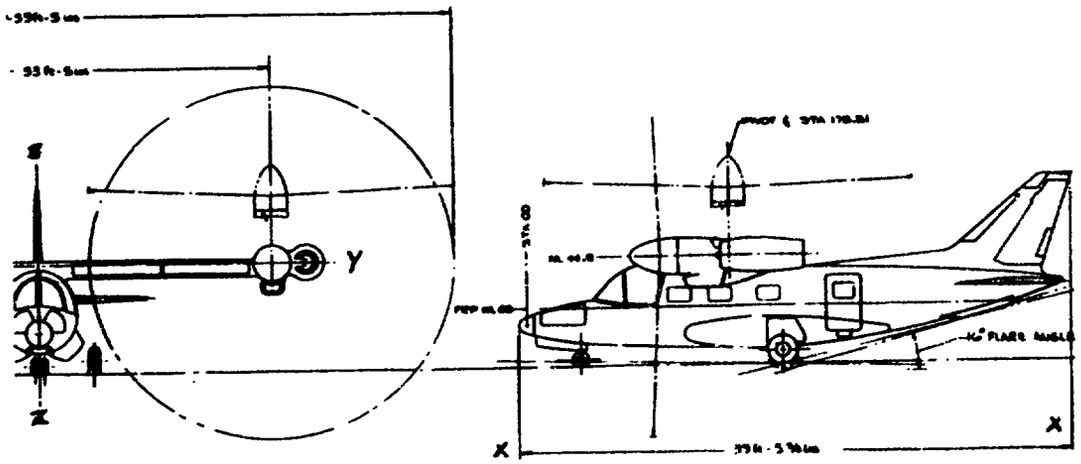

NOTES

MAC	71.8 IN.
L.E. MAC	F.S. 144.6
ROTOR PLANE	F.S. 114.1
WING ¼ CHORD	F.S. 162.5
PIVOT POINT	F.S. 173.3

		NACELLE HORIZ.						NACELLE VERTICAL					
		BALANCE			INERTIA - SLUG FT.^{2}			BALANCE			INERTIA - SLUG FT.^{2}		
SUB-GROUPS	WEIGHT	X (F.S.)	Y (B.L.)	Z (W.L.)	I_{XX} (ROLL)	I_{YY} (PITCH)	I_{ZZ} (YAW)	X (F.S.)	Y (B.L.)	Z (W.L.)	I_{XX} (ROLL)	I_{YY} (PITCH)	I_{ZZ} (YAW)
°FUSE. & CONTENTS													
FWD	159	14.2	-	-19.6	4	11	11						
CENTER	2642	140.4	-	- 7.9	376	2321	2321						
AFT	366	304.0	-	.6	35	259	259						
°HORIZONTAL TAIL	190	413.3	27.7	18.5	16	12	28			SAME			
°VERTICAL TAIL	131	391.3	-	55.5	12	33	21						
°WING CONTENTS	1410	171.2	101.0	41.0	926	130	1060						
°NACELLE & CONTENTS	4732	148.1	207.6	45.3	243	1007	1140	174.1	207.6	69.7	1140	1007	243
OPER. WT. EMPTY	9630	161.6	-	26.9	50030	11957	58919	174.1	-	39.0	52090	12737	57639
FUEL - INBOARD	2000	171.3	93.0	40.5	884	128	1012						
- OUTBOARD													
CARGO	370	171.3	-	.5	200	150	105						
DESIGN GROSS WEIGHT	12000	163.5	-	28.4	54946	12386	63822	173.8		38.1	56998	11098	62453

NOTE: ROTOR BLADE INERTIAS (I_o)
BLADE WT. EA = 107 LB (WITH CUFF) I_{XX} (ROLL) 46, I_{YY} (PITCH) 5, I_{ZZ} (YAW) 50 SLUG FT^2

TABLE G-2 MASS PROPERTIES

(1) Wing Group 800 lbs

$$W_w = 220(K)^{0.585}$$

where

W_w = *weight of wing (lbs)*

and

$$K = \left(\frac{R_m W_x S_w}{100}\right)\left(\log \frac{b}{B}\right)\left(\sqrt{\frac{1+\lambda}{2k_r}}\right)^{\sqrt{N}} \log V_D \log AR$$

LEGEND:

R_m = *relief term*	=	*1.0*	
W_x = *gross weight less tip pod*	=	*7000*	
S_w = *planform area of wing*	=	*200*	*(sq.ft)*
b = *wing span*	=	*33.42*	*(ft)*
B = *maximum fuselage width*	=	*5.6*	*(ft)*
λ = *taper ratio*	=	*1.0*	
k_r = *relative wing root thickness*	=	*.21*	
N = *ultimate load factor*	=	*4.0*	
V_D = *dive velocity*	=	*350*	*(kts)*
AR = *aspect ratio*	=	*5.61*	

The wing weight equation predicted the weight of the Model 222 tilt-rotor wing. For conventional wings, designed primarily for airloads resulting from forward flight, the term $R_m W_x$ indicates the magnitude of the resultant wing shear and bending loads located at the semispan center of lift in forward flight.

Figure G-1 represents the results of wings analyzed in this manner. In the tilt-rotor, the wing design requirements results from vertical flight and transitional modes and the term $R_m W_x$ is reinterpreted by locating the center of lift at the thrust line of the rotor and defining W_x as the aircraft gross weight less the weight of the nacelle and contents. The trend weight represents the total wing structure as defined in AN-9103D MIL-STD weight specification.

The wing weight was determined from layout drawings. Honeycomb construction torque-box was stress-checked to the available loads. The remaining wing structure ribs, fittings, leading and trailing edges, etc., were calculated from scale drawings. The calculated weights* are as follows:

Torque Box	436 lbs
Nacelle Carry-Through Structure	50
Ribs, Doublers, Hardware	100
Leading and Trailing Edges	250
Fittings and Miscellandous	50
TOTAL	886 lbs

*Stress-Checked

Wing structure weight review meetings are currently in progress for the purpose of reducing the wing weight below the predicted trend value of 800 pounds.

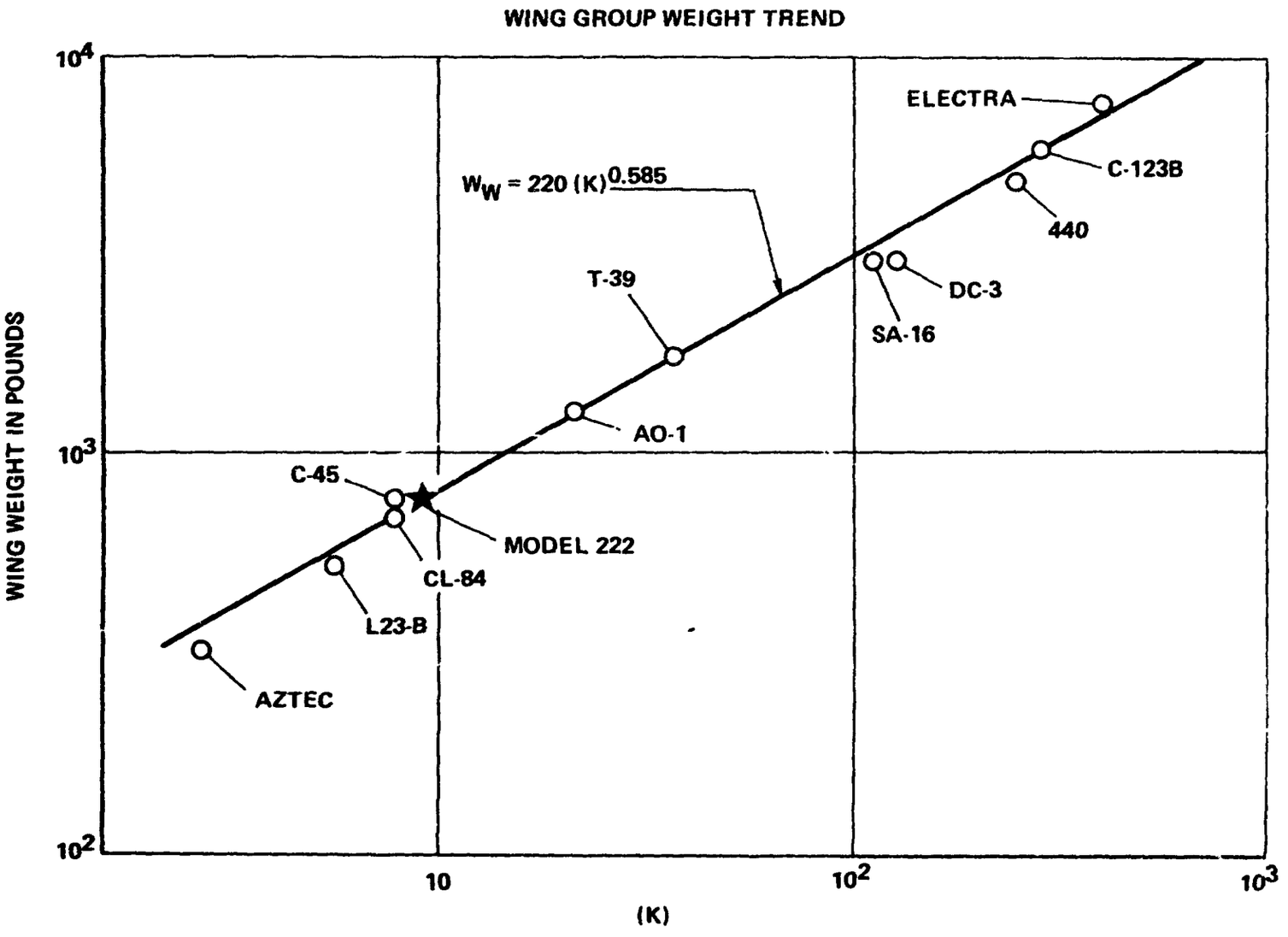

FIGURE G-1 WING GROUP WEIGHT TREND

(2) Tails

The weights of the horizontal and vertical tails are determined from the weight trend equations presented below.

Horizontal Tail 122 lbs

$$W_h = 360(K)^{0.54}$$

where W_h = *weight of horizontal tail (lbs)*

$$K = F_h\left(\frac{S_h}{10^2}\right)\left(\frac{\log V_D}{TMA(t)}\right) \quad \text{and} \quad F_h = \left(\frac{W_G k_y b_h}{10^6}\right)\left(\frac{1 + 2\lambda_h}{1 + \lambda_h}\right)$$

Vertical Tail 91 lbs

$$W_v = 380(K)^{0.54}$$

where W_v = *weight of vertical tail (lbs)*

$$K = \left(F_v + \frac{a(F_h)}{2(b_v)}\right)\left(\frac{S_v}{100}\right)\left(\frac{\log V_D}{TMA(t)}\right) \quad \text{and} \quad F_v = \left(\frac{W_G k_z b_v}{10^6}\right)\left(\frac{1 + 2\lambda_v}{1 + \lambda_v}\right)$$

LEGEND:

F	= *tail load parameter*	
S	= *planform area*	*(sq.ft.)*
V_D	= *dive velocity*	*(kts)*
TMA	= *tail moment arm (measured from wing 1/4 chord to tail 1/4 chord)*	*(ft)*
t	= *root thickness*	*(ft)*

W_G = *design gross weight* (lbs)

k_y = *pitch radius of gyration* (ft)

k_z = *yaw radius of gyration* (ft)

b = *tail span* (ft)

λ = *taper ratio; (chord at tip)/(chord at root)*

a = *height of horizontal tail attachment to vertical tail (measured from root of vertical tail)*

Subscripts:

h *denotes horizontal tail*

v *denotes vertical tail*

The trends consider the tail loads which are a function of the gross weight, span, radius of gyration and point of load application (distance of the mean aerodynamic chord from the point of support). The *"a"* term in the vertical tail equation accounts for *"T"* tail configurations. Figures G-2 and G-3 present the aircraft used to develop the trends.

Refer to Figures G-4 and G-5 to determine the values of k_y and k_z to be placed in the structural box of the weight equations for F_h and F_v, respectively. The weight trend equations over-predict the weights of both horizontal and vertical tails (Figures (G-2 and G-3) of the Mitsubishi MU-2J aircraft as received from Mitsubishi Aircraft International, Inc., San Angelo, Texas.

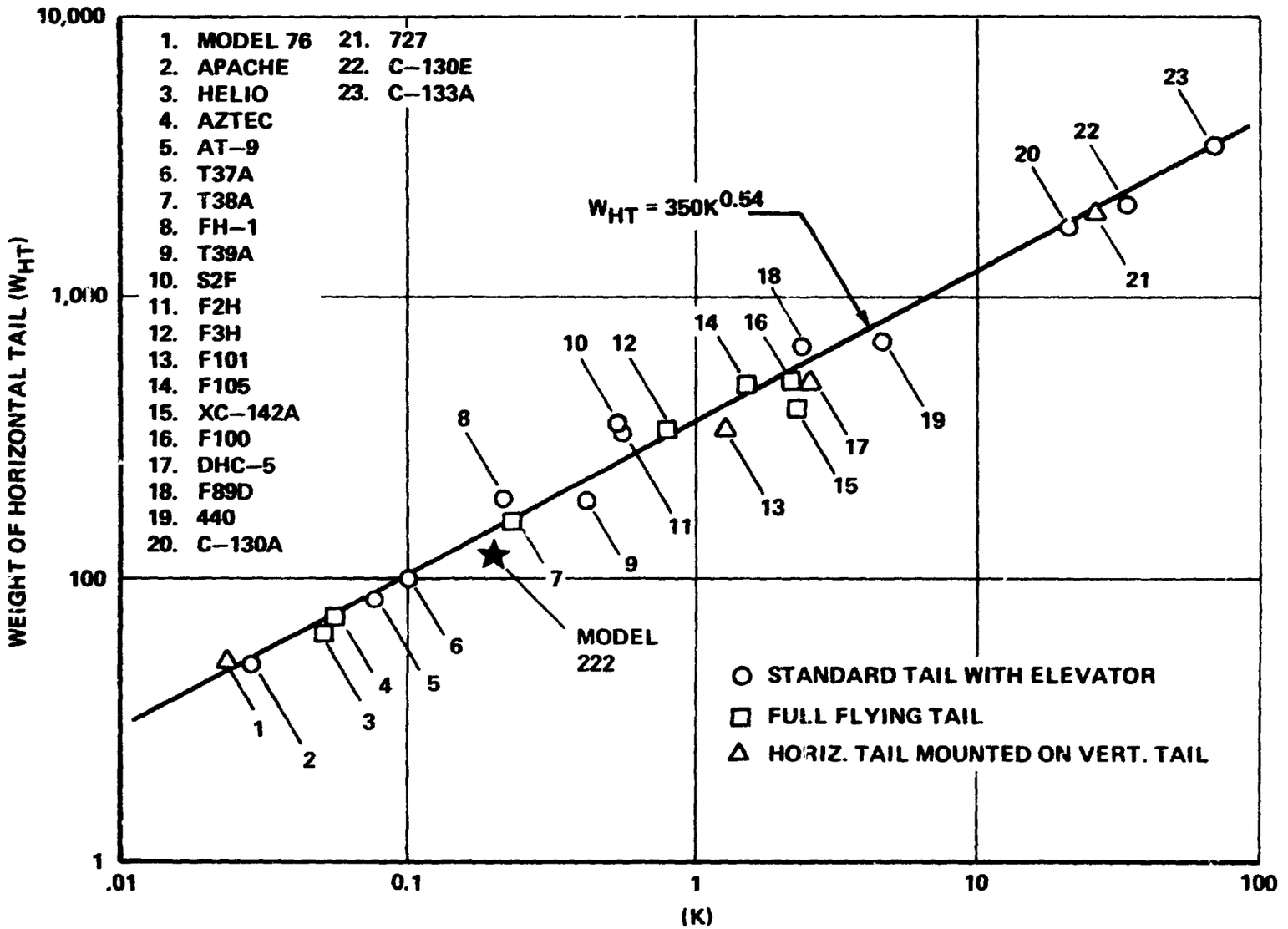

FIGURE G-2 HORIZONTAL TAIL WEIGHT TREND

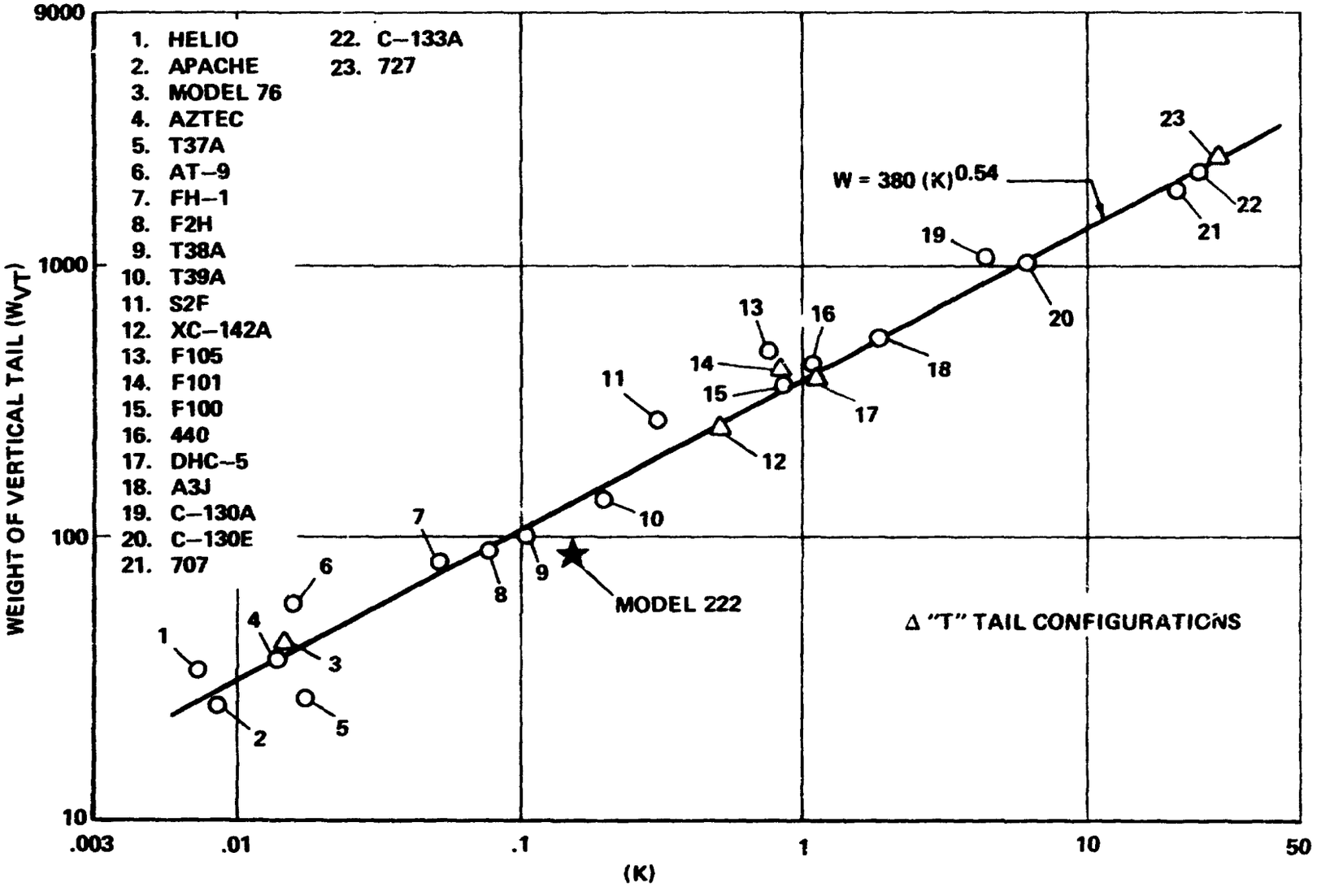

FIGURE G-3 VERTICAL TAIL WEIGHT TREND

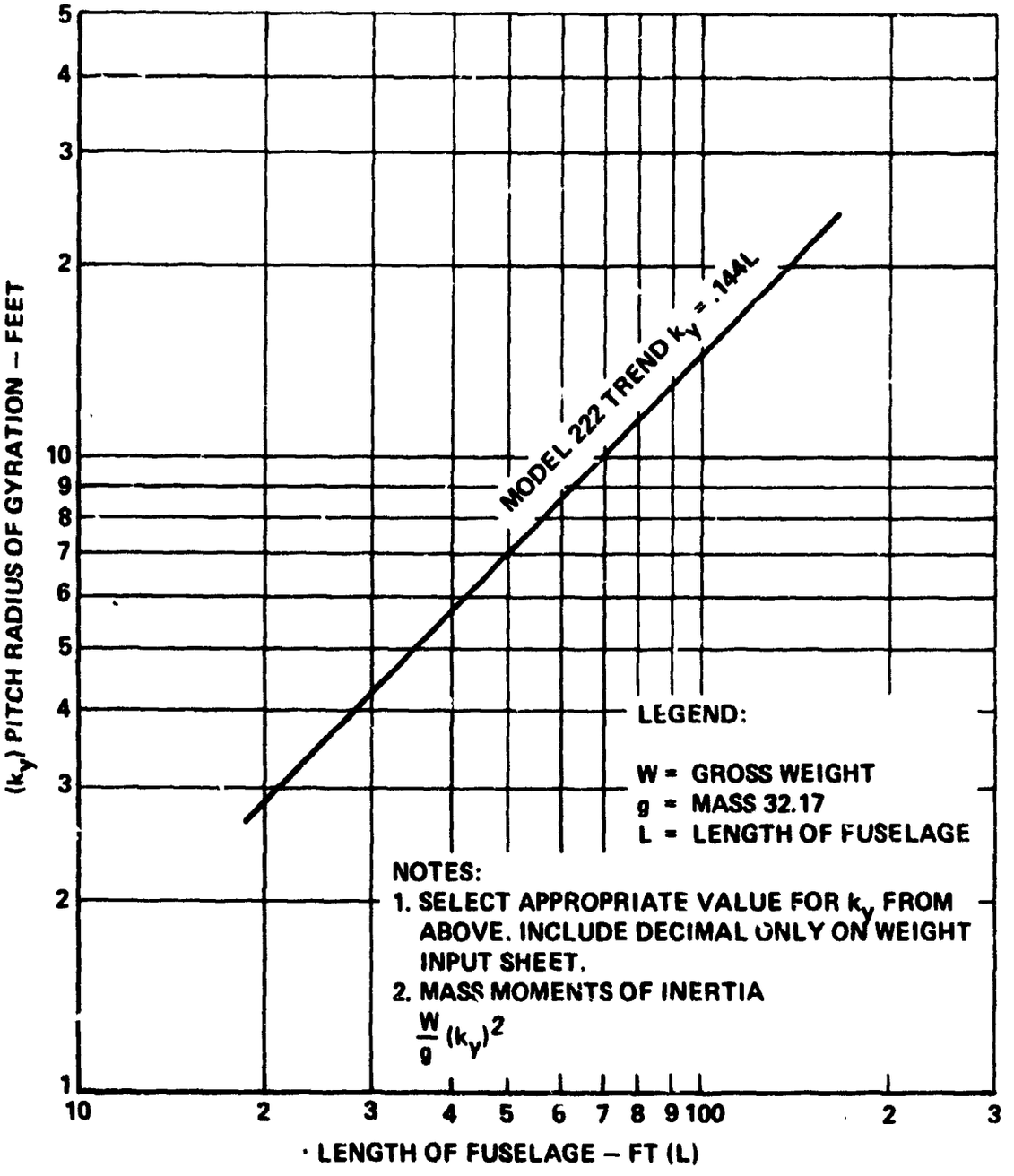

FIGURE G-4 RADIUS OF GYRATION - PITCH

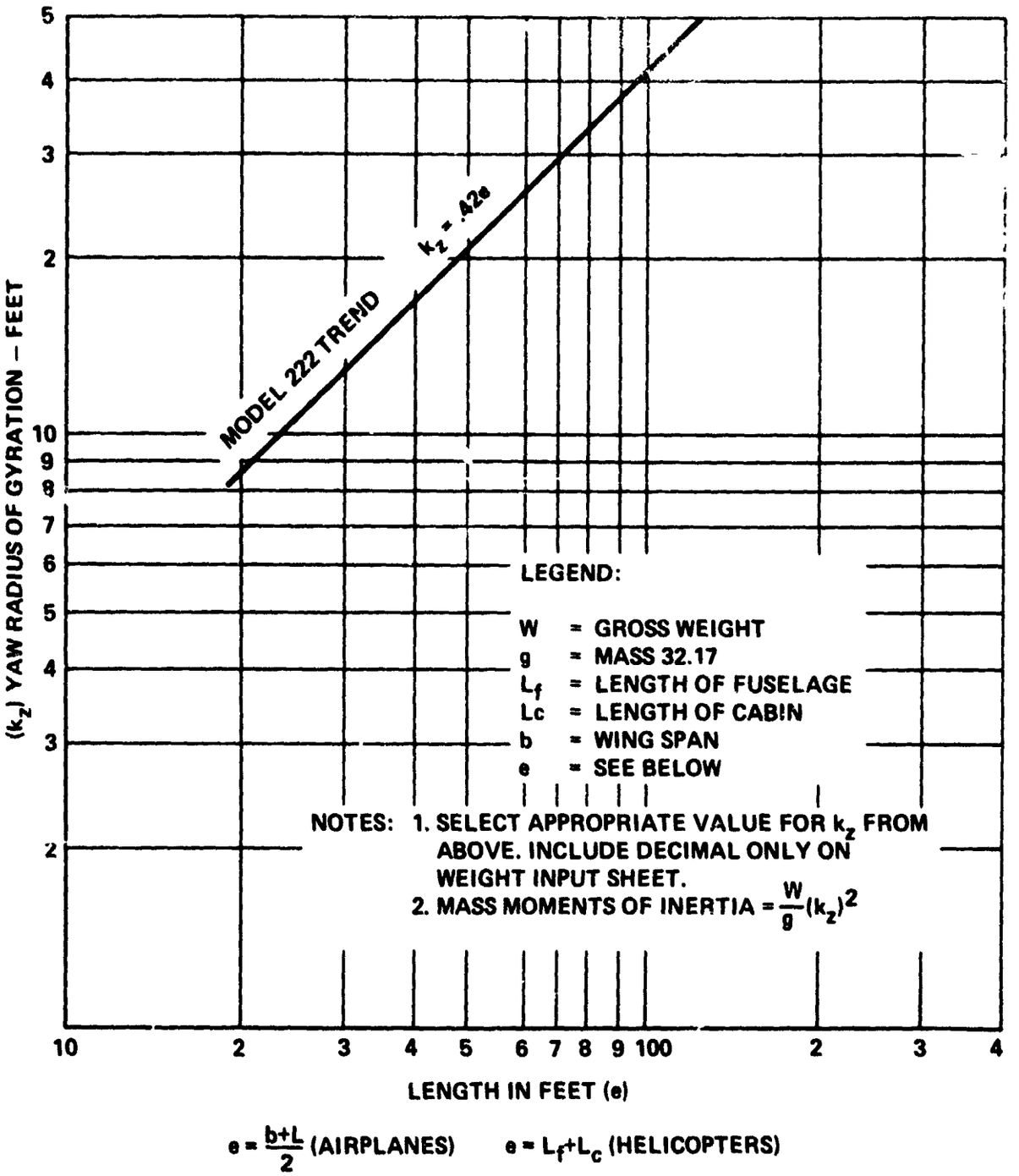

FIGURE G-5 RADIUS OF GYRATION - YAW

Therefore, the constants 360 for the horizontal tail and 380 for the vertical tail were changed to 305 and 256, respectively. This assures that the aircraft in the Sensitivity Study and the new quiet design tail weights are all based on the same design criteria as represented by the Weight Trend Line.

(3) Body and Alighting Gear 1,801 lbs

The weights of the body and landing gear are actual weights of the Mitsubishi MU-2J aircraft.

(4) Flight Controls

The weights of the flight controls were determined from the following:

Cockpit Controls	$W_{CC} = 26(GW/10)^{0.41}$	= 71 lbs
Upper Controls	$W_{UC} = .35(W_R - W_{spin})$	= 360 lbs
Hydraulics	$W_H = 25(W_R - W_{spin}/100)^{0.64}$	= 178 lbs
Fixed-Wing Controls	$W_{FW} = .012(GW)$	= 144 lbs
SAS and Mix Box		= 75 lbs
Tilting Mechanism	$.023(GW)$	= 355 lbs

where:

GW = *gross weight*

W_R = *propeller weight*

W_{spin} = *spinner weight*

Miscellaneous flight control components have been calculated and are in general agreement with the trend weights.

(5) Engine Section

(a) Internal Structure 400 lbs

The weights comprising the engine section were determined from layout drawings. The internal structure supporting the engine and transmissions is as follows:

Internal Structure	200 lbs
Fairing	140
Fire Walls	40
Engine Mounts	15
Miscellaneous	5
TOTAL	400 lbs

(b) Engines 1026 lbs

The engine weight was obtained from the manufacturer. The engines (2) are Lycoming Turboshaft T53-L-13B. The engine was modified by removing the speed decreaser gearing (engine gearbox). Vertol is designing its own drive system for the Model 222. The engine weight, including resudual fluids (fuel and oil), is 513 pounds each.

(c) Engine Installation 200 lbs

The items comprising the engine installation package were calculated and estimated from layout drawings. The weights are as follows:

Air Induction (no foreign object separator)	35 lbs
Exhaust	40
Cooling System (includes core, fan and drive unit)	60
Lubrication	20
Engine Controls	20
Starting System (cables, etc.)	25
TOTAL	200 lbs

(6) Fuel System 200 lbs

The weight of the fuel system is based on a fuel capacity of 308 gallons carried internally in the wing. A statistically-derived weight factor of .65 pounds per gallon was used to deterine the fuel system weight of 200 pounds. The weight includes crash-resistant fuel bladders, pumps, valves, filters, plumbing and installation hardware.

(7) Rotor Installation 1100 lbs

The rotor installation weight was determined from detail drawings of the individual components of the rotor assembly. The details represent the rotor system designed and fabricated at Vertol for NASA under Contract NAS2-6598. A summary of the items and weights comprising the rotor installation are as follows:

Hub and Hardware (2)	300 lbs
Blade Retention	88

Spinners (2)	60
Blades (6)	625
TOTAL	1100 lbs

The rotor installation weight was also checked using the weight equation shown below. The weight of the spinners must be added to the end result to compare it to the calculated values.

$$W_R = 14.2\ a(K)^{0.67}$$

where

W_R = *weight of rotor installation (lbs)*

a = *propeller group adjustment factor (1.10) (rigid, articulated, etc.)*

$$K = r^{.25}\left(\frac{HP_r}{100}\right)^{.5}\left(\frac{V_{tl}Rbc}{10}\right)\left|\left(\frac{R^{1.6}}{100K_dt}\right)\right.$$

NOTE: The last term is a droop factor. It is used only if the result is greater than 1.

LEGEND:

r	= *centerline of rotation to average blade attachment point*	*.98 ft.*
HP_r	= *horsepower (Xmsn limit 1264 per prop)*	
V_{tl}	= *design limit tip speed (750 × 1.15)*	*863 ft/sec*
R	= *prop radius*	*13.0 ft*
b	= *number of blades per prop*	*3*

c = *blade chord (average)* *1.57 ft*

K_d = *droop constant*

t = *blade thickness at 0.25 ft*

In the trend equation, the (14.2) constant is the average for the articulated rotor system presented in Figure G-6. The (16.0) constant is the estimated average line for rigid or hingeless systems based on the limited number of points shown. The *"a"* factor for the Model 222 is *1.10*. The trend weight for the rotor is 515 pounds, plus 30 pounds for the spinner.

(8) Drive System 1107 lbs

The weight of the drive system was determined from design layout drawings. A second method of checking the weight was with the weight trend equation shown below:

$$W_{BOX} = 150(QPUA/N\bar{S}B)^{0.8}$$

where

W_{BOX} = *weight of the individual gearbox*

and

Q = *nondimensional weight factor for gear set or planetary stage*

P = *design horsepower*

U = *function of use factor*

A = *gearbox support factor*

N = *rpm*

$\bar{S}$ = *average Hertz factor*

B = *bearing support factor*

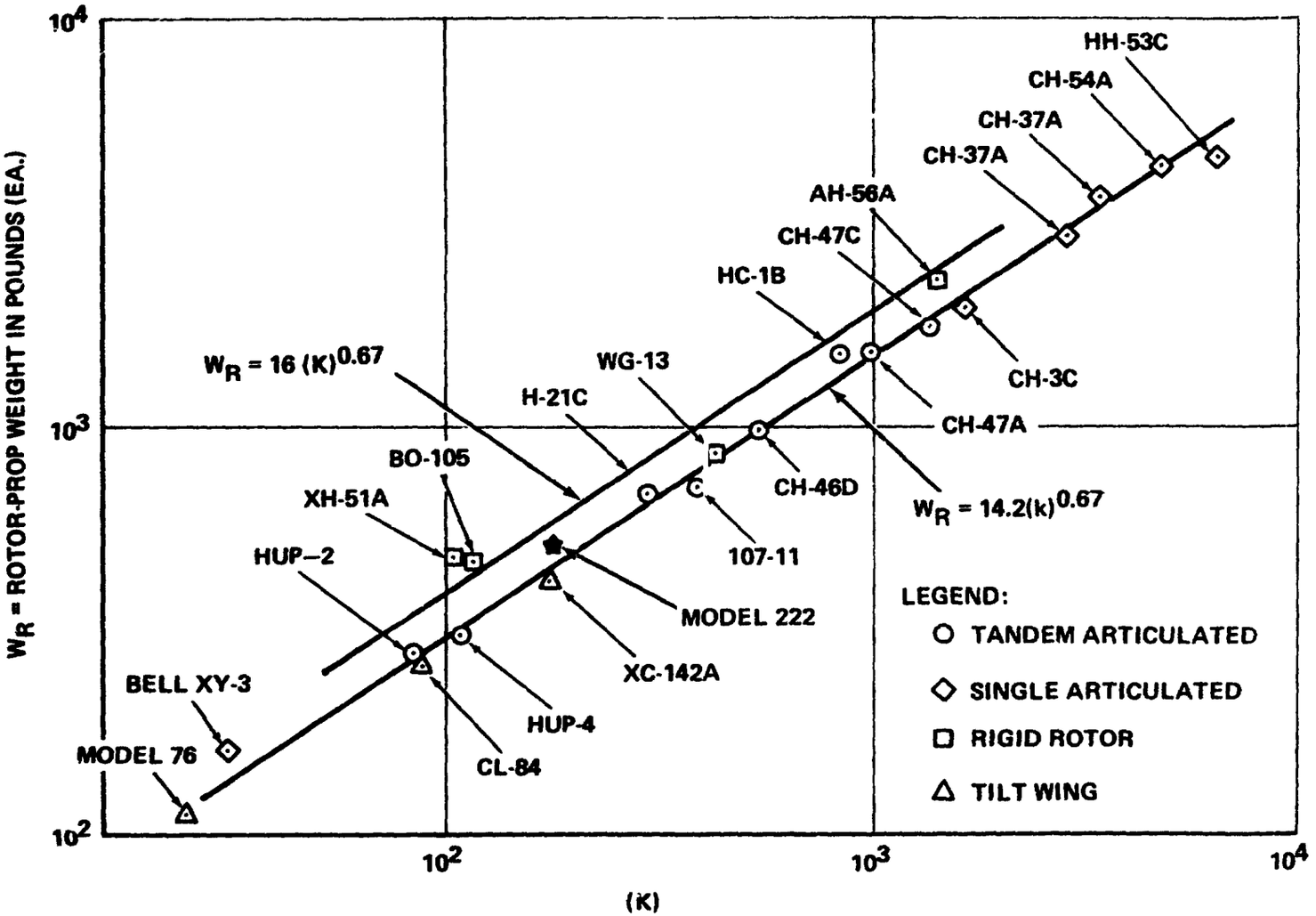

FIGURE G-6 ROTOR/PROP WEIGHT TREND

The trend permits a box-by-box building block approach to determine the drive system weight. It allows for actual design considerations to be used in predicting the weight of the individual gearboxes. The trend includes the weights of the gears, bearings, seals, spacers, case, etc. The weight of the lubrication system and interconnect cross-shafting is not included in the trend values; these must be added separately. Figure G-7 presents a plot of the actual weights of some existing aircraft gearboxes. The trend weights are presented below along with the weights of the various boxes, lubrication system and shafting determined from calculating layout drawings.

	Calculated Weight	Trend Weight
Engine Box	174	150
Rotor Box (includes accessory drive)	624	589
Bevel Box	65	90
Cross-Shaft	100	100
Miscellaneous Shafting	26	26
Lubrication	18	112
TOTALS	1107	1067 lbs

(9) Fixed Equipment

The fixed-equipment group includes the items beginning with the auxiliary powerplant and ending with the auxiliary gear group on the Summary Weight Statement, Table G-1. The weights were

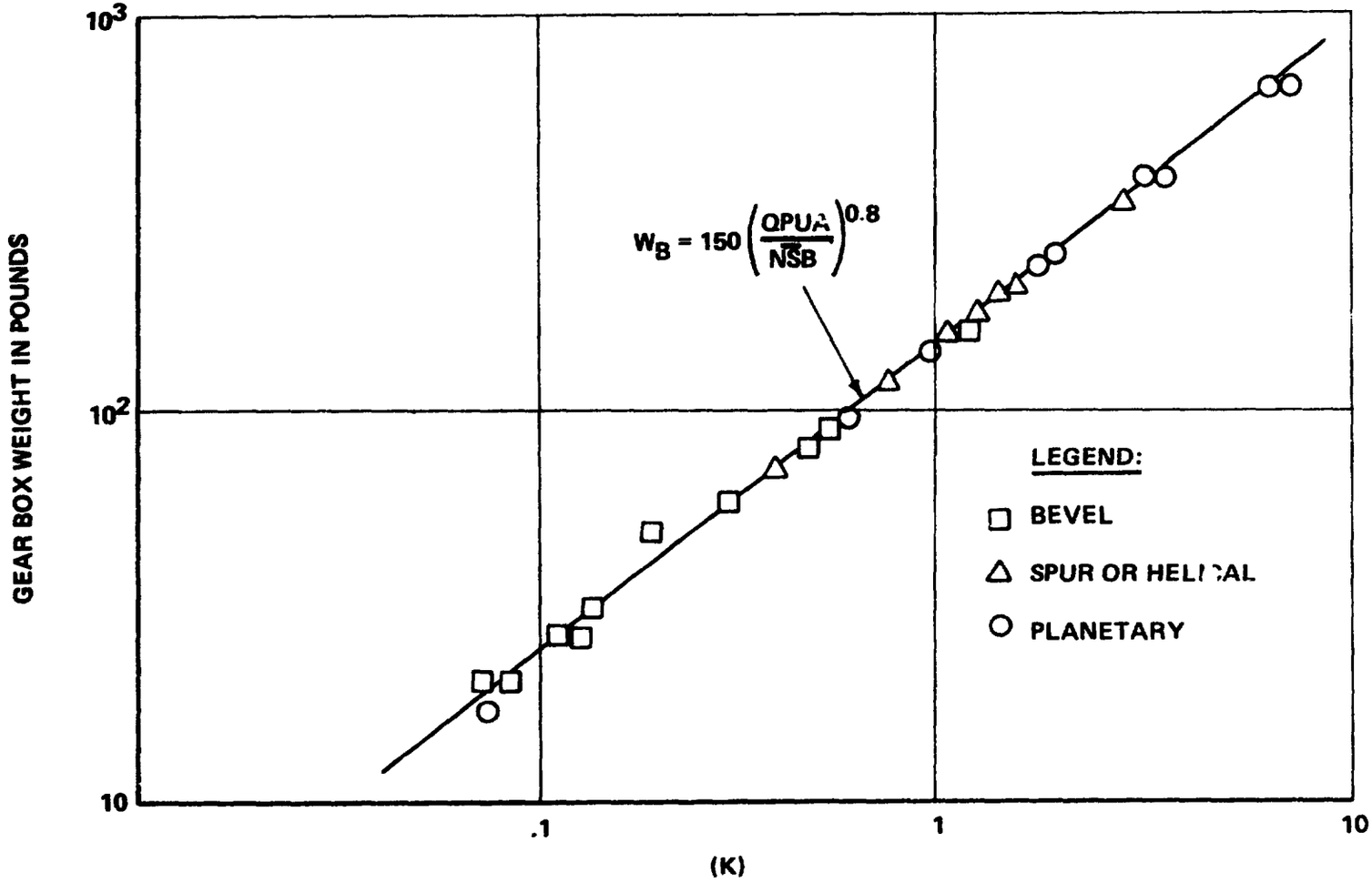

FIGURE G-7 GEAR BOX WEIGHT TREND

determined from equipment lists developed around the tilt-rotor research aircraft requirements. A summary of the items and the weights of the individual groups are tabulalated below:

(a) Instruments		108 lbs
Flight	50	
Engine	25	
Drive/Rotor	26	
Hydraulics	7	
TOTAL	108 lbs	
(b) Electrical Group		305 lbs
Power Supply (starter/generator, batteries)	133	
Power Conversion	46	
Power Distribution (controls. circuit breakers, junction boxes, connectors, wiring, supports, etc.)	106	
Lights (interior, exterior, landing, taxi, etc.)	20	
TOTAL	305 lbs	
(c) Electronics		230 lbs
AN/ARC-51A Radio (UHF)	36	
AN/ARC-115 Radio	6	
AN/ARN-52 Radio (TACAN)	47	
AN/A1C-14 Interphone	19	

AN/ASN-73 Attitude and Heading Reference System	49	
AN/APN-171(V) Electronic Altimeter Set	20	
Shelves, Wiring & Supports	53	
TOTAL	230 lbs	

(d) Furnishings and Equipment — 439 lbs

Accommodations for Personnel: (pilots ejection seats (2) (No. American Aviation LW-3B), seat rails, relief tubes, litter supports)	299	
Miscellaneous Equipment: (data cases, windshield wiper/washer, instrument boards, consoles)	63	
Furnishings: (floor covering, trim, soundproofing	35	
Emergency Equipment: (fire detection and extinguishing equipment, portable fire ext., first-aid kit)	42	
TOTAL	439 lbs	

(e) Airconditioning: — 108 lbs

Environmental Control Unit, Fan, Plumbing, Ducting, Supports and Hardware

(f) Auxiliary Gear 10 lbs

Fittings and Supports for Tiedowns
(jacking, leveling, hoisting, etc.)

(g) Useful Load 2770 lbs

The useful load for the 12,000-pound DGW configuration includes:

(a)	Pilots (2) - 180 lbs each	360
(b)	Trapped Liquid & Engine Oil	40
(c)	Mission Fuel for 100 n.mi. radius	1072
(d)	Mission Payload	1298
	TOTAL	2770 lbs

LIST OF REFERENCES

1. V/STOL Tilt Rotor Aircraft Study, Vol. II , Preliminary Design of Research Aircraft, The Boeing Company, Vertol Div., NASA CR-114438, March 1972.

2. Schmitz, F. H., Stepniewski, W. Z., Gibs, J., Hinterkeuser, A Comparison of Optimal and Noise Abatement Trajectories of a Tilt-Rotor Aircraft, NASA CR-2034, May, 1972.

3. Lowson, M. V., and Ollerhead, J. B., Studies of Helicopter Rotor Noise.

   USAAVLABS Technical Report 68-60, Jan. 1969.

4. Stepniewski, W. Z., and Schmitz, F. H., Possibilities and Problems of Achieving Community Noise Acceptance of VTOL, The Aeronautical Journal, Vol. 77, No. 750, June 1973.

5. Sternfeld, H., Spencer, R. H., and Schairer, J.O., An Investigation of Noise Generation on a Hovering Rotor Part I, Boeing Vertol Report D210-10229-1, January 1971.

6. Hubbard, H. H., and Maglieri, D. J., Noise Characteristics of Helicopter Rotors at Tip Speeds up to 900 Feet per Second, J. Acoustical Soc. Amer., Vol. 32, No. 9, Sept. 1969.

7. Stuckey, T. J., and Goddard, J. O., Investigation and Prediction of Helicopter Rotor Noise, J. Sound Vib., Vol. 5, No. 1, Jan. 1967.

8. Leverton, J. W., The Sound of Rotorcraft, The Aero J. of Royal Aero. Soc., Vol. 75, June 1971.

9. Hilton, D. A. and Henderson, H.R., Standard and Two Modified Hughes OH-6A Helicopters with Some Initial Results, Langley Working Paper 838, Dec. 1969.

10. Schlegel, R., King, R., and Mull, H., Helicopter Rotor Noise Generation and Propagation, USAAVLABS Tech. Rep. 66-4, Oct. 1966.

11. Pollard, J. S., and Leverton, J.W., Effect of Blade Tip Planform on the Noise and Aerodynamics of a Helicopter Rotor, Westland Helicopters Ltd. Research Paper No. 414, April 1972

12. Sternfeld, H., Bobo, C., Carmichael, D., Fukushima, T. and Spencer, R., An Investigation of Noise Generation on a Hovering Rotor Part II, Boeing Vertol Report D210-10550-1.

13. Metzger, F.B., and Magliozzi, B., Noise Characteristics of Quiet Propellers for STOL Aircraft, Noise and Vibration Control Engineering: Proceedings of the Purdue Noise Control Conference (620.23 - PU976N).

14. Feiler, C.E., Groeneweg, J.F., Rice, E.J., Smith, E.B., and Tucker, R.H., Fan Noise Suppression, Paper presented at Aircraft Engine Noise Reduction Conference, NASA SP-311, May 1972.

15. Magee, J.P., Maisel, M.D., and Davenport, F.J., The Design and Performance Prediction of Propeller/Rotor for VTOL Applications, Proceedings of the 25th Annual AHS Forum, No. 325, May 1969.

16. Schoen, A.H., User's Manual for VASCOMP II. The V/STOL Aircraft Sizing and Performance Program, Boeing Document No. D8-075, Volume VI, March 1968, NASA Contract No. NAS 2-3142.

17. Hinterkeuser, E., A Preliminary Investigation of the Properties of a Model Rotor in Nonaxial Flight, Addendum to Contract NAS2-5473, Boeing Vertol Document No. D210-10666-1, July 1973.

18. Ward, J. F. and Young, W.H., Jr., A Summary of Current Research in Rotor Unsteady Aerodynamics with emphasis on work at Langley Research Center, AGARD-CPP-111, September 1972.

19. White, R.P., Jr. and Balcerak, J.C., Investigation of the Dissipation of the Tip Vortex of a Rotor Blade by Mass Injection, USAAMRDL TR72-43, AD 750634, August 1972.

20. Soderman, P.T., Leading-Edge Serrations which Reduce the Noise of Low-Speed Rotors, Unpublished. Ames Research Center.

21. Cox, C., Property for Acoustic and Aerodynamic Testing of a High Mach No. Rotor Tip Model, Bell Helicopter Report No. 299-199-004, May 1970.

22. Boeing Vertol Company, Investigation of the Performance of Low Disc Loading Tilt Rotors in Hovering Flight, Vol. I, Analysis and Results, Boeing Document No. D160-10013-1, March 1971.

23. Stepniewski, W. Z., Basic Aerodynamics of Convertible Rotor/Propeller Aircraft, AGARD NATO Lectures on The Aerodynamics of V/STOL Aircraft, AGARDograph 126, May 1968.

24. Durand, W.F., Aerodynamic Theory, Vol. IV, Div. L, Durand Reprinting Committee, Cal Tech., 1943.

FOLDOUT FRAME

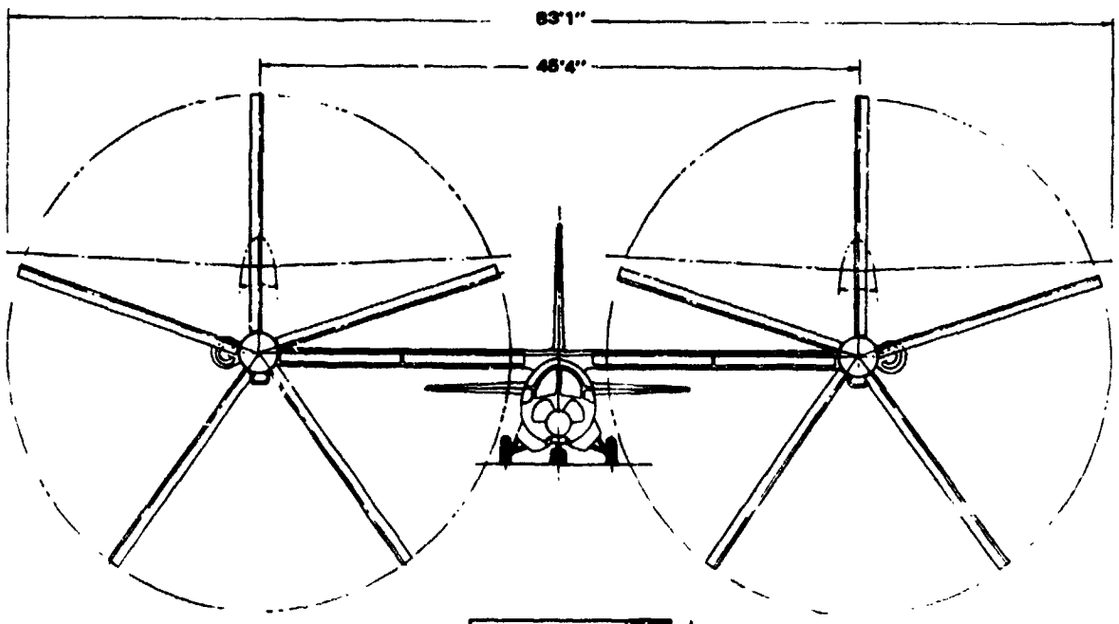

FOLDOUT FRAME

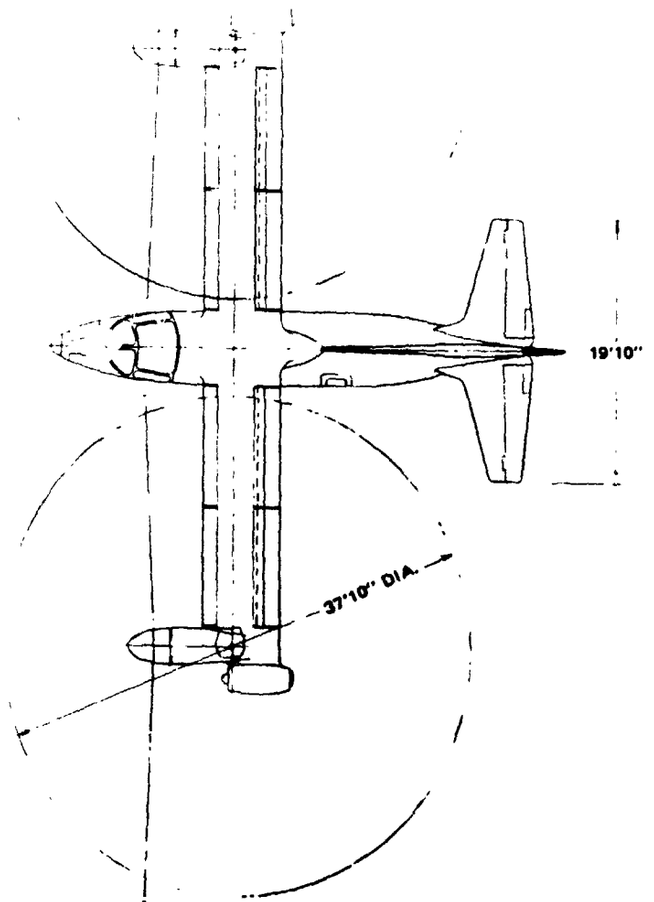

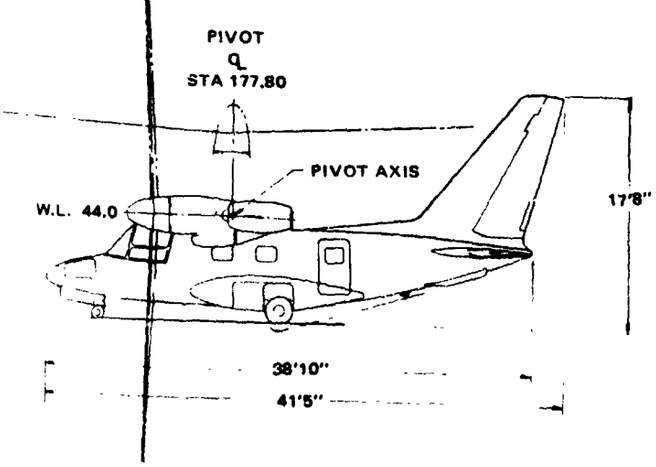

WING

ASPECT RATIO		7.28
AREA		281.4 SQ FT
SPAN		45 3 FT
GEOM. MEAN CHORD		6.2 FT
TAPER RATIO		1
ROOT THICKNESS		.210
TIP THICKNESS	.210	.210
WING LOADING		45.2 LB/SQ FT

HOR. TAIL

ASPECT RATIO		4.61 FT
AREA		85.3 SQ FT
SPAN		19.8 FT
MEAN CHORD	4.3	4.3 FT
THICKNESS/CHORD		0.1

VERT. TAIL

ASPECT RATIO	1.77
AREA	82.8 SQ FT
SPAN	12.1 FT
MEAN CHORD	6.8 FT
THICKNESS CHORD	.060

PROPELLER

DIAMETER	37.8 FT
SOLIDITY	.075
DISC LOADING	5.6 LB/SQ FT
THRUST COEFF./SOLIDITY	.076
BLADES/ROTOR	6.0

WEIGHTS

WEIGHT EMPTY	10,064.0
GROSS WEIGHT	12,707.0

NASA ACOUSTIC PERFORMANCE DESIGN STUDY
TILT ROTOR WITH REDUCED DISK LOADING
SK 25034

SK-25034

FOLDOUT FRAME

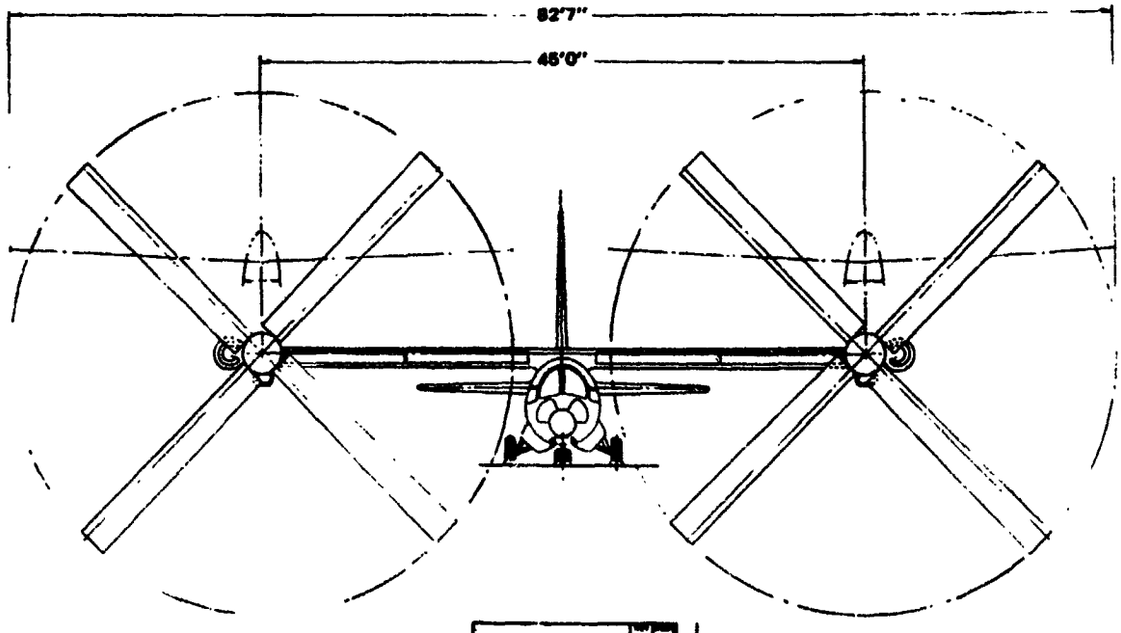

FOLDOUT FRAME

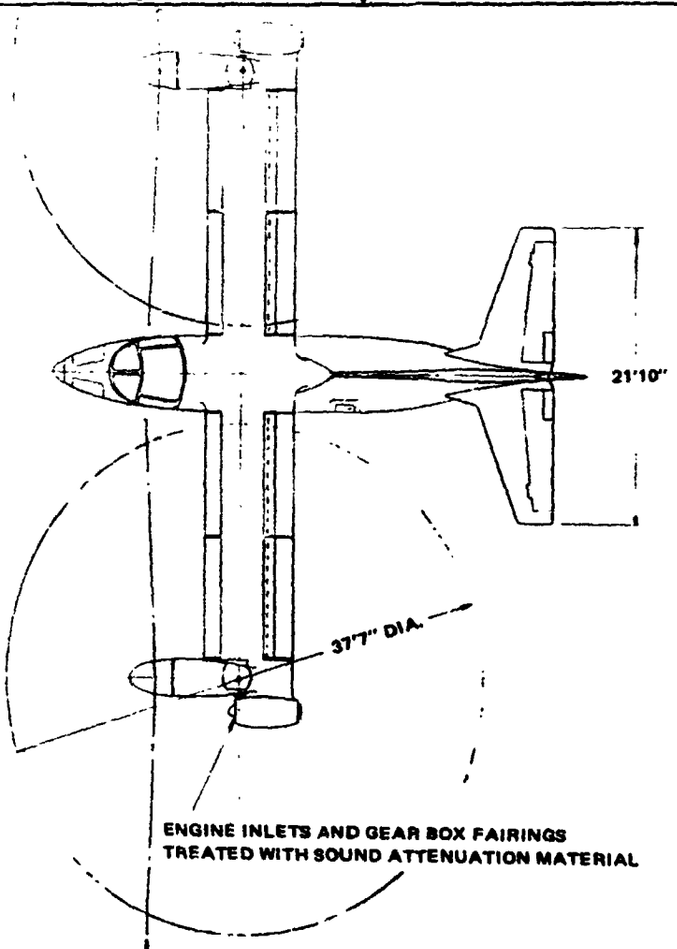

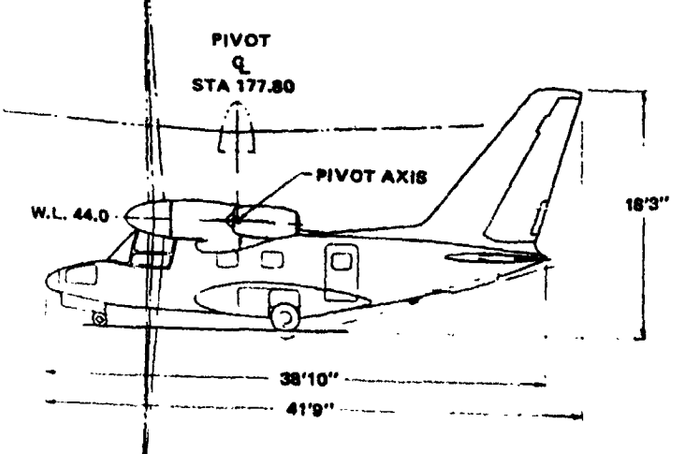

WING

ASPECT RATIO	6.57
AREA	308.3 SQ FT
SPAN	45.0 FT
GEOM. MEAN CHORD	6.9 FT
TAPER RATIO	1.0
ROUT THICKNESS	0.210
TIP THICKNESS	0.210
WING LOADING	48.8 LB/SQ FT

HOR. TAIL

ASPECT RATIO	4.61
AREA	103.0 SQ FT
SPAN	21.8 FT
MEAN CHORD	4.7 FT
THICKNESS/CHORD	0.1

VERT. TAIL

ASPECT RATIO	1.77

ASPECT RATIO	1.77
AREA	89.9 SQ FT
SPAN	12.6 FT
MEAN CHORD	7.1 FT
THICKNESS/CHORD	0.090

PROPELLER

DIAMETER	37.6 FT
SOLIDITY	0.153
DISC LOADING	6.8 LB/SQ FT
THRUST COEFF./SOLIDITY	0.076
BLADES/ROTOR	4.0

WEIGHTS

WEIGHT EMPTY	12,167
GROSS WEIGHT	16,046

SK-25035

NASA ACOUSTIC PERFORMANCE DESIGN STUDY
TILT ROTOR WITH REDUCED DIA.
SK-25035